Heme/Iron-driven microglia polarization in Parkinson's disease

Illyane Sofia Martins Lima

Dissertation presented to obtain the Ph.D degree in Molecular Bioscience

Instituto de Tecnologia Química e Biológica António Xavier | Universidade Nova de Lisboa

Research work coordinated by: INSTITUTO GULBENKIAN DE CIÊNCIA

Oeiras, July, 2021

AKNOWLEDMENTS

Em primeiro lugar quero agradecer à minha supervisora Raffaella Gozzelino por me ter aceite no laboratório. Pela paciência “dos Deuses”. Pela forma amiga e generosa com que sempre me incentivou e ajudou, e pelo estímulo sentido após cada conversa, que me faziam “carregar baterias”. Ao meu co-supervisor Luís Moita por me aceite e ajudado imenso, um muito abrigada.

À Joana Sá pela grande oportunidade, que me permitiu evoluir profissionalmente e não só, permitiu-me conhecer pessoas que levo pela vida toda, a minha família PGCD.

Às minhas colegas de laboratório, quero agradecer-lhes os momentos, que passamos. Cathy querida, quem me ensinou quase tudo. Muito agradecida por tudo, pela paciência. Saudade (ish) das noitadas de facs. Ahah. Inêzinha, obrigada por tudo, oh meu Deeus! Miss you! À minha pequena “bola” de mau feitio, Ana obrigada pela companhia, amizade e por compartilhares comigo o gosto de músicas de qualidade duvidosa, como disseste. Bohemian Rhapsody acho que equilibrou as coisas.

Aos meus colegas e amigos, Daniela, Nuninho, Pedro e Bitoquinho, um especial obrigado pela amizade, nossas conversas “de café” pela força nos momentos não tão bons.

À minha família um especial obrigado. Cre nhos txeu!! Mina, Cafi, Paulo, Dada, Biu, Nunas, Melainas!! Thanks for all the suport. Cowzinha of my heart! Thank you for all the support and for making me laugh like a crazy person! Mamy poderosa nada disso seria possível sem ti e Papito obrigada pelo apoio e motivação para nunca desistir.

Ao meu namorado, AMO-TE. Obrigada pela enorme paciência e extrema calma que sempre me transmitiste e que foi essencial para que tudo corresse bem. Ao meu Tosinho, amor da sua mãe, this was all thanks to you! Amo-te muito amor.

Agradeço a todos que diretamente ou indiretamente ajudaram-me durante todo esse processo!

ABSTRACT

Parkinson Disease (PD) is a neurodegenerative disorder characterized by the progressive loss of dopaminergic neurons in the *substantia nigra pars compacta* of the brain, which is often accompanied by the abnormal aggregation of α-synuclein, forming Lewy bodies. Although the etiology of PD remains to be fully elucidated, there are several causes underlying this disease, which are known to play an important role. Among these, the activation of microglia towards a proinflammatory phenotype, fueled by disruption of heme metabolism, stands out. Although provided systemically, exogenous heme administration was shown to trigger brain iron accumulation, which is known to physiologically occur during aging. This crosstalk between the periphery and the brain was investigated *in vivo* by using flow cytometry. The phenotypic switch of microglia and resulting neuroinflammation in mice exposed to heme was assessed. Our study demonstrates that, at higher doses, heme suppresses microglia to further release pro-inflammatory cytokines and generate radical oxygen species. Our data show that, after certain thresholds, microglia become unresponsive. Whether this could increase the accumulation of iron in the brain during aging is likely to be the case, given that microglia are no longer functioning. Our findings also allow to determine the consequences of brain microvascular impairment in promoting the development of neurodegenerative diseases, like PD.

RESUMO

A doença de Parkinson é uma doença neurodegenerativa caracterizada pela perda progressiva de neurônios dopaminérgicos localizados na *substância nigra pars compacta* e pela agregação anormal de α-sinucleína no cérebro. Embora a etiologia não esteja totalmente elucidada, existem várias causas subjacentes a esta doença, conhecidas por desempenharem um papel importante no desenvolvimento da mesma. Entre estas, destacam-se a dirupção do metabolismo de heme, seguido pela ativação do fenótipo pró-inflamatório da microglia. Apesar de ser administrado na periferia, heme demonstrou a capacidade de desencadear a acumulação de ferro no cérebro, que é conhecida por ocorrer fisiologicamente durante o envelhecimento. A comunicação entre a periferia e o cérebro foi posteriormente investigado *in vivo* através da utilização da citometria de fluxo. Foi avaliada a mudança fenotípica da microglia e a neuroinflamação resultante em ratinhos expostos a heme. O nosso estudo demonstra que, em doses mais elevadas, o heme suprime a libertação de citocinas pró-inflamatórias pela microglia e a produção de espécies reativas de oxigénio, tornando-se inertes. Este evento poderá levar a uma acumulação exacerbada de ferro no cérebro dado que a microglia não consegue desempenha o seu papel. Os nossos resultados também permitem determinar as consequências da disrupção da barreira hematoencefálica do desenvolvimento de doenças neurodegenerativas, incluindo a doença de Parkinson.

INDEX

FIGURE INDEX

ABBREVIATIONS

6-OHDA	6-hydroxydopamine
ABCG2	ATP-binding cassette
ALA	δ-aminolevulinic acid
AD	Alzheimer's disease
CNS	Central nervous system
CO	Carbon monoxide
CoQ10	Coenzyme Q10
CLR	C type lectin receptors
CRY1-2	Cryptochrome 1 and 2
DAR	Dopamine agonists receptors
DFO	Deferoxamine
DFN	Deferiprone
DMT1	Divalent metal transporter 1
DCF	5-(and-6)-chloromethyl-2',7'-dichrlorodihydro-fluorescein di-acetate
DXM	Dexamethasone
Fe	Iron
Fer-1	Ferrostatin-1
Fr	Ferritin
FPN	Ferroportin
FLVCR1	Feline leukemia virus subgroup C receptor 1
GPXs	Glutathione peroxidases
GPX4	Glutathione peroxidase 4
GSH	Glutathione
GSSG	Glutathione disulfide
HAS	Heme A synthase
HCP-1	Heme carrier protein 1
HDL	High density lipoproteins
HMB	Hydroxymethylbilane
HO	Heme oxygenase
HOS	Heme O synthase
HRG-1	Heme Responsive Gene 1
HSAN	Hereditary sensory and autonomic neuropathy
H_2O_2	Hydrogen peroxide
Hx	Hemopexin
ICH	Intracerebral Hemorrhage
IL-6	Interleukin 6
IL-1 β	Interleukin 1 beta
IL-10	Interleukin 10
IRF3	Interferon regulatory factor-3 (
LDL	Low density lipoproteins

MAO-B	Monoamine oxidase B
Mb	Myoglobin
MPP+	1-methyl-4-phenylpyridinium
MPTP	1-metil-4-fenil-1,2,3,6-tetraidropiridina
MyD88	Myeloid differentiation factor 88
NAC	N-Acetylcysteine
NPAS2	Neuronal PAS domain protein 2
NLR	NOD-like receptors
PD	Parkinson's Disease
PER2	Period 2
PBG	Porphobilinogen
PPIX	Proto- porphyrin IX
PUFA-PLs	Poly-unsaturated fatty acids phospholipids
TH	Tyrosine-Hydroxylase
TLR	Toll-like receptors
TNF-a	Tumor necrosis factor alpha
TNFR1	Tumor necrosis factor receptor 1
TRAIL	Tumour necrosis factor (TNF)-related apoptosis-inducing ligand
TREM	Triggering receptor expressed on myeloid cells
TRIF	TIR-domain containing adapter-inducing interferon-γ
RBC	Red blood cells
RIG	RIG-like receptors
RIPK	Receptor-Interacting Protein Kinase
ROS	Reactive oxygen species
RSL-3	RAS-selective lethal 3
RP	Retinitis pigmentosa
TBI	Traumatic brain injury
TLR	Toll-like receptor
Tf	Transferrin
TfR	Transferrin receptor
TGF-β	Transforming growth factor β
Xc^- system	Membrane system for cysteine uptake

INTRODUCTION

CHAPTER 1

1.1 HEME

Heme is a metallo-compound, i.e. a tetrapyrrole containing an iron (Fe^{2+}) atom, which acts as prosthetic group of proteins, known as hemoproteins [1]–[3]. Heme is essential to ensure a wide range of biological processes [4]. It is capable to control oxido-reducing reactions, it is used for oxygen transport and storage, it plays a crucial role for respiration, gas synthesis and sensing, drug detoxification and signal transduction [3], [5], [6]. Heme also participates in antioxidant responses and influences circadian rhythms, microRNA processing, cell differentiation and cell proliferation [7].

Heme is a major source of iron (Fe), which explains its abundance in red blood cells (RBC), where is part of the hemoglobin structure. About 80% of heme is produced to sustain hematopoiesis, while 20% is stored by other tissues [8].

Heme is present in different forms: *a, b* and *c.* Their nature and function are defined by substituent's groups on the porphyrin macrocycle. Heme *a* is derived from Heme *b* through two enzymatic chain reactions: First Heme O synthase (HOS) converts the C-2 vinyl group of Heme *b* into Heme *o;* second, Heme A synthase (HAS) catalyzes the C-8 methyl group of Heme O into to a formyl group. Heme *a* reduces molecular oxygen and forms the proton pump pathway of cytochrome c and quinol oxidase. Therefore, it is an essential co-factor

for respiratory terminal oxidases and is vital for respiration in aerobic organisms [9][10].

Heme *b* is the most common variant in mammals. It is an iron-protoporphyrin IX and binds non-covalently to proteins. It is a precursor of Heme *c* and transports gas when in hemoproteins, as hemoglobin (Hb) and myoglobin (Mb) [2].

Heme *c* is the second most common variant. It is characterized by the presence of two covalent thioether bonds, formed between Cys side chains and the Heme's vinyl groups at the 2^{nd} and 4^{th} position. Heme *c* is present in the cytochrome c protein. It can act as a redox site for intramolecular and/or intermolecular electron transfer [11].

1.2 HEME SYNTHESIS

There are two tissues where Heme synthesis mostly occurs, the bone marrow and the liver (Ogun and Valentine, 2019 – Biochemistry, Heme synthesis). Heme synthesis requires the participation of eight conserved enzymes [12], as shown in Fig.1, and occurs between the mitochondria and cytosol. It begins in the mitochondria, with a reaction catalyzed by the enzyme δ-aminolevulinic acid synthase 1 (ALAS-1), producing δ-aminolevulinic acid (ALA) from the amino acid glycine and succinyl-CoA. This is the rate-limiting step of heme biosynthesis, as ALAS-1 determines how much Heme is synthetized [13][14]. Two molecules of ALA are then used to produce a pyrrole ring, known as porphobilinogen (PBG), by the action of ALA dehydratase. This reaction occurs in the cytosol. The condensation of four molecules of porphobilinogen to form the linear hydroxymethylbilane (HMB) is catalyzed by hydroxymethylbilane synthase [15]. The production of an asymmetric pyrrole ring, called uroporphyrinogen III, followed by the formation of the porphyrin ring III,

is promoted by the action of uroporphyrinogen-III synthase and of the uroporphyrinogen decarboxylase, respectively. The coproporphyrinogen oxidase, located at the mitochondrial intermembrane space, turns coproporphyrinogen III into protoporphyrinogen IX [15][16], which is then converted into protoporphyrin IX by the protoporphyrinogen oxidase. Inside the mitochondria, the ferrochelatase promotes the insertion of the Fe atom within the porphyrin structure, leading to the formation of heme [2], [14], [17], [18].

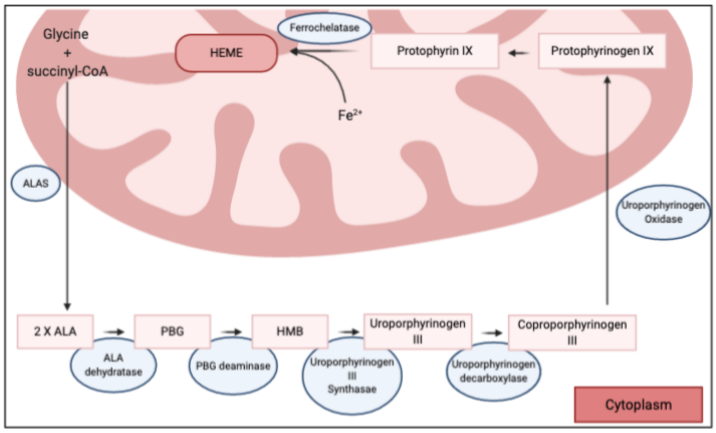

Fig. 1- Schematic representation of Heme synthesis.

1.3 HEME HOMEOSTASIS

At systemic levels, Heme homeostasis can be achieved by the action of two scavenger proteins: haptoglobin (Hp) and hemopexin (Hx).

Hp prevents the release of cell-free hemoglobin upon red blood cell (RBC) disruption, a process occurring as a consequence of Hb oxidation. The release of heme from non-hemoglobin bound heme is scavenged by Hx, which delivers this molecule to the liver for iron recycling (Fig.2).

Other molecules with similar scavenging properties include albumin, α1-microglobulin, and high- and low-density lipoproteins (HDL and LDL). However, Hx binds Heme with highest affinity.

1.4 HEME CATABOLISM

Free Heme causes inflammation. It intercalates in lipid membranes and changes cellular structures. By acting as pro-oxidant, Heme is able to activate immune cells [19]. Thus, Heme homeostasis must be tightly regulated both at systemic and cellular levels. At cellular levels, Heme degradation contributes to maintain this equilibrium and occurs by the action of stress-response proteins, known as Heme oxygenases (HO) [20]. Biliverdin, carbon monoxide (CO) and iron (Fe) are the by-products of Heme catabolism by these enzymes. Once produced biliverdin is converted into Bilirubin by biliverdin reductase, while the released Fe is stored and neutralized into the multimeric ferritin. By converting it into an inert state, ferritin prevents Fe participation to the generation of cytotoxic compounds [21]–[23] (Fig.2).

To date, three isoforms of HO have been described, being HO-1 and HO-2 the most common. HO-1 is induced in almost all tissues, as responding to a variety of stressors, like pro-oxidants, and pathologic conditions, such as hemorrhages, trauma, or inflammatory reactions. Contrarily, HO-2 is constitutively and ubiquitously expressed, already under physiologic conditions. In the brain, HO-2 is the most prevalent form. Those enzymes are encoded by *Hmox-1* and *Hmox-2* genes, respectively, and they share 45% of sequence homology. Few studies describe HO-3, which, despite presenting a lower Heme degrading capacity, is likely to play a role in oxygen sensing [6], [22], [23].

Heme can also be degraded through non-enzymatic reactions. In the presence of high content of Hydrogen peroxide (H_2O_2) [24], Heme is catabolized in a pH-dependent manner, a reaction occurring in neutral or alkaline solution [25]. In these cases, Heme is degraded into verdoheme, which is then hydrolyzed to free, approximately, the same amount biliverdin IXα and CO as enzymatic reactions [26][27].

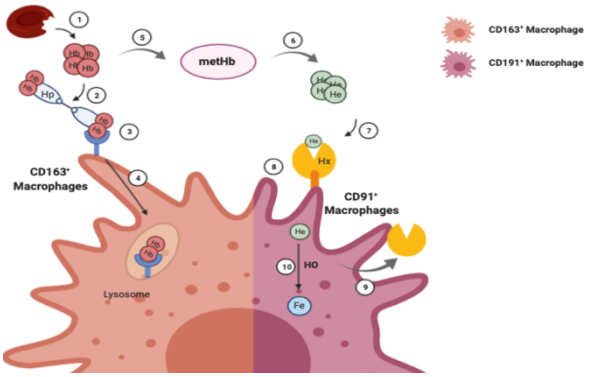

Fig. 2- Heme homeostasis. The disruption of RBCs releases Hb (1), which is scavenged by Hp (2). The complex Hb:Hp is then internalized by the binding to its receptor CD163 on the extracellular membrane of macrophages (3). Complex endocytosis is followed by degradation (4). If Hp capacity is exceeded, cell-free Hb is oxidized to metHb (5), which is highly unstable and rapidly releases Heme into circulation (6). Heme is immediately scavenged by Hx (7), which complex is internalized by binding to Hx receptor CD91 (8). Once entered cells by endocytosis (9), Heme is then degraded by HO (10).

1.5 HEME TRANSPORT

The lipophilic nature of Heme allows its diffusion between different compartments. However, several transporters have been identified as capable to mediate Heme trafficking (Fig.3) [7].

Heme is uptaken through the diet, in the intestine, via the Heme carrier protein 1 (HCP1). HCP-1 is a 50kDa protein, highly conserved and expressed in the duodenum and small intestine, as shown in Fig.4.

This Heme importer was shown as capable to also transport folic acid, for which it has a high affinity. As demonstrated in competition experiments and although HCP-1 showed enhanced affinity for folic acid, the concentration of Heme in the intestine is higher, turning the protoporphyrin the preferential HCP-1 substrate to be transported [28][29][30].

Another Heme importer is the Heme Responsive Gene 1 (*HRG-1*), which is the first to be described. Functioning at low pH, HRG-1 co-localizes on endosomes and lysosomes [28], where responsible for Heme uptake. Inside these organelles, Heme is then degraded by HO-1 [30]. HRG family members was first discovered in *C. elegans*, organisms that cannot synthesize Heme and need to uptake it from the environment. Loss of function approaches, where *HRG-1* and *HRG-4* genes were depleted, confirmed their role as Heme importers [15][31]. In humans, the transmembrane protein *HRG-1* is highly expressed in brain, kidney, heart, and skeletal muscle [31].

The Feline leukemia virus subgroup C receptor 2 (FLVCR2) also acts as Heme importer. FLVCR2 is ubiquitously expressed and involved in Heme endocytosis processes. FLVCR2 mutation, in humans, leads to the development of the Fowler Disease, a condition characterized by the lack of complex III and IV in mitochondria, which causes vessel thickening and vascular impairment [3], [32].

Heme can be exported from cells via the Feline leukemia virus subgroup C receptor 1 (FLVCR1) and ATP-binding cassette (ABCG2). FLVCR1 is a cell surface protein, highly conserved, and expressed in humans in brain, liver, kidney, lung, spleen, lung, placenta, and bone marrow [28][33]. ABCG2 was shown as capable to mediate intracellular proto-porphyrin IX (PPIX) exit and deliver Heme to extracellular Heme scavengers [2]. It is expressed in multiple tissues including the nervous system, intestine, kidney, liver and placenta. [28]

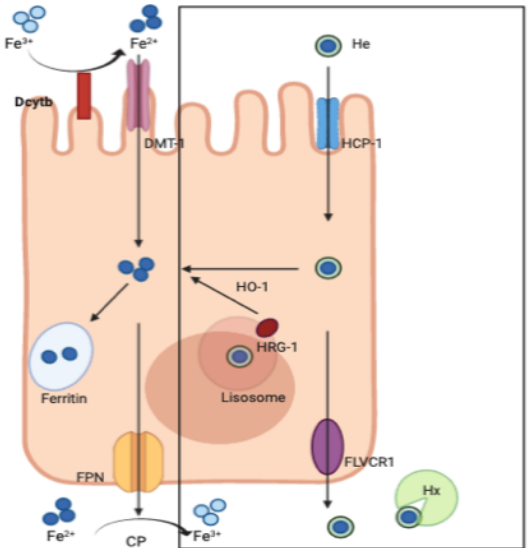

Fig. 3- Heme intracellular trafficking. Dietary Heme is uptaken by HCP-1, which is located in the duodenum. Inside cells, Heme is degraded by HO-1, releasing Fe2+, which is then neutralized and stored into ferritin. The lysosomal Heme importer HRG-1 allows Heme transport into the cytoplasm, which is then degraded by HO. Excess Heme exits the cell through Heme exporter FLVCR1 and is released into circulation.

CHAPTER 2

2.1 THE HEME ROLE IN THE BRAIN

Heme is a metallo-compound capable to promote neuronal growth and survival in the central nervous system (CNS), where is used to produce the energy necessary for neuronal activity [3]. Likewise, Heme also serves to detoxify neurotoxic compounds causing oxidative insults in the brain, an effect achieved by its incorporation into cytoprotective proteins as neuroglobin, neudesin, neuroferricin [34]. Neuroglobin is mainly expressed in neurons of the central and peripheral nervous system (CNS, PNS, respectively). It provides oxygen to the respiratory chain [35] and detoxifies neurotoxic and oxidative products [3]. Neudesin is a secreted protein, which promotes neural differentiation and proliferation. Neuferricin is abundantly expressed during developmental stages and plays an important role in neurogenesis [36][34].

In the brain, Heme also regulates the circadian rhythm. It influences the clock function by binding to circadian proteins, including cryptochrome 1 and 2 (CRY1-2), neuronal PAS domain protein 2 (NPAS2), Period 2 (PER2), and the nuclear hormone receptors REV-ERBα and REV-ERBβ [37]. This direct binding regulates the stability and transcriptional activity of these clock components [38]. On the other hand, it is also important to highlight that the transcription of ALAS-1 and enzymes involved in Heme catabolism and transport are regulated by the circadian clock [37], [39], thus resulting in a positive feedback loop. Therefore, disruption of Heme metabolism directly affects the circadian clock [16] and vice-versa.

2.2 HEME SYNTHESIS, CATABOLISM AND TRANSPORT IN THE BRAIN

Like in other organs, Heme metabolism in the brain is tightly regulated [32], [40].

As for other organs, Heme synthesis occurs between the cytosol and the mitochondria, a process regulated by the eight enzymes, as previously mentioned [18], [41].

Heme uptake into the brain occurs mainly through the action of HRG-1, which is highly expressed in the brain [18]. Studies in zebrafish showed that HRG-1 deficiency leads to malformation and neurological impairment. FLVCR2 is also responsible for Heme import into the CNS, and is expressed in the brain and spinal cord [32]. Mutations related to this gene are responsible for the development of the Fowler syndrome, a proliferative glomerular vasculopathy that was previously mentioned [40].

ABCG2 and FLVCR1 are responsible for Heme export also in the brain. ABCG2 is mainly expressed by neurons and glia, while FLVCR1 plays an important role in maintaining the proper neuronal function [3]. Mutations in FLVCR1 results in posterior column ataxia and retinitis pigmentosa (PCARP), as well as in a non-syndromic retinitis pigmentosa (RP) and hereditary sensory and autonomic neuropathy (HSAN).

HOs are also expressed in the brain. Responsible for Heme degradation, the expression of HO-1 is almost undetectable in this organ under physiological conditions. However, its levels increase upon injury. HO-1 is mainly upregulated by glial cells in the attempt to revert inflammation and protect the brain against oxidative stress. The levels of HO- and the duration of its enzymatic activity vary according to cell types [42]. Conversely, the constitutive HO-2 is

commonly expressed, under physiological conditions, in both neurons and glia. In addition, the levels of HO-2 might also increase upon ischemia or hemorrhagic injury [3], [42], [43].

2.3 PATOPHYSIOLOGY OF AGING

It is known that Heme accumulation in the brain occurs gradually and throughout life. Several diseases have been described as significantly contributing to this phenomenon, like ischemia, traumatic brain injury (TBI), intracerebral hemorrhage (ICH), vascular hemorrhage and stroke [44]. Microhemorrhage events, in particular, could be highly deleterious, as clinically silent [45], but their incidence increases during aging. Thus, it is likely that these occurrences increase the susceptibility to develop other pathologies [45], [46].

The release of heme in circulation also affects the integrity of the blood brain barrier (BBB) (Fig.4) [45], as enhancing the sensibility of the brain to external insults by disrupting endothelial cells' adhesion. The infiltration of immune cells from the periphery into the brain activates microglia, which release pro-inflammatory molecules and cause neuroinflammation. The reduced effectiveness of these cells during aging, in terms of patrolling, reparative and phagocytic capacity, is combined to the increased susceptibility of aged brains to neuronal pathologies [47]. Microhemorrhages increase the risk for developing neurodegenerative diseases of up to 3-fold [40][47]. Combined to the decreased effectiveness of detoxifying mechanisms, occurring during aging, this can be a leading cause for tissue malfunctioning, oxidative stress and neuroinflammation [48].

Although, during aging, the accumulation of Heme and, subsequently, of Fe in the CNS has been correlated with the occurrence of neurodegenerative diseases, it is still not known whether cause or consequence of specific brain pathologies [49], [50].

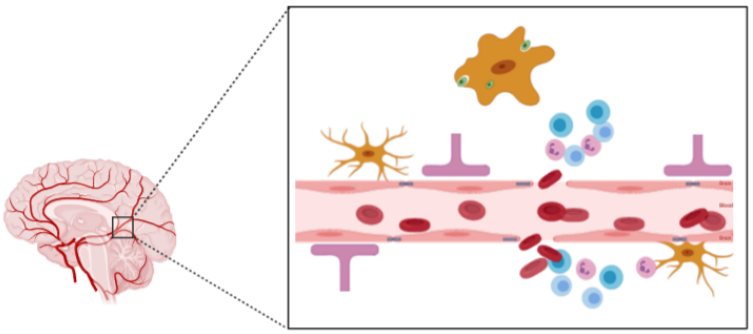

Fig. 4- BBB disruption. BBB disruption during aging leads to the accumulation of Heme/Fe in the brain, which can be highly cytotoxic and increase neuroinflammation. The infiltration of immune cells also contributes to this phenomenon.

CHAPTER 3

3.1 THE INFLAMMATORY SIDE OF HEME

Inflammation is a defense mechanism, elicited in response to disturbances, like injury, infection, trauma, etc. It can be acute, if the damage is coped in a short period of time, or chronic, if requiring the activation of complex defense mechanisms. This might contribute to cause neuroinflammation [51][52], meaning that beneficial effects of inflammatory responses, elicited to reestablish cell homeostasis and protect against specific insults, is associated with costs that might harm the brain and contribute to the development of

neurodegenerative pathologies [48][53]. Neuroinflammatory responses increase with advancing age, also in view of damaged proteins' accumulation, increased oxidative stress, disrupted energy homeostasis, etc. which physiologically occur in elderly brain [54], [55].

The main cells, responsible for the development of neuroinflammatory phenotypes, are resident brain immune cells. These were firstly described by Ramon y Cajal, in 1913, and named microglia [56], [57]. Like peripheral macrophages, microglia are capable to phagocytose foreigner bodies and death cells, thus acting as antigen-presenting cells (APC) and producing inflammatory mediators [58].

The origins of microglia have been the object of several controversies. At first, from mouse experiments, it seemed they derive from a monocytic bone marrow precursor. However, it was discovered that the origin of microglia are hematopoietic stem cells (HSCs), present in the embryonic yolk sac and migrating to the brain at embryonic day 9.5 (E9.5). Persisting during adulthood and self-renewing [56], [58]–[64] microglia possesses a unique set of markers that differentiate these cells from peripheral macrophages, mentioning TMEM119 as an example [60]. Under physiological conditions, microglia support CNS development and function. They have a ramified morphology, are highly motile and sense the environment, eliminating non-active neurons through their phagocytic activity [63], [65]. Microglia are capable to control neuron synaptic plasticity, survival, and proliferation (Fig.5) [58], [66]. Upon activation, they can act as pro- or anti-inflammatory cells, according to their ability to switch towards a M1 and M2 phenotype (Fig.5) [58] [63] [67] [68].

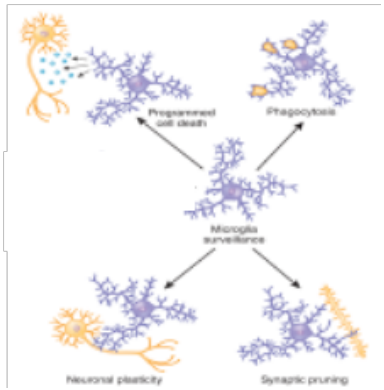

Fig. 5- Microglia: the immune cell of the brain. Resting microglia surveil the environment, with their extended processes. On the contrary, ramified and activated microglia contribute to neuroinflammation, as illustrated herein (Adapted from Salter & Stevens, 2017; doi:10.1038/nm.4397).

Microglia recognize both endogenous and exogenous insults, through the expression of pattern recognition receptors (PRRs). The sub-families of PRRs includes: specific toll-like receptors (TLRs), NOD-like receptors (NLR), C type lectin receptors (CLRs), triggering receptor expressed on myeloid cells (TREMs), RIG-like receptors (RLRs), etc. [69][70]. However, microglia activation by TLRs and NLRs are, to date, the most characterized [69]. These receptors bind to pathogen-associated molecular patterns (PAMPs) or DAMPs, thus initiating proper cellular defense response [68].

TLRs are broadly expressed in the CNS, since besides microglia, are also present in astrocytes [71], neurons, oligodendrocytes and neural stem cells (NSC). In humans, microglia express TLR1, TLR2, TLR3, TLR4, TLR5, TLR7, TLR8, TLR9 and co-receptor CD14 TLR [69][72]. TLR activation occurs in a myeloid differentiation factor 88 (MyD88)- or TIR-domain containing adapter-inducing interferon-γ (TRIF)-dependent pathway [73].

MyD88 is recruited through TIR-TIR domain interactions. This activates IL-1R-associated kinases (IRAK), which signals through TRAF6 and catalyzes the formation of a complex that phosphorylates IκBα. This leads to IκBα degradation and the nuclear translocation of NF-κB, which causes the transcription of inflammatory mediators.

Through the activation of TRAF3, the TRIF signaling pathway activates interferon regulatory factor-3 (IRF3) and IRF7, which triggers the production of type I interferons and leads to anti-viral immunity [73]. To note that TLRs can also drive the NLRs to produce pro-inflammatory mediators [69] NLRs respond to pathogens and cellular stress through their C-terminal leucine-rich repeats (LRRs). They form a large multiprotein complex by self-oligomerization at their central NACHT domain. When activated, NLRs respond by binding through homotypic interactions at N-terminal domains, typically at pyrin or CARD domain. This activates NF-kB through the NODosome pathway or caspase-1 through inflammasome activation [74].

Inflammatory microglia release cytokines among which TNF-α, IL-6, IL-1β and reactive oxygen species (ROS). Their anti-inflammatory phenotype is characterized by the secretion of IL-4, IL-10, IL-13 and TGFβ, among others, which aid to repair injuries by clearing debris and promoting neuronal survival (Fig.6) [75], [76].

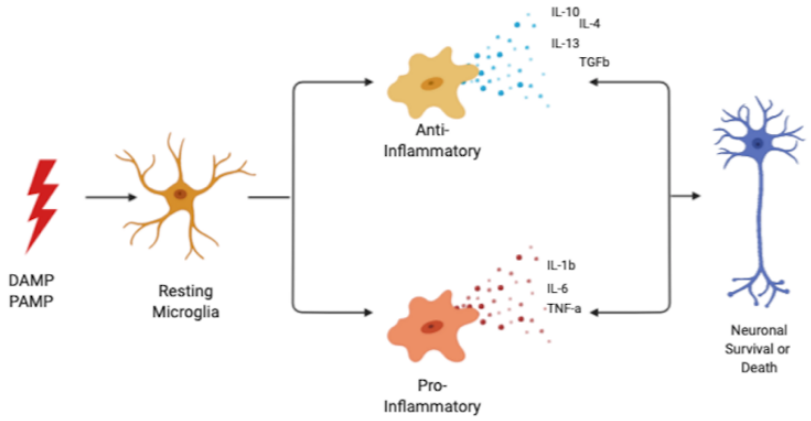

Fig. 6- Microglia polarization. Upon activation, microglia acquire a round morphology, becoming pro- or anti- inflammatory.

In case of disturbances, microglia rapidly migrate to the injured site, to resolve the damage and restore tissue homeostasis. If microglia activation persists overtime, sustained neuroinflammation occurs as well as neuronal loss [75], [77]. A variety of receptors regulate microglia function, including those responsible for microglia-neuronal communication, environmental sensing and interaction [78], [79]. Most molecules used by neurons to modulate microglial activation bind to “On/Off” types of receptors, capable to induce alert signals according to the level of expression. An example of "Off" receptor is CD200, which belongs to the immunoglobulin family [80]. When binding to neuronal produced CD200L, microglia are maintained in a steady and inactivated state. In the absence of this ligand, the number of microglia increases and these cells become activated [58], [60], [81]. Similarly, CX3CL1 is released by neurons and binds to microglia receptor CX3CR1, an interaction regulating microglia motility and synaptic plasticity [58][81]. The release of regulatory membrane glycoprotein SIRPα by

neurons and its binding to $CD47^+$ microglia decreases cytokine secretion and microglia-induced pro-inflammatory response [60]. Microglia-driven inflammation is also modulated when TREM2, an activating phospholipid-binding receptor exclusively expressed on these cells, forms a complex with TYROBP also known as DAP12, to strengthen their phagocytic activity or with, to favor the production of an anti-inflammatory response [60],[81],[82].

It is worth to mention that the neuronal-microglia communication is a bi-directional interaction, which regulates the function of both cells. Importantly, the contact that microglia establish with neurons' dendrite spines occurs not only during early development but is maintained throughout adulthood, aiding to control both their number and size [58][82].

3.3 HEME AND MICROGLIA POLARIZATION

From a metabolical point of view, the brain is the most active organ, as justified by the high demand for Heme/Fe used for energy production. However, the accumulation of this metal during aging [3], [83], turns microglia Heme/Fe-loaded and cause their switch towards a pro-inflammatory phenotype. When microglia are activated, they release pro-inflammatory cytokines, like IL-1β, IL-6 and TNF-α, besides expressing the histocompatibility complex (MHC) II markers on their surface. This indicates that Heme promotes microglia polarization, enhances neuroinflammation and sustains neuronal loss (Fig.7) [48], [75], [84].

Despite the mechanism through which Heme activates microglia is not totally elucidated, it is plausible to hypothesize that it enters cells through TLR-4. The activation of the MyD88 signaling pathway then result in the transcription of pro-inflammatory

cytokines via the nuclear factor kappa (NF-κB) transcription factor. This leads to M1 microglia polarization, as demonstrated by the induction of TLR-4 caused by the oxidative form of hemoglobin, i.e. metHb [85][86]. Interestingly, *in vivo* and *in vitro* studies showed that a decreased TLR-4 expression diminishes microglia activation and neuroinflammation by also reducing inflammatory cytokine production [48], [87].

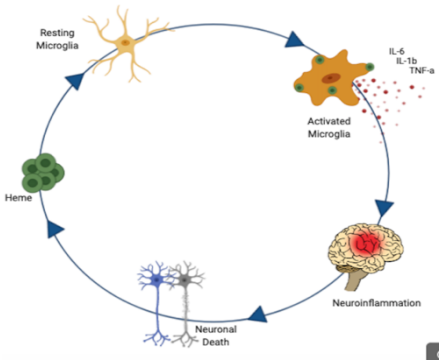

Fig. 7- Heme primes microglia toward a pro-inflammatory state. This cause neuroinflammation and neuronal loss.

CHAPTER 4

4.1 THE CYTOTOXIC EFFECT OF HEME

Heme cytotoxicity is also due to its pro-oxidant effect, which generates oxidative stress and promote ROS-driven cell death. This means that heme metabolism needs to be tightly controlled, maintaining a strict balance between its synthesis and degradation. When disturbances occur, the accumulation of Fe, resulting from heme catabolism by HOs, promotes the generation of highly reactive hydroxyl radicals through the Fenton reaction [32]. Thus, anti-

oxidant treatments are capable to confer cytoprotection against Heme [2].

In the brain, its cytotoxicity [81], [88], [89] might lead to different types of cell death. While astrocytes are reported to undergo Heme-mediated necrosis [1], the same molecule mainly induce apoptosis in microglia [88] and brain vascular endothelial cells [1]. As for neurons, Heme is likely to induce different kind of cell death-osis according to its accumulation [90].

4.2 THE INFLAMMATORY EFFECT OF HEME

The oxidative stress caused by excess Heme increases, in the brain, with advancing age, also due to a diminished expression of antioxidant proteins. Its cytotoxicity and pro-oxidant effects impair neuronal functions, and Fe, contained within the protoporphyrin ring, is the real responsible for Heme-mediated harmful effects [32].

Fe is abundant and fundamental to most organisms. In the brain, it participates in biological processes, as ensuring mitochondrial respiration, myelin production, DNA replication, neurotransmitter synthesis, oxygen transport, etc. [91]. Fe is also used as co-factor for the enzymatic activity of neurotransmitter production, like Tyrosine-Hydroxylase (TH), which is responsible for dopamine synthesis [92]. Thus, maintaining Fe homeostasis is fundamental especially during aging when protective mechanisms seem to physiologically fail. While this could explain the increase in iron-neutralizing and storing proteins, like ferritin or neuromelanin, their levels are often not enough [91]. This turns regions that are already richer in iron, like basal ganglia, as potentially sensitive to neuronal damage [92]. This is the reason for which iron is considered

the leading cause of neuronal death, as underlying the pathogenesis of neurodegenerative diseases, like Parkinson's Disease (PD).

The implication of Fe in PD was firstly introduced by McGeer and colleagues, reporting abnormal Fe concentration in *post-mortem* brain samples of PD patients [48]. By then, the association between brain Fe overload and neuroinflammation was already established, in view of the oxidative stress observed in microglia [91]. This notion was then supported by the decreased activity of mitochondrial complex I and reduced glutathione (GSH) in PD patients, due to the increase expression of iron proteins. This aided to further confirm that disruption of Fe metabolism plays a crucial role in in PD development [50][91][93][94]. Later, it was proven that Fe accumulation enhanced cytokine release, exacerbating neuroinflammation in *post-mortem* samples of PD affected individuals [95]–[97].

Concluding, impaired Heme/Fe metabolism compromises brain function [32], impairing mitochondrial activity, affecting axonal myelination, promoting neurite fragmentation and disrupting dendritic microtubule, all effects leading to neuronal loss [40][98].

However, it is worth to mention that also heme deficiency affects neuronal survival, since neurons need Fe for their metabolic function [3].

CHAPTER 5

5 PARKINSON'S DISEASE

5.1 PATHOGENISIS AND SYMPTOMATHOLOGY

PD is the second most common neurodegenerative disorder, after Alzheimer's disease (AD) [99], and affects about 2-3% of the elderly population (60-80 years old). This number is estimated to double until 2030, as increasing life expectancy enhances the incidence of this neurodegenerative disease. It is important to mention that men are more susceptible than women, also in terms of disease severity [49].

Histologically, PD is characterized by the depigmentation of the Substantia Nigra (SN) of the brain, indicating the progressive loss of dopaminergic neurons (DN). Abnormal aggregation of alpha-synuclein (α-syn) in the brain, known as Lewy bodies, is also a hallmark of this disease ([99][100].

Clinically, PD patients manifest motor and non-motor symptoms. Among motor symptoms: bradykinesia, resting tremor, rigidity, postural instability stands out. Non-motor symptoms include cognitive decline, anxiety, sleep disturbance, depression, dysautonomia and anosmia [101]. Other features like hypomimia, hypophonia, dysphagia, vision changes and gait freezing are also PD features [49], [101].

PD has a genetic or sporadic origin. However, only 5 - 10% of all PD cases are due to genetic mutations and in this case the pathology is manifested early in life [100]. Mutations in genes as SNCA, PINK-1, PARKIN, LRRK2, DJ-1 have been reported [102]. Yet, in most cases, PD is an idiopathic and multifactorial neuropathology, characterized by a neuroinflammatory phenotype and neuronal loss caused by mitochondrial impairment, proteasomal dysfunction, Fe accumulation, and oxidative stress [101][103]. Hence, to better understand the interaction between the different mechanisms involved might aid to develop new therapeutic strategies against this disorder.

5.2 HEME AND ALPHA-SYNUCLEIN AGGREGATION

Heme/Fe increases in the brain during aging, and this leads to generation of oxidative stress, causing DN loss, as already mentioned. The accumulation of Heme/Fe in the brain was found to promote α-syn aggregation, an effect enhancing PD progression [104][105].

α-Syn is a protein of 140 amino acids, with a not fully elucidated function. Its expression in neurons was shown to regulate the dynamics of synaptic vesicles. α-syn was also described as involved in intracellular trafficking, playing a role of chaperone, when monomeric [100]. However, when forming large insoluble fibrils, it becomes cytotoxic and causes cell death [100], [106], [107].

Heme/Fe fosters α-syn aggregation [108] by inducing conformational changes to generate β-sheet forming fibrils [104], an effect also observed by different oxidants [109]. Treatments with Fe chelators confirm that this metal can cause α-syn aggregation, as shown to also decrease α-syn mRNA level [110]. In addition, Fe was found capable to regulate α-syn expression at post-transcriptional level [111], increasing translation and facilitating secretion, a phenomenon able to impair neuronal survival [112]. It is important to mention that the ferrireductase activity of α-syn leads to the reduction of Fe^{3+} into Fe^{2+}, in the presence of copper (Cu^{2+}) [104]. This further enhances Fe-driven α-syn aggregation, creating a positive feedback loop that activates microglia and triggers neuroinflammation [113], [114].

CHAPTER 6

6 NEURONAL DEATH

6.1 APOPTOSIS IN PARKINSON'S DISEASE

Dysfunctional neurons die physiologically. However, patients developing neurodegenerative diseases, like PD, present DNs loss, as the main reason for the symptomatology previously described.

Among the different types of cell death neurons undergo to, apoptosis is the most studied. Apoptosis is a programed cell death (PCD), firstly described by Kerr et al., in 1972 [115], characterized by specific morphological changes [116]. These include cell shrinkage, membrane blebbing, nuclear fragmentation, DNA cleavage and chromatin condensation [117]–[119]. Biochemical alterations start with the externalization of the phosphatidylserine, which represents an "alert" signal for recognition by cleaning immune cells 117]–[119.

Apoptosis is a complex machinery that can be initiated by two distinct pathways, the extrinsic and intrinsic cell death signaling. The extrinsic pathway is mediated by death receptors, as TNF, Fas-L and TNF related apoptosis-inducing ligand (TRAIL). The formation of a death-inducing signaling complex (DISC) [120] activates initiator caspase-8, a proteolytic enzyme responsible for the activation of the executioner caspase-3. The intrinsic apoptotic signaling is regulated at mitochondrial level [95]. Once cleaved by initiator caspase-8, the BCL-2 homology (BH3)-interacting domain death agonist (BID) migrates to the mitochondria and activates the pro-apoptotic pore-forming proteins BCL-2-associated X protein (BAX) or BCL-2 antagonist/killer (BAK), located at the surface of this organelle. This

leads to the release of cytochrome *c*, which forms a multi-protein complex, known as apoptosome, with the apoptotic protease-activating factor 1 (APAF-1) and pro-caspase-9. The subsequent activation of caspase-9, leads to a caspase 3-driven cell death [121], [117], [122].

During apoptosis, the integrity of the cellular membrane is maintained. Upon degradation of intracellular structures by effector caspases, these are released in small extracellular vesicles and phagocytosed by immune cells, without affecting neighboring cells or generating inflammatory responses [96], [118]. Although the presence of apoptotic neurons has been shown in post-mortem brain of PD patients [97], [123], different types of cell deaths are also observed. This occurs also in the brain of experimental animal models, where neurotoxin 1-methyl-4-phenylpyridinium (MPP+) and 6-hydroxydopamine (6-OHDA) were used to induce pharmacological PD. Indeed, higher doses of these compounds were showed to elicit neuronal necroptosis [96].

6.2 NECROPTOSIS IN PARKINSON'S DISEASE

Necroptosis is a regulated necrosis, a cell death pathway discovered to share many features with the activation of the apoptotic machinery. Necroptosis can be initiated by death receptors (DRs), like tumor necrosis factor receptor 1 (TNFR1), Fas, TRAIL, etc. However, it can also be triggered by inflammatory molecules binding TLRs [124]. In caspase-inhibiting conditions, the interaction between TNF and its receptor leads to the activation of the Receptor-Interacting Protein Kinase 1 (RIPK1), which recruits and auto-phosphorylates RIPK3, through interaction with RHIM domain, forming the necrosome [125]–[127]. The oligomerization of RIPK3

activates the Mixed lineage Kinase-Like Protein (MLKL), which translocate to the plasma membrane, where it forms pores lysing the cell. Contrarily to apoptosis, this process induces a strong pro-inflammatory response, since the intracellular content is released in the surrounding environment [128].

The involvement of necroptosis in PD has been described in the recent years. *In vitro* studies showed that 6-OHDA increases necroptosis markers, as RIPK1, RIPK3 and MLKL, in cortical neurons. This effect is inhibited pharmacologically, by specific necroptosis inhibitors, known as necrostatins (Nec). In particular, Nec-1 significantly decreases this type of cell death, preventing neurite degeneration. The role of necroptosis in PD-driven neuronal loss was also determined analyzing post-mortem samples of PD patients. Increased levels of MLKL phosphorylation were found in DNs, by histological assessment [124]. This observation was also confirmed in experimental animal models, showing upregulation of RIPK3 [129]. Again, the pharmacological inhibition of necroptosis in PD mice, using Nec-1, was found to be effective in significantly decreasing RIPK3 and protecting neuronal death [124].

6.3 FERROPTOSIS IN PARKINSON'S DISEASE

Ferroptosis is a non-apoptotic and Fe-dependent regulated form of cell death [107][130][131], characterized morphologically by mitochondria shrinkage, increased membrane density, cytoplasmic swelling and disappearance of mitochondrial cristae [132] [133].

The oxidation of polyunsaturated fatty acid (PUFA)-containing phospholipids, the availability of redox-active Fe and the loss of lipid peroxide clearance mechanism by glutathione peroxidase 4 (GPX4) are typical features of this cell death [131].

The role of PUFAs in ferroptosis was demonstrated through a loss of function approach, showing that deletion of acyl-CoA synthetase long-chain family member-4 (ACSL4) and lysophosphatidylcholine acyltransferase-3 (LPCAT3), essential for PUFAs activation and incorporation into phospholipid membranes, inhibits ferroptosis [131].

Fe or Fe-containing lipoxygenase enzyme leads to PUFAs oxidation and ROS generation. The use of Fe chelators further proved the involvement of this metal in this programmed cell death, in addition to the modulation of Fe-dependent genes, as shown to downregulate Fe-uptake receptor gene, i.e. Transferrin receptor (TfR) [131].

GPX4 is a selenoprotein that converts glutathione (GSH) into oxidized glutathione (GSSG), thus allowing to reduce the cytotoxic lipid peroxides (L-OOH) to the corresponding alcohols (L-OH). It is essential for normal mammalian development, since its deletion was shown to be lethal in mice [131], [134].

The use of ferroptosis inducers, like Erastin and Ras-selective lethal small molecule 3 (RSL-3), allowed to better understand the molecular mechanisms underlying this cell death [132][133]. The same for inhibitor compounds, which include Ferrostatins. Although their ability to prevent ferroptosis is highly significant, it is important to also refer liproxstatins (LIP-1), α-tocopherol, iron chelators deferiprone (DFN), deferoxamine (DFO) and ciclopirox as potent ferroptosis inhibitors [107].

Despite that the physiological role of Ferroptosis remains to be elucidated, this cell death was already observed in neurodegenerative disease, like PD [135], where lipid peroxidation is a main feature [136]. *In vivo* studies demonstrated that ferrostatin treatment prevents the severity of MPTP-induced PD, rescuing DNs

and motor dysfunction [137]. The involvement of ferroptosis in this pathology was also observed by the increase of GPX4 expression in the cerebrospinal fluid (CSF) of PD patients under iron chelator therapy, as DFN, which also ameliorates their motor impairment [138].

CHAPTER 7

7 THERAPEUTIC APPROACHES IN PARKINSON'S DISEASE

For being a multifactorial neurodegenerative disorder, it is still a challenge to develop a therapeutic approach that can prevent and/or fully retard PD symptoms.

The common treatment is dopamine restoring therapy, which aims to increase dopamine levels seeking to improve motor deficits.

7.1 DOPAMINE MODULATORS

7.1.1 DOPAMINE PRECURSORS

The first treatment used against PD was considered a breakthrough in defeating this pathology. It was named as levodopa (3,4-dihydroxy-l-phenylalanine), also known as L-Dopa. It was developed by Birkmayer and Hornykiewicz in 1967 [139]. It is a dopamine precursor, which in the brain is biosynthetically transformed to dopamine by the action of aromatic L-amino acid decarboxylase (AADC). By replenishing dopamine pool, L-Dopa alleviates PD symptoms without restoring DN loss, which leads its effectiveness to decrease overtime. Side effects [140], like "on-off"

periods of motor fluctuation, L-Dopa-induced dyskinesia (LID), impulse control disorder, sleepiness and dopamine dysregulation were observed after long treatment [139]. Often combined with carbidopa, to lessen the systemic metabolism of L-DOPA and increase central exposure, this association allows to lower the doses of dopamine precursors and to maintain longer efficacy [141].

7.1.2 DOPAMINE AGONISTS

Dopamine agonists are chemical compounds that recognize and bind to dopamine receptors, in the absence of the endogenous neurotransmitter. Dopamine agonist receptors (DARs) are predominantly expressed in the brain, although not restricted to [142]. Two families of DARs have been identified so far. D_1-like receptor family members comprise D_1 and D_5 receptors, while D_2-like includes D_2, D_3 and D_4 receptors [141]. Among the five receptors of D_1-like family members, D_1 is the most abundant in the CNS, followed by D_2, D_3, D_5 and D_4. D_1 and D_5 receptors are highly expressed in the striatum, nucleus accumbens, olfactory bulb, and SN. D_2, D_3 and D_4 receptors are expressed in the striatum, mesencephalon, external globus pallidus, hippocampus, basomedial amygdaloid nucleus, and cerebral cortex [143][142].

Dopamine agonists are divided in two groups, ergoline- and non-ergoline-derived compounds. Ergoline is a chemical compound found in a variety of alkaloids and firstly characterized in the fungus *Claviceps purpurea*, ergot [144]. Ergoline-based molecules are the first generation of dopamine agonists. Their use is associated though with an increased risk of developing peritoneal, pulmonary, and cardiac/valvular fibrosis. Drugs belonging to this group are:

bromocriptine, cabergoline, pergolide, and lisuride [145]. However, due to their side effects are rarely used [142].

Non-ergoline-derived agonists cause less collateral damages and include compounds like: pramipexole, ropinirole, rotigotine, piribedil, and apomorphine [142].

Ergot derivatives stimulate both D_1-like and D_2-like receptors, while non-ergot derivatives stimulate only D_2-like family members [146]

It is worth to mention that dopamine agonists are not as potent as L-dopa, although often prescribed in combination to decrease doses and side effects.

7.1.3 MONOAMINE OXIDASE B (MAO-B) INHIBITORS

MAO are flavin adenine dinucleotide (FAD) co-factor-dependent enzymes, responsible for the oxidation of endogenous and xenobiotic monoamine. MAO exists in two isoforms, MAO-A and MAO-B [147], both metabolizing substrates like dopamine, adrenaline, and noradrenaline. While MAO-A presents a higher affinity for serotonin, dopamine is the substrate of MAO-B [148]. MAO-B is produced by glial cells and is largely expressed in the *substantia nigra* [149]. Increased MAO-B activity was associated with the loss of dopamine in the brain. Thus, MAO-B inhibitors were shown to enhance L-Dopa effect [150].

Among the most used compounds belonging to this family, there are Selegiline (N-Propargyl-methamphetamine) and Rasagiline [141], with the first being a selective and irreversible MAO-B inhibitor [149]. Selegiline monotherapy provides neuroprotection and reduces motor fluctuations. The combination of Selengiline with vitamin E also showed promising results, improving

the Unified Parkinson's Disease Rating Scale (UPDRS) score after three months. UPDRS score is used to measure the severity and to follow the progression of PD. The scale is divided in four sections: Part I- mention, mood and behavior, Part II- activities of daily living; Part III- motor examination; Part IV- therapy complications. Each subscale varies from 0-4, where 0 means normal, 1- slight, 2- mild 3- moderate and 4- severe [151].

7.2 ANTI-INFLAMMATORY COMPOUNDS

It is known that neuroinflammation plays an important role in PD. Exacerbated microglia activation induces neuronal damage by secreting pro-inflammatory compounds [152]. Hence, anti-inflammatory drugs could be promising, if combined to current therapies.

7.2.1 DEXAMETHASONE (DXM)

DMX is a potent anti-inflammatory agent, preventing the synthesis of enzymes involved in cyclogenase-2 (COX-2) and phospholipase A2 signaling pathways [153]. In MPTP-induced mice, DMX was shown to modulate microglia activation, decreasing cytokine and nitric oxide (NO) production. It was also observed to prevent catecholamine depletion and TH decrease as well as the infiltration of peripheral immune cells into the brain. Thus, DMX exerts its neuroprotective effect by diminishing microglia pro-inflammatory status [140][153].

Non-steroidal anti-inflammatory drugs (NSAIDs) are commonly used as analgesics and antipyretics. NSAIDs, as aspirin (acetylsalicylic acid), ibuprofen and indomethacin, inhibit COX-2

activity by blocking the synthesis of pro-inflammatory mediators via NF-kB activation. These drugs are also capable to activate the anti-inflammatory peroxisome proliferator-activated receptor γ (PPARSγ) pathway, reducing microglia activation by also acting as ROS and NOS scavenger [154], [155]. While Ibuprofen was shown to protect DNs increasing TH positive cells [156][157], aspirin was shown to inhibit COX-1, by acetylating the active site of this enzymes and producing salicylic acid (SA). Its neuroprotective effect, as ROS scavenger, was demonstrated in a pharmacological PD mouse model, where the antioxidant action of SA prevents dopamine depletion. Pre-treatment with SA improved the motor activity of PD-induced mice [156]. Also, indomethacin was shown to protect DNs in PD mice, decreasing microglial activation and peripheral immune cell infiltration into the brain parenchyma. Although these anti-inflammatory drugs presented clear effects in reducing neuroinflammation, its positive action was observed only in mice, more studies are needed to investigate theirs effects in PD patients, probably as a complementary treatment [156].

7.2.2 MINOCYCLINE

Minocycline is a second-generation tetracycline analog, with lipophilic properties that allow this compound to cross the BBB [154]. In PD mice, Minocycline presents anti-inflammatory, neuroprotective, antimicrobial, anti-apoptotic, and antioxidant roles in the brain. It decreases the production of cytokines, chemokines and lipid mediators of inflammation, reducing microglia activation and neuroinflammatory-driven damage [158]. However, despite neuroprotective in PD animal models, clinical studies failed to show beneficial effects in PD patients [158] [159].

7.3 ANTIOXIDANTS

As mentioned in previous chapters, the brain is prone to accumulate Fe during aging, which then contributes to neurodegeneration. The ability of Fe to catalyze ROS production, exacerbated also as a consequence of dopamine synthesis and catabolism, boosts oxidative stress and neuronal loss [160]. Thus, antioxidants might constitute a potential therapy for PD, in view of their ability to protect against different types of cell death. Among those, α-tocopherol (vitamin E), Coenzyme Q10 (CoQ10), Mitoquinone (MitoQ), N-acetylcysteine (NAC) have been investigated as therapeutic approach [160].

7.3.1 NAC

N-Acetylcysteine (NAC) is a GSH precursor [177]. It is the acetylated form of the amino acid residue, L-cysteine, which is susceptible to undergo a rapid oxidation and generate an inactive disulfide [177]. NAC is a membrane-permeable cysteine precursor, which does not require active transport to enter cells. Once diffusing through the cell membrane, NAC is rapidly hydrolyzed to release a GSH precursor, cysteine [179], this being the limiting rate for GSH synthesis [179]. NAC supplementation increases cysteine/GSH concentration in cells, which then is capable to scavenge free radicals, promote neurogenesis and aid mitochondrial function [181]. NAC is likely to regulate dopamine release by modulating the cellular redox status, via the antioxidant effects of GSH and L-cysteine. Dopamine *per se* is a potent pro-oxidant, as capable to generate free radicals by auto-oxidation [183], [184]. Pre-clinical studies showed that NAC increases the level of GSH in mouse brains, while reducing

oxidative damage and enhancing synaptic connections [180]. In PD-induced mice, NAC significantly protects dopaminergic terminals [185]. This finding was also supported by *in vitro* experiments, conducted in human neuronal cells, where NAC was found to prevent membrane depolarization caused by oxidative stress [186], [187]. A randomized study with 42 PD patients showed that NAC treatment increases dopamine transport in the caudate and putamen regions, improving PD symptoms [188].

7.3.2 COENZYME Q10

CoQ10, also known as ubiquinone, is an important constituent of the mitochondria electron transport chain. Its main function is to generate cellular energy [160] [161] by converting carbohydrates, lipids, and proteins into ATP. The reduced form, ubiquinol (CoQH2), is a potent antioxidant [162]. PD patients presented significantly lower levels of CoQ10 in the mitochondria. Thus, when tested, the administration of CoQ10 in pre-clinical PD animal models significantly prevents DN loss [163]. The combination of CoQ10 and creatine, which also functions an antioxidant, exhibited a significant neuroprotective effect in chronic PD-induced mice [164], thus constituting a potential treatment against PD [163]. *In vitro* and *in vivo* studies showed that creatine is already neuroprotective against DNs loss by 6-OHDA and MPTP treatment. Since Vit E is capable to enhance CoQ10 antioxidant effect, it was also tested on pre-clinical models. However, so far, it showed to be inefficient to retard PD progression [164] [165], possibly due to its inability to cross the BBB [160].

7.3.3 MITOQUINONE

MitoQ is the active antioxidant moiety of CoQ10 [166]. It was reported to be highly effective against mitochondrial-driven oxidative stress and demonstrated neuroprotective effects by scavenging peroxynitrite, and superoxide. Protecting mitochondria against lipid peroxidation [167], it was tested in a PD clinical trial, where it was shown uncapable to retard disease progression [160].

7.3.4 VITAMIN E

Vit E is a fat-soluble vitamin with high antioxidant properties. It acts as a scavenger of peroxyl radical, peroxynitrite, and hydroxyl radical, being capable to inhibit lipid peroxidation [164]. Vit E was the first drug to be considered for the treatment for PD [168]. Although several studies have been conducted, to uncover its role as possible therapy, the conclusions are contradictory. Pre-clinical PD model showed that Vit E supplementation is effective in ameliorating PD progression [169]. Using *PINK1*$^{-/-}$ mice, the administration of Vit E fully restore corticostriatal synaptic plasticity, reducing PD severity [170]. However, further studies are required to understand the effectiveness of Vit E administration in humans. In fact, clinical trial combining Vit E and selegiline showed no improvement in patients in early stages of PD [171].

7.4 IRON CHELATORS

7.4.1 DEFEROXAMINE (DFO)

DFO is one of the first Fe chelators used in clinical practice, to treat iron-overload related diseases [189]. For decades, it was the

only available treatment [190]. DFO is a multifunctional therapeutic drug, since capable to chelate, detoxifying non-transferrin-bound Fe (NTBI), and scavenge free radicals and hemeprotein by ferryl reduction. Thus, DFO is a reducing agent, which prevents membrane lipids oxidation by removing high-oxidation states of Heme/Fe, as in ferryl myoglobin (Mb) or Hb [191]. DFO was shown to be effective in hematologic diseases, characterized by Fe overload, like β-thalassemia major, sickle cell disease (SCD) and myelodysplasia. One of the limitations of DFO treatment relies on the fact that is not orally absorbed [189], [192]. This means that it needs to be administered parenterally, for 8 to 12 hours, as nightly infusions, from five to seven days/week [193], resulting in patient non-compliance. This leaded to the development of a new compound, which is orally active [189]. In PD, DFO significantly decreases Fe deposition in the SN, known to exacerbate DNs loss and cause motor impairment, in PD-induced mice models. Since DFO does not cross the BBB, it raises the hypothesis that a peripheral Fe chelation might already confer protection against the development of Fe toxicity in the brain [194]. When administered intranasally, DFO was also proven to improve motor disabilities, decreasing DNs loss, in PD mice [195]–[197].

7.4.2 DEFERIPRONE (DFP)

DFP (3-hydroxy-1,2-dimethylpyridin-4-one) is a water-soluble Fe chelator synthesized in the 1980s with the intent to substitute DFO [172]. DFP is orally administrated and peaks in circulation 45 minutes after administration. Its absorption can be

delayed by food [173]. DFP is quickly eliminated in urine, as presenting a half-life of approximately 2 hours [172]. The affinity of DFP for Fe is in a 3:1 ratio [172] [173]. Although effective in excess Fe removal, side effects, like agranulocytosis, were observed [172][173].

Neuroprotective effect of DFP were proven in PD [172], [174], with the completion of four clinical trials, where shown to decrease Fe content in the SN, dentate and caudate nucleus, improve motor symptoms and reduce disease progression. Nevertheless, once the treatment was suspended, Fe accumulation reappeared [175].

7.5 NECROPTOSIS INHIBITORS

Several studies have associated necroptosis with PD [176] (Nec-1 is the main pharmacological inhibitor of necroptosis and was showed to reduce axonal degeneration [177]. Pre-clinical studies also demonstrated that the genetic deletion of RIPK3 in PD-induced mice affords protection against DNs loss [178]. In vitro, both pharmacologic or genetic inhibition of necroptosis revert cell death [179] and DNs loss. In $RIP3^{-/-}$ and $MLKL^{-/-}$ PD-induced mice, lower pro-inflammatory cytokine release was observed during disease progression [180]. In addition, mesencephalic neuronal degeneration in PD-induced mice, which is characterized by fragmentation and neurite beading, was shown to be fully abrogated by Nec-1 treatment [124].

7.6 FERROPTOSIS INHIBITORS

As mentioned, ferroptosis is one of the programmed cell deaths involved in PD, as the accumulation of Fe in the brain of PD

patients increases lipid peroxidation [181]. Whether ferroptosis inhibitors could be beneficial to PD treatment is still under investigation. However, Fer-1 was shown to increase TH-positive neurons and improve motor impairment in PD-induced mice. Moreover, *in vivo* and *ex-vivo* studies reveal that pharmacological and genetic inhibition of protein kinase C (PKC), an inducer of ferroptosis, can efficiently inhibit this pathway in dopamine precursor-derived neuronal cell line [137].

Many reports describe Fe accumulation, increased oxidative stress, lipid peroxidation [182], reduced levels of GSH and GPX4 in *post-mortem* PD patients brain tissue [136][183] and PD mice models [138], [184]. The use of Fe chelators, such as DFP and DFO, was also shown to counteract these events [138], [185], decreasing the level of labile Fe [186] and increasing the expression of GSH and GPX4 in different regions of the brain [138], [184], [187].

Similarly, antioxidants, such as NAC and vitamin E, were shown to confer protection against oxidative damage in neuronal cell lines and PD mice by repressing ferroptosis [137]. Therefore, the combination of Fe chelators and antioxidants might constitute a promising treatment to retard ferroptosis-driven PD progression [137].

AIMS

Heme/Fe accumulation and exacerbated inflammation has been described to occur in aged brains. Interestingly, this was also observed in the context of neurodegenerative diseases, including PD. Hence, in this project we aimed at understanding the role of Heme/Fe imbalance during aging, as underlying cause of PD. The work in this thesis was conducted to test the following hypotheses:

- Heme/Fe overload exacerbates inflammation by inducing infiltration of peripheral immune cells into the brain, causing microglia polarization towards a pro-inflammatory phenotype.
- Heme/Fe physiologically accumulates in the brain during aging, becoming per se a risk factor for neuroinflammation.
- Exogenous administration of Heme/Fe to aged mice aggravates their inflammatory profile and sensitize to neuronal damage.
- Alpha-synuclein (α- syn) is capable to protect against Heme-driven inflammatory profile.
- Heme/Fe accumulation is the leading cause of PD development.
- Fe chelators can be used to prevent Heme-driven neuroinflammation.

METHODS

1 ANIMALS

C57BL/6 mice were used for the study and purchased from the animal facility production of the Instituto Gulbenkian de Ciência (IGC), Oeiras, Portugal and Champalimaud Foundation Center of the Unknown (CFCU). Animal care and experimental procedures were conducted in accordance with Portuguese guidelines and regulations after approval by the respective local (IGC) and governmental committee (DGAV). Wild-type mice were used as experimental controls.

For primary microglia cell culture, brains from C57BL/6 at P1 to P3 were harvested. For flow cytometry analysis, young (8 to 12-week-old) and old mice (40 to 52 week-week-old) were used.

2 HEME TREATMENT IN VIVO

Mice were injected intraperitoneally (i.p.) with hemin (Sigma, Ref. No. H9039), 15mg/kg of body weight. Hemin was injected once a day for three days. On the fourth day animals were sacrificed with Carbon Dioxide (CO_2) and organs collected for processing.

3 DEFERIPRONE TREATMENT IN VIVO

Mice were injected intraperitoneally (i.p.) with DFN (Sigma, Ref. No. H9039), once a day, i.p., administered every other day 15mg/kg of body weight. Animals were sacrificed with Carbon Dioxide (CO_2) and organs collected for processing.

4 MPTP TREATMENT IN VIVO

Mice were injected intraperitoneally (i.p.) with (1-metil-4-fenil-1,2,3,6-tetraidropiridina (MPTP) (Sigma, Ref. No. M0896). Three doses of 15mg/kg of body weight were administered every 2 hours. After 30 days animals were sacrificed with Carbon Dioxide (CO_2) and organs collected for processing.

5 α-SYNUCLEIN TREATMENT IN VIVO

Mice were injected intravenously (i.v.) with the Pertussis (PTX) toxin (List Biological laboratories, INC, Ref. No. 181). One dose of 1.5μ/kg of body weight was administered per day, for 3 days. On the third day, animals were administered intranasally (i.n.), with 40μg/25g of body weight, once a day for five days. Purified α-Syn was kindly offered by Prof. Cláudio Gomes, working at BioISI, Faculty of Science, University of Lisbon. Animals were then administered hemin or not, as previously described. After 15 days, animals were sacrificed with Carbon Dioxide (CO_2) and the organs collected for processing.

6 IMMUNE CELL ANALYSIS BY FLOW CYTOMETRY

Brain, spleen, and blood were collected to assess inflammatory state by flow cytometry.

6.1 BRAIN ANALYSIS

After blood collection, mice were perfused with cold PBS 1X (Gibco, Ref. No. 100-10-56) before harvesting the organs. The brain was placed in a 6mm petri dish with 7 mL of collagenase VIII (0.2 mg/mL) (Sigma, Ref. No C2139-100MG) diluted in HBSS (Gibco, Ref. No. 14170-138) and then homogenized using two glass slides. The tissue was then incubated at 37ºC for 30 minutes. After this time, using a Pasteur pipette, cell suspension was transferred to a 50mL falcon through a 100µm strainer (Falcon, Ref. No. 352360) and PBS 1X was added until 20 mL to stop the enzymatic reaction. Cells were centrifuged at 1500 rpm for 12 min at 4ºC, and the supernatant was discarded. 10mL PBS 1X was again added and the cell suspension centrifuged at 1500 rpm for 12 min at 4ºC. The supernatant was newly discarded. The cell pellet was resuspended with 10 mL of Percoll 33.3% (GE Healthcare, Ref. No.17-0891-01) and the samples centrifuged at 2500 rpm for 22 min at 22ºC, with no acceleration and no brake. The supernatant was discarded and 30 mL of PBS 1X was added to the samples to wash off the Percoll. The cell suspension was centrifuged at 1500 rpm for 12 min at 4ºC. The supernatant was discarded. Cells were resuspended with 1mL of FACS buffer (PBS 1X with 2% heat inactivated FBS (Gibco, Ref. No. 10270-106) and centrifuged at 2000 rpm for 3 min at 4ºC. After this last wash, the samples were resuspended with 450µL of FACS buffer and plated for staining with antibodies.

6.2 BLOOD ANALYSIS

Blood was collected by cardiac puncture and placed in an Eppendorf tube with heparin (LEO Pharma A/S, Ref. No. 014425-03). The total volume of blood was marked on the respective

collection tube and the plasma was removed by centrifugation for 5 min at 1600G twice, at room temperature. The cell pellet was resuspended in RBCs lysis buffer (2x) (BioLegend, Ref. No. 420301) in a 1:1 proportion and left for 10 min at room temperature. Then, samples were centrifuged for 5 min at 1500rpm, at room temperature, and the supernatant was discarded. RBCs lysis was repeated twice, as described above. After the last centrifugation, cells were washed twice with FACS buffer and the pellet resuspended in the initial volume previously marked of FACS buffer.

6.3 SPLEEN ANALYSIS

In a 6mm petri dish, the spleen was smashed using a 100µm mesh (LINKER Industry- Technik, Ref. No. 11774539) in FACS buffer. The single cell suspension obtained was transferred to a 2mL Eppendorf tube. The cell suspension was centrifuged for 2 min at 2000 rpm, at room temperature. The supernatant was discarded. Pellet cells were resuspended with RBCs Lysis buffer (1X) and the samples were left for 10 min at room temperature. Samples were then centrifuged for 5 min at 1500rpm, at room temperature, and washed twice with FACS buffer. After the last wash, the supernatant was discarded, and the cells were resuspended in 2mL of FACS buffer.

7 CELLS COUNTING FOR FLOW CYTOMETRY ANALYSIS

For counting cells, 5uL from all cell suspensions were transferred to a counting mix containing FACS buffer, propidium iodide (PI - a viability dye) (Fluka) and reference beads with known concentration (Bangs Laboratories, SureCount^{TM}, Ref. No. CC10N). The counting mix was run in the BD FACSCanto II Flow

Cytometer (BD Bioscience) and the number of cells per µL was obtained based on the following equation:

$$\text{Cells } per\ \mu\text{L} = \frac{\text{Counted Cells x Volume Beads Added}}{Beads\ Counted\ x\ Volume\ Cells\ Added} \text{ x Beads Concentration}$$

8 ANTIBODIES

The aim of the experiments was to assess the level of inflammation upon different treatments, comparing distinct responses in young and old animals. To do so, antibody mixes for surface antigen were specifically designed to analyze and quantify immune cell populations, differentiating innate from adaptive subsets. To assess innate immune cells, "Granulocyte Mix" was used. This was composed by several antibodies that allowed to distinguish peripheral inflammatory cells from resident ones and measuring its activation. These were, APC/Cy7 anti-mouse CD45 Antibody (BioLegend, Ref. No. 103115), PE/Cy7 anti-mouse/human CD11b Antibody (BioLegend, Ref. No. 101216), FITC anti-mouse F4/80 Antibody (BioLegend, Ref. No. 123107), PerCP/C5.5 anti-mouse Ly-6C Antibody (BioLegend, Ref. No. 128012), APC anti-mouse Ly-6G Antibody (BioLegend, Ref. No. 127613), Pacific Blue anti-mouse MHC II Antibody (BioLegend, Ref. No. 107620), PE anti-mouse CCR2 Antibody (R&D SYSTEMS, Ref. No. FAB5538P), Zombie Aqua Fixable Viablity Kit™ (BioLegend, Ref. No. 423101). These cells were then stained with the Calcein Mix-1, designed to identify the accumulation of Iron in immune cells and which cells were more prone to carry this metal. This mix was composed by

PE/Cy7 anti-mouse/human CD11b Antibody, APC/Cy7 anti-mouse CD45 Antibody, APC anti-mouse Ly-6G Antibody, PE RAT anti-mouse GR-1 Antibody (BD Biosciences, Ref. No. 553128), Pacific Blue anti-mouse CD4 Antibody (BD Bioscience, Ref. No. 558107), Brilliant Violet 510 anti-mouse TCR β Antibody (BioLegend, Ref. No. 109233), Calcein AM Permeant Dye (ThermoFisher, R. No C1430).

To assess adaptive immune cells, "T Mix" and "Myeloid Mix" were used. These mixes were composed by several antibodies that allowed to identify and study the different leukocytes subtypes. T Mix contained antibodies identifying lymphocytic cells, as T and B leukocytes, and their activation. This mix was composed by Alexa Fluor 488 anti-mouse TCR β antibody (BioLegend, Ref No. 109216), PE/Cy7 anti-mouse CD62L Antibody (BioLegend, Ref. No. 104417), Brilliant Violet 510 anti-mouse CD19 Antibody (BioLegend, Ref. No. 115545), PE anti-mouse CD4 Antibody (BioLegend, Ref. No. 100408), APC/Cy7 anti-mouse CD8 Antibody (BioLegend, Ref. No. 100714), APC anti-mouse CD44 Antibody (BioLegend, Ref. No. 103012), APC/Cy7 anti-mouse CD45 Antibody.

For the Myeloid Mix, a set of antibodies were designed to distinguish peripheral from resident inflammatory cells, as well as their activation. The mix was constituted by, PE/Cy7 anti-mouse/human CD11b Antibody, APC/Cy7 anti-mouse CD45 Antibody, Pacific Blue anti-mouse MHC II Antibody, PE anti-mouse CCR2 Antibody, Brilliant Violet 510 anti-mouse TCR β Antibody, Brilliant Violet 510 anti-mouse CD19 Antibody, FITC anti-mouse Ly-6C Antibody (BD Biosciences, Ref. No. 553104). The Calcein Mix-2 was design with the same purpose as the Calcein Mix-1, although applied to a different antibody panel. It was composed by PE/Cy7 anti-mouse/human CD11b Antibody, APC/Cy7 anti-mouse CD45 Antibody, Brilliant Violet 510 anti-mouse CD19 Antibody, PE anti-

mouse TCR β chain Antibody (BioLegend, Ref No. 109208), APC anti-mouse NK1.1 chain Antibody (BD Biosciences, Ref No. 561117), Pacific Blue anti-mouse CD4 Antibody (BD Biosciences, Ref No. 558107). The dye used with Calcein Mix-1 and 2, T and Myeloid mix, to measure cell viability was propidium iodide (PI) (ThermoFisher, Cat No. P1304MP).

8.1 SURFACE STAINING

Cells were seeded in a round, non-coated 96-well-plate. Cells suspension from brain and blood were evenly divided for each staining. Cells derived for spleen were seeded at 10^6 cells/well. The plate was centrifuged at 2000 rpm for 2 minutes and the supernatant was removed. To cells, subsequently stained, Fc-block (BD Bioscience, Ref. No. 553141) was added, to block unspecific immunoglobulin binding. Incubation lasted 30 min, at 4ºC. The plate was then centrifuged at 2000 rpm for 2 minutes and the supernatant was removed. The respective antibodies mix was added, and the staining occurred at 4ºC, in the dark, for 45 minutes. After this period, FACS buffer was added to the wells and the plate was centrifuged for 2 min at 2000 rpm. Cells were washed twice with FACS buffer. For FACS data acquisition, stained cells were resuspended in FACS buffer and PI in a 1:1 proportion and collected in FACS tubes.

To cells stained with M and G Mix, PBS 1X was added to each well and the plate centrifuged at 2000 rpm for 2 minutes, twice. The viability dye, Zombie aqua, was added to each well and incubated for 15 minutes at room temperature. After this time, FACS buffer was added, and the plate centrifuged at 2000 rpm for 2 minutes. The supernatant was discarded. Cells were resuspended with Fc-block and incubated for 30 min, at 4ºC. The plate was

centrifuged at 2000 rpm for 2 minutes and the supernatant was removed. The respective antibodies mix was added, and the staining occurred at 4ºC, in the dark, for 45 minutes. After this period, FACS buffer was added to the wells and the plate was centrifuged for 2 min at 2000 rpm. Cells were washed two more times with FACS buffer.

For each organ and condition an unstained sample was used as a negative control and to set-up the acquisition parameters in BD FACSCanto II Flow Cytometer. Data analysis was performed using FlowJo software (version 7, Tree Star Inc.) and GraphPad Prism (v. 6.0) (GraphPad Software).

9 BLOOD BRAIN BARRIER PERMEABILITY MEASUREMENT

Mice were injected with 200uL of 2% Evans Blue (Sigma, Ref. No. 2129) (i.v). After 1 hr, mice were sacrificed and perfused with 20mL of PBS 1X. The organs were removed, weighed and placed in 2mL of formamide (Sigma, Ref. No. F9037-0100) at 37ºC for 48 hrs. Organs were kept at 4ºC until analysis. This was performed by diluting the supernatant of each sample with formamide (1:20). The data were represented as ug of Evans blue per g of organ.

10 IRON MEASUREMENT

Mice were sacrificed and perfused with 20mL of PBS 1X. The organs were removed, dried at 95ºC, overnight, and then weighted. 3M of Hydrochloric acid (HCL) (Sigma, Ref. No. 258148) and 10% of Trichloroacetic acid (TCA) (Sigma, Ref. No. T0699) were added (1mL/100mg tissue). Samples were kept at 65 ºC, overnight. After this time, each sample was diluted in distilled H_2O (1:30). To this,

10μL of β-Mercaptoethanol (Sigma, Ref. No. M3148) was added, followed by 500μL of 3M Sodium acetate (Sigma, Ref. No. S2889), pH 4.5, and 80μL of BPTS. Samples were mixed by inversion and incubated at 37ºC for 1 hr. 200uL were then transferred to a round bottom non-coated 96-well-plate and read at λ= 535nm, with the spectrophotometer (Biotrak II Plate Reader, Amersham Biosciences).

11 *IN VITRO* ASSAYS

11.1 CELL LINES

10.1.1 BV-2

Microglia BV-2 cells were purchased at ATCC cell bank, grown in T-75 Flasks and cultured in RPMI 1640 Medium (1x) GlutaMAX™ Supplement (Gibco™, Ref. No. 61870-010), supplemented with 10% Fetal Bovine Serum (FBS) (Gibco® by Life Technologies, Ref. No. 10500-064), 1% Penicillin-Streptomycin (10,000 U/mL) (Gibco® by Life Technologies, Ref. No. 15140-122) and 2% L-Glutamine solution 200 mM (Sigma Aldrich, Ref. No. 59202C). To maintain BV-2 cells in culture, cells were split every two days. To do so, PBS 1X was used to wash off the complete medium and cell debris. Cells were then trypsinized with Trypsin-EDTA (1x) (0.05%) (Gibco™, Ref. No. 25300-054), for 2 minutes at 37ºC. Trypsin activity was then neutralized with complete RPMI medium, at a 1:4 dilution. This cell line was obtained by the immortalization of brain macrophage resident cells from apparently normal 10-day old mouse (*Mus musculus*) and used to characterize their response upon insult treatment.

11.1.2 PRIMARY MICROGLIA ISOLATION

Primary microglia were isolated from newborn C57BL/6 mice (1-3-day old). The brain was removed and placed in a Falcon tube containing complete medium supplemented 20% FBS. The organ was homogenized using a P1000 pipette and then filtered through a 100μM mesh. The cell suspension was centrifuged at 1000 rpm for 5 minutes, and the pellet resuspended in 7.5mL of complete DMEM/F12 medium (with 20% FBS). Cells were then plated in 6-well plates (1.5mL/well). After 7 days, the medium was replaced by the complete medium supplemented with 10% FBS. This procedure was conducted for three weeks and without washing cells with PBS 1X to avoid their detachment. After this period, mild trypsinization was performed (1:4 dilution of trypsin in PBS 1X) in order to remove the astrocytes layer, a procedure that left microglia at the bottom of the flask. Microglia were then incubated with a dilution 1:1 of fresh and conditioned media. This refers to the supernatant collected from growing astrocyte and microglia, which contains growth factors needed for cell survival. After 48-72 hours, cells were trypsinized and cultured in DMEM/F-12 GlutaMAX™ (1:1 mixture) (Gibco® by Life Technologies, Ref. No. 31331-028), supplemented with 10% Fetal Bovine Serum (FBS) (Gibco® by Life Technologies, Ref. No. 10500-064) and 1% Penicillin-Streptomycin (10,000 U/mL) (Gibco® by Life Technologies, Ref. No. 15140-122).

11.2 CELL TREATMENT

Primary microglia and BV-2 cells were treated with hemin (Sigma Aldrich, Ref. No. H9039), 1S,3R-RSL-3 98% (HPLC) (Sigma

Aldrich, Ref. No. SML2234), Erastin 98% (Sigma, Ref. No. E7781), Deferiprone (DFP) (Sigma Aldrich, Ref. No. 379409), Deferoxamine (DFO) (Sigma Aldrich, Ref. No. D9533) and Ferrostatin-1 (Fer-1) (Sigma Aldrich, Ref. No. SML0583). These treatments were performed with two-time points, 4 and 24 hours. The 4 hrs treatments were carried out in a serum deprived medium HBSS (Gibco® by Life Technologies, Ref. No. 24020-091), while the 24 hours treatments were performed in complete medium.

11.2.1 VIABILITY ASSAY

Cell viability was determined by performing a Crystal Violet assay, in 96-well plates. A volume of 50µL of Crystal Violet (0,05g/100mL of 20% EtOH) (Sigma, Ref. No. C-0775) was added to each well. After 20 minutes incubation at room temperature, excess Crystal Violet solution was removed and washed twice with 100µL of MiliQ water. Wells were left drying completely. Cells were then resuspended in 50µL of acetic acid glacial (1:1 dilution in MiliQ water) (AnalaR NORMAPUR® VWR Prolabo Chemicals, Ref. No. 20104.298) and optical density was measured at λ= 590nm with the spectrophotometer (Biotrak II Plate Reader, Amersham Biosciences). Data analysis was performed using GraphPad Prism (v. 6.0) (GraphPad Software).

11.2.2 INTRACELLULAR MEASUREMENT OF RADICAL OXYGEN SPECIES

The production of radical oxygen species (ROS) was measured by using two different probes: 5-(and-6)-chloromethyl-2′,7′-dichlorodihydro-fluorescein di-acetate, acetyl ester (CM-

H_2DCFDA) (Life Technologies, Ref. No. C6827), a cell-permeable probe that allows evaluating all ROS produced within a cell, and MitoSOX™ (Thermo Fisher, Ref. No. M36008), a mitochondrial specific ROS probe.

For ROS quantification, BV-2 cells were seeded at 200,000 cell/well, in a 12-well plate with complete medium. At confluence, cells were treated with different compounds/conditions for 4 hrs in a serum-deprived medium (HBSS).

After this period, cells were washed with PBS 1X, trypsinized and transferred to 15mL falcon containing the respective complete medium, for trypsin inactivation. The cell suspension was then centrifuged at 1000 rpm for 5 minutes. The supernatant was discarded. Cells were resuspended with 500μL of PBS 1X and centrifuged again, as mentioned above. The supernatant was discarded. Cells were resuspended with 200μL of 1μM CM-H_2DCFDA (DCF) /1μM MitoSOX™ and incubated for 15 minutes at 37ºC, in the dark. After this period, PBS 1X was added and cell suspension were centrifuged at 1000 rpm for 5 min. Cells were washed one more time with PBS 1X, resuspended with 120μL of PBS 1X and ROS quantified in a BD FACSCanto II Flow Cytometer (BD Bioscience).

11.2.3 CYTOKINE ANALYSIS

Supernatants from treated cells and plasma collected from blood samples were kept at -20ºC, in order to quantify pro-inflammatory cytokines and define their proinflammatory profile. The cytokines quantified were TNF-α (using Mouse Uncoated ELISA kit with Plates, Invitrogen, Ref. No. 88-7324-22) and IL-6 (IL-6 Mouse Uncoated ELISA Kit with Plates, Invitrogen, Ref. No. 88-7064-22).

The quantification was performed according to the manufacturer's instruction.

RESULTS

CHAPTER 1

Heme is an essential metalloprotein and acts as co-factor in proteins involved in a variety of biological processes [3], [5], [6]. Its role in brain is to support neurogenesis and neuronal growth, since crucial for energy production. It is worth to mention that Heme contributes to neuronal survival, by enhancing neuronal activity [3].

However, for being a pro-oxidant and an inflammatory molecule, Heme homeostasis needs to be strictly maintained to avoid its accumulation and the generation of ROS, an effect particularly deleterious in sensible organs as the brain.

Hence, in this study we assessed the effects of physiological Heme/Fe accumulation in the brain of young, if any, and old mice, comparing the impact of exogenous peripheral Heme treatment in promoting a neuroinflammatory phenotype.

1 Heme-driven BBB disruption

It is known that, during aging, disruption of brain capillaries and/or microhemorrhage occurs, a phenomenon that can also favor Heme/Fe accumulation in the brain parenchyma. Thus, we assessed vascular impairment by injecting Heme in young C57BL/6 (8-12 weeks) and measuring the extravasation of Evans Blue into the brain. We expected no major differences when evaluating the permeability of BBB in Heme-peripherally treated young mice and control animals. However, Fig. 8 shows that Heme treatment in these mice significantly

disrupts the integrity of BBB, when compared to non-manipulated control young mice.

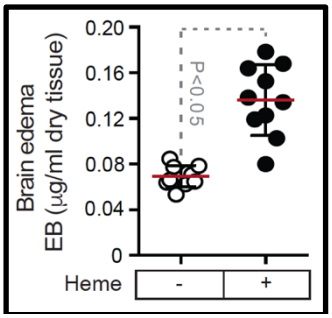

Fig. 8- Peripheral injections of Heme primes BBB disruption. Mice were injected i.p. with hemin. On the fourth day, animals were sacrificed and injected i.v. with Evans Blue to assess BBB permeability. Young mice treated with Heme (+) present higher BBB disruption, as assessed by quantifying the extravasation of the dye into the brain when compared to young non manipulated mice (-). This increase in permeability was significant, according to a non-parametric Student's t test. The results are expressed as mean ± standard deviation (n = 10 animals per group).

1.1 Heme-driven increased HRG-1 expression in the brain

To further confirm whether Heme can in fact enter the brain and accumulate, we quantified the expression of the Heme importer HRG-1 in the brain. There is a significant increase in the expression of HRG-1 in treated young mice when compared with young non-manipulated mice (Fig.9).

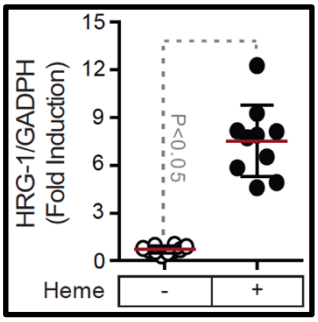

Fig. 9- Quantification of Heme importer-HRG-1- in the brain. Mice were injected i.p. with hemin. On the fourth day, animals were sacrificed. Harvested brains were collected and analyzed by qRT-PCR. The results are expressed as mean ± standard deviation (n = 10 animals per group). Non-parametric Student's t test was used to assess the significancy of the results obtained.

1.2 Heme-caused Fe accumulation in the brain

Whether the administration of exogenous Heme, in the periphery, leads to Fe accumulation in the brain was assessed and found to be the case (Fig.10).

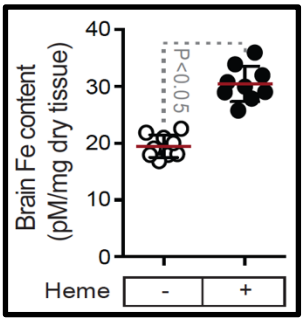

Fig. 10- Fe quantification in the brain after exogenous and peripheral Heme administration. Fe content was assessed, by colorimetric assay, as described in the method section. The results were referred to young control mice and expressed as pM per mg of dry tissue ± standard deviation (n = 9 animals per group). Non-parametric Student's t test was used to assess the significancy of the results obtained.

1.3 Heme-mediated immune cells infiltration into the brain

To assess the effect of exogenous and peripheral Heme administration in the brain of 8-12 weeks mice (from now on named as young), we used the flow cytometry technique. The gating strategy was set to analyze different immune cell types and to quantify populations of interest. Statistical difference was presented as *p < 0.05; ** p < 0.01; *** p <0.001, **** p <0.0001 and defined by applying a non-parametric Student's t test.

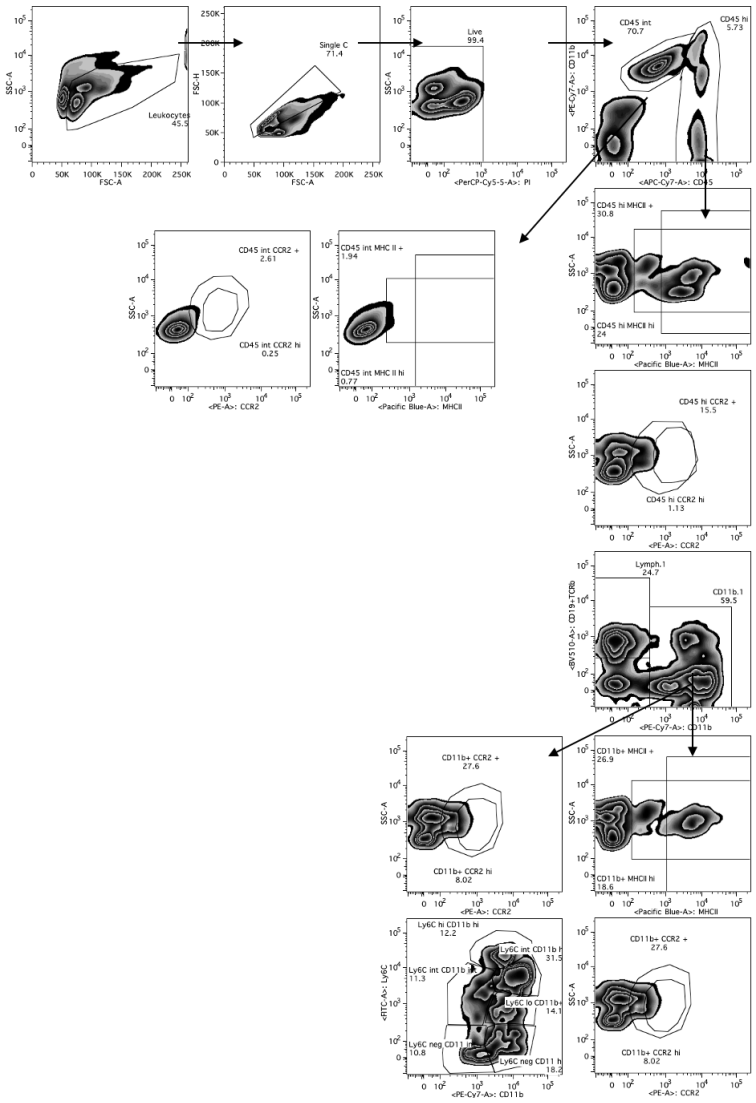

Fig. 11- Representative gating strategies to assess the infiltration of the immune cell population into the brain. Leukocytes were identified by size and granularity using FSC-A and SSC-A, respectively. Discrimination of doublets was performed through FSC-H and FSC-A combination. Then, combining SSC-A/PI, it was possible to identify viable cells (impermeable to PI). Using a combination of SSC-A and CD45, a pan marker of leukocytes, it was possible to distinguish microglia from peripheral immune cells. By gating SSC-A/CD45hi, we assessed whether leukocytes (CD45hi), among which lymphocytes, express inflammatory markers, as the Major Histocompatibility II (MHC II) [188] and the recruiting chemokine CCR2 [189]. The combination of Ly6C and Ly6G markers allowed identifying monocytes and neutrophils, respectively. Within cells expressing Ly6G, the combination of Ly6G/CD11b

confirms those be neutrophils. CCR2 marker was used to verify neutrophils' activation. Similar to previous gating strategy, the combination CD19/TCRβ were used as "dump channel" to exclude B and T cells. The same strategy was used to detect monocyte population. Withing CD11b+ cells, MHC II and CCR2 were used to determine the inflammatory state. The monocyte marker, Ly6C, was also used to identify inflammatory monocytes. Ly6Chi, inside CCR2+, showed whether Ly6C+ cells recruited to the site of inflammation [188], [189]. Inside CD11b+CD45int population, the levels of MHC II and CCR2 were assessed to determine microglia activation.

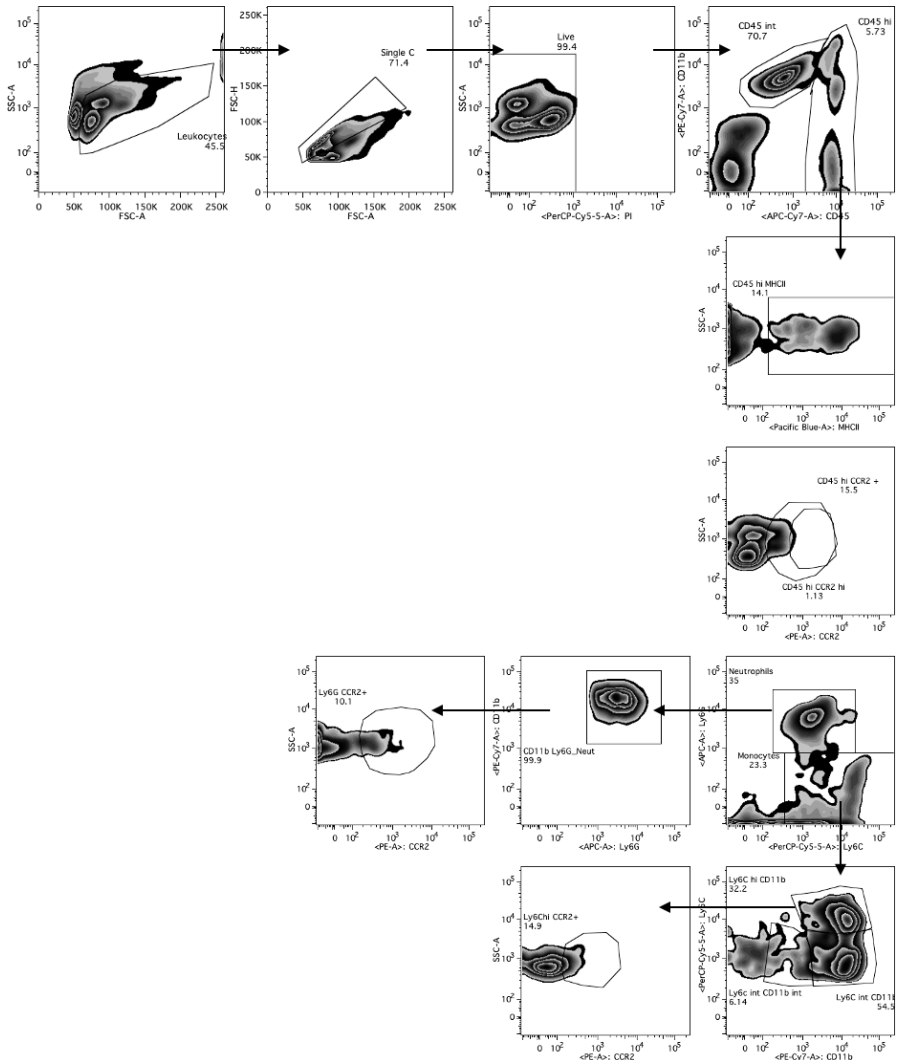

Fig. 12- Representative gating strategies to identify the levels of inflammation in the immune cell populations. Leukocytes were identified by size and granularity using FSC-A and SSC-A, respectively. Discrimination of doublets was performed through FSC-H and FSC-A combination. Then, combining SSC-A/PI, it was possible to identify viable cells (impermeable to PI). Using the combination of SSC-A and CD45, a pan marker of leukocytes, is possible to distinguish microglia from immune cells from the periphery. From SSC-A/CD45hi, it was possible to assess whether leukocytes (CD45hi), including lymphocytes, express inflammatory markers, among which the Major Histocompatibility II (MHC II) [188] and the recruiting chemokine CCR2 [189] Afterwards, the combination of Ly6C and Ly6G allowed identifying monocytes and neutrophils, respectively. Inside Ly6G, the combination of Ly6G/CD11b confirms that they are in fact neutrophils (as found in the literature), CCR2

marker was used to assess the level of activation of neutrophils. Similar to the previous mix CD19/TCRβ were used together as a "dump channel" to exclude B and T cells, since granulocytes are the population under the scope. Regarding the monocyte's population, we used the same strategy. Inside CD11b+, MHC II and CCR2 were used to assess the inflammatory state. Monocyte's marker, Ly6C, was also used to identify inflammatory monocytes. Ly6Chi and inside CCR2+ showed whether Ly6C+ cells are recruiting to the site of inflammation [188], [189]. Inside CD11b+CD45int population, the levels of MHC II and CCR2 were assessed to determine microglia activation.

1.4 Heme-driven peripheral immune cells infiltration into the brain

Heme-treated mice, in the periphery, presented an increased number of infiltrated immune cells into the brain, when compared to non-treated control animals of the same age (Fig. 13). The gating strategies used were presented in Fig.11 and Fig.12.

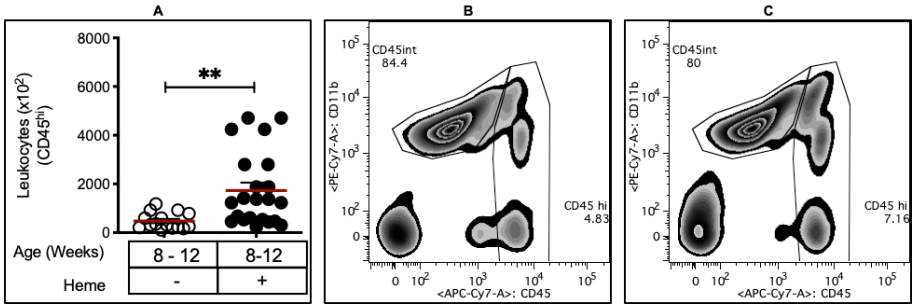

Fig. 13- Analysis of peripheral immune cells infiltration into the brain. Graph (A) shows the number of peripheral leukocytes (CD45hi) in the brain. This difference was also observable in plots obtained for freshly isolated brain leukocytes from (B) non-treated and (C) Heme-treated mice. The results were expressed as mean ± standard deviation (of 15-20 mice per group). Asterisks refer to a statistically significant difference. ** $p < 0.01$, defined by applying a non-parametric Mann-Whitney test.

1.5 Heme-driven activation of leukocytes in the brain

We then assessed the inflammatory state of peripheral leukocytes, infiltrating into the brain, upon peripheral injection of Heme. As shown in the figure below (Fig.14), Heme is capable to significantly

increase the activation of infiltrated immune cells into the brain, when compared to young non-manipulated mice, as quantified by the number of CCR2 positive cells.

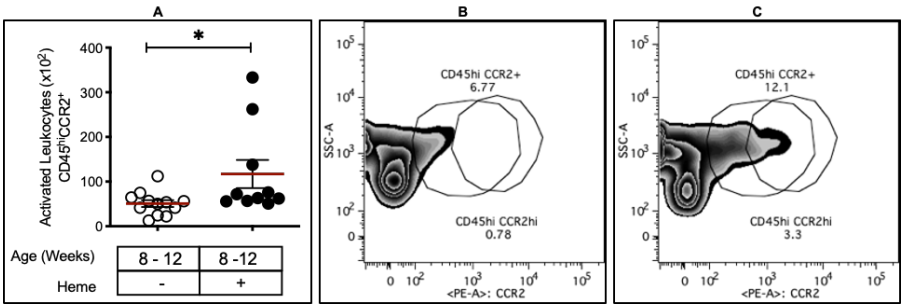

Fig. 14- Analysis of the inflammatory profile of infiltrated immune cells into the brain. Young mice (8-12 weeks old) were injected i.p. with hemin. Graph (A) shows the activation profile of leukocytes (CD45hiCCR2+). Significant differences were also observed in plots obtained from (B) non-treated and (C) Heme-treated mice. The results were expressed as mean ± standard deviation (11 animals per group). Asterisks refer to a statistically significant difference. *p < 0.05, defined by applying a non-parametric Mann-Whitney test.

1.6 Heme-driven activation of monocytes and neutrophils into the brain

Studies have shown that Heme/Fe activates immune cells towards a pro-inflammatory phenotype [1]. Among these, neutrophils, monocytes and tissue macrophages are common targets [1]. In our experiments, these same populations, more precisely activated neutrophils and monocytes, were those infiltrating the most into the brain. In Fig. 15 and 16, it is possible to observe a significant increase of neutrophils and monocytes, respectively, upon peripheral Heme treatment.

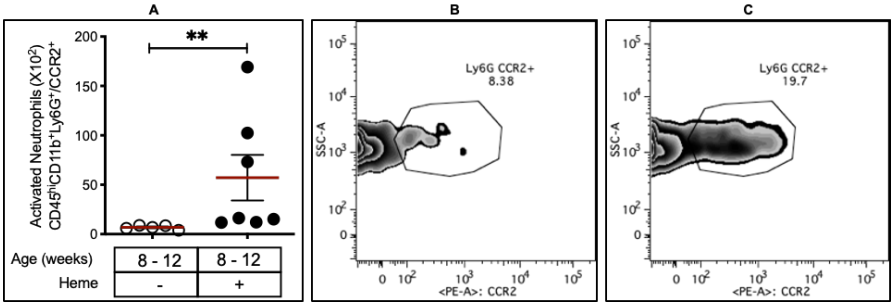

Fig. 15- Neutrophil activation in the brain after Heme administration. Young mice (8-12 weeks old) were injected i.p. with hemin. Graph (A) shows neutrophils activation profile (Ly6G+CCR2+). The differences were also observed in plots obtained from (B) non-treated and (C) Heme-treated mice. The results were expressed as mean ± standard deviation (5-7 animals per group). Asterisks refer to a statistically significant difference. *p < 0.05, defined by applying non-parametric Mann-Whitney test.

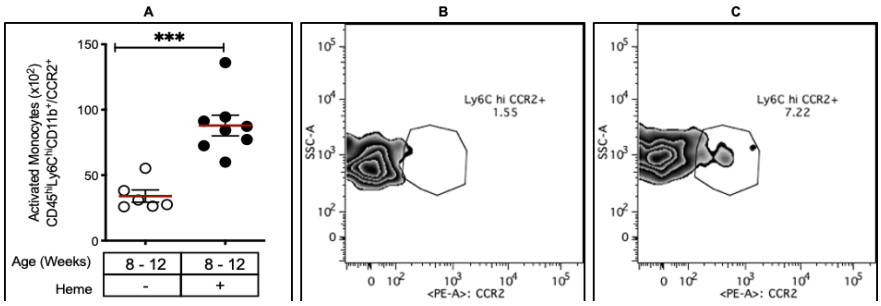

Fig. 16- Monocyte activation in the brain after peripheral Heme administration. Young mice (8-12 weeks old) were injected i.p. with hemin. Graph (A) shows monocytes activation (Ly6ChiCD11b+/CCR2+). The differences were also observed in plots obtained from freshly isolated brain monocytes from (B) non-treated and (C) Heme-treated mice. The results were expressed as mean ± standard deviation (6-8 animals per group). Asterisks refer to a statistically significant difference. ***p < 0.001, defined by applying non-parametric Mann-Whitney test.

1.7 Heme primes microglia towards a pro-inflammatory profile

Once Heme/Fe enters the brain, it boosts the infiltration of pro-inflammatory cells into this organ, where activates resident microglia. To investigate the influence of this treatment on these cells, we first assess if Heme could influence the total number of microglia. As shown

in the graph below (Fig.17), the Heme-treated animal group presents a significantly higher number of microglia when compared to controls.

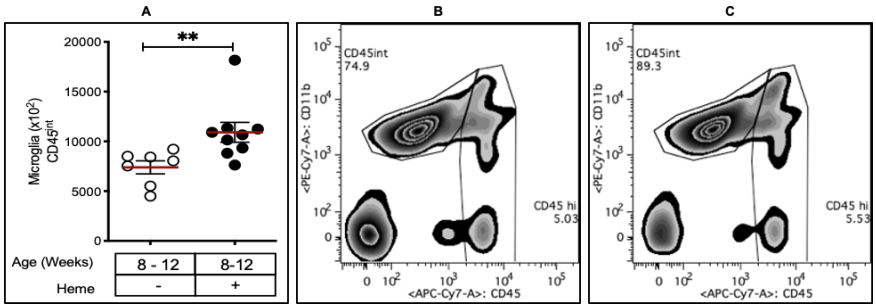

Fig. 17- Microglia proliferation after peripheral Heme administration. Young mice (8-12 weeks old) were injected i.p. with hemin. Graph (A) shows the number of microglial (CD45int). The differences were also observed in plots obtained from freshly isolated brain microglia from (B) non-treated and (C) Heme-treated mice. The results were expressed as mean ± standard deviation (7-9 animals per group). Asterisks refer to a statistically significant difference. ** $p < 0.01$, defined by applying non-parametric Mann-Whitney test.

Using inflammatory markers, we assessed microglia inflammatory state. As shown in Fig.18 and 19, even when injected in the periphery, Heme shifts microglia towards an inflammatory state, as assessed by quantifying inflammatory markers, as MHCII and CCR2.

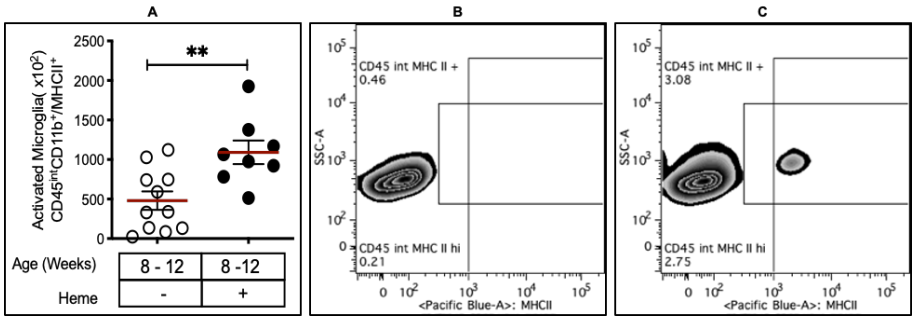

Fig. 18- Microglia activation after peripheral Heme administration. Young mice (8-12 weeks old) were injected i.p. with hemin. Graph (A) shows microglia activation in the brain (CD45intCD11b+/MHCII+). The differences were also

observed in plots obtained from freshly isolated brain microglia from (B) non-treated and (C) Heme-treated mice. The results were expressed as mean ± standard deviation (8-11 animals per group). Asterisks refer to a statistically significant difference. ** $p < 0.01$, defined by applying non-parametric Mann-Whitney test.

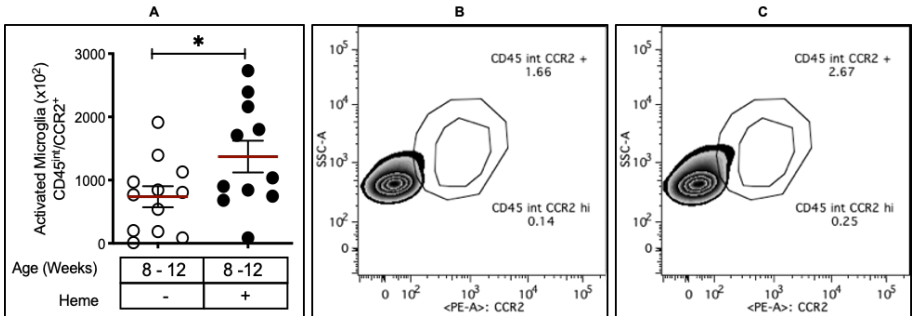

Fig. 19- Microglia activation after Heme administration. Young mice (8-12 weeks old) were injected i.p. with hemin. Graph (A) shows microglia activation in the brain (CD45intCD11b+/CCR2+). This difference was also observed in plots obtained from freshly isolated brain microglia from non-treated (B) and Heme-treated mice (C). The results were expressed as mean ± standard deviation (11-12 mice per animal group). Asterisks refer to a statistically significant difference. * $p < 0.05$, defined by applying non-parametric Mann-Whitney test. Parametric t test, as appropriate.

1.8 Heme-Driven infiltration of T cells into the Brain

In addition to the myeloid population, also T cells can enter the brain through an increased BBB permeability caused by the exogenous and peripheral administration of Heme. Therefore, brain samples were harvested from young mice treated with Heme and analyzed by flow cytometry, with the aim to identify different T cells subsets in the brain, like helper and cytotoxic cells, and to evaluate their activation. This allowed to subdivide T cells into naïve, activated, and memory lymphocyte. The gating strategy used to determine our populations of interest is described in Fig. 20.

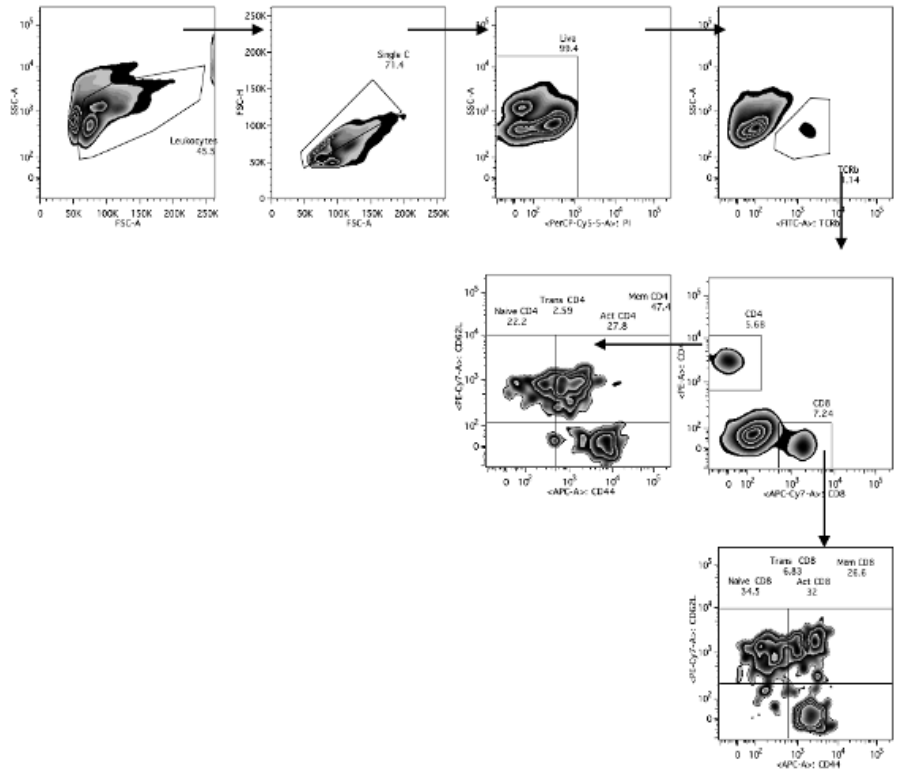

Fig. 20- Representative gating strategies to identify the levels of activation of the lymphocytic population. First, leukocytes were identified by size and granularity using FSC-A and SSC-A, respectively. Doublet discrimination was performed through FSC-H and FSC-A. Then, viable cells (impermeable to PI) were analyzed by combining SSC-A/PI. T cells were identified by gating on TCRβ+ cells and these were then subdivided in CD4+ T and CD8+ T cells. Inside of each T cells subtype, the activation of these cells was determined by quantifying the expression of CD44 and CD62L, as follows: naïve cells, when express CD62L+, CD44-, activated cell when express CD62L- CD44+ and memory, when expressed CD44+CD62L+.

The results showed in Fig.21 demonstrate that Heme significantly increases the number of T cells in the brain.

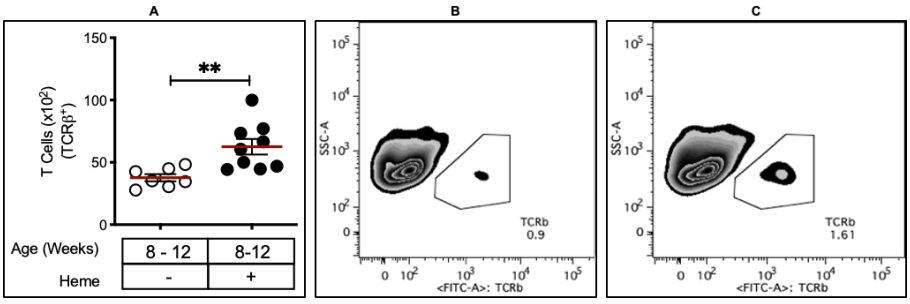

Fig. 21- T cells infiltration into the brain after peripheral Heme administration. Young mice (8-12 weeks old) were injected i.p. with hemin. Graph (A) shows the number of T cells (TCRβ+) in the brain. The differences were also observed in plots from freshly isolated brains from (B) non-treated and (C) Heme-treated mice. The results were expressed as mean ± standard deviation (8 animals per group). Asterisks refer to a statistically significant difference. ** $p < 0.01$, defined by applying non-parametric Mann-Whitney test.

1.9 Heme-Driven activation of T helper cells

The same profile is observed for the two subsets of T cells, namely T helper (CD4+) and cytotoxic T cells (CD8+) (Fig. 22A and Fig. 23A, respectively). As we expected, these latter become activated upon a peripheral Heme exposure, invading the brain along with myeloid cells, to then exert their cytotoxicity.

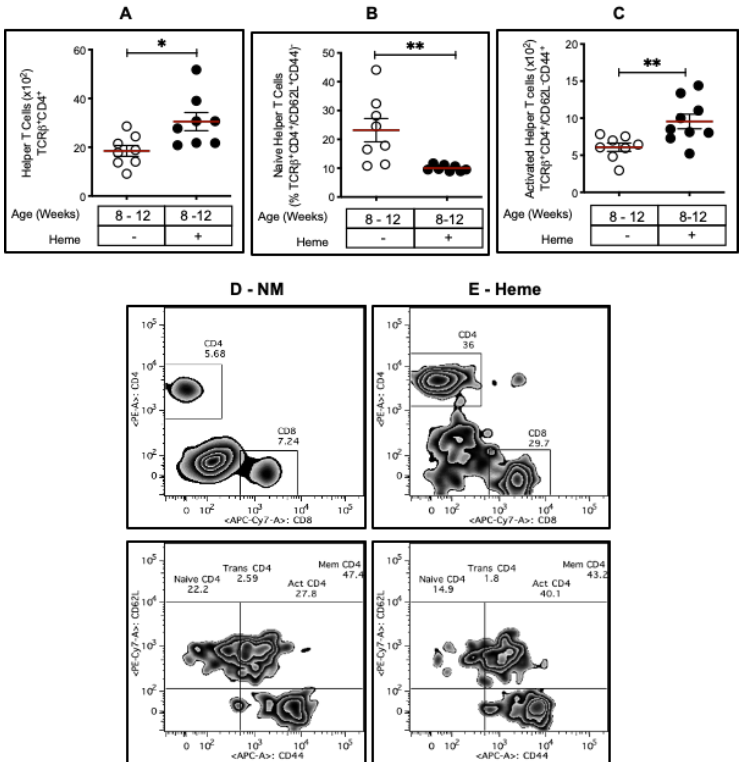

Fig. 22- Helper T Cells activation after peripheral Heme administration. Young mice (8-12 weeks old) were injected i.p. with hemin. Graph (A) represents the number of T helper cells, (B) naive and (C) activated CD4+.The differences were also observed in plots from freshly isolated brains from (D) non-treated and (E) Heme-treated mice. The results were expressed as mean ± standard deviation (8 animals per group). Asterisks refer to a statistically significant difference. * $p < 0.05$; ** $p < 0.01$, defined by applying non-parametric Mann-Whitney test.

Heme had the same effect on CD8+ cell. Peripheral Heme administration significantly increases the number of CD8+ (Fig.23A). As expected, similar data were obtained concerning the number of activated CD8+ cells.

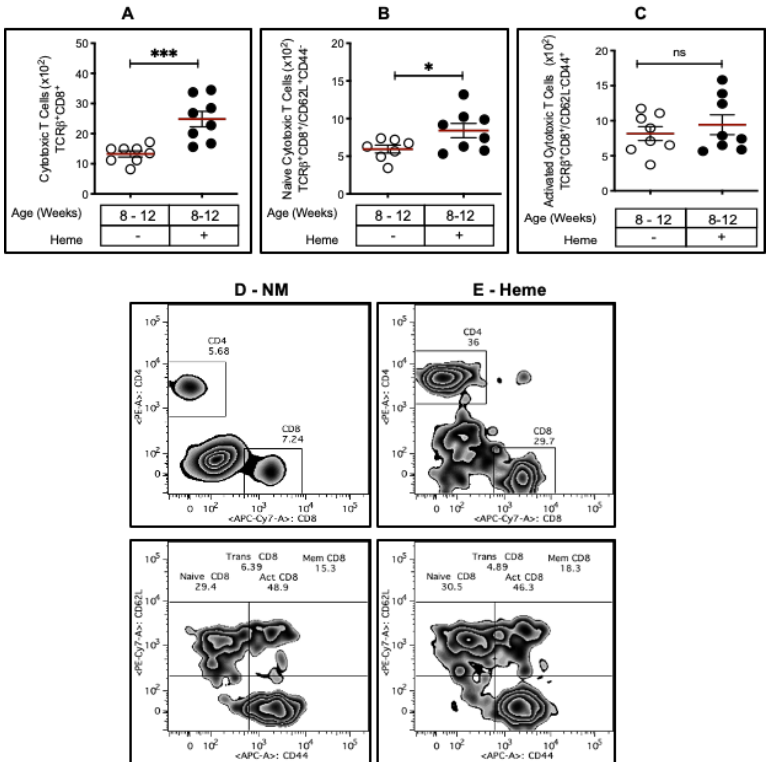

Fig. 23- Cytotoxic T Cells activation after peripheral Heme administration. Young mice (8-12 weeks old) were injected i.p. with hemin. Graph (A) represents the number of Cytotoxic CD8+ T cells, while graph (B) and (C) naïve and activated CD8+ cells, respectively. These results were also observed in plots from freshly isolated brains from (D) non-treated and (E) Heme-treated mice. The results were expressed as mean ± standard deviation (8 animals per group). Asterisks refer to a statistically significant difference. * $p < 0.05$; *** $p < 0.001$, defined by applying non-parametric Mann-Whitney test.

1.10 Peripheral immune cells analysis

To support our hypothesis that the circulating compartment contributes to the development of a neuroinflammatory phenotype sensitizing the brain to neurodegenerative diseases, we analyzed the inflammatory states of spleen and blood (PBLs) compartment as well as the changes in Fe accumulation in quantified immune cells.

1.10.1 Peripheral Heme administration effect on spleen leukocytes

The analysis of spleen leukocytes showed no major effects upon peripheral Heme administration. Whether lower counts correspond to leukocytes that already left the spleen could be the case.

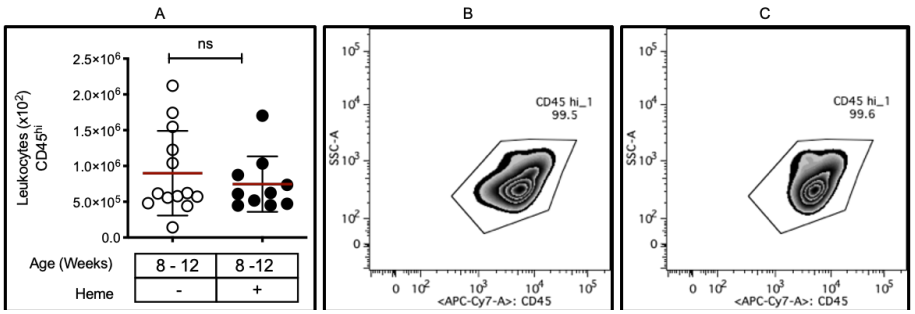

Fig. 24- Immune response in the spleen after peripheral Heme administration. Young mice (8-12 weeks old) were injected i.p. with hemin. Graph (A) represents the number of activated leukocytes (CD45+MHCII+). These results were also observed in plots from freshly isolated brains from (B) non-treated and (C) Heme-treated mice. The results were expressed as mean ± standard deviation (10-12 animals per group). Asterisks refer to a statistically significant difference. ns $p > 0.05$, defined by applying non-parametric Mann-Whitney test.

No increase in activated leukocytes was observed in the spleen of tested animals upon peripheral Heme treatment, possibly indicating that activated cells left this organ at the time of the analysis (Fig.25).

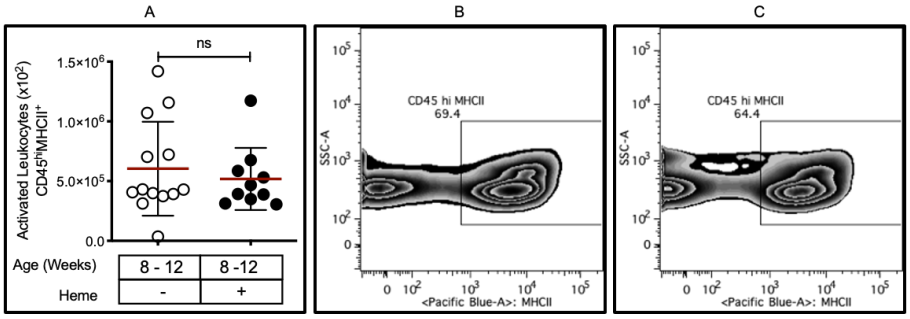

Fig. 25- Analysis of spleen immune response after Heme administration. Young mice (8-12 weeks old) were injected i.p. with hemin. Graph (A) represents the number of activated leukocytes (CD45+MHCII+). These results were also observed in plots from freshly isolated brains from (B) non-treated and (C) Heme-treated mice. The results were expressed as mean ± standard deviation (10-12 animal per group). Asterisks refer to a statistically significant difference. ns p >0.05, defined by applying non-parametric Mann-Whitney test.

No significant changes were observed also when analyzing the number and activation of monocytes in the spleen (Fig.26).

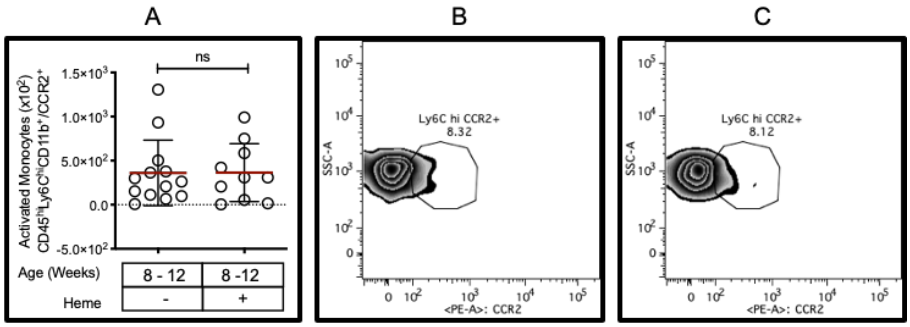

Fig. 26- Analysis of spleen immune response after Heme administration. Young mice (8-12 weeks old) were injected i.p. with hemin. Graph (A) represents the number of activated monocytes (Ly6C+CCR2+). These results were also observed in plots obtained from fresly isolated brains from (B) non-treated and (C) Heme-treated mice. The results were expressed as mean ± standard deviation (10-12 animal per group). Asterisks refer to a statistically significant difference. ns p >0.05, defined by applying non-parametric Mann-Whitney test.

1.10.2 Peripheral Heme administration effect on circulating leukocytes

When assessing whether immune cells could migrate from the spleen and reach the circulation, we observed that the number of total leukocytes in the blood of young mice increases upon Heme administration (Fig.27). These results demonstrate the existing complementarity between the data obtained in the different compartments of Heme-treated animals.

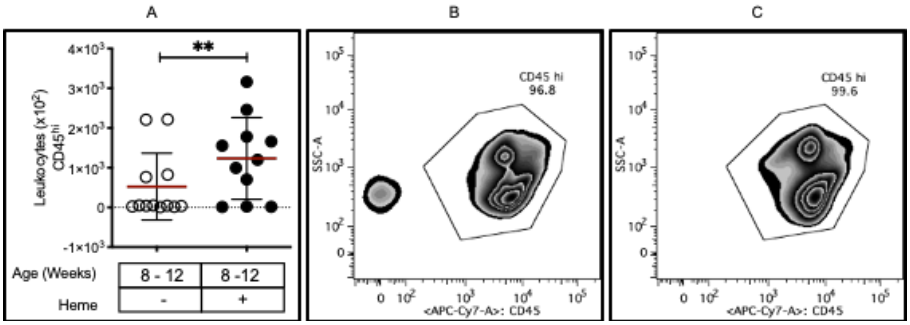

Fig. 27- Analysis of PBLs immune response after peripheral Heme administration. Young mice (8-12 weeks old) were injected i.p. with hemin. Graph (A) represents the number of leukocytes (CD45+). These results were also observed in graphs from (B) non-treated and (C) Heme-treated mice. The results were expressed as mean ± standard deviation (10-12 animal per group). Asterisks refer to a statistically significant difference. ** p <0.01, defined by applying non-parametric Mann-Whitney test.

Similar graphs were obtained regarding leukocytes activation, where peripheral Heme administration induces an inflammatory profile.

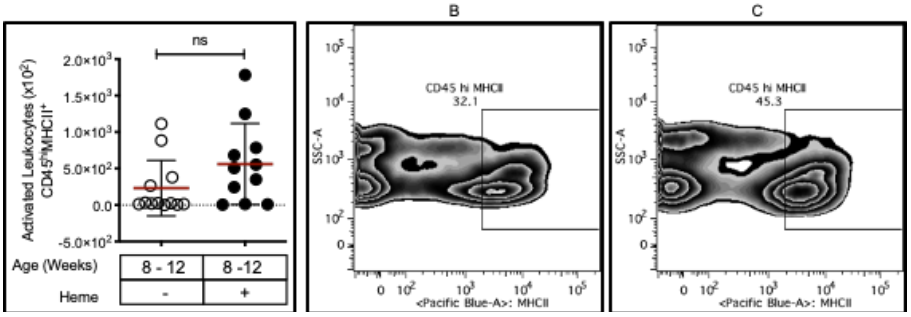

Fig. 28- Leukocytes activation after Heme administration. Young mice (8-12 weeks old) were injected i.p. with hemin. Graph (A) represents the number of activated leukocytes (CD45+MHCII+). These results were also observed in plots from (B) non-treated and (C) Heme-treated mice. The results were expressed as mean ± standard deviation (10-12 animal per group). Asterisks refer to a statistically significant difference. ns p >0.05, defined by applying non-parametric Mann-Whitney test.

When analyzing the number of activated monocytes, we observed a decreased count in response to peripheral Heme injection. This reflects the increased number of these cells in the brain, where they infiltrate.

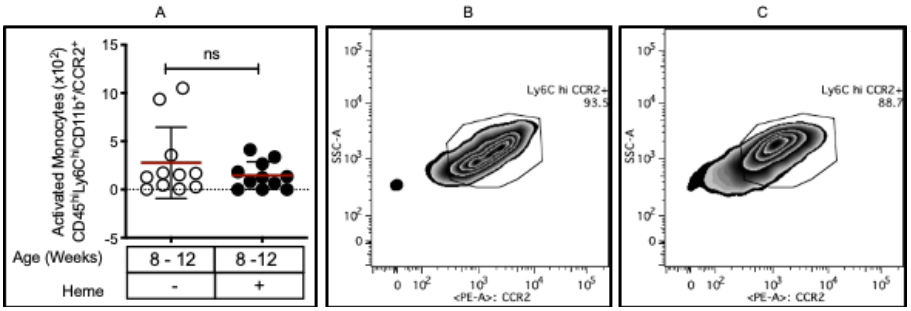

Fig. 29- Analysis of PBLs immune response after peripheral Heme administration. Young mice (8-12 weeks old) were injected i.p. with hemin. Graph (A) represents the number of activated monocytes (Ly6C+CCR2+). These results were also observed in plots from (B) non-treated and (C) Heme-treated mice. The results were expressed as mean ± standard deviation (11-12 animal per group). Asterisks refer to a statistically significant difference. ns p >0.05, defined by applying non-parametric Mann-Whitney test.

The same results were observed when quantifying the number and activation of neutrophils in young mice after peripheral Heme administration, corroborating the hypothesis that these cells infiltrate into the brain.

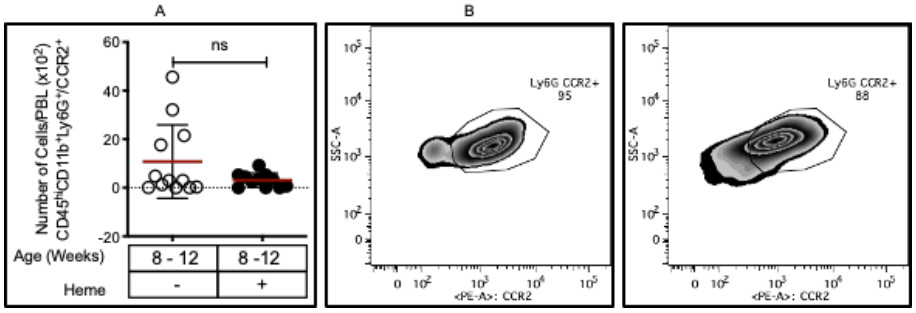

Fig. 30- PBLs immune response after Heme administration. Young mice (8-12 weeks old) were injected i.p. with hemin. Graphs (A) represents the number of activated neutrophils (Ly6G+CCR2+). These results were also observed in plots from (B) non-treated and (C) Heme-treated mice. The results were expressed as mean ± standard deviation (11-12 animal per group). Asterisks refer to a statistically significant difference. ns p >0.05, defined by applying non-parametric Mann-Whitney test.

1.11 Iron accumulation in brain immune cells

We observed that Heme was capable to sensitize young mice to develop a neuroinflammatory profile. We then tested whether the administration of Heme leads to Fe accumulation in the brain when injected into the periphery. Our hypothesis is that immune cells might act as buffering cells for Fe and, entering the brain, they favor its accumulation.

To assess that, we conducted experiments by combining immune cell markers with Calcein AM. This is a fluorescent cell-permeable probe that quickly binds Fe^{2+}. Quenching this metal, Calcein fluorescence decreases. Although this is not a direct method to

quantify intracellular Fe, it is accepted that calcein quenching might indicate the presence of oxidative stress caused by the accumulation of intracellular labile Fe (LIP). This means that the lower the fluorescence of calcein, the higher the amount of Fe within cells [190][191].

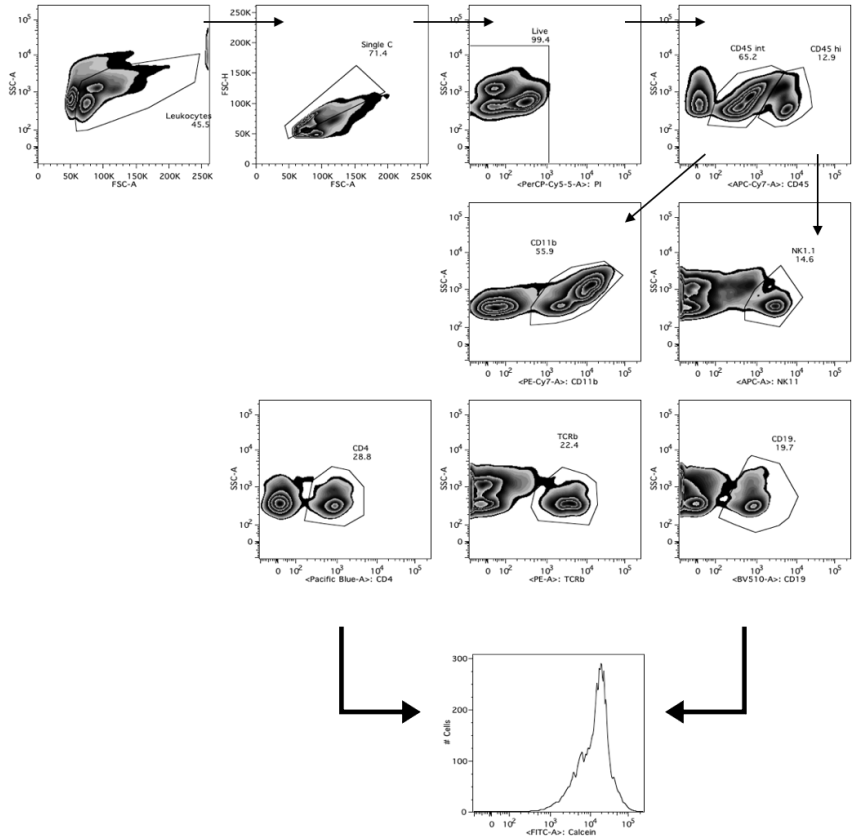

Fig. 31- Representative gating strategies to identify Fe accumulation into immune cells, using calcein AM probe. Leukocytes were identified through their size and granularity using FSC-A and SSC-A, respectively. Doublet discrimination was performed through FSC-H and FSC-A. Then, viable cells (impermeable to PI) were analyzed by combining SSC-A/PI. CD45 was used to discriminate resident immune cells, microglia (CD45int) and infiltrated leukocytes (CD45hi). Inside these latter, T cells (TCRβ), Helper T cells (TCRβCD4+), B cells (CD19), Macrophages (CD11b) and natural killer cells (NK1.1) were identified. Inside each population the intensity of CA was quantified and expressed as histograms.

The results demonstrated that young mice accumulate less Fe in the brain, although increases upon peripheral Heme administration. This goes in accordance with previous results (Fig.10), confirming that increasing the levels of circulating Heme causes brain Fe overload.

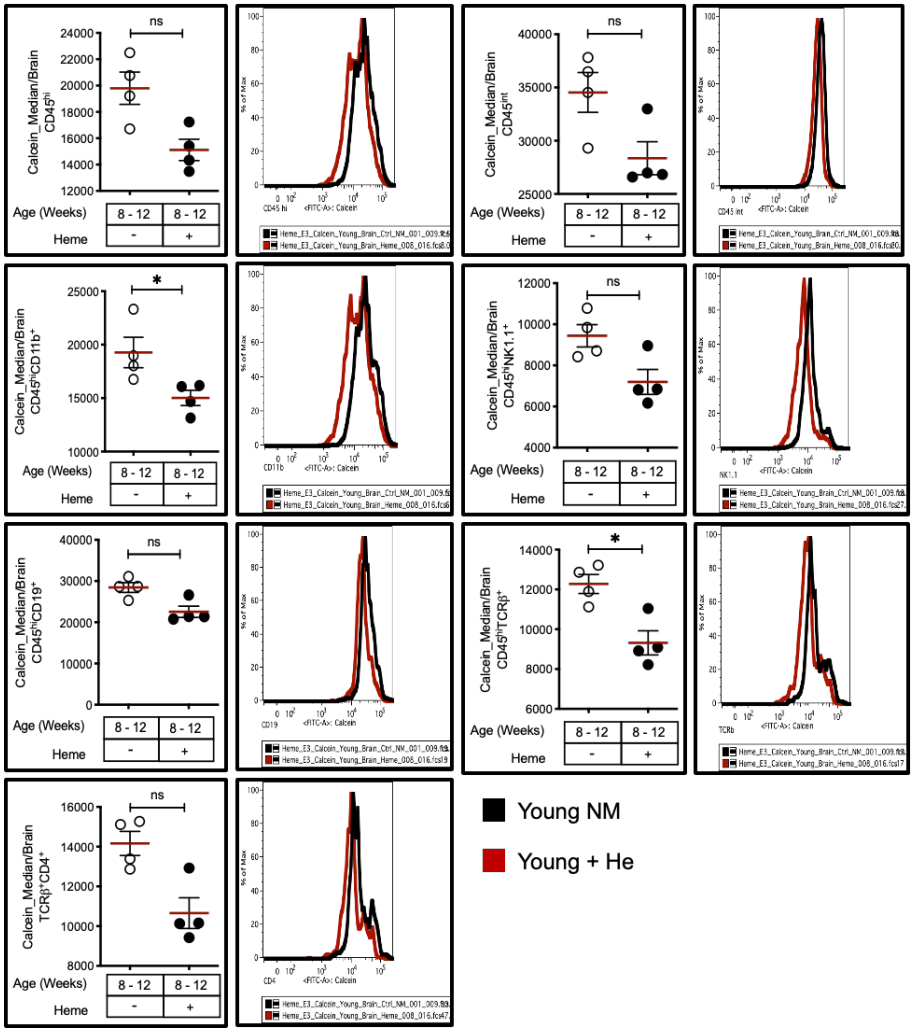

Fig. 32- Quantification of brain Fe accumulation in infiltrated peripheral and resident immune cells. Young non-manipulated (NM; 8-12 weeks old) and Heme-treated young mice were used for the experiment. Both peripheral invading cells: CD45hi-Leukocytes, CD11b- Macrophages, CD19- B cells, NK1.1- Natural killer cells, TCRβ- T cells, TCRβCD4+- Helper T cells; and

resident cells: CD45int-Microglia, were evaluated. The results were expressed as mean ± standard deviation (4 animals per group). Asterisks refer to a statistically significant difference. ns $p > 0.05$, * $p < 0.05$, defined by applying non-parametric Mann-Whitney test.

1.12 Iron accumulation in PBL immune cells

Whether the Fe found in the brain could come from the circulation is our starting hypothesis. To prove it, we measured the Fe content in PBL immune cells. Fig.33 shows that peripheral Heme administration significantly increases Fe in immune cells.

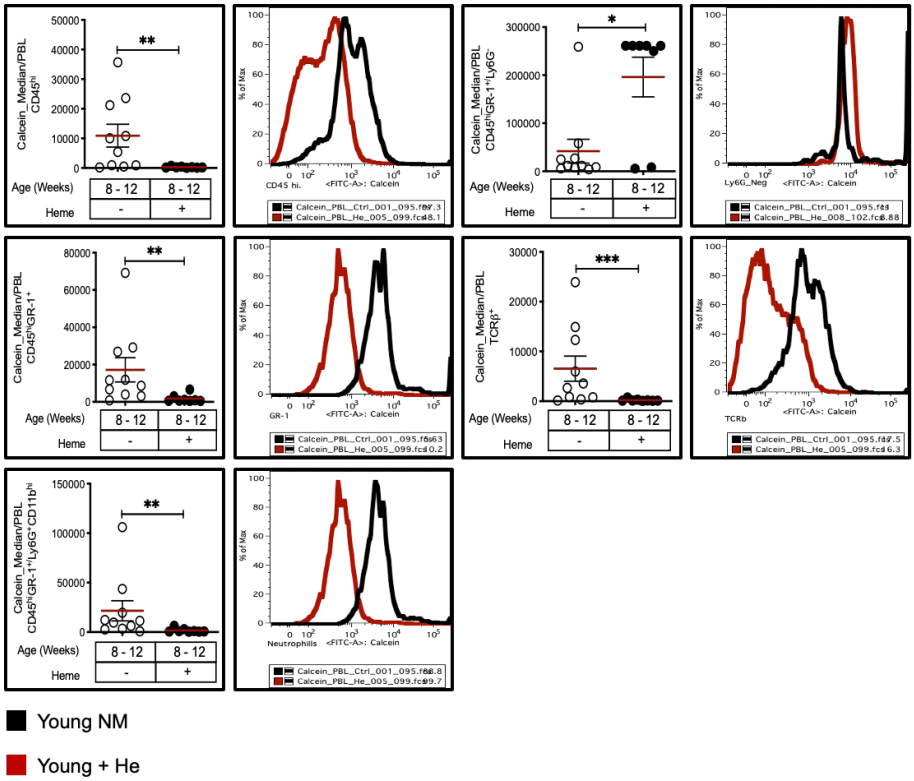

Fig. 33- Quantification of Fe accumulation PBLs immune cells. Young NM (8-12 weeks old) and Heme-treated young mice were used for the experiment. The graphs represent: CD45hi-peripheral Leukocytes, CD11b- Macrophages, CD19- B cells, NK1.1- Natural killer cells, TCRβ- T cells, TCRβCD4+- Helper T cells. The results were expressed as mean ± standard deviation (10 animals

per group). Asterisks refer to a statistically significant difference. * $p < 0.05$, ** $p < 0.0$, *** $p < 0.001$, defined by applying non-parametric Mann-Whitney test.

CHAPTER 2

2 Aging

Aging is a sub-chronic pro-inflammatory pathology and represents the main risk factor for several diseases, among which neurodegenerative diseases, like PD. This physiological process is characterized by an increased oxidative stress, which compromises brain physiological functions [192], [193]. Evidence suggests that during aging there might exist sub-acute vascular events, like microhemorrhages, which promote an increased Heme accumulation in the brain and neural cells cytotoxicity. Whether this could contribute to disrupt the BBB is likely the case [45], as aging is a main cause of neuroinflammation and neuronal death [83].

To assess whether aging increases BBB permeability, we compared BBB integrity in young NM mice (8-12 weeks) and aged animals (52-60 weeks). As shown in Fig.31, older mice have an enhanced BBB permeability, as measured by the extravasation of Evans Blue into the brain, in relation to young mice.

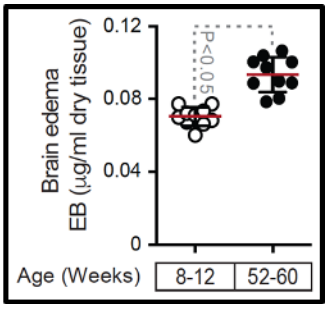

Fig. 34- BBB disruption quantification. Young (8-12 weeks old) and old (52-60 weeks old) animals were injected i.v. with Evans Blue and then sacrificed, to assess BBB permeability. Old mice present a significantly higher BBB disruption when compared to young mice, used as controls. The results are

expressed as mean ± standard deviation (n = 10 animals per group), defined by applying non-parametric Mann-Whitney test.

To understand whether this might impair Fe accumulation, the level of this metal was measured in young (8-12 weeks) and old NM mice (52-60 weeks). As shown in Fig. 32, an increased Fe accumulation was observed in the brain of old mice, as it occurs in humans.

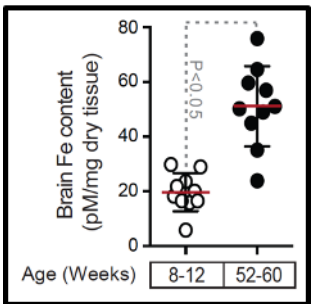

Fig. 35- Fe quantification in the brain of young and old animals. Increased Fe accumulation in the brain of old mice when compared to young animals. The level of Fe in the brain was measured by colorimetric assays as described in the Material and Methods session. The results were expressed as pM per mg of dry tissue ± standard deviation (n = 10 animals per group). Statistical significance was defined by applying non-parametric Mann-Whitney test.

2.1 The pathophysiology of Aging

We then assessed whether an increased BBB permeability and Fe accumulation in aged mice was associated with the infiltration of peripheral immune cells, considered as underlying cause of these events and what subsequently triggers neuroinflammation and neuronal death.

As shown below, NM old mice presents a significantly higher number of infiltrated immune cells when compared to young control animals.

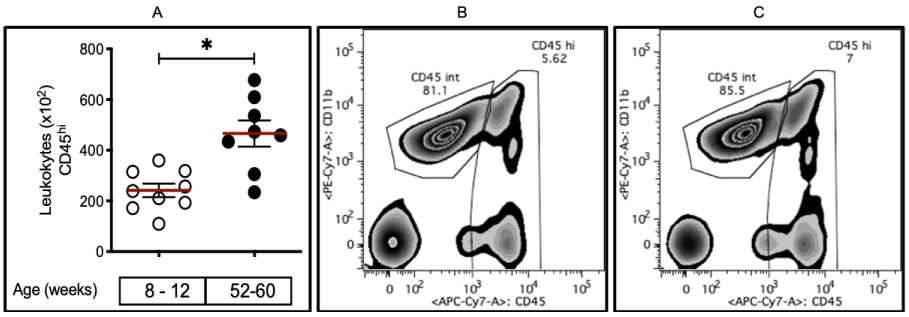

Fig. 36- Peripheral leukocytes infiltration in aged mice. Young (8-12 weeks old) and old (52-60 weeks old) animals were used for the experiment. Graph (A) shows the number of peripheral leukocytes (CD45hi). Differences were also observed in graphs obtained from freshly isolated brain leukocytes from (B) young and (C) old mice. The results were expressed as mean ± standard deviation (7 animals per group). Asterisks refer to a statistically significant difference. * $p < 0.05$, defined by applying non-parametric Mann-Whitney test.

2.2 Age-driven inflammation

In addition to a higher infiltration of peripheral immune cells, old animals show enhanced recruitment of inflammatory leukocytes, quantified by flow cytometry, using $CCR2^+$ (Fig. 34) and MHC II^+ markers (Fig.35). This demonstrates that old mice present an increased brain inflammation even in physiological conditions.

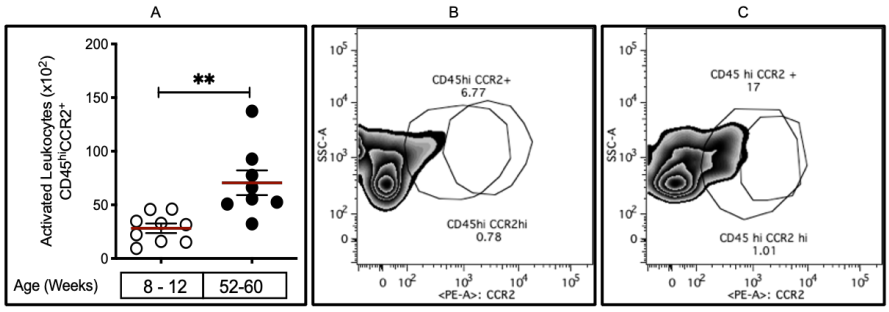

Fig. 37- Peripheral leukocytes activation in aged mice. Young (8-12 weeks old) and old (52-60 weeks old) animals were used for the experiment. Graph (A) shows the number of activated leukocytes (CD45hiCCR2+). The differences were also observed in graphs obtained from freshly isolated brain

leukocytes from (B) young and (C) old mice. The results were expressed as mean ± standard deviation (7 animals per group). Asterisks refer to a statistically significant difference. ** p < 0.01, defined by applying non-parametric Mann-Whitney test.

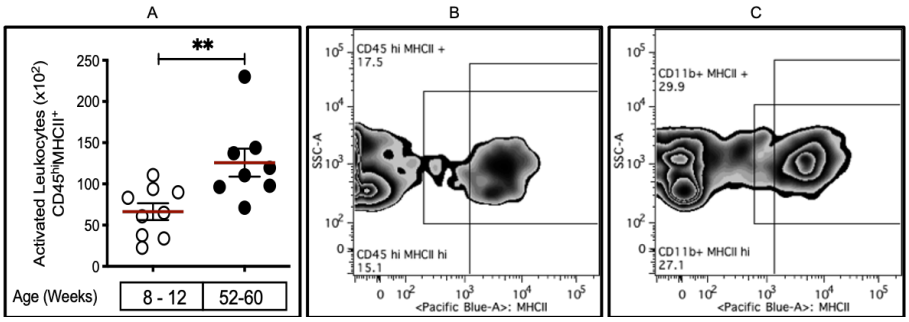

Fig. 38- Peripheral leukocytes activation in aged mice. Young (8-12 weeks old) and old (52-60 weeks old) animals were used for the experiment. Graph (A) shows the number of activated leukocytes (CD45hiMHCII2+). The differences were also observed in graphs obtained from freshly isolated brain leukocytes from (B) young and (C) old mice. The results were expressed as mean ± standard deviation (7 animals per group). Asterisks refer to a statistically significant difference. ** p < 0.01, defined by applying non-parametric Mann-Whitney test.

2.3 Increased neutrophil count in the brain during aging

An increased BBB permeability enhances the infiltration of leukocytes. To assess which immune cell population mostly enters the bran, we performed a series of experiments and observed a greater neutrophils' infiltration (Fig. 39). Our results demonstrated that both neutrophil count and activation were significantly higher in older mice (Fig.40).

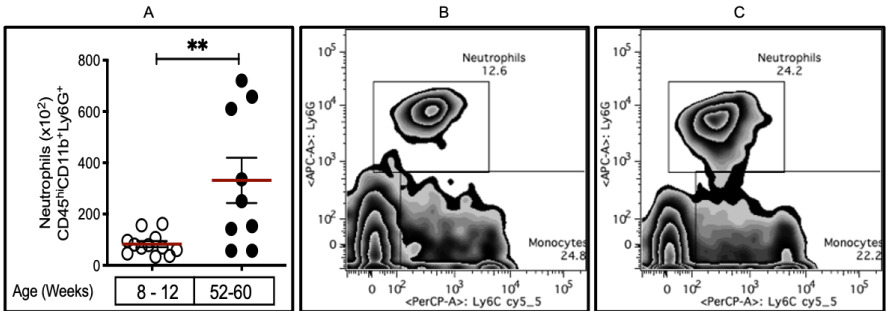

Fig. 39- Neutrophils infiltrates into the brain of aged mice**.** Young (8-12 weeks old) and old (52-60 weeks old) animals were used for the experiment. Graph (A) shows the number of neutrophils (Ly6G+). The differences were also observed in graphs obtained from freshly isolated brain leukocytes from (B) young and (C) old mice. The results were expressed as mean ± standard deviation (9-11 animals per group). Asterisks refer to a statistically significant difference. ** $p < 0.01$ defined by applying non-parametric Mann-Whitney test.

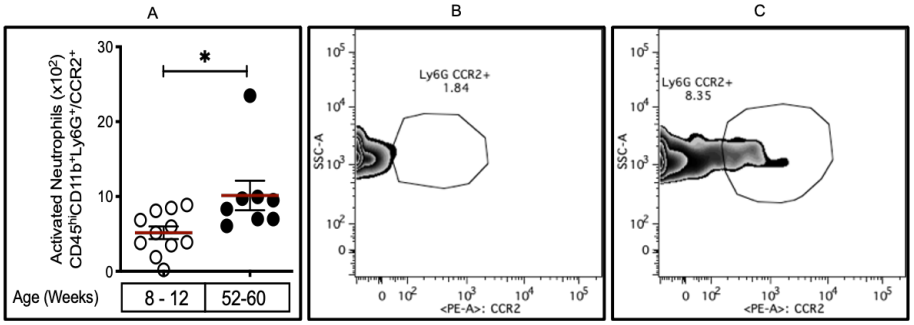

Fig. 40- Neutrophil's activation into the brain of aged mice. Young (8-12 weeks old) and old (52-60 weeks old) animals were used for the experiment. Graph (A) shows the number of activated neutrophils (Ly6G+CCR2+). The differences were also observed in graphs obtained from freshly isolated brain leukocytes from (B) young and (C) old mice. The results were expressed as mean ± standard deviation (8-11 animal per group). Asterisks refer to a statistically significant difference. * $p < 0.05$, defined by applying non-parametric Mann-Whitney test.

2.4 Increased number of infiltrating monocytes into the brain during aging

Monocyte counts were found to be higher in the brain of old animals when compared to young animals (Fig. 41), as the number of activated and inflammatory monocytes (Fig. 42).

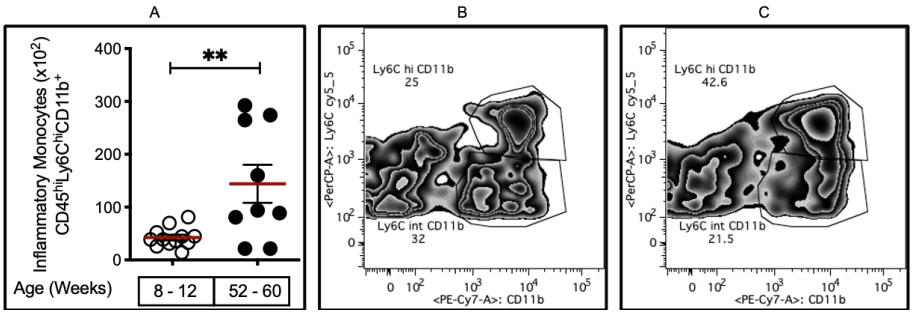

Fig. 41- Inflammatory monocytes in the brain of aged mice. Young (8-12 weeks old) and old (52-60 weeks old) animals were used for the experiment. Graph (A) shows the number of monocytes (Ly6Chi). The differences were also observed in graphs obtained from freshly isolated brain leukocytes from (B) young and (C) old mice. The results were expressed as mean ± standard deviation (9-12 animals per group). Asterisks refer to a statistically significant difference. * $p < 0.05$, defined by applying non-parametric Mann-Whitney test.

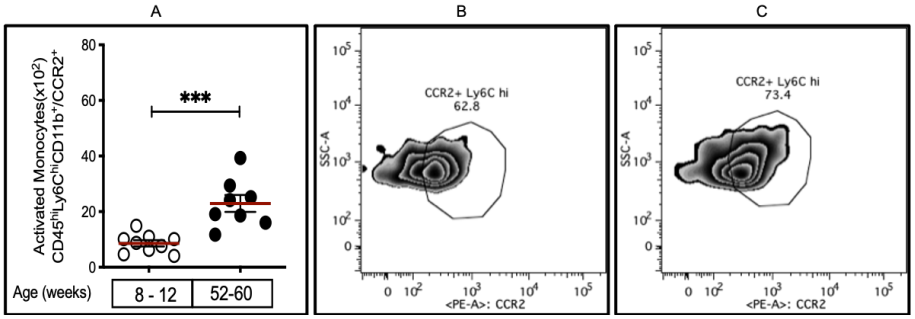

Fig. 42- Activated monocytes in the brain of aged mice. Young (8-12 weeks old) and old (52-60 weeks old) animals were used for the experiment. Graph (A) shows the number of activated monocytes (Ly6C+CCR2+). The differences were also observed in graphs obtained from freshly isolated brain leukocytes from (B) young and (C) old mice. The results were expressed as mean ± standard deviation (8-9 animals per group). Asterisks refer to a statistically significant difference. * $p < 0.05$, defined by applying non-parametric Mann-Whitney test.

2.5 Microglia activation in old mice

Infiltrating immune cells boost brain inflammation, which hallmark is microglia activation. According to the gating strategy shown in Fig.11, the activation of microglia was quantified through the

expression of MHC II and CCR2 marker. Our expectation was to observe an increased number of total microglia counts with animal age. However, despite their enhanced activation, this was not the case, as observed in Fig. 43.

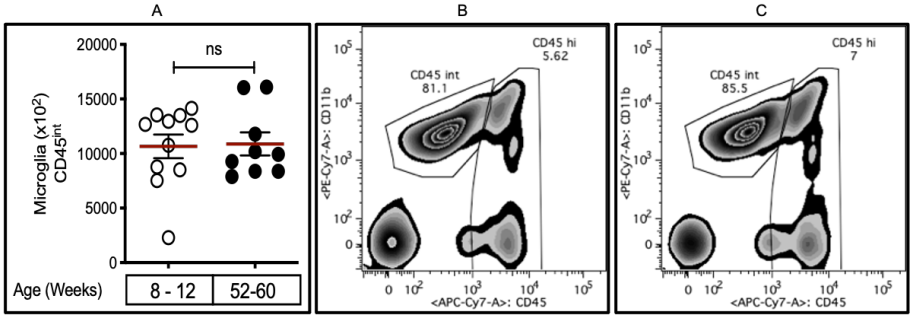

Fig. 43- Microglia proliferation in the brain of aged mice. Young (8-12 weeks old) and old (52-60 weeks old) animals were used for the experiment. Graph (A) shows the number of microglia cell (CD45int). The differences were also observed in graphs obtained from freshly isolated brain leukocytes from (B) young and (C) old mice. The results were expressed as mean ± standard deviation (9-11 animals per group). Asterisks refer to a statistically significant difference. Ns $p > 0.05$, defined by applying non-parametric Mann-Whitney test.

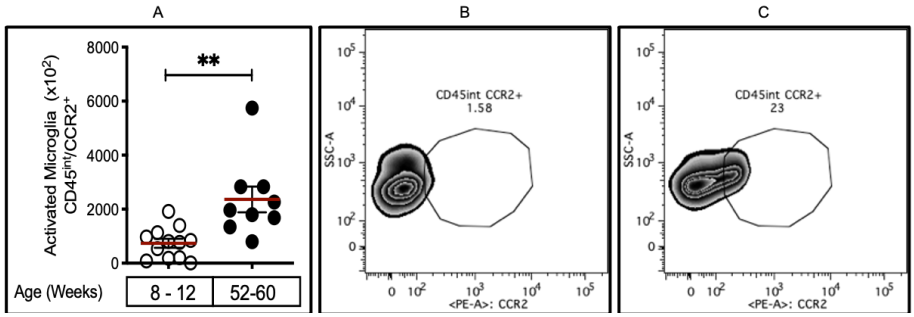

Fig. 44- Microglia activation in the brain of aged mice. Young (8-12 weeks old) and old (52-60 weeks old) animals were used for the experiment. Graph (A) shows the number of activated microglia (CD45intCCR2+). The differences were also observed in graphs obtained from freshly isolated brain leukocytes from (B) young and (C) old mice. The results were expressed as mean ± standard deviation (9-12 animals per group). Asterisks refer to a statistically significant difference. Ns $p > 0.05$, defined by applying non-parametric Mann-Whitney test.

2.6 Increased infiltration of T lymphocytes into the aged brain

When brain samples were analyzed to identify T cells, using the gating strategy shown in Fig.20, we observed a significant increase in the activation of these cells in the brain of old mice, when compared to young animals.

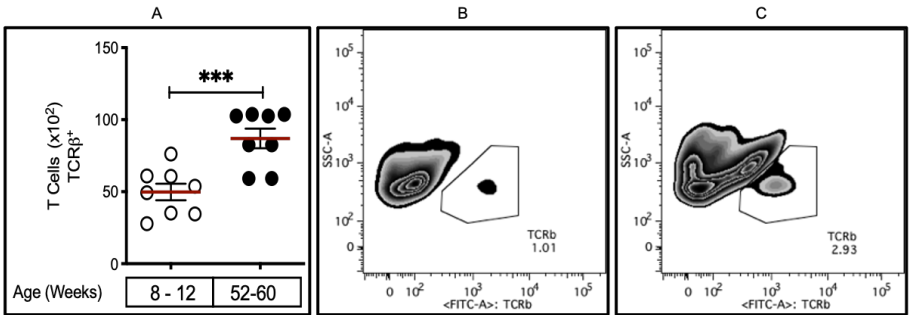

Fig. 45- T cells quantification in the brain of aged mice. Young (8-12 weeks old) and old (52-60 weeks old) animals were used for the experiment. Graph (A) shows the number of T cells (TCRβ+). The differences were also observed in graphs obtained from freshly isolated brain leukocytes from (B) young and (C) old mice. The results were expressed as mean ± standard deviation (8 animals per group). Asterisks refer to a statistically significant difference. *** $p > 0.001$, defined by applying non-parametric Mann-Whitney test.

No significant difference was observed in the number of helper T cells ($CD4^+$) between the two groups of animals (Fig.46A). Similar results were obtained for naïve CD4 T cells ($CD4^+CD62L^-CD44^-$) (Fig.46B). Contrarily, the activation of helper T ($CD4^+CD62L^-CD44^+$) significantly increases in aged animals (Fig.42C).

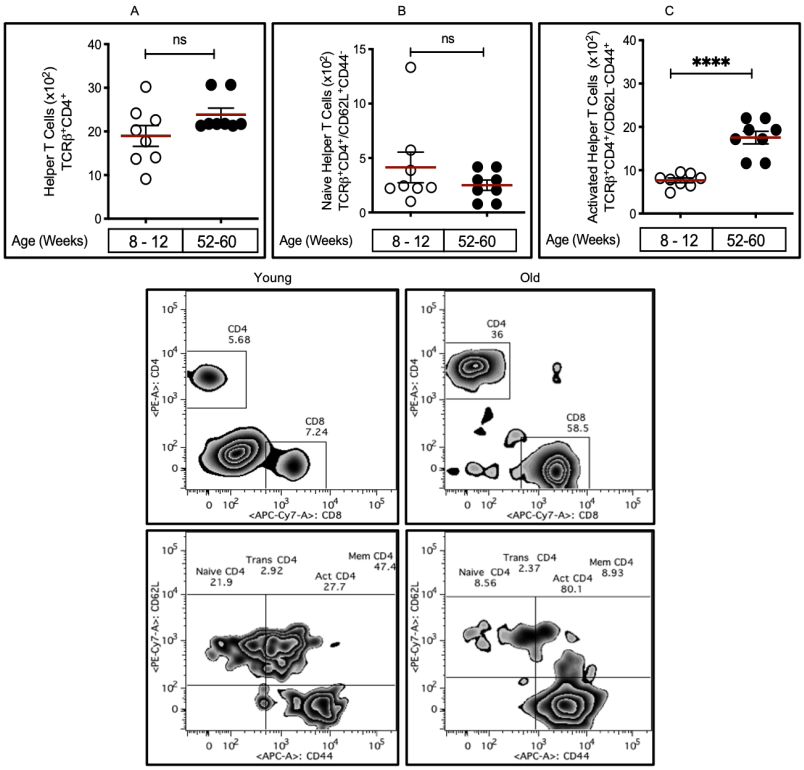

Fig. 46- Helper T cells activation in the brain of aged mice. Young (8-12 weeks old) and old (52-60 weeks old) animals were used for the experiment. Graph (A) shows the number of Th cells (TCRβ+CD4+), (B) naïve Th cells and (C) activated Th cells. The differences were also observed in graphs obtained from freshly isolated brain leukocytes. The results were expressed as mean ± standard deviation (8 animals per group). Asterisks refer to a statistically significant difference. ns $p>0.05$, **** $p > 0.0001$, defined by applying non-parametric Mann-Whitney test.

When referring to cytotoxic T cells (CD8+ cells), a significant difference was observed in the number of these lymphocytes, between young and old mice (Fig 47A), in the sense that their count increases during aging. Despite no significant differences in the number of naïve cells (Fig 47B), their activation was significantly enhanced in old mice (Fig 47C).

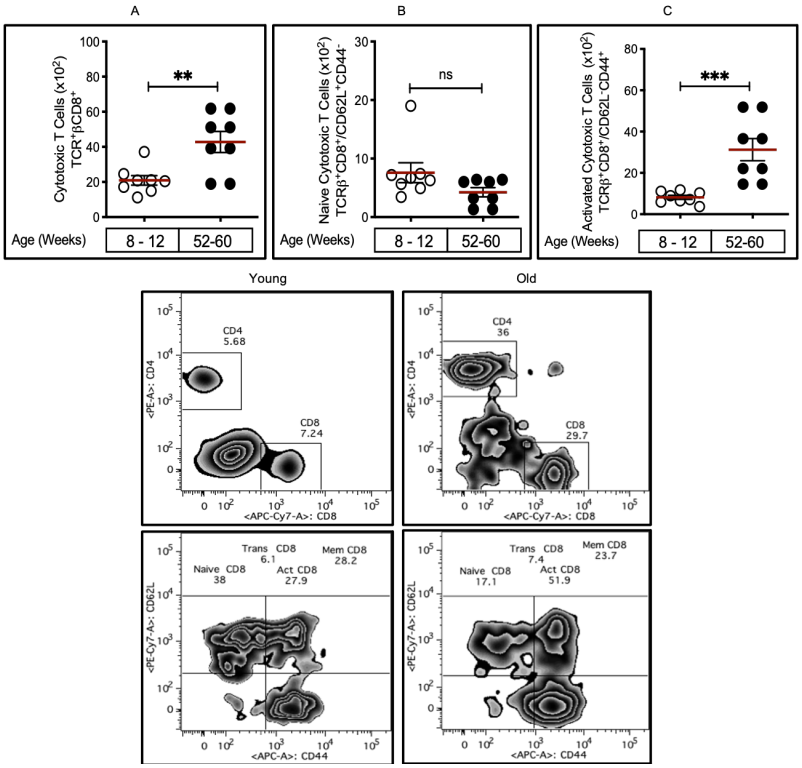

Fig. 47- cytotoxic T cells activation in the brain of aged brain. Young (8-12 weeks old) and old (52-60 weeks old) animals were used for the experiment. Graph (A) shows the number of T cells (TCRβ+CD8+), (B) naïve and (C) activated cytotoxic T cells. The differences were also observed in graphs obtained from freshly isolated brain leukocytes. The results were expressed as mean ± standard deviation (8 animals per group). Asterisks refer to a statistically significant difference. ns $p>0.05$, **** $p > 0.0001$, defined by applying non-parametric Mann-Whitney test.

2.7 Peripheral immune cells analysis

To support our hypothesis that the circulating compartment contributes to the development of a neuroinflammatory phenotype sensitizing the brain to neurodegenerative diseases, like PD, we analyzed the inflammatory states of spleen and blood (PBLs) and the respective changes in the accumulation of Fe, in specific tested immune cells.

2.7.1 Spleen immune profile in aged mice

The analysis of spleen leukocytes showed the same profile as in the brain of old non-manipulated mice, meaning that old animals present highest levels of inflammation (Fig.48).

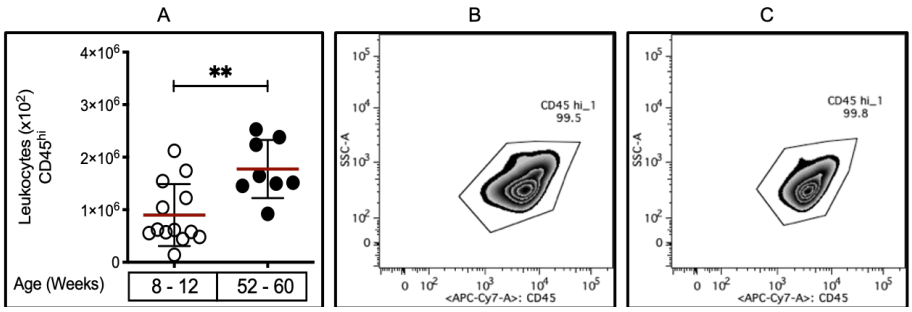

Fig. 48- Analysis of spleen immune response in aged mice. Young (8-12 weeks old) and old (52-60 weeks old) animals were used for the experiment. Graph (A) represents the number of leukocytes (CD45+). These results were also observed in plots from (B) young and (C) old mice. The results were expressed as mean ± standard deviation (9-13 animal per group). Asterisks refer to a statistically significant difference. ** p <0.05, defined by applying non-parametric Mann-Whitney test.

Similar data were also obtained when assessing leukocytes activation. As showed in Fig.49, the inflammatory profile was found even at peripheral level, in aged mice when compared young.

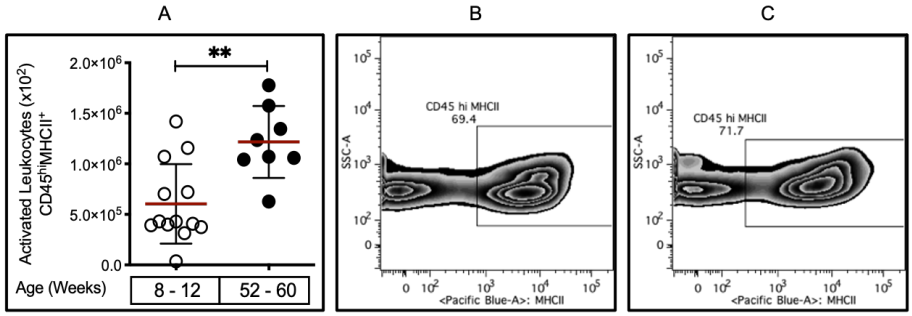

Fig. 49- Activated leukocytes response in aged mice. Young (8-12 weeks old) and old (52-60 weeks old) animals were used for the experiment. Graph (A) represents the number of activated leukocytes (CD45+MHCII+). These results were also observed in plots from (B) young and (C) old mice. The results were expressed as mean ± standard deviation (8-13 animals per group). Asterisks refer to a statistically significant difference. ** p <0.05, defined by applying non-parametric Mann-Whitney test.

We observed a different profile when we quantified the number of activated monocytes, as aged mice presented the same counts of young animals (Fig.50). Probably, these inflammatory cells already left this organ.

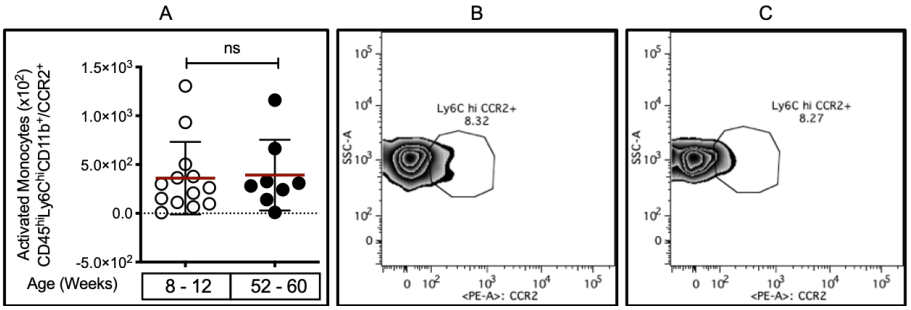

Fig. 50- Monocyte's activation in aged mice. Young (8-12 weeks old) and old (52-60 weeks old) animals were used for the experiment. Graph (A) represents the number of activated monocytes (Ly6C+CCR2+). These results were also observed in plots from (B) young and (C) old mice. The results were expressed as mean ± standard deviation (9-13 animal per group). Asterisks refer to a statistically significant difference. ns p >0.05, defined by applying non-parametric Mann-Whitney test.

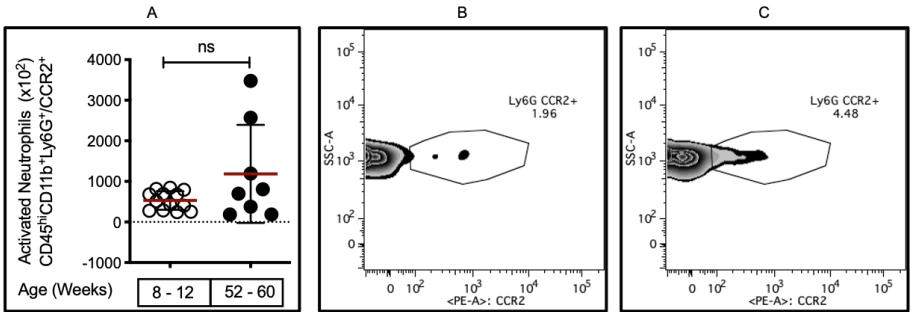

Fig. 51- Neutrophil's response in aged mice. Young (8-12 weeks old) and old (52-60 weeks old) animals were used for the experiment. Graph (A)

represents the number of activated neutrophils (Ly6G+CCR2+). These results were also observed in plots from (B) young and (C) old mice. The results were expressed as mean ± standard deviation (9-13 animals per group). Asterisks refer to a statistically significant difference. ns p >0.05, defined by applying non-parametric Mann-Whitney test.

2.7.2 PBL immune profile in aged mice

Observing an increased inflammation in the spleen, we assessed whether similar data could be obtained also in circulation. However, this was not the case, as shown in the Fig.51, where old non-manipulated mice have lower circulating leukocyte count, possibly indicating they might have infiltrated other tissues, like the brain.

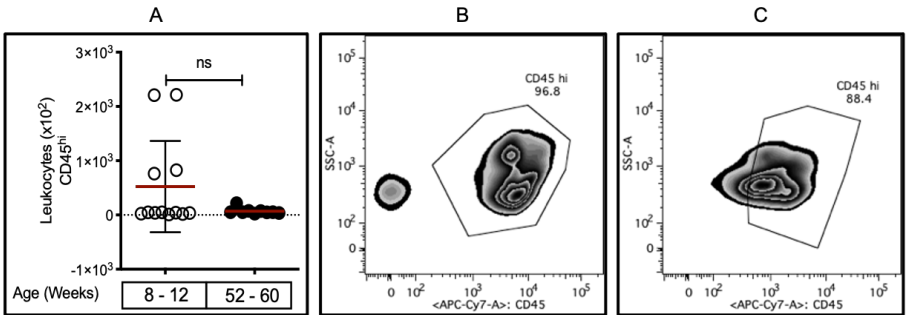

Fig. 52- PBL response in aged mice. Young (8-12 weeks old) and old (52-60 weeks old) animals were used for the experiment. Graph (A) represents the number of circulating leukocytes (CD45). These results were also observed in plots from (B) young and (C) old mice. The results were expressed as mean ± standard deviation (9-13 animals per group). Asterisks refer to a statistically significant difference. ns p >0.05, defined by applying non-parametric Mann-Whitney test.

The number of activated leukocytes confirms previous result. Inflammation levels in blood circulation seems to be maintained throughout aging (Fig.52).

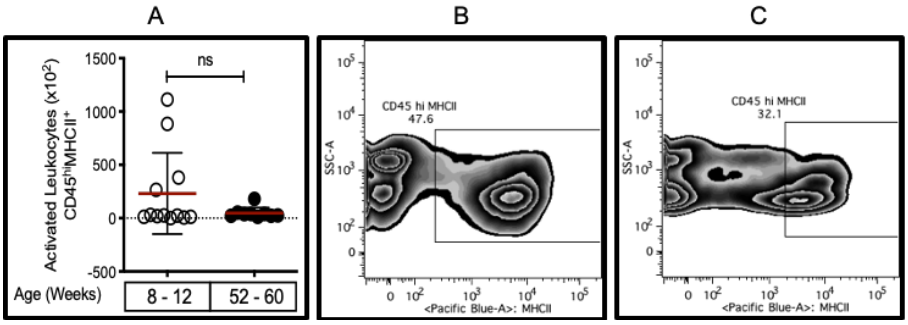

Fig. 53- PBL activation in aged mice. Young (8-12 weeks old) and old (52-60 weeks old) animals were used for the experiment. Graph (A) represents the number of activated leukocytes (CD45hiMHCII+). These results were also observed in plots from (B) young and (C) old mice. The results were expressed as mean ± standard deviation (9-13 animals per group). Asterisks refer to a statistically significant difference. ns p >0.05 defined by applying non-parametric Mann-Whitney test.

We observed similar tendency when we quantified and also analyzed the number of activated monocytes. Although the lack of significance, counts appear to decrease in old mice.

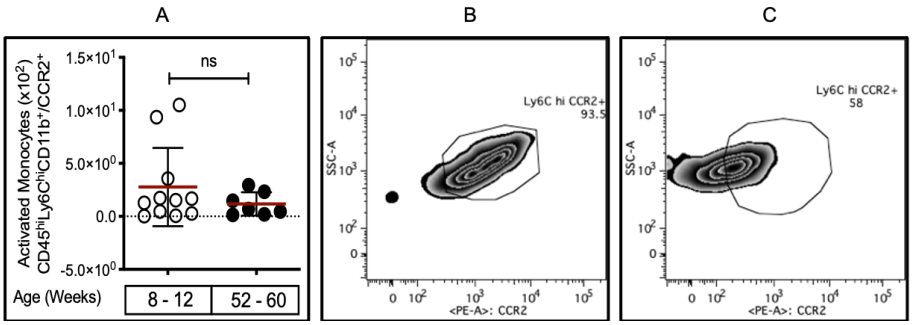

Fig. 54- Circulating monocytes activation in aged mice. Young (8-12 weeks old) and old (52-60 weeks old) animals were used for the experiment. Graph (A) represents the number of activated monocytes (Ly6ChiCCR2+). These results were also observed in plots from (B) young and (C) old mice. The results were expressed as mean ± standard deviation (7-11 animals per group). Asterisks refer to a statistically significant difference. ns p >0.05, defined by applying non-parametric Mann-Whitney test.

The same results were observed when quantifying the number and activation of neutrophils (Fig.55). We obtained results with the same profile, regardless of the population analyzed.

Keeping in mind the results obtained from cells isolated from brain, spleen and PBLs, we hypothesized that inflammatory cells have already left the circulation and infiltrated in tissues such as brain.

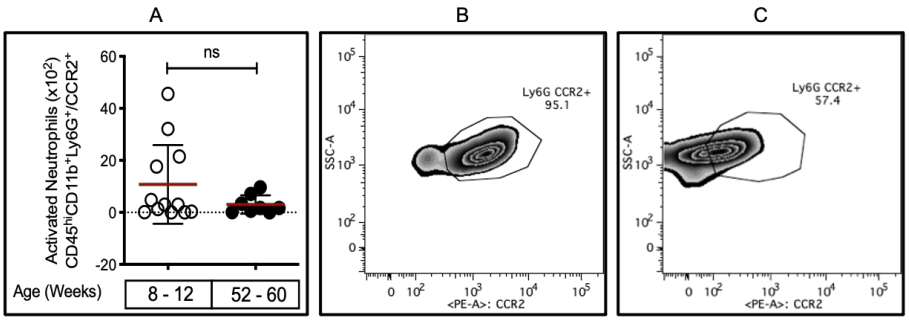

Fig. 55- Circulating neutrophils activation in aged mice. Young (8-12 weeks old) and old (52-60 weeks old) animals were used for the experiment. Graph (A) represents the number of activated neutrophils (Ly6G+CCR2+). These results were also observed in plots from (B) young and (C) old mice. The results were expressed as mean ± standard deviation (8-12 animals per group). Asterisks refer to a statistically significant difference. ns $p > 0.05$, defined by applying non-parametric Mann-Whitney test.

2.8 Iron accumulation in immune cells of aged brains

Considering the increased Fe content and inflammation in aged brain, we wanted to know whether this could be due to the accumulation of this metal into immune cells. Thus, we quantified calcein fluorescence in each brain population. Fig.56 shows that old mice has considerably higher amount of Fe in immune cells, regardless of the population analyzed.

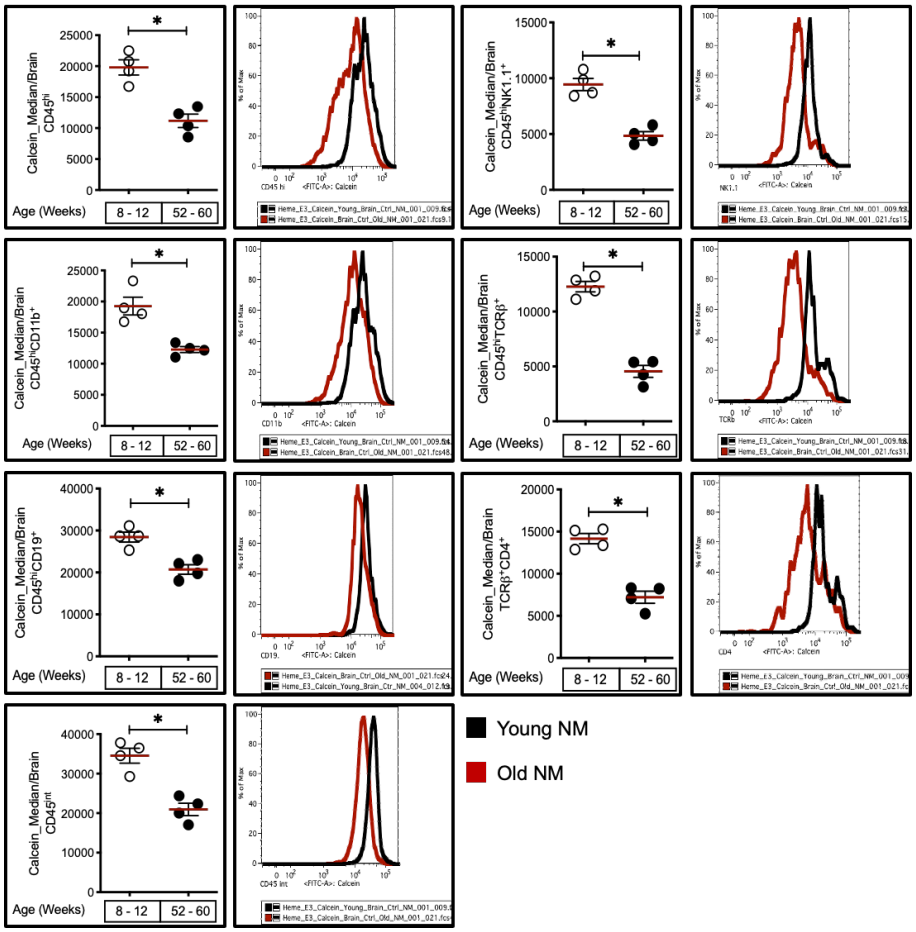

Fig. 56- Quantification of brain Fe accumulation in infiltrated peripheral and resident immune cells. Young (8-12 weeks old) and old (52-60 weeks old) mice were used for the experiment. The graphs represent: CD45hi- peripheral leukocytes, CD11b- Macrophages, CD19- B cells, NK1.1- Natural killer cells, TCRβ- T cells, TCRβCD4+- Helper T cells and the resident cells: CD45int- Microglia. The results were expressed as mean ± standard deviation (4 animals per group). Asterisks refer to a statistically significant difference. * $p < 0.05$, defined by applying non-parametric Mann-Whitney test.

2.9 Iron accumulation in PBL immune cells of aged brains

We tested whether infiltrated peripheral immune cells were Fe-loaded, when entering the brain. To confirm the hypothesis, we measured calcein fluorescence in PBLs immune cells.

The data shows no significant difference between young and old mice (Fig.57), suggesting that Fe loaded inflammatory cells have mostly infiltrated tissues, like the brain.

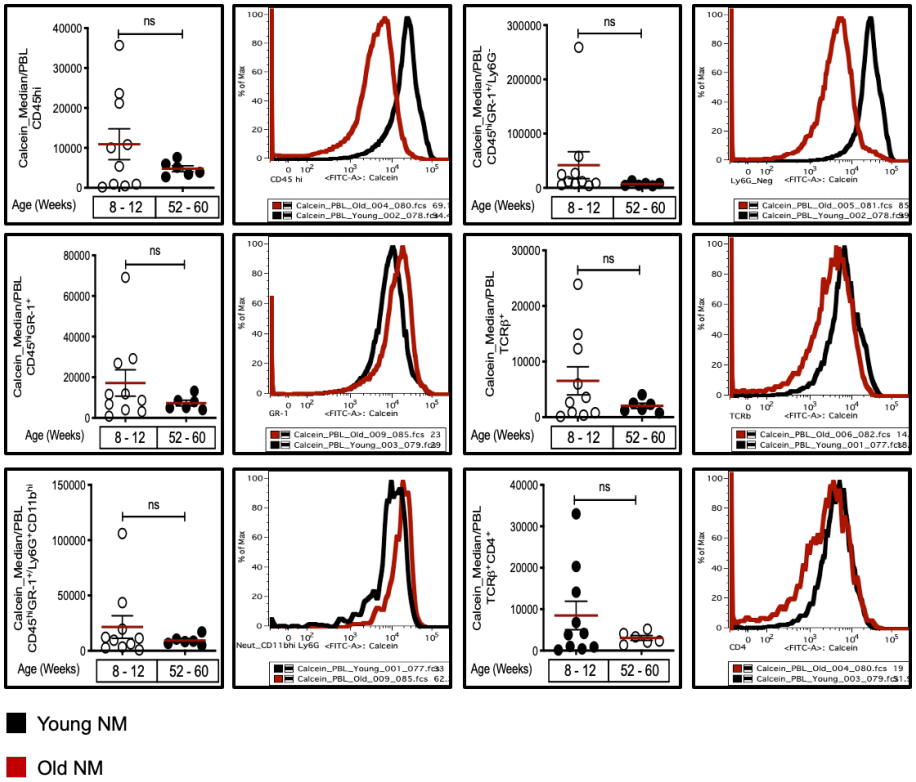

Fig. 57- Quantification of brain Fe accumulation in PBL cells. Young (8-12 weeks old) and old (52-60 weeks old) were used for the experiment. The graphs represent: CD45hi-Leukocytes, CD11b- Macrophages, CD19- B cells, NK1.1- Natural killer cells, TCRβ- T cells, TCRβCD4+- Helper T cells, and the resident cells: CD45int-Microglia. The results were expressed as mean ± standard deviation (10 animals per group). Asterisks refer to a statistically significant difference. * $p < 0.05$, defined by applying non-parametric Mann-Whitney test.

CHAPTER 3

3 Heme accumulation during aging

As previously shown, Heme is a pro-inflammatory molecule capable to disrupt BBB integrity and prime the brain to neuroinflammation, regardless of age. To assess whether an exogenous and peripheral Heme administration fosters this phenomenon and causes neuronal damage by promoting immune cells infiltration, we investigated its effects when injected into old mice.

3.1 Decreased peripheral immune cell infiltration in old mice upon Heme administration

As observed in the graph below and contrary to our expectations, exogenous and peripheral Heme administration reduced the number of infiltrated immune cells and their activation, in the brain of old mice.

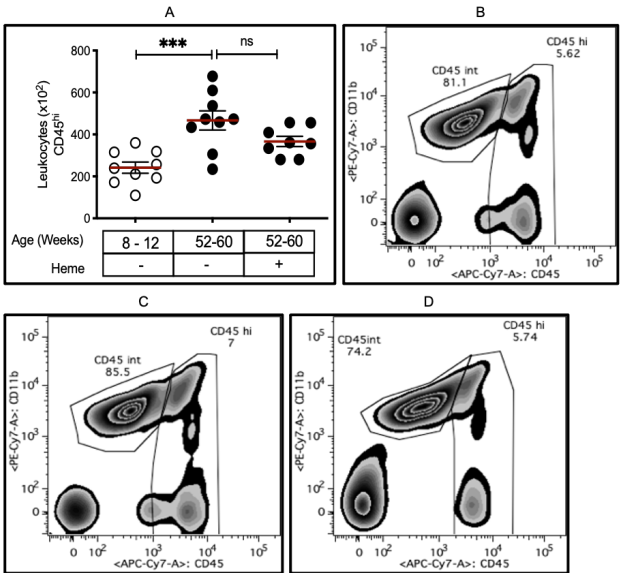

Fig. 58- Peripheral leukocytes infiltration in the brain of aged mice upon Heme injection. Young (8-12 weeks old), old (52-60 weeks old) and Heme-treated old animals were used for the experiment. Graph (A) shows the number of peripheral leukocytes (CD45hi). The differences were also observed in freshly isolated brain leukocytes from (B) young, (C) old and (D) Heme-treated old mice. The results were expressed as mean ± standard deviation (8-9 animals per group). Asterisks refer to a statistically significant difference. ns $p>0.05$, *** $p > 0.001$, defined by applying one-way ANOVA test.

3.2 Heme administration reduces the brain inflammatory profile in old mice

Given the decrease of leukocytes infiltration into the brain, we assessed whether the same tendency was maintained for their inflammatory profile. As shown in Fig.59, peripheral Heme administration significantly decreases leukocytes activation in old mice, reaching approximately the same levels than young animals.

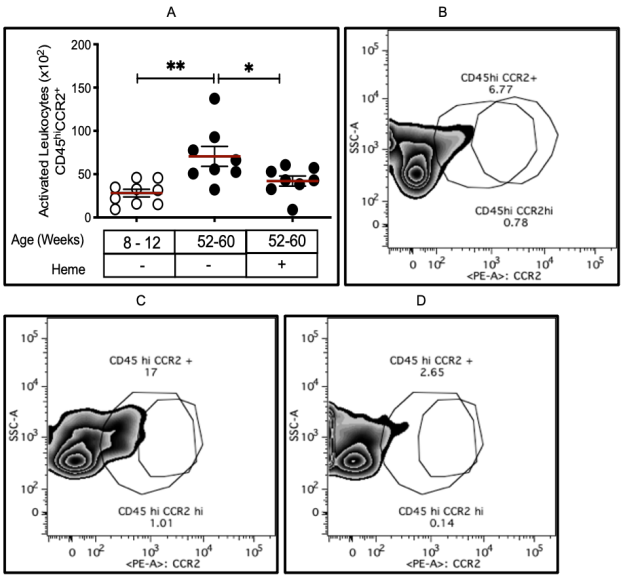

Fig. 59- Peripheral leukocytes activation in the brain of aged mice after Heme injection. Young (8-12 weeks old), old (52-60 weeks old) and Heme-treated old animals were used for the experiment. Graph (A) shows the number of peripheral leukocytes (CD45hiCCR2+). The differences were also observed in freshly isolated brain leukocytes from (B) young, (C) old and (D) Heme-

treated old mice. The results were expressed as mean ± standard deviation (8-9 animal per group). Asterisks refer to a statistically significant difference. *p <0.05, ** p > 0.01, defined by applying one-way ANOVA test.

Similar patterns were observed in relation to the quantification of MHCII expression on these cells, which was significantly lower in injected old mice, when compared to non-manipulated aged-matched controls (Fig.60).

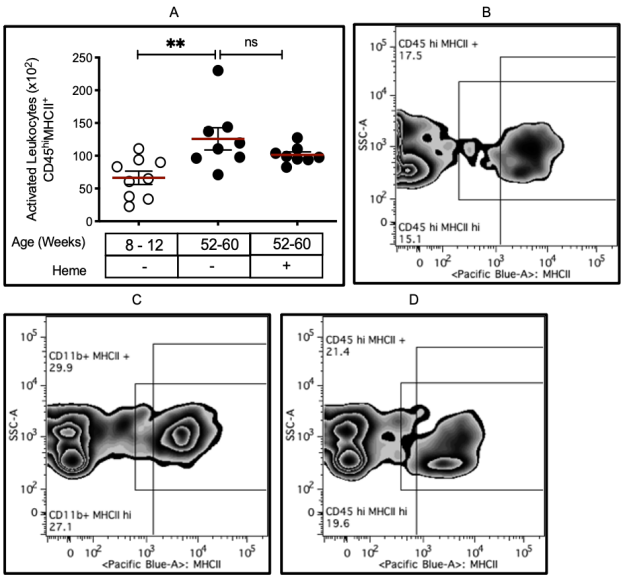

Fig. 60- Peripheral leukocytes activation in the brain of aged mice after Heme injection. Young (8-12 weeks old), old (52-60 weeks old) and Heme-treated old animals were used for the experiment. Graph (A) shows the number of peripheral leukocytes (CD45hiMHCII+). The differences were also observed in freshly isolated brain leukocytes from (B) young, (C) old and (D) Heme-treated old mice. The results were expressed as mean ± standard deviation (8 animals per group). Asterisks refer to a statistically significant difference. *p <0.05, ** p > 0.01, defined by applying one-way ANOVA test.

3.3 Heme administration in old mice decreased neutrophils activation in the brain

Although no significant difference was observed in old mice, treated or not with Heme, when injected, aged mice presented a

reduced neutrophil count. The number of these cell and their activation decreased closer to young non-manipulated animals (Fig.61-62).

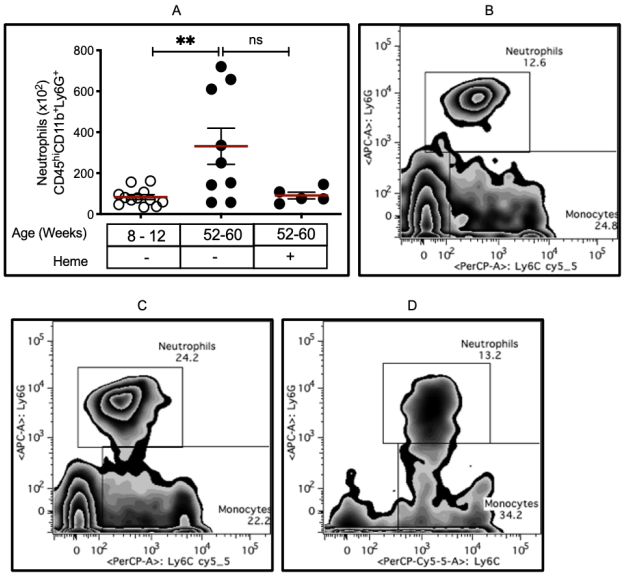

Fig. 61- Neutrophils´ infiltration into the brain of aged mice after peripheral Heme injection. Young (8-12 weeks old), old (52-60 weeks old) and Heme-treated old animals were used for the experiment. Graph (A) shows the number of neutrophils (Ly6G+). The differences were also observed in freshly isolated brain leukocytes from (B) young, (C) old and (D) Heme-treated old mice. The results were expressed as mean ± standard deviation (5-12 animal per group). Asterisks refer to a statistically significant difference. *p <0.05, ** p > 0.01, defined by applying the non-parametric Kruskal-Wallis test.

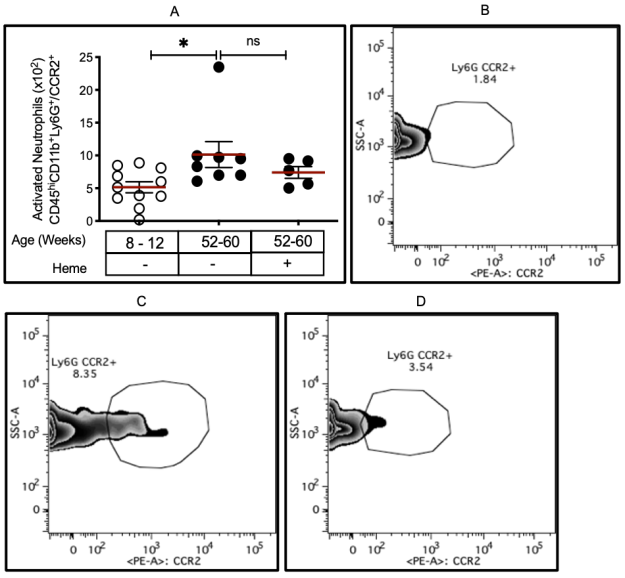

Fig. 62- Neutrophils' activation in the brain of aged mice after peripheral Heme injection. Young (8-12 weeks old), old (52-60 weeks old) and Heme-treated old animals were used for the experiment. Graph (A) shows the number of inflammatory neutrophils (Ly6G+CCR2+). The differences were also observed in freshly isolated brain leukocytes from (B) young, (C) old and (D) Heme-treated old mice. The results were expressed as mean ± standard deviation (5-11 animals per group). Asterisks refer to a statistically significant difference. ns $p > 0.05$, * $p > 0.05$, defined by applying the non-parametric Kruskal-Wallis test.

3.4 Heme administration in old mice decreased the number of monocytes and their activation into the brain

Tendencies similar to the data previously described were obtained for infiltrating inflammatory monocytes/macrophages (Fig.63). Their activation was assessed by measuring the expression of CCR2 marker within $Ly6C^+$. In this condition, the decrease in CCR2 was not significant (Fig.64).

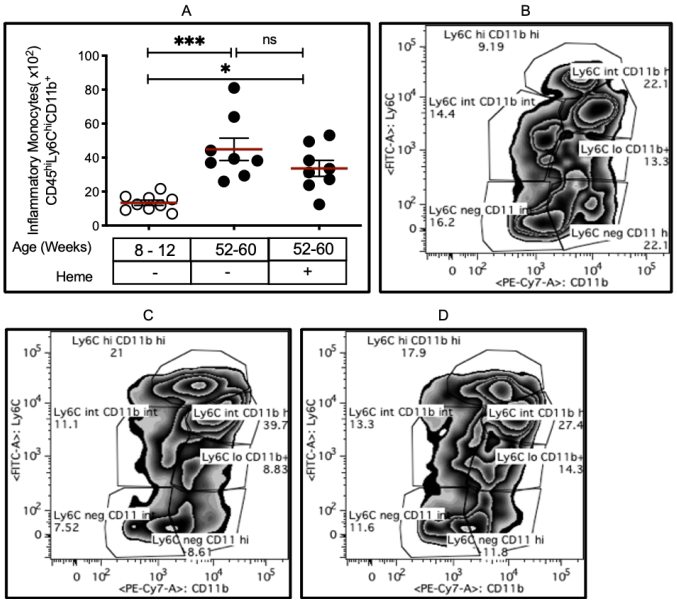

Fig. 63- Monocyte's infiltration into the brain of aged mice after peripheral Heme injection. Young (8-12 weeks old), old (52-60 weeks old) and Heme-treated old animals were used for the experiment. Graph (A) shows the number of monocytes (Ly6C+) The differences were also observed in freshly isolated brain leukocytes from (B) young, (C) old and (D) Heme-treated old mice. The results were expressed as mean ± standard deviation (8 animals per group). Asterisks refer to a statistically significant difference. ns $p > 0.05$, *** $p > 0.001$, defined by applying one-way ANOVA test.

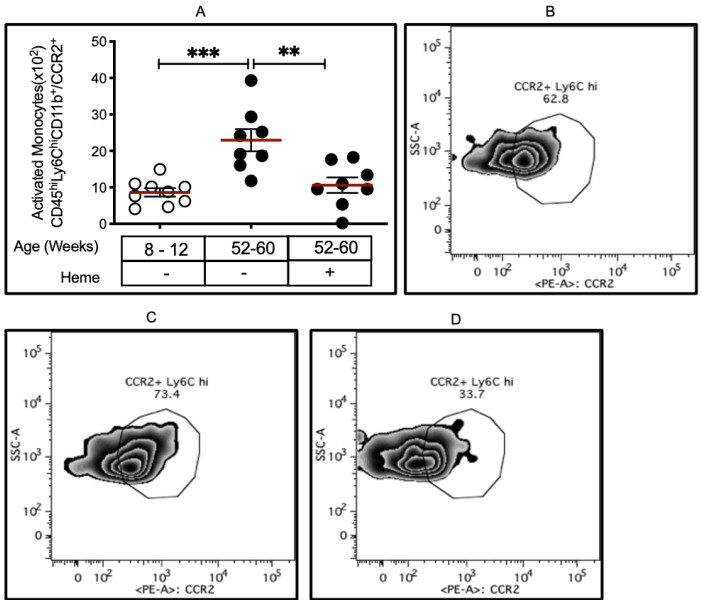

Fig. 64- Monocytes' activation in the brain of aged mice after peripheral Heme injection. Young (8-12 weeks old), old (52-60 weeks old) and Heme-treated old animals were used for the experiment. Graph (A) shows the number of inflammatory monocytes (Ly6C+CCR2+) The differences were also observed in freshly isolated brain leukocytes from (B) young, (C) old and (D) Heme-treated old mice. The results were expressed as mean ± standard deviation (8-9 animals per group). Asterisks refer to a statistically significant difference. ** $p < 0.01$, *** $p > 0.001$, defined by applying one-way ANOVA test.

3.5 Heme administration in old mice decreased the number microglia and their activation in the brain

When assessing microglia, we observed that peripheral Heme administration in old mice significantly decreases their number, in relation to old non-manipulated controls. Interestingly, their count was significantly lower even in relation to young non-treated animals (Fig.65).

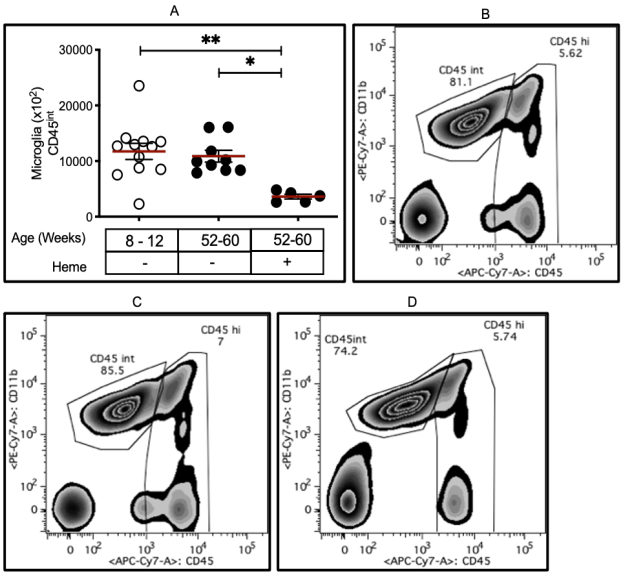

Fig. 65- Microglia proliferation in the brain of aged mice after peripheral Heme injection. Young (8-12 weeks old), old (52-60 weeks old) and Heme-treated old animals were used for the experiment. Graph (A) shows the number of microglia cells (CD45int). The differences were also observed in freshly isolated brain leukocytes from (B) young, (C) old and (D) Heme-treated old mice. The results were expressed as mean ± standard deviation (5-11 animals per group). Asterisks refer to a statistically significant difference. * $p < 0.05$, ** $p > 0.01$, defined by applying the non-parametric Kruskal-Wallis test.

Regarding the inflammatory profile, microglia became less inflammatory upon peripheral Heme administration to old mice, as evaluated by measuring the expression of MHCII marker (Fig.66).

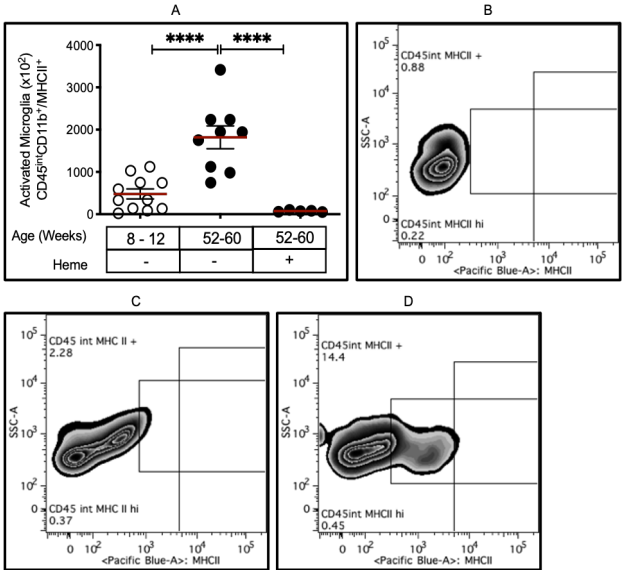

Fig. 66- Microglia activation in the brain of aged mice after peripheral Heme injection. Young (8-12 weeks old), old (52-60 weeks old) and Heme-treated old animals were used for the experiment. Graph (A) shows the number of activated microglia (CD45intMHCII+). The differences were also observed in freshly isolated brain leukocytes from (B) young, (C) old and (D) Heme-treated old mice. The results were expressed as mean ± standard deviation (5-11 animals per group). Asterisks refer to a statistically significant difference. **** $p < 0.0001$, defined by applying the non-parametric Kruskal-Wallis test.

Despite the lack of significance, the analysis of CCR2 levels in these cells shows similar results, in the sense they present a reduced recruitment capacity when compared to non-manipulated old mice, resembling that of young non-manipulated mice (Fig.67).

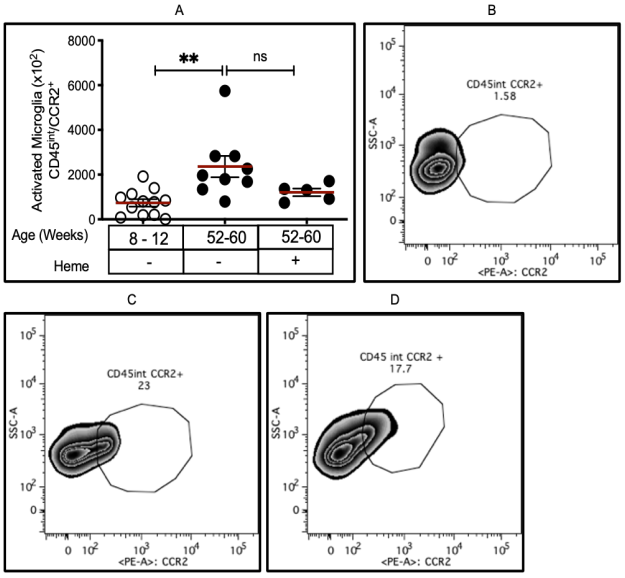

Fig. 67- Microglia activation in the brain of aged mice after peripheral Heme injection. Young (8-12 weeks old), old (52-60 weeks old) and Heme-treated old animals were used for the experiment. Graph (A) shows the number of activated microglia (CD45intCCR2+). The differences were also observed in freshly isolated brain leukocytes from (B) young, (C) old and (D) Heme-treated old mice. The results were expressed as mean ± standard deviation (5-11 animals per group). Asterisks refer to a statistically significant difference. ns $p > 0.05$, ** $p > 0.01$, defined by applying the non-parametric Kruskal-Wallis test.

3.6 Heme administration in old mice decreased the number of T cells in the brain

We then characterized the lymphocytic compartment in old mice peripherally injected with Heme, as expecting potential differences in the ability of these cells to invade the brain and contribute to neuroinflammation. The analysis and quantification of our results lead to conclusions similar to previous findings.

In the figure below, we can observe an increased number of T cells in the brain of old mice in relation to young animals, which diminishes if the formers were administered with exogenous peripheral Heme (Fig.68). To note that Heme-treated old mice display similar number of TCRβ positive cells, as young non-manipulated mice.

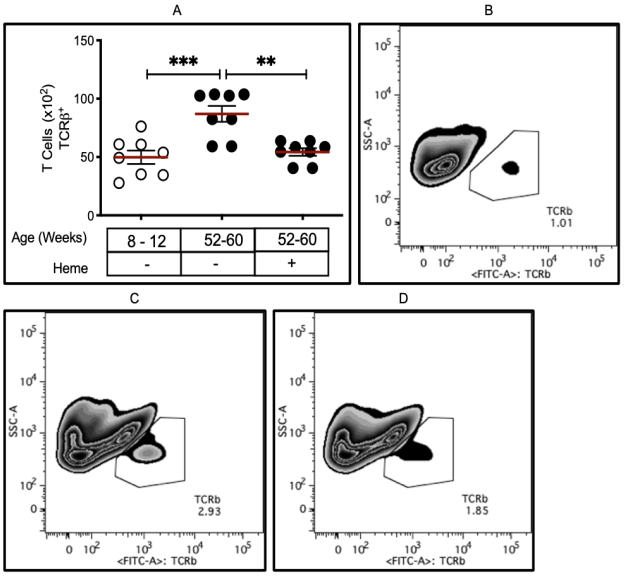

Fig. 68- T Cells infiltration in the brain of aged mice after Heme injection. Young (8-12 weeks old), old (52-60 weeks old) and Heme-treated old animals were used for the experiment. Graph (A) shows the number of T cells (TCRβ+). The differences were also observed in freshly isolated brain leukocytes from (B) young, (C) old and (D) Heme-treated old mice. The results were expressed as mean ± standard deviation (8 animals per group). Asterisks refer to a statistically significant difference. ** $p < 0.01$, *** $p > 0.001$, defined by applying the one-way ANOVA test.

We evaluated the expression of CD4 and CD8 T cells as well as their activation, obtaining similar trends than in previous figures (Fig.69). A decrease in both CD4+ and CD8+ T cell count was found in the brain of peripherally Heme-treated old mice, when compared to non-manipulated controls, reaching levels similar to young non-manipulated mice.

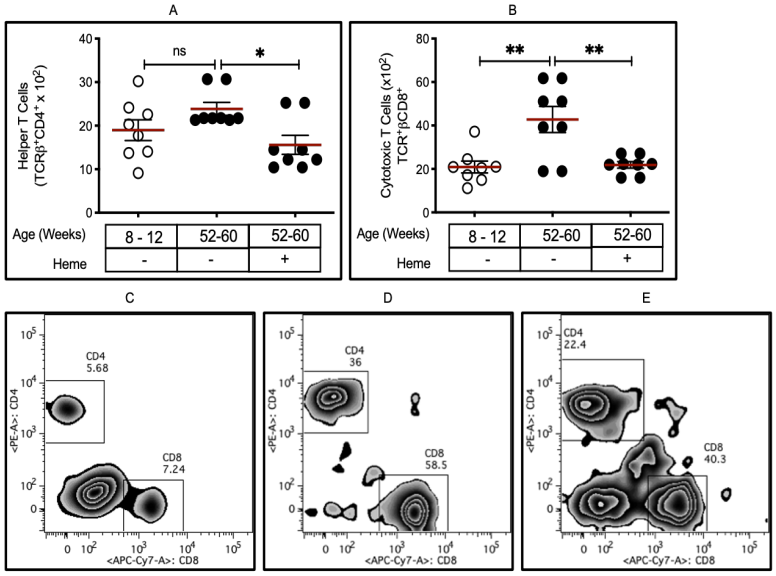

Fig. 69- Helper T cells and cytotoxic T cell infiltration into the brain of aged mice after peripheral Heme injection. Young (8-12 weeks old), old (52-60 weeks old) and Heme-treated old animals were used for the experiment. Graph (A) shows the number of helper T cells (TCRβ+CD4+), while (B) illustrates cytotoxic T cell count (TCRβ+CD8+). Differences were also observed in freshly isolated brain leukocytes from (C) young, (D) old and (E) Heme-treated old mice. The results were expressed as mean ± standard deviation (8 animals per group). Asterisks refer to a statistically significant difference. ns $p > 0.05$, * $p > 0.05$, defined by applying the one-way ANOVA test.

When characterizing the activation of lymphocyte sub-populations, we observed that old animals showed a slight and not significant decrease in naïve T cells, when compared to young mice, which does not change in response to exogenous peripheral Heme administration. The number of activated $CD4^+$ T cells, which were significantly increased in old non-manipulated mice in relation to young animals, drastically diminishes in the brain of aged Heme-treated mice.

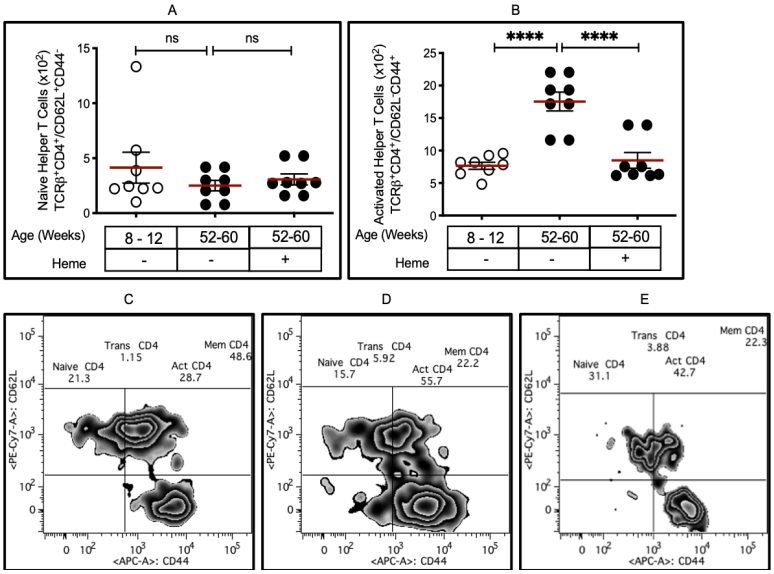

Fig. 70- Helper T cells activation in the brain of aged mice after peripheral Heme injection. Young (8-12 weeks old), old (52-60 weeks old) and Heme-treated old animals were used for the experiment. Graph (A) shows the number of naïve helper T cells (CD4+CD62L+CD44-) and (B) illustrates activated helper T cells (CD4+CD62L-CD44+). Differences were also observed in freshly isolated brain leukocytes from (C) young, (D) old and (E) Heme-treated old mice. The results were expressed as mean ± standard deviation (7-8 animals per group). The results were expressed as mean ± standard deviation. Asterisks refer to a statistically significant difference. ns $p>0.05$ **** $p < 0.0001$, defined by applying the one-way ANOVA test.

A similar pattern was found when analyzing cytotoxic T cells. The number of naïve cells decreases in old NM mice in relation to young animals, although no further reduction was observed upon peripheral Heme treatment. Contrarily, the number of activated CD8 T cells in the brain of old non-manipulated mice is significantly higher than in young animals. However, the activation of CD8 T cells, in aged mice, significantly diminishes upon peripheral Heme injection (Fig.71).

It is worth noticing that we obtained the same trend profile, regardless of the population analyzed, indicating that exogenous

peripheral Heme administration decreases the neuroinflammation presented by old mice.

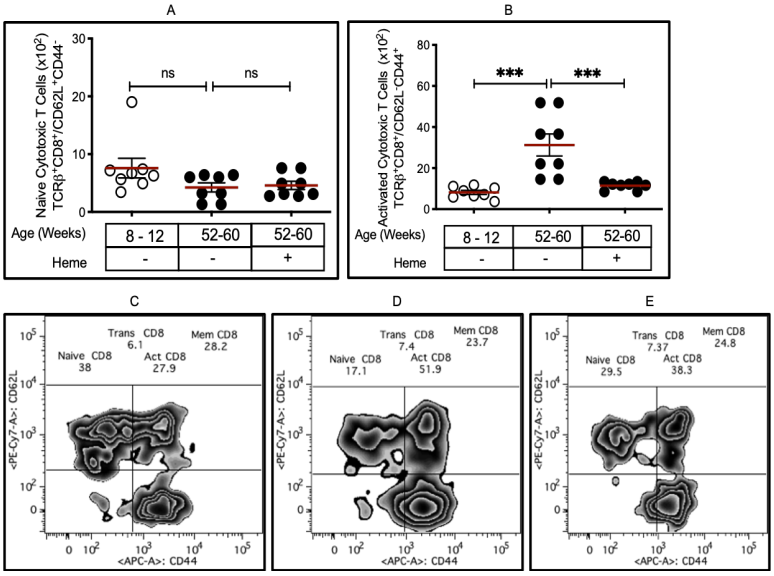

Fig. 71- Cytotoxic T cells activation in the brain of aged mice after peripheral Heme injection. Young (8-12 weeks old), old (52-60 weeks old) and Heme-treated old animals were used for the experiment. Graph (A) shows the number of naïve cytotoxic T cells (CD8+CD62L+CD44-) and (B) illustrates activated cytotoxic T cells (CD4+CD62L-CD44+). Differences were also observed in freshly isolated brain leukocytes from (C) young, (D) old and (E) Heme-treated old mice. The results were expressed as mean ± standard deviation (8 animals per group). Asterisks refer to a statistically significant difference. Ns $p>0.05$, *** $p < 0.001$, defined by applying the one-way ANOVA test.

3.7 Peripheral immune cells analysis in Heme-treated old mice

Considering that Heme induces a significant decrease in inflammation, in the brain of old mice, we aimed to assess whether this effect is due to the retention of inflammatory cells into the peripheral compartment. Thus, we analyzed the inflammatory states of spleen and PBL cells as well as the changes in the accumulation of Fe in those tested immune cells.

3.7.1 Spleen immune cells' profile in Heme-treated old mice

Although not significant, we observed in the spleen the same profile found in the brain, of mice treated or not with peripheral injections of Heme (Fig.72).

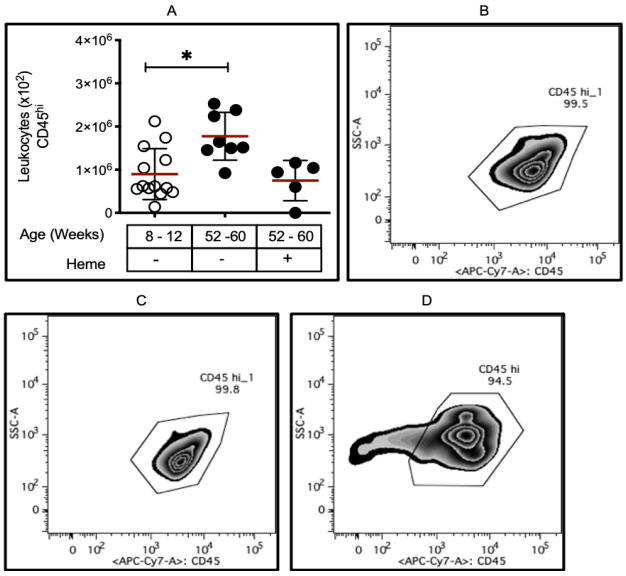

Fig. 72- Leukocytes' profile in aged mice after Heme injection. Young (8-12 weeks old), old (52-60 weeks old) and Heme-treated old animals were used for the experiment. Graph (A) shows the number of peripheral leukocytes (CD45hi). The differences were also observed in freshly isolated spleen from (B) young, (C) old and (D) Heme-treated old mice. The results were expressed as mean ± standard deviation (5-13 animals per group). Asterisks refer to a statistically significant difference. * $p<0.05$, defined by applying the non-parametric Kruskal-Wallis test.

When we assessed total leukocytes activation, we observed in the spleen a profile similar to what found in the brain. Exogenous peripheral Heme administration into old mice significantly decreased the level of inflammation (Fig.73).

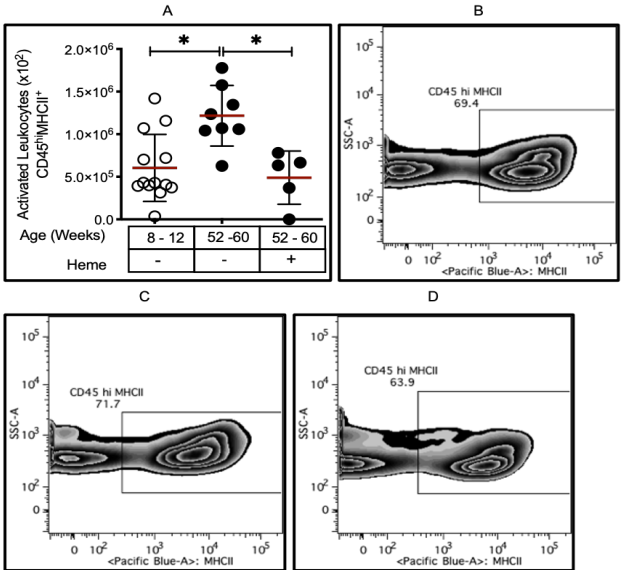

Fig. 73- Leukocytes' activation in aged mice after peripheral Heme injection. Young (8-12 weeks old), old (52-60 weeks old) and Heme-treated old animals were used for the experiment. Graph (A) shows the number of activated leukocytes (CD45hiMHCII+). The differences were also observed in freshly isolated spleen from (B) young, (C) old and (D) Heme-treated old mice. The results were expressed as mean ± standard deviation (5-13 animals per group). Asterisks refer to a statistically significant difference. * $p<0.05$, defined by applying the non-parametric Kruskal-Wallis test.

When assessing the number and activation of monocytes in the spleen, we observed that Heme-treated old mice present a slightly higher number of activated monocytes in relation to old non-manipulated mice. However, these results were not significant (Fig.74).

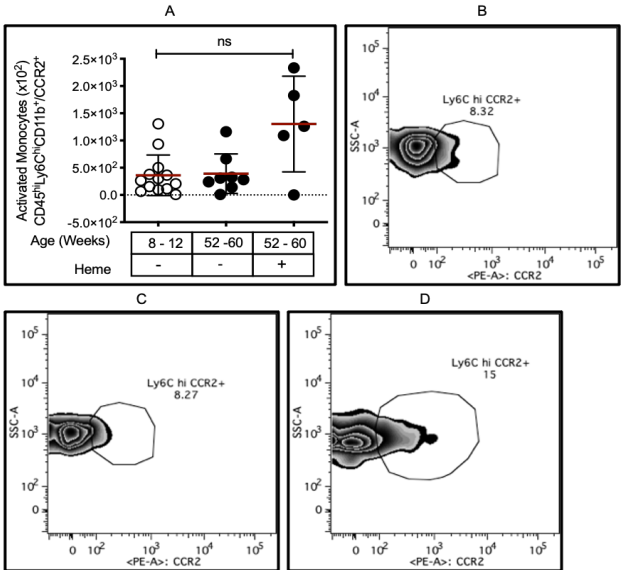

Fig. 74- Monocytes' activation in aged mice after Heme injection. Young (8-12 weeks old), old (52-60 weeks old) and Heme-treated old animals were used for the experiment. Graph (A) shows the number of activated monocytes (Ly6C+CCR2+). The results were also observed in freshly isolated spleen from (B) young, (C) old and (D) Heme-treated old mice. The results were expressed as mean ± standard deviation (5-13 animals per group). Asterisks refer to a statistically significant difference. ns $p > 0.05$, defined by applying the non-parametric Kruskal-Wallis test.

Neutrophils' activation also follows the same pattern than activated monocytes, in the sense that Heme slightly enhances inflammation when administered to old mice (Fig.75).

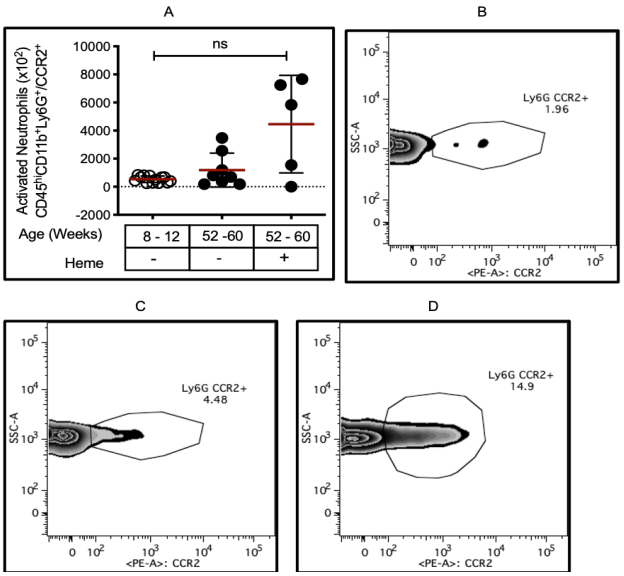

Fig. 75- Neutrophils' activation in aged mice after peripheral Heme injection. Young (8-12 weeks old), old (52-60 weeks old) and Heme-treated old animals were used for the experiment. Graph (A) shows the number of activated monocytes (Ly6G+CCR2+). The results were also observed in freshly isolated spleen from (B) young, (C) old and (D) Heme-treated old mice. The results were expressed as mean ± standard deviation (5-13 animals per group). Asterisks refer to a statistically significant difference. ns $p > 0.05$, defined by applying the non-parametric Kruskal-Wallis test.

3.7.2 PBLs immune profile in Heme treated old mice

Considering previous results, demonstrating that old mice present a similar trend for activation in relation to young mice, we assessed the ability of Heme to modulate this profile. Thus, we observed that total leukocytes in the blood of old mice decreases significantly upon Heme administration (Fig.76).

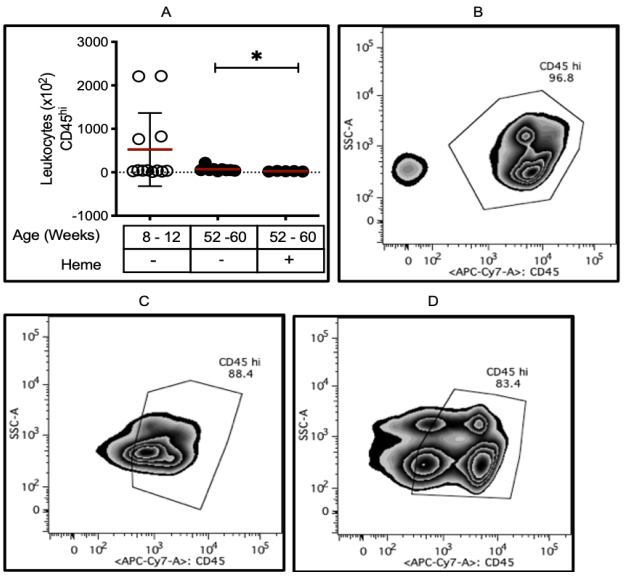

Fig. 76- PBLs immune profile in aged mice after peripheral Heme injection. Young (8-12 weeks old), old (52-60 weeks old) and Heme-treated old animals were used for the experiment. Graph (A) shows the number of leukocytes (CD45+). The results were also observed in freshly isolated spleen from (B) young, (C) old and (D) Heme-treated old mice. The results were expressed as mean ± standard deviation (5-13 animals per group). Asterisks refer to a statistically significant difference. * $p < 0.05$, defined by applying the non-parametric Kruskal-Wallis test.

When assessing the activation of these cells, we observed a similar profile, despite the lack of significance (Fig.77).

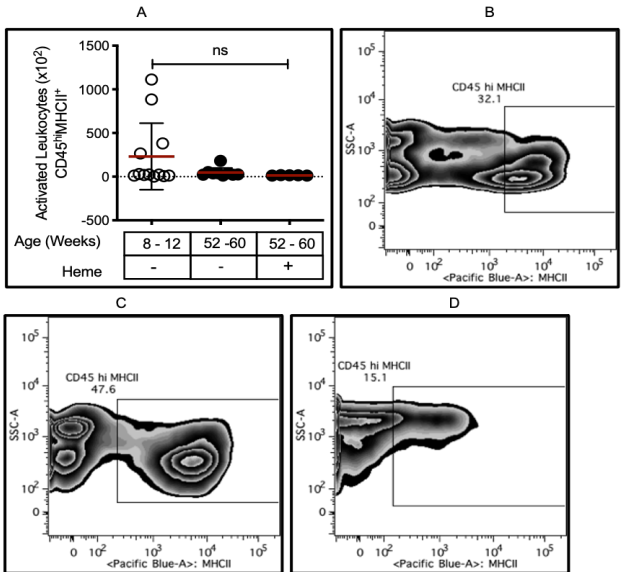

Fig. 77- PBLs activation profile in aged mice after peripheral Heme injection. Young (8-12 weeks old), old (52-60 weeks old) and Heme-treated old animals were used for the experiment. Graph (A) shows the number of activated leukocytes (CD45+MHCII+). The results were also observed in freshly isolated spleen of (B) young, (C) old and (D) Heme-treated old mice. The results were expressed as mean ± standard deviation (5-13 animals per group). Asterisks refer to a statistically significant difference. ns $p > 0.05$, defined by applying the non-parametric Kruskal-Wallis test.

When we assessed monocytes levels of activation, we found the same pattern as in previous results (Fig.78). Similar data were also obtained when analyzing the neutrophil population, i.e. inflammation is reduced upon peripheral Heme injections (Fig.79).

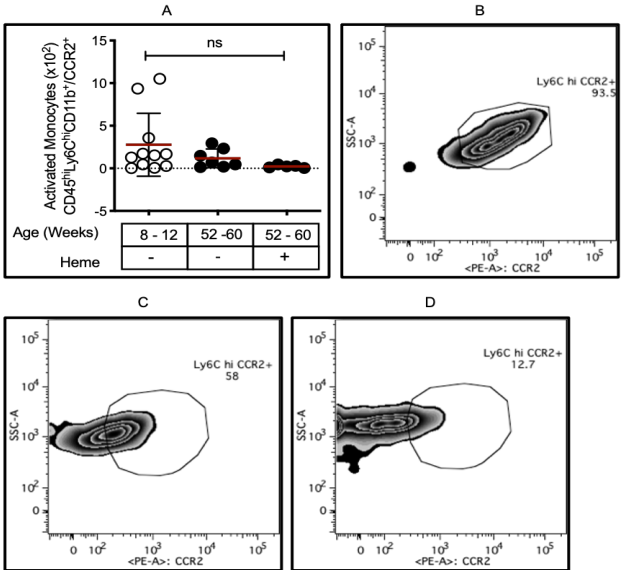

Fig. 78- PBLs activated monocytes profile in aged mice after peripheral Heme injection. Young (8-12 weeks old), old (52-60 weeks old) and Heme-treated old animals were used for the experiment. Graph (A) shows the number of activated monocytes (Ly6C+CCR2+). The results were also observed in freshly isolated spleen from (B) young, (C) old and (D) Heme-treated old mice. The results were expressed as mean ± standard deviation (5-13 animals per group). Asterisks refer to a statistically significant difference. ns p >0.05, defined by applying the non-parametric Kruskal-Wallis test.

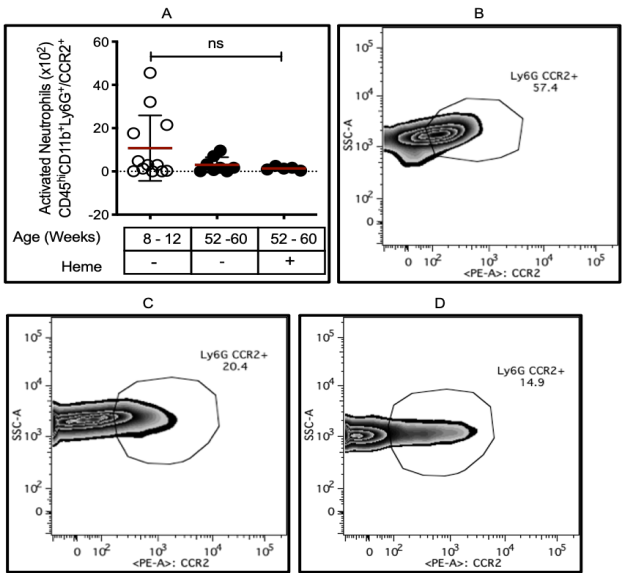

Fig. 79- PBLs activated neutrophils profile in aged mice after peripheral Heme injection. Young (8-12 weeks old), old (52-60 weeks old) and Heme-treated old animals were used for the experiment. Graph (A) shows the number of activated neutrophils (Ly6G+CCR2+). The results were also observed in freshly isolated spleen from (B) young, (C) old and (D) Heme-treated old mice. The results were expressed as mean ± standard deviation (5-13 animals per group). Asterisks refer to a statistically significant difference. ns $p > 0.05$, defined by applying the non-parametric Kruskal-Wallis test.

3.7 Iron accumulation in Brain immune cells

We observed that Heme sensitizes young mice to develop a neuroinflammatory profile, an effect not observed in older animals, where exogenous peripheral Heme administration was found to diminish the increase in immune cells' activation into the brain, which physiologically occurs during aging. We then assessed the ability of Heme to cause brain Fe accumulation, possibly induced by the infiltration of immune cells in this organ during aging. Contrarily to the expectation, exogenous Heme administration does not increase the amount of Fe in the immune cells of these animals (Fig.80). Whether this could be explained by the high level of intracellular Fe that immune cells already present during aging, which prevents the further entry of this metal, is likely the case, and supported by similar values of Calcein-quenched Fe.

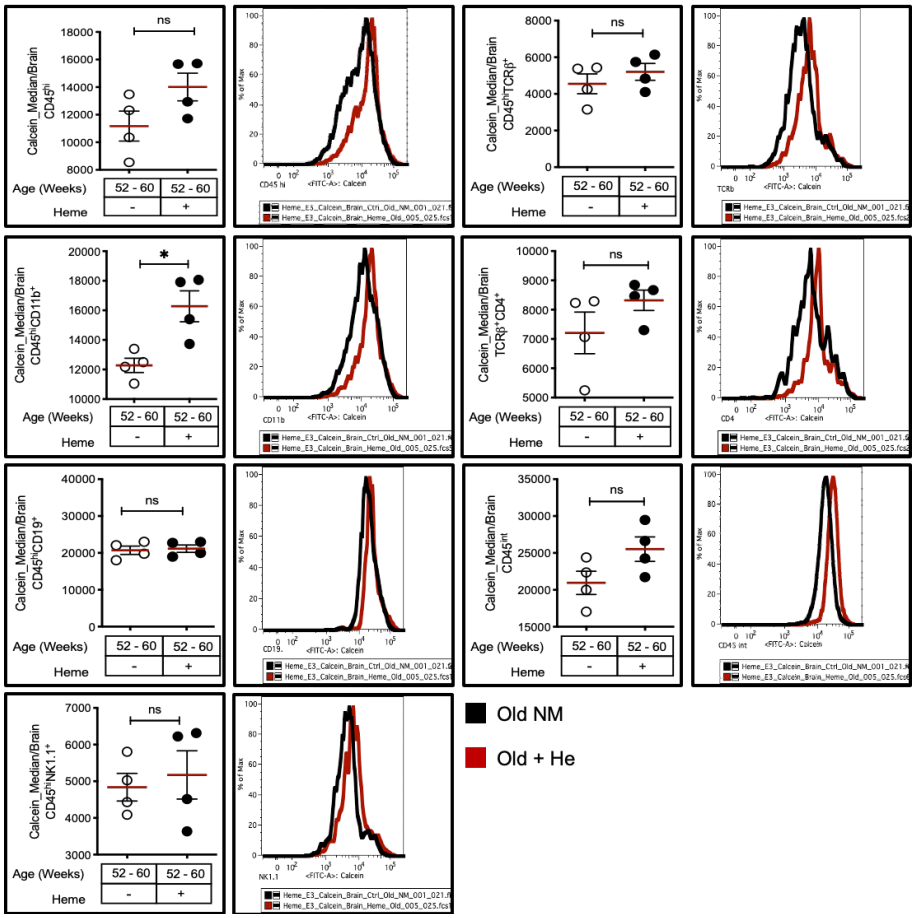

Fig. 80- Quantification of brain Fe accumulation in infiltrated peripheral and resident immune cells. Old (52-60 weeks old) and peripherally Heme-treated old mice were used for the experiment. The graphs show: CD45hi- peripheral leukocytes, CD11b- Macrophages, CD19- B cells, NK1.1- Natural killer cells, TCRβ- T cells, TCRβCD4+- Helper T cells and the resident cells: CD45int- Microglia. The results were expressed as mean ± standard deviation. Asterisks refer to a statistically significant difference. ns $p > 0.05$ * $p < 0.05$, defined by applying the non-parametric Mann-Whitney t test.

3.8 Iron accumulation in PBL immune cells

Given the unexpected results, obtained in the brain of peripheral Heme-treated old mice, we assessed the effect of Heme/Fe administration into circulation by measuring calcein fluorescence in

PBL immune cells. The figure below shows an enhanced Fe accumulation in old Heme-treated mice (Fig.81).

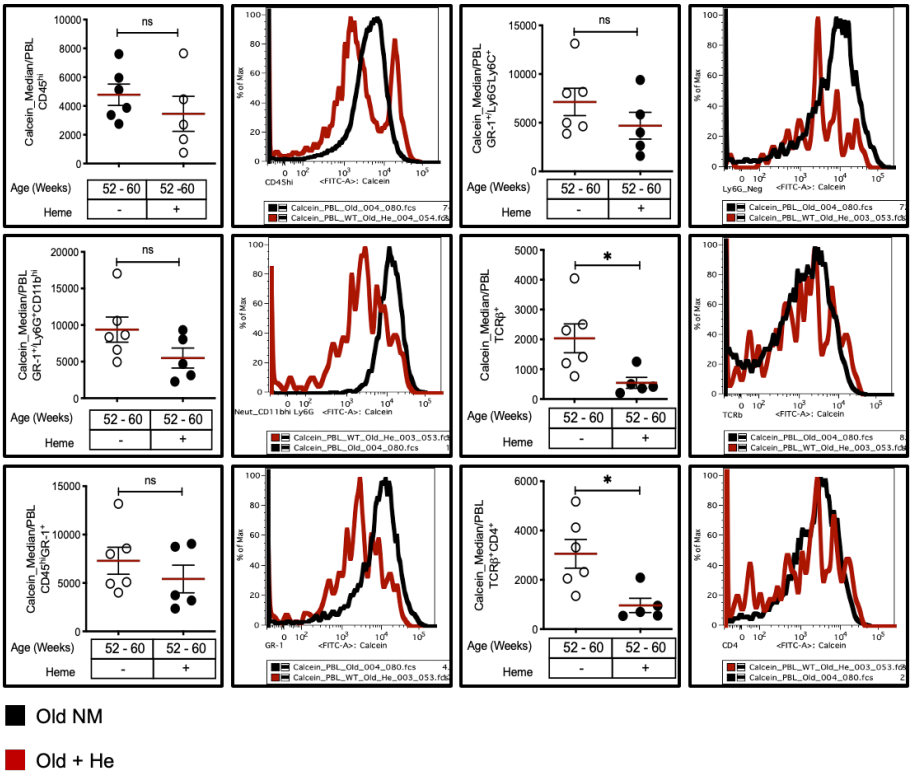

Fig. 81- Quantification of Fe accumulation PBL immune cells. Old (52-60 weeks old) and peripheral Heme-treated old mice were used for the experiment. The graphs show: CD45hi-Leukocytes, Ly6G+/Ly6G+CD11b+-neutrophils, Ly6G-Ly6C+- monocytes, TCRβ- T cells, TCRβCD4+- Helper T cells. The results were expressed as mean ± standard deviation. Asterisks refer to a statistically significant difference. ns $p > 0.05$ * $p < 0.05$, defined by applying the non-parametric Mann-Whitney t test.

CHAPTER 4

4 Immune system modulation

Aging is a physiological sub-chronic inflammatory disease, which leads to develop a neuroinflammatory phenotype, characterized by the accumulation of Fe in the brain. Disruption of Heme/Fe homeostasis, both at systemic or tissue levels, occurs physiologically during aging, being presumably the cause of altered brain function and neuronal death. One of the possible contributors for brain Fe overload, in advancing age, is BBB disruption, which increased permeability leads immune cells to infiltrate into the brain. Since Fe accumulates also in peripheral tissues, including circulating immune cells, when breaching the BBB, this Fe-loaded compartment, might increase the brain content of this metal. Capable to switch immune cell phenotype towards a pro-inflammatory status, we can consider that this potential chain of events might serve as a trigger for the development of neurodegenerative diseases, like PD. This hypothesis was tested by assessing the inflammatory profile of infiltrated and resident immune cells, in the brain of immunocompromised mice-RAG2-KO (which lack mature T and B lymphocytes) and TCRβ-KO (which lack mature T lymphocytes) animals [194]. The ability of this mice to be less susceptible to Fe-driven inflammation was expected.

4.1 Lymphocytic compartment's depletion decreases brain inflammation in young mice

Immune cells were quantified by flow cytometry, in the brain of young immunocompromised mice, as shown in the figure below. The number of infiltrated peripheral immune cells is similar in non-

manipulated mice, regardless of being WT or deficient animals. However, the level of CD45hi cells in RAG2-KO slightly increased upon peripheral Heme administration, when compared to TCRβ-KO. Heme treatment increases the number of infiltrated cells in WT mice, but not in immunocompromised animals. Regardless, peripherally Heme-treated RAG2-KO mice present a significantly lower number of infiltrated immune cells (Fig.82).

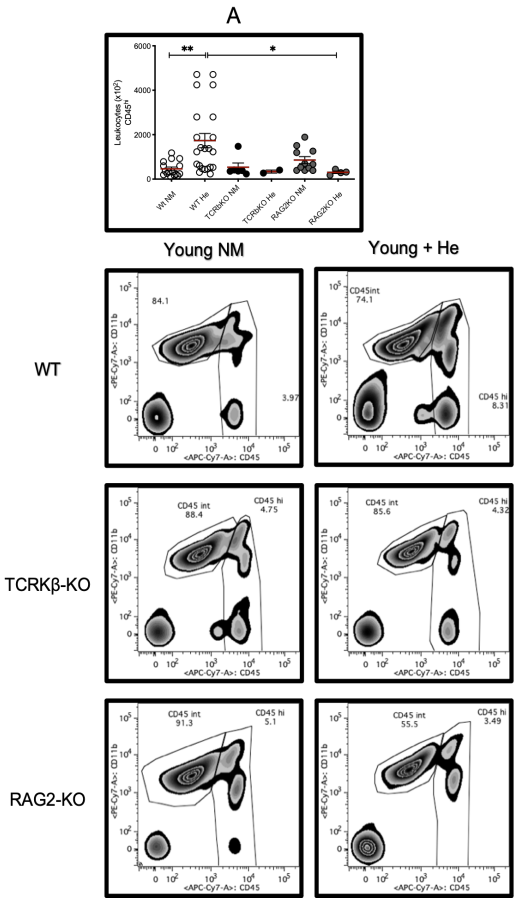

Fig. 82- Infiltration of immune cells in the brain of immunocompromised deficient mice. Young (8-12 weeks old) mice - WT, TCRKβ-KO and RAG2-KO - were used for the experiment. Graph (A) shows the number of peripheral leukocytes (CD45hi) after peripheral Heme injection. The differences were also observed in graphs obtained from freshly isolated brain leukocytes. The

results were referred to young NM mice, used as control in each genotype and expressed as mean ± standard deviation (2-11 animals per group). Asterisks refer to a statistically significance. * p <0.05, ** p <0.01, defined by applying the non-parametric Kruskal-Wallis test.

We next evaluated whether immunocompromised animals also present a different inflammatory profile. When administered to young WT mice, peripheral Heme injections promote a significant increase in CCR2+ leukocytes. Importantly, RAG2-KO mice already present a basal expression of CCR2, which is significantly higher than in non-manipulated WT and TCRβKO animals (Fig.83).

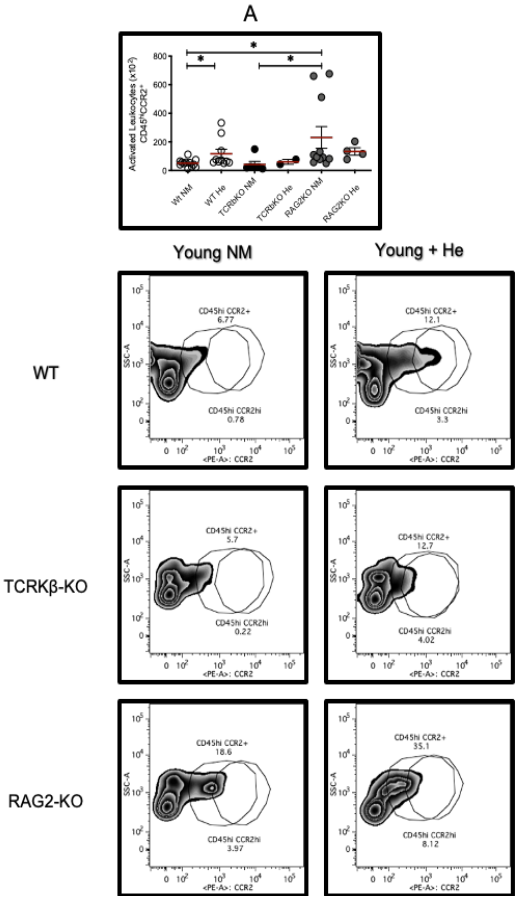

Fig. 83- Infiltration of immune cells in the brain of immunocompromised deficient mice. Young (8-12 weeks old) mice - WT, TCRKβ-KO and RAG2-KO - were used for the experiment. Graph (A) shows the number of activated leukocytes (CD45hiCCR2) after peripheral Heme injection. The differences were also observed in graphs obtained from freshly isolated brain leukocytes. The results were referred to young NM mice, used as control in each genotype and expressed as mean ± standard deviation (2-11 animals per group). Asterisks refer to a statistically significance. * $p<0.05$, defined by applying the non-parametric Kruskal-Wallis test.

It was interestingly to observe that the expression pattern of MHC II in infiltrated brain leukocytes differs. As shown in Fig.84, RAG2-KO NM mice present a significant decrease in brain inflammation when compared to WT NM and TCRβ-KO NM mice. However, Heme administration reverses this profile and increases the expression of MHC II in these cells.

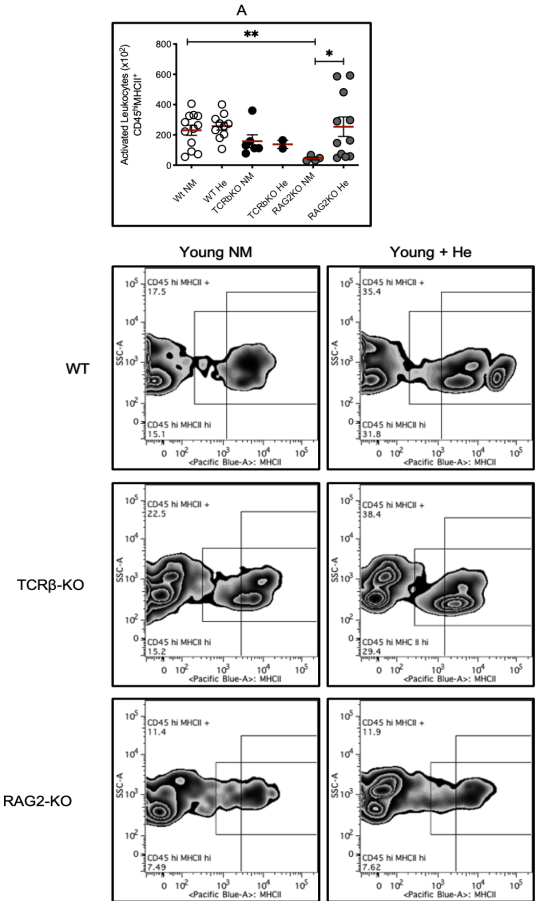

Fig. 84- Infiltration of immune cells in the brain of immunocompromised deficient mice. Young (8-12 weeks old) mice - WT, TCRKβ-KO and RAG2-KO - were used for the experiment. Graph (A) shows the number of activated leukocytes (CD45hiMHCII+) after peripheral Heme injection. The differences were also observed in graphs obtained from freshly isolated brain leukocytes. The results were referred to young NM mice, used as control in each genotype and expressed as mean ± standard deviation (2-11 animals per group). Asterisks refer to a statistically significance. ** $p<0.01$, defined by applying the non-parametric Kruskal-Wallis test.

Since Heme is capable to activate neutrophils and monocytes in the brain of young mice, we assessed whether lymphocyte depletion could affect the inflammatory profile driven by the exogenous peripheral administration of this molecule. We found an increased number of activated cells in young and NM RAG2-KO mice, these

being statistically higher in relation to NM WT or TCRβ-KO mice. However, this profile was significantly inhibited by Heme treatment (Fig.85).

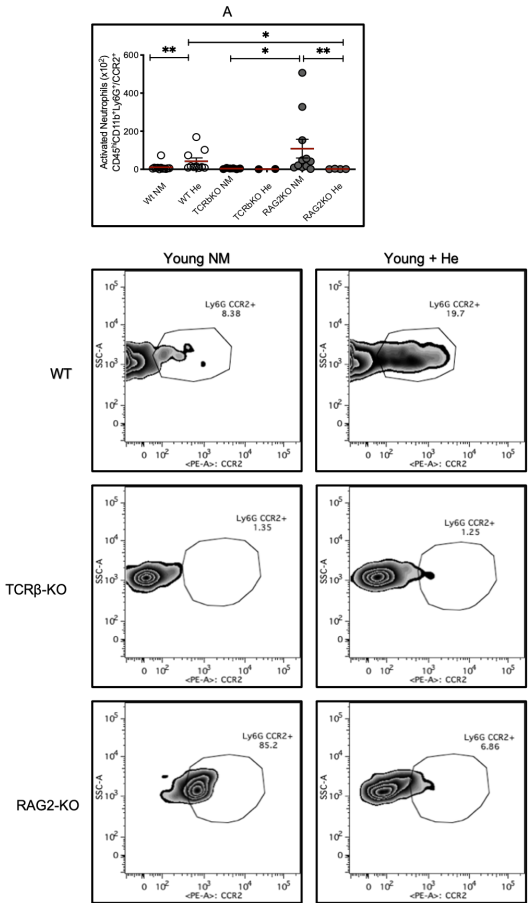

Fig. 85- Neutrophils' infiltration in the brain of immunocompromised mice. Young (8-12 weeks old) mice - WT, TCRKβ-KO and RAG2-KO - were used for the experiment. Graph (A) shows the number of activated neutrophils (Ly6G+CCR2+) after peripheral Heme injection. The differences were also observed in graphs obtained from freshly isolated brain leukocytes. The results were referred to young NM mice, used as control in each genotype and expressed as mean ± standard deviation (2-11 animals per group). Asterisks refer to a statistically significance. * $p<0.05$, ** $p<0.01$, defined by applying the non-parametric Kruskal-Wallis test.

Despite the lack of a statistically significant difference, the profile of monocytes activation is similar to that obtained for neutrophils.

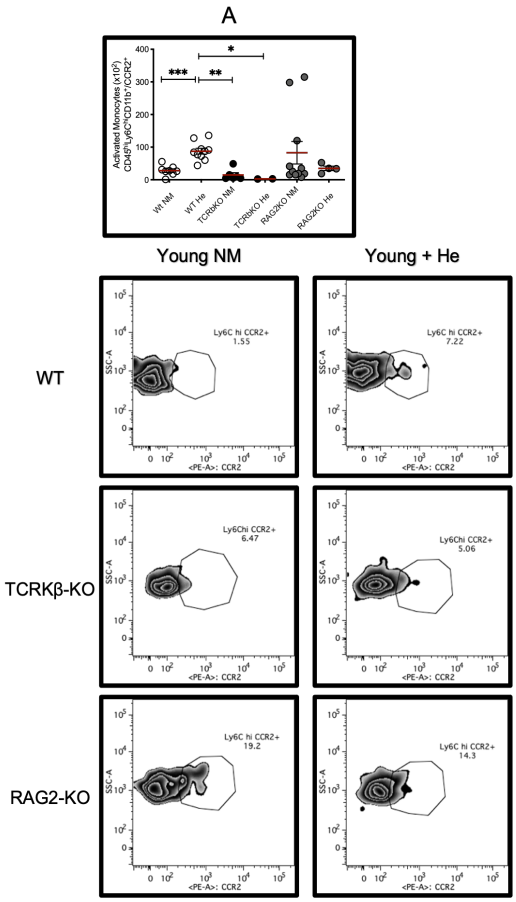

Fig. 86- Monocytes' infiltration in the brain of immunocompromised mice. Young (8-12 weeks old) mice - WT, TCRKβ-KO and RAG2-KO - were used for the experiment. Graph (A) shows the number of activated monocytes (Ly6C+CCR2+) after peripheral Heme injection. The differences were also observed in graphs obtained from freshly isolated brain leukocytes. The results were referred to young NM mice, used as control in each genotype and expressed as mean ± standard deviation (2-11 animals per group). Asterisks refer to a statistically significance. * $p<0.05$, ** $p<0.01$, *** $p<0.001$, defined by applying the non-parametric Kruskal-Wallis test.

We then assessed the inflammatory status of microglia in NM TCRβ-KO mice, which showed similar numbers as in NM WT. Although no significant difference was shown between microglia activation in NM and peripherally Heme-treated TCRβ-KO, the inflammatory profile of resident immune cells in these mice tended to decrease. The profile of microglia in RAG2-KO is shown in Fig.87 and Fig. 88. NM RAG2-KO mice presented an increased number of microglia when compared to other NM genotypes, resembling counts observed in peripheral Heme-treated WT mice. To note that the exogenous administration of Heme significantly diminished the number of microglia (Fig.87).

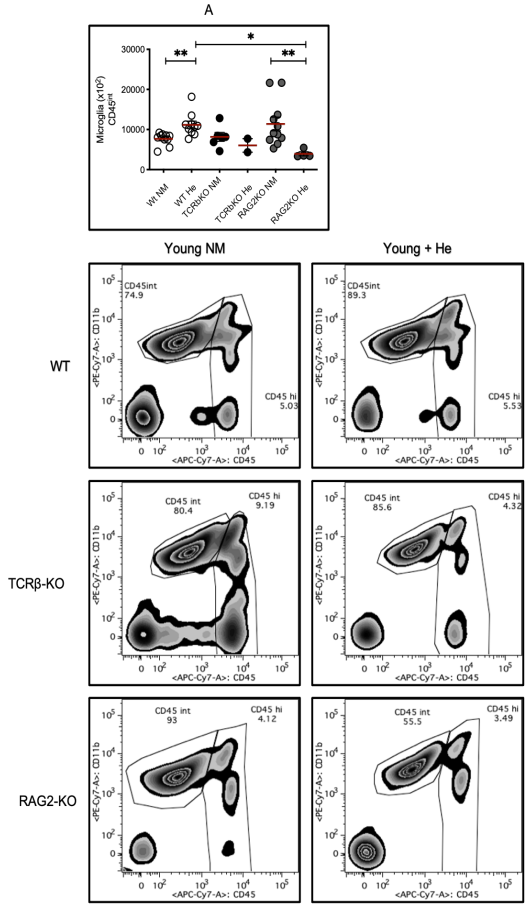

Fig. 87- Microglia analysis in the brain of immunocompromised mice. Young (8-12 weeks old) mice - WT, TCRKβ-KO and RAG2-KO - were used for the experiment. Graph (A) shows the number of microglia state (CD45int) after peripheral Heme injection. The differences were also observed in graphs obtained from freshly isolated brain leukocytes. The results were referred to young NM mice, used as control in each genotype and expressed as mean ± standard deviation (2-11 animals per group). Asterisks refer to a statistically significance. * $p<0.05$, ** $p<0.01$, defined by applying the non-parametric Kruskal-Wallis test.

We then quantified the activation of microglia in the different genotypes, assessing the expression MHCII and CCR2 marker. Peripheral Heme exogenous administration in TCRβ-KO mice decreased the expression of MHCII marker, to levels that are even lower than NM WT mice. No significant difference was observed in

RAG2-KO, receiving or not Heme administration, although the activation of microglia tends to decrease upon Heme treatment (Fig.88).

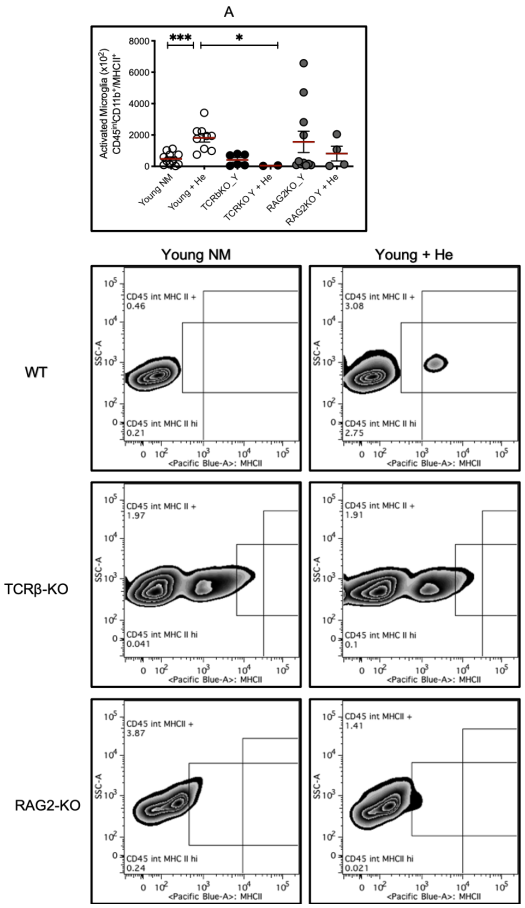

Fig. 88- Microglia activation in the brain of immunocompromised mice. Young (8-12 weeks old) mice - WT, TCRKβ-KO and RAG2-KO - were used for the experiment. Graph (A) shows the number of microglia activation (CD45intMHCII+) after peripheral Heme injection. The differences were also observed in graphs obtained from freshly isolated brain leukocytes. The results were referred to young NM mice, used as control in each genotype and expressed as mean ± standard deviation (2-11 animals per group). Asterisks refer to a statistically significance. * $p<0.05$, ***$p<0.001$, defined by applying the non-parametric Kruskal-Wallis test.

As in previous results, peripheral Heme-treated TCRβ-KO mice showed a reduced expression of CCR2 in microglia, when compared to the same treatment in WT mice. This profile was also observed in RAG2-KO mice, although the tendency was not significant. Remarkably, the activation of microglia in NM RAG2-KO at basal level is already higher and the expression of CCR2+ resembles that found in peripheral Heme-treated WT mice (Fig.89).

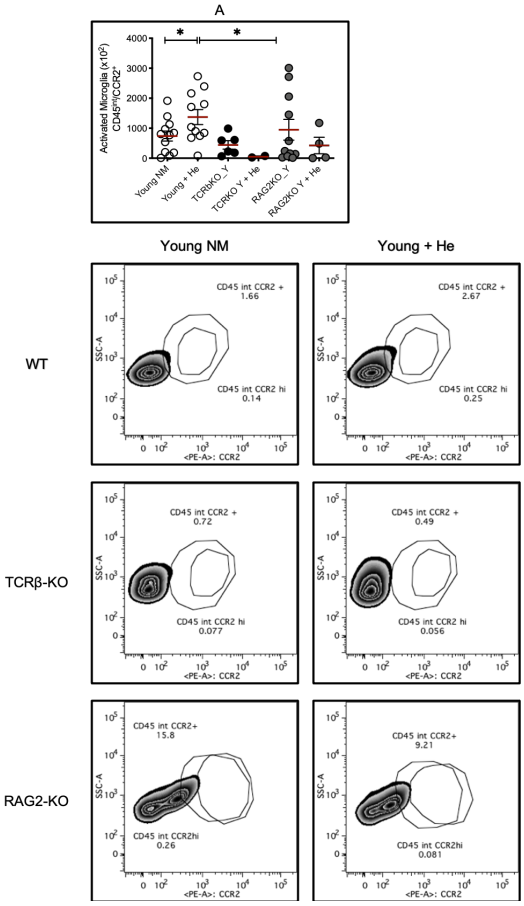

Fig. 89- Microglia activation in the brain of immunocompromised mice. Young (8-12 weeks old) mice - WT, TCRKβ-KO and RAG2-KO - were used for the experiment. Graph (A) shows the number of microglia activation (CD45intCCR2+) after peripheral Heme injection. The differences were also observed in graphs obtained from freshly isolated brain leukocytes. The results were referred to young NM mice, used as control in each genotype

and expressed as mean ± standard deviation (2-11 animals per group). Asterisks refer to a statistically significance. * $p<0.05$, defined by applying the non-parametric Kruskal-Wallis test.

4.2 Peripheral immune cells analysis in Heme-treated young mice

Considering that the depletion of the lymphocytic compartment renders the brain less inflammatory, we evaluated whether this could affect the periphery, in terms of spleen and PBL.

4.2.1 Lymphocyte depletion decreases inflammation in the spleen

While no major effects are observed between the different genotypes and their respective controls, immunocompromised mice presented lower immune cell counts when compared to WT mice, indicating a lower inflammatory profile, also in response to peripheral administration Heme, in agreement with the immune cell deficiency.

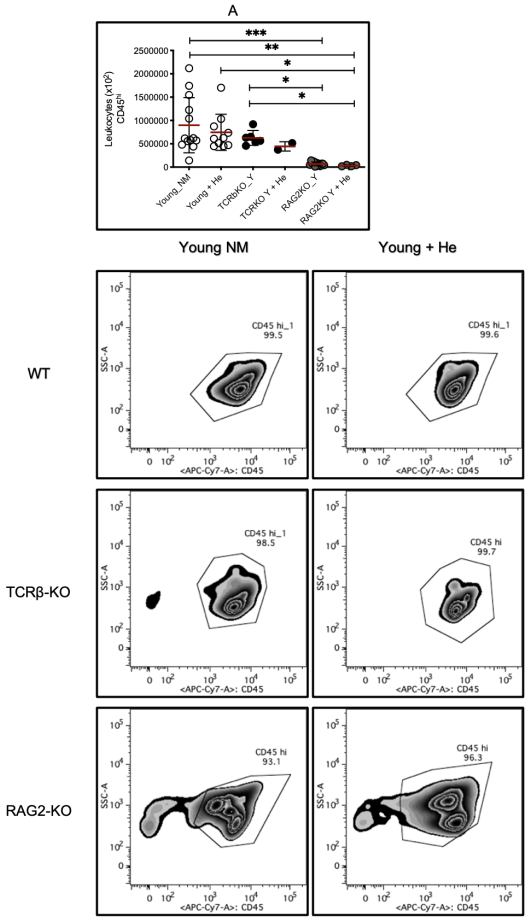

Fig. 90- Spleen immune response in immunocompromised mice. Young (8-12 weeks old) mice - WT, TCRKβ-KO and RAG2-KO - were used for the experiment. Graph (A) shows the number of peripheral leukocytes (CD45hi) after peripheral Heme injection. The differences were also observed in graphs obtained from freshly isolated spleen leukocytes. The results were referred to young NM mice, used as control in each genotype and expressed as mean ± standard deviation (2-11 animals per group). Asterisks refer to a statistically significance. * p <0.05, ** p <0.01, *** p <0.001, defined by applying the non-parametric Kruskal-Wallis test.

The mice were unresponsive to the peripheral Heme administration, when compared to each respective control. However, differences were observed among genotypes. TCRKβ-KO and RAG2-

KO animals present a lower leukocyte count, with RAG2-KO even lower (Fig.91).

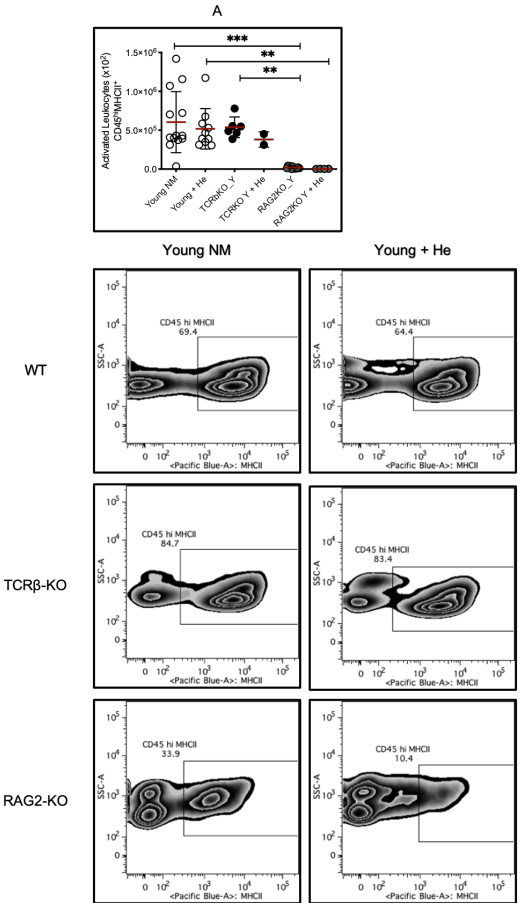

Fig. 91- Spleen immune response in immunocompromised mice. Young (8-12 weeks old) mice - WT, TCRKβ-KO and RAG2-KO - were used for the experiment. Graph (A) shows the number of activated leukocytes (CD45hiMHCII+) after peripheral Heme injection. The differences were also observed in graphs obtained from freshly isolated spleen leukocytes. The results were referred to young NM mice, used as control in each genotype and expressed as mean ± standard deviation (2-11 animals per group). Asterisks refer to a statistically significance. * $p < 0.05$, ** $p < 0.01$, *** $p < 0.001$, defined by applying the non-parametric Kruskal-Wallis test.

No significant changes were observed when analyzing the number and activation of monocytes, in all genotypes.

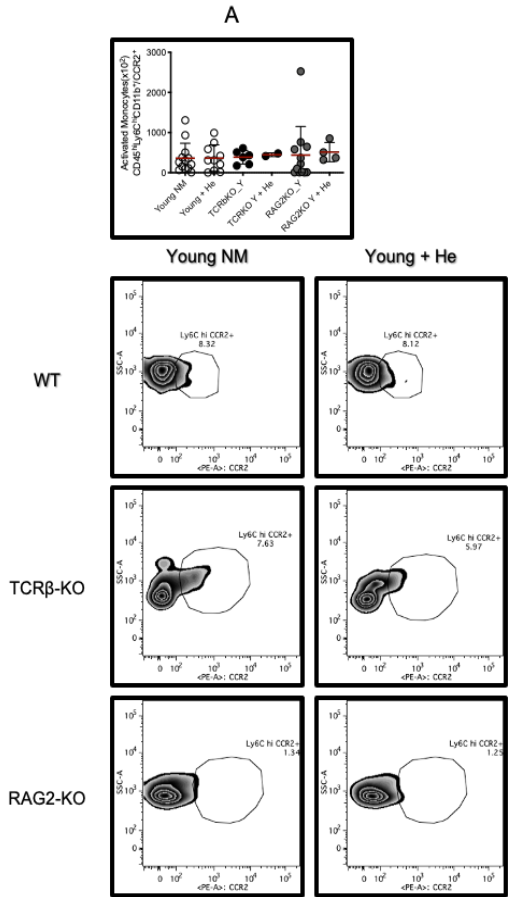

Fig. 92- Spleen immune response in immunocompromised mice. Young (8-12 weeks old) mice - WT, TCRKβ-KO and RAG2-KO - were used for the experiment. Graph (A) shows the number of activated monocytes (Ly6ChiCCR2+) after peripheral Heme injection. The differences were also observed in graphs obtained from freshly isolated spleen leukocytes. The results were referred to young NM mice, used as control in each genotype and expressed as mean ± standard deviation (2-11 animals per group). Asterisks refer to a statistically significance. ns p >0.05, defined by applying the non-parametric Kruskal-Wallis test.

4.2.2 Lymphocyte depletion decreases inflammation in circulation

WT mice present a significantly higher number of circulating leukocytes than TCRβ-KO or in RAG2-KO animals (Fig.93).

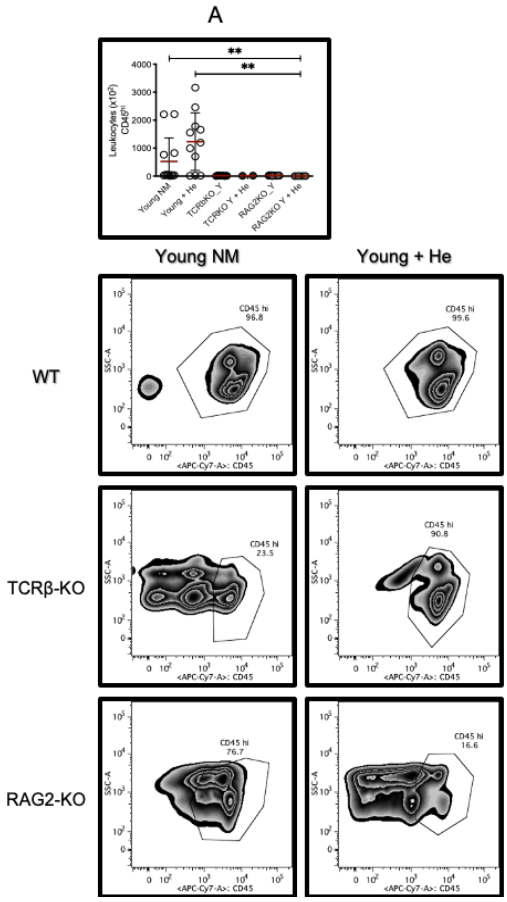

Fig. 93- PBLs immune response in immunocompromised mice. Young (8-12 weeks old) mice - WT, TCRKβ-KO and RAG2-KO - were used for the experiment. Graph (A) shows the number of circulating leukocytes (CD45+) after peripheral Heme injection. The differences were also observed in graphs obtained from freshly isolated PBLs. The results were referred to young NM mice, used as control in each genotype; expressed as mean ± standard deviation (2-11 animals per group). Asterisks refer to a statistically significance. ** p <0.01, defined by applying the non-parametric Kruskal-Wallis test.

Similar results were also obtained when evaluating leukocytes activation. Whether the lack of increased activated immune cells in TCRβ-KO or in RAG2-KO mice when compared to WT animals could be due to a lack of response to Heme treatment would require further

investigations. So far, only WT young mice were sensitive to Heme administration, as shown in the graphs below.

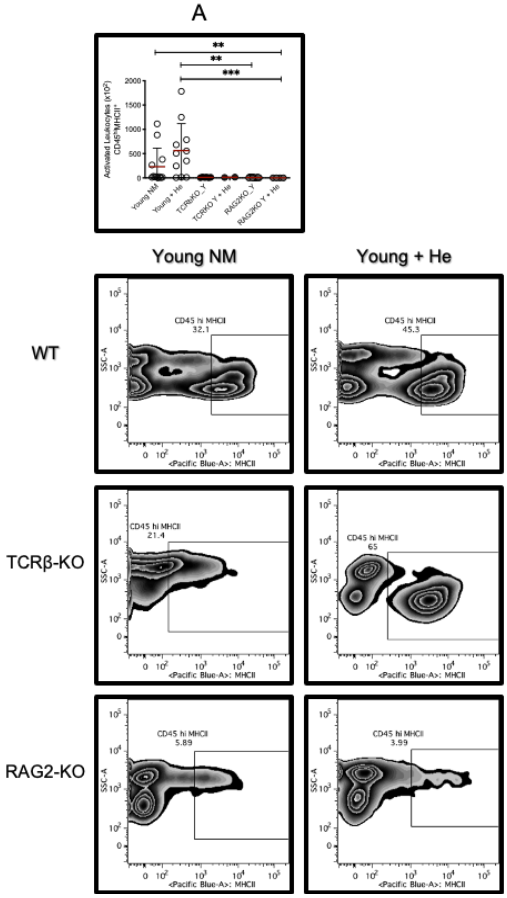

Fig. 94- PBLs immune response in immunocompromised mice. Young (8-12 weeks old) mice - WT, TCRKβ-KO and RAG2-KO - were used for the experiment. Graph (A) shows the number of activated leukocytes into circulation (CD45+MHCII+) after peripheral Heme injection. The differences were also observed in graphs obtained from freshly isolated PBLs. The results were referred to young NM mice, used as control in each genotype; expressed as mean ± standard deviation (2-12 animals per group). Asterisks refer to a statistically significance. * $p < 0.05$, ** $p < 0.01$, defined by applying the non-parametric Kruskal-Wallis test.

Activated monocytes present a similar tendency, meaning that higher values were found in WT mice when compared to TCRβKO or

RAG2-KO animals. To note that the levels of activation of immune cells in peripheral Heme-treated immunocompromised mice are lower than in young NM mice.

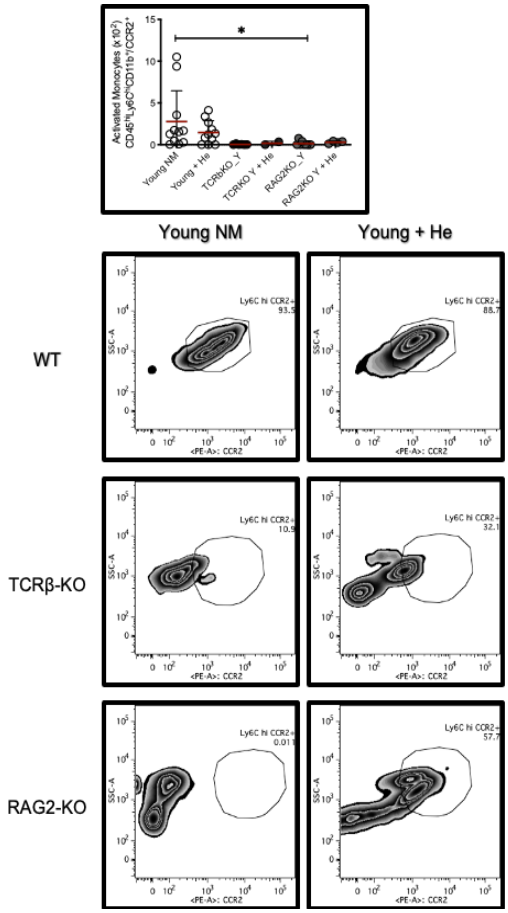

Fig. 95- PBLs immune response in immunocompromised mice. Young (8-12 weeks old) mice - WT, TCRKβ-KO and RAG2-KO - were used for the experiment. Graph (A) shows the number of activated monocytes into circulation (Ly6C+CCR2+) after peripheral Heme injection. The differences were also observed in graphs obtained from freshly isolated PBLs. The results were referred to young NM mice, used as control in each genotype; and expressed as mean ± standard deviation (2-12 animals per group). Asterisks refer to a statistically significance. * p <0.05, defined by applying the non-parametric Kruskal-Wallis test.

We observed the same results when quantifying the number and activation of neutrophils in WT and immunocompromised mice (Fig.96).

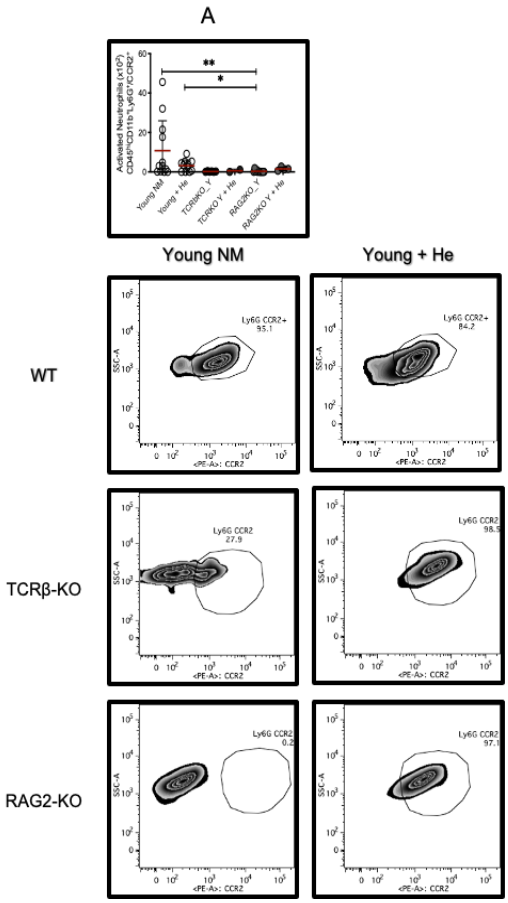

Fig. 96- PBLs immune response in immunocompromised mice. Young (8-12 weeks old) mice - WT, TCRKβ-KO and RAG2-KO - were used for the experiment. Graph (A) shows the number of activated neutrophils in the circulation (Ly6G+CCR2+) after peripheral Heme injection. The differences were also observed in graphs obtained from freshly isolated PBLs. The results were referred to young NM mice, used as control in each genotype; and expressed as mean ± standard deviation (2-12 animals per group). Asterisks refer to a statistically significance. * p <0.05, ** p <0.01, defined by applying the non-parametric Kruskal-Wallis test.

4.3 Can Lymphocyte depletion in old mice reverse the Heme-driven induced phenotype?

Heme treatment in old WT animals reduces their pro-inflammatory brain phenotype. Since we demonstrated that immune cells infiltration into the brain strongly contributes to develop neuroinflammation, we assessed the effects of Heme treatment in the brain of old immunocompromised animals.

Heme administration significantly diminishes the infiltration of immune cells in old NM RAG2-KO, when compared to WT old NM mice. Despite the lack of significance in TCRKβ-KO condition, CD45hi count in NM TCRKβ-KO mice is lower compared to old NM (Fig.97). Interestingly, the profile observed in RAG2-KO is the opposite of what observed in WT mice.

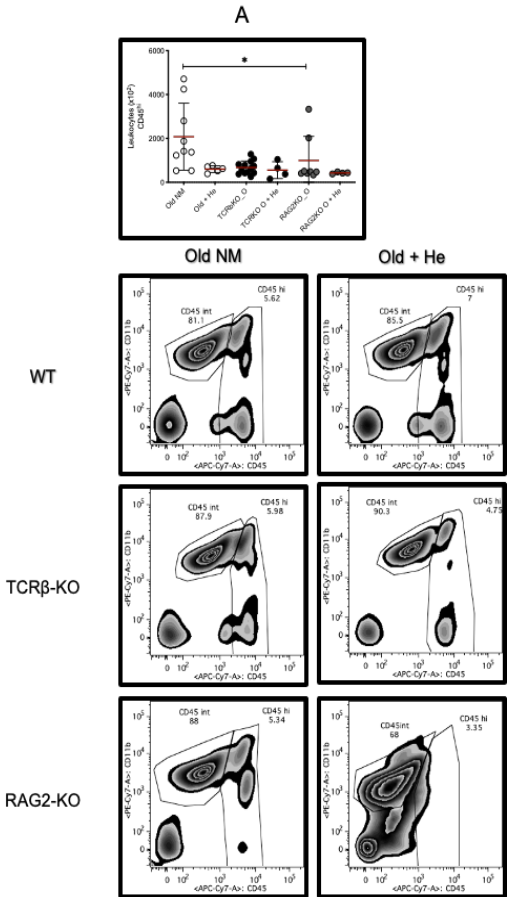

Fig. 97- Leukocytes' infiltration in the brain of old immunocompromised mice. Old (52-60 weeks old) mice - WT, TCRKβ-KO and RAG2-KO - were used for the experiment. The graph (A) shows the number of peripheral leukocytes (CD45hi) after peripheral Heme injection. The differences were also observed in graphs obtained from freshly isolated brain leukocytes. The results were referred to old NM mice, used as control in each genotype; and expressed as mean ± standard deviation (4-10 animals per group). Asterisks refer to a statistically significance. ns p>0.05, defined by applying the non-parametric Kruskal-Wallis test.

When evaluating the inflammatory profile, we observed that peripheral Heme-treated old TCRβ-KO and RAG2-KO mice present an increased number of CCR2 expressing cells in the brain (Fig.98). Old mice showed no statistical difference after exogenous Heme administration. However, the number of infiltrated immune cells in

immunocompromised mice slightly increased, when compared to their respective controls. As shown in the graph below, Heme-treated RAG2-KO mice had significantly higher CCR2 expressing leukocytes than WT old NM mice.

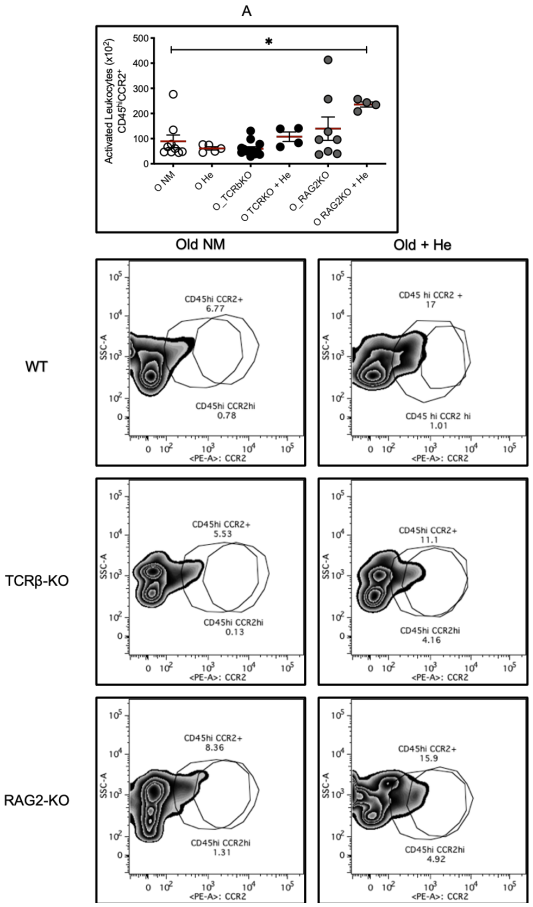

Fig. 98- Activated leukocytes infiltration in the brain of old immunocompromised mice. Old (52-60 weeks old) mice - WT, TCRKβ-KO and RAG2-KO - were used for the experiment. Graph (A) shows the number of peripheral leukocytes (CD45hiCCR2+) after peripheral Heme injection. The differences were also observed in graphs obtained from freshly isolated brain leukocytes. The results were referred to old NM mice, used as each genotype in NM control; and expressed as mean ± standard deviation (4-10 animals per group). Asterisks refer to a statistically significance. * $p<0.05$, defined by applying the non-parametric Kruskal-Wallis test.

While counts in TCRβ-KO mice did not change between tested conditions, the levels of MHC II expression were lower when compared to WT. Consistently, peripheral Heme administration in RAG2-KO decreases the expression of MHC II in peripheral infiltrated immune cells (Fig.99).

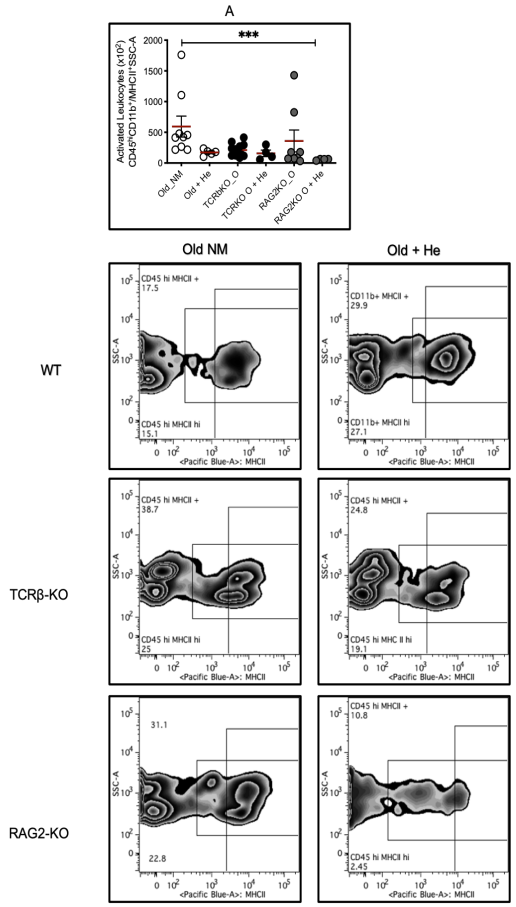

Fig. 99- Activated leukocytes infiltration in the brain of old immunocompromised mice. Old (52-60 weeks old) mice - WT, TCRKβ-KO and RAG2-KO - were used for the experiment. Graph (A) shows the number of peripheral leukocytes (CD45hiMHCII++) after peripheral Heme injection. The differences were also observed in graphs obtained from freshly isolated brain leukocytes. The results were referred to old NM mice, used as controls in each genotype; and expressed as mean ± standard deviation (4-10 animals

per group). Asterisks refer to a statistically significance. *** p>.05, defined by applying the non-parametric Kruskal-Wallis test.

No differences in activated neutrophils were observed between TCRβ-KO conditions. Nevertheless, exogenous peripheral Heme administration in RAG2KO mice decreased neutrophils count, regardless of the genotype.

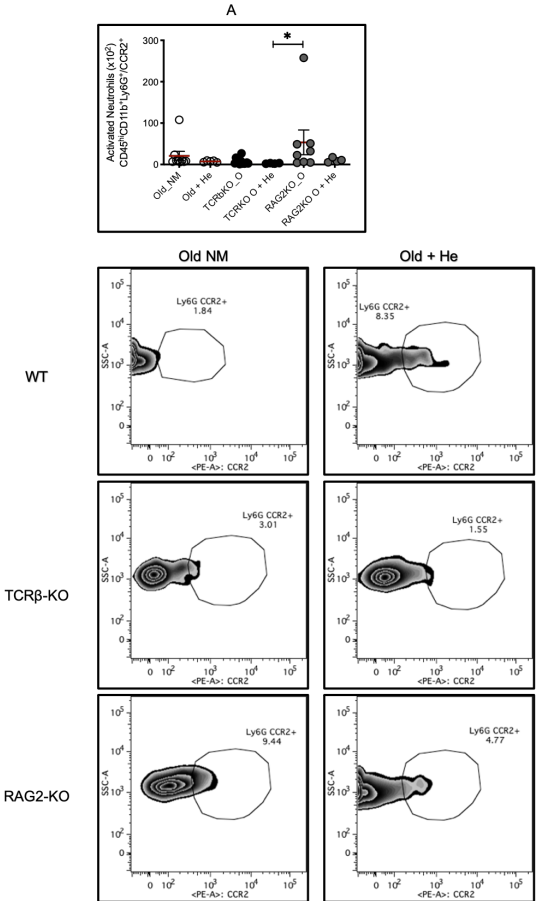

Fig. 100- Activated neutrophils in the brain of old immunocompromised mice. Old (52-60 weeks old) mice - WT, TCRKβ-KO and RAG2-KO - were used for the experiment. Graph (A) shows the number of peripheral leukocytes (CD45hiMHCII++) after peripheral Heme injection. The differences were also observed in graphs obtained from freshly isolated brain leukocytes. The results were referred to old NM mice, used as control in each genotype; and expressed as mean ± standard deviation (4-10 animals per group). Asterisks

refer to a statistically significance. * p<0.05, defined by applying the non-parametric Kruskal-Wallis test.

Microglia were unresponsive to Heme in old TCRβ-KO mice, contrarily to what we observed in RAG2KO animals, where Heme decreases the pro-inflammatory phenotype of these cells in aged mice.

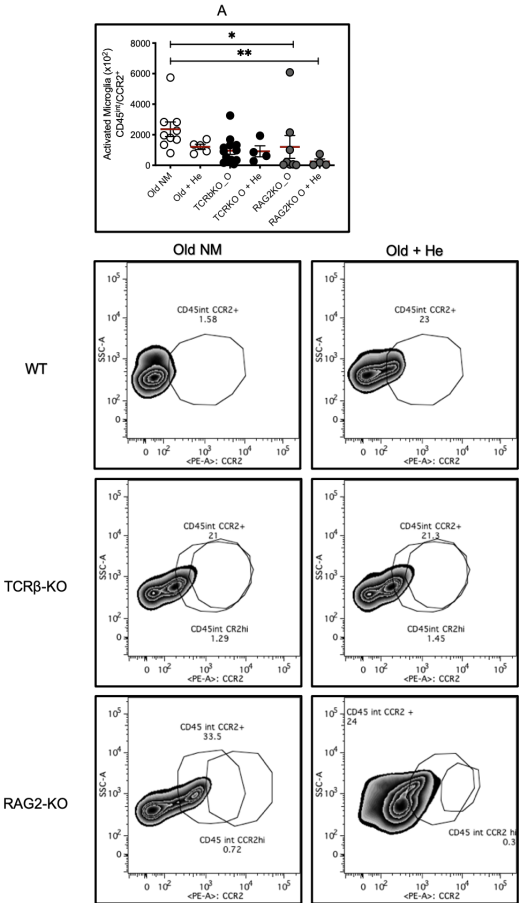

Fig. 101- Activated microglia in the brain of old immunocompromised mice. Old (52-60 weeks old) mice - WT, TCRKβ-KO and RAG2-KO - were used for the experiment. Graph (A) shows the number of peripheral leukocytes (CD45hiMHCII++) after peripheral Heme injection. The differences were also observed in graphs obtained from freshly isolated brain leukocytes. The results were referred to old NM mice, used as controls in each genotype; expressed as mean ± standard deviation (4-10 animals per group). Asterisks refer to a statistically significance. * p<0.05, ** p<0.01, defined by applying the non-parametric Kruskal-Wallis test.

4.3.1 Lymphocyte depletion decreases inflammation in the spleen of old mice

Spleen leukocytes of old mice are more sensitive to Heme overload (Fig.102). The differences between genotypes suggests immunocompromised mice are more protected to inflammation.

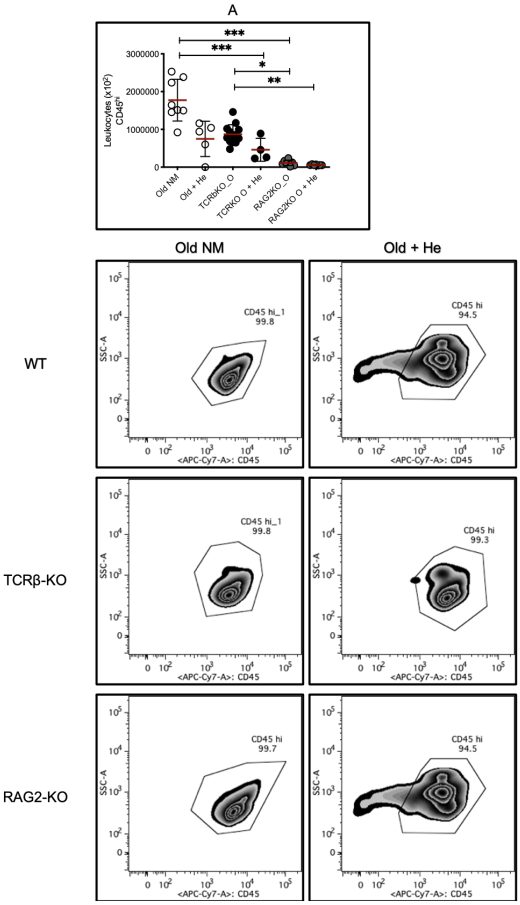

Fig. 102- Spleen immune cells response in old immunocompromised mice. Old (52-60 weeks old) mice - WT, TCRKβ-KO and RAG2-KO - were used for the experiment. Graph (A) shows the number of peripheral leukocytes (CD45+) after peripheral Heme injection. The differences were also observed in graphs obtained from freshly isolated spleen leukocytes. The results were referred to old NM mice, used as controls in each genotype; and expressed as mean ± standard deviation (4-10 animals per group). Asterisks refer to a

statistically significance. * p<0.05, ** p<0.01, *** p<0.001, **** p<0.0001, defined by applying the non-parametric Kruskal-Wallis test.

Activation of leukocytes in the spleen was not observed upon peripheral Heme treatment. Similar to previous results, TCRKβ-KO and RAG2-KO mice present lower inflammation, especially RAG2-KO animals, where inflammation is significantly lower than in TCRKβ-KO mice.

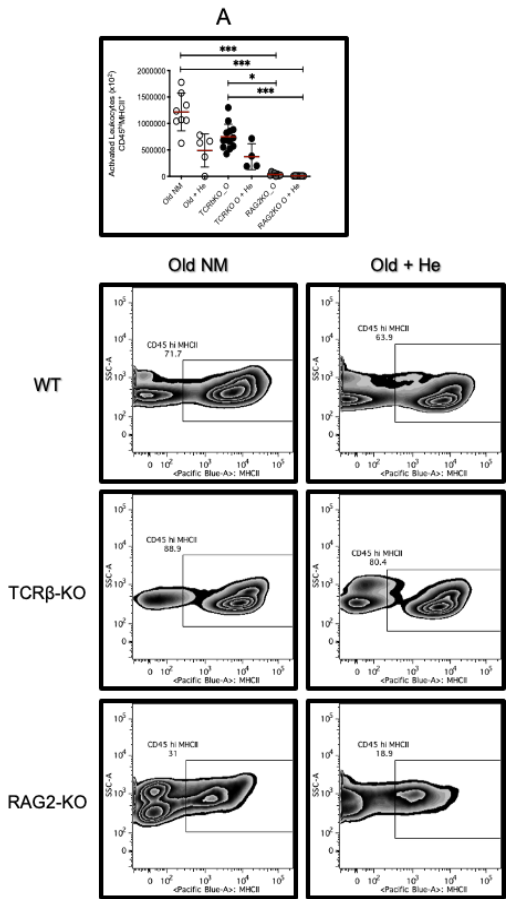

Fig. 103- Spleen immune cells response in old immunocompromised mice. Old (52-60 weeks old) mice - WT, TCRKβ-KO and RAG2-KO - were used for the experiment. Graph (A) shows the number of peripheral leukocytes (CD45+MHCII+) after peripheral Heme injection. The differences were also observed in graphs obtained from freshly isolated spleen leukocytes. The

results were referred to old NM mice, used as controls in each genotype; expressed as mean ± standard deviation (4-10 animals per group). Asterisks refer to a statistically significance. * p<0.05, ** p<0.01, *** p<0.001, defined by applying the non-parametric Kruskal-Wallis test.

Evaluating the monocytes population, we observed no changes between different conditions.

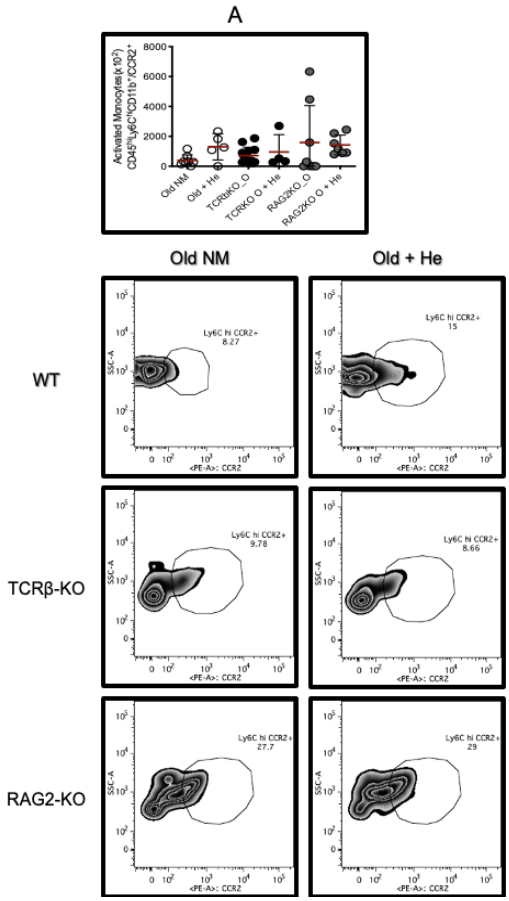

Fig. 104- Spleen immune cells response in old immunocompromised mice. Old (52-60 weeks old) mice - WT, TCRKβ-KO and RAG2-KO - were used for the experiment. Graph (A) shows the number of peripheral leukocytes (CD45+MHCII+) after peripheral Heme injection. The differences were also observed in graphs obtained from freshly isolated spleen leukocytes. The results were referred to old NM mice, used as controls in each genotype; and expressed as mean ± standard deviation (4-10 animals per group). Asterisks refer to a statistically significance. ns p>0.05, defined by applying the non-parametric Kruskal-Wallis test.

4.3.2 Lymphocyte depletion decreases inflammation in PBLs of old mice

WT old NM mice present lower circulating leukocyte count (Fig.105), as also found in the spleen of these animals. However, WT mice present a significantly higher number of circulating leukocytes than in TCRβ-KO or RAG2-KO mice.

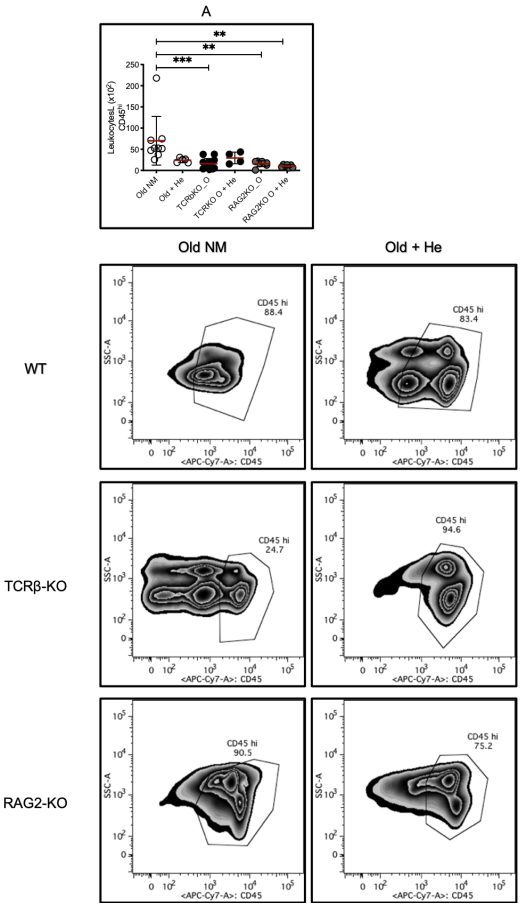

Fig. 105- PBLs immune response in old immunocompromised mice. Old (52-60 weeks old) mice - WT, TCRKβ-KO and RAG2-KO - were used for the experiment. Graph (A) shows the number of circulating leukocytes (CD45+) after peripheral Heme injection. The differences were also observed in graphs obtained from freshly isolated PBLs. The results were referred to old NM mice, used as controls in each genotype; expressed as mean ± standard deviation

(4-10 animals per group). Asterisks refer to a statistically significance. ** p<0.01, ** *p<0.001, defined by applying the non-parametric Kruskal-Wallis test.

Similar results were also obtained for leukocytes activation (Fig.106). Whether the lack of increased activated immune cells in TCRβ-KO or RAG2-KO mice, when compared to WT animals, could be due to a lack of response to peripheral Heme injection would require further investigations.

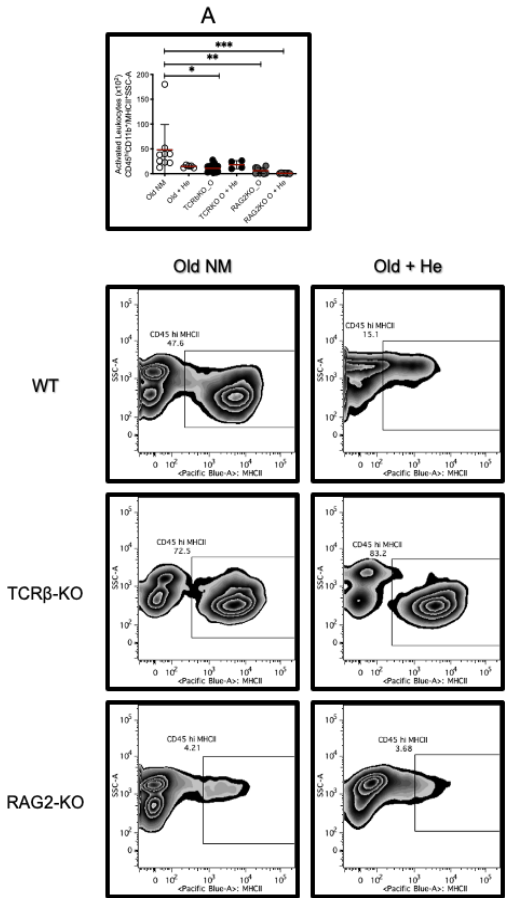

Fig. 106- PBLs immune response in old immunocompromised mice. Old (52-60 weeks old) mice - WT, TCRKβ-KO and RAG2-KO - were used for the experiment. Graph (A) shows the number of activated leukocytes (CD45+MHCII) after peripheral Heme injection. The differences were also observed in graphs obtained from freshly isolated PBLs. The results were

referred to old NM mice, used as controls in each genotype; and expressed as mean ± standard deviation (4-10 animals per group). Asterisks refer to a statistically significance. * $p<0.05$, ** $p<0.01$, defined by applying the non-parametric Kruskal-Wallis test.

Despite the lack of significance, only WT animals were sensitive to peripheral Heme administration. Immune cell counts in the Immunocompromised mice were significantly lower.

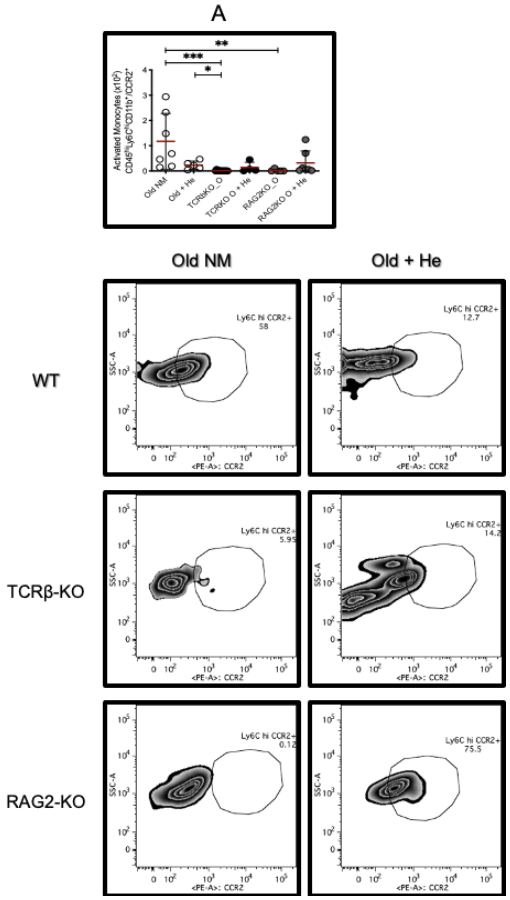

Fig. 107- PBLs immune response in old immunocompromised mice. Old (52-60 weeks old) mice - WT, TCRKβ-KO and RAG2-KO - were used for the experiment. Graph (A) shows the number of activated monocytes (Ly6ChiMHCII) after peripheral Heme injection. The differences were also observed in graphs obtained from freshly isolated PBLs. The results were referred to old NM mice, used as controls in each genotype; and expressed as mean ± standard deviation (4-10 animals per group). Asterisks refer to a

statistically significance. * p<0.05, ** p<0.01, *** p<0.001, defined by applying the non-parametric Kruskal-Wallis test.

Similar results were observed when quantifying the number and activation of neutrophils in WT and immunocompromised mice. Regardless of the population assessed, the pattern was the same. Heme-treated and non-treated WT animals presented enhanced inflammation when compared to their immunocompromised counterpart.

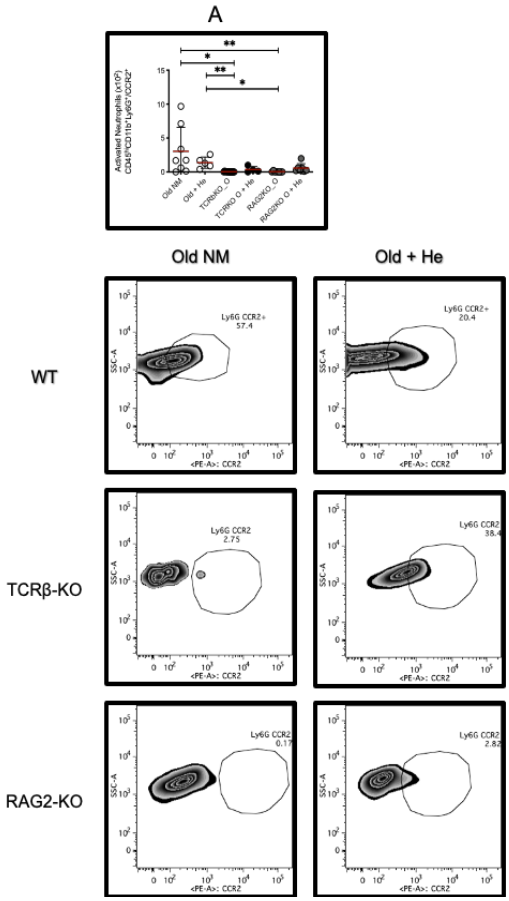

Fig. 108- PBLs immune cells response in old immunocompromised mice. Old (52-60 weeks old) mice - WT, TCRKβ-KO and RAG2-KO - were used for the experiment. Graph (A) shows the number of activated neutrophils (Ly6G+MHCII+) after peripheral Heme injection. The differences were also

observed in graphs obtained from freshly isolated PBLs. The results were referred to old NM mice, used as controls in each genotype; and expressed as mean ± standard deviation (4-10 animals per group). Asterisks refer to a statistically significance. * $p<0.05$, ** $p<0.01$, defined by applying the non-parametric Kruskal-Wallis test.

4.4 Iron accumulation in the Brain immune cells of immunocompromised mice

Lymphocytic depletion confers protection against Heme-driven inflammation in young mice, while decreasing inflammation in old mice, even though maintaining the profile previously observed, i.e. peripheral Heme administration reverts the inherent inflammation of old mice. Therefore, we quantified Fe in immune cells from these mice.

We found that Heme administration in young TCRKβ-KO mice reduces Fe accumulation (Fig.109). Despite the lack of significance, differences displayed in the histograms clearly indicate the difference between the two groups.

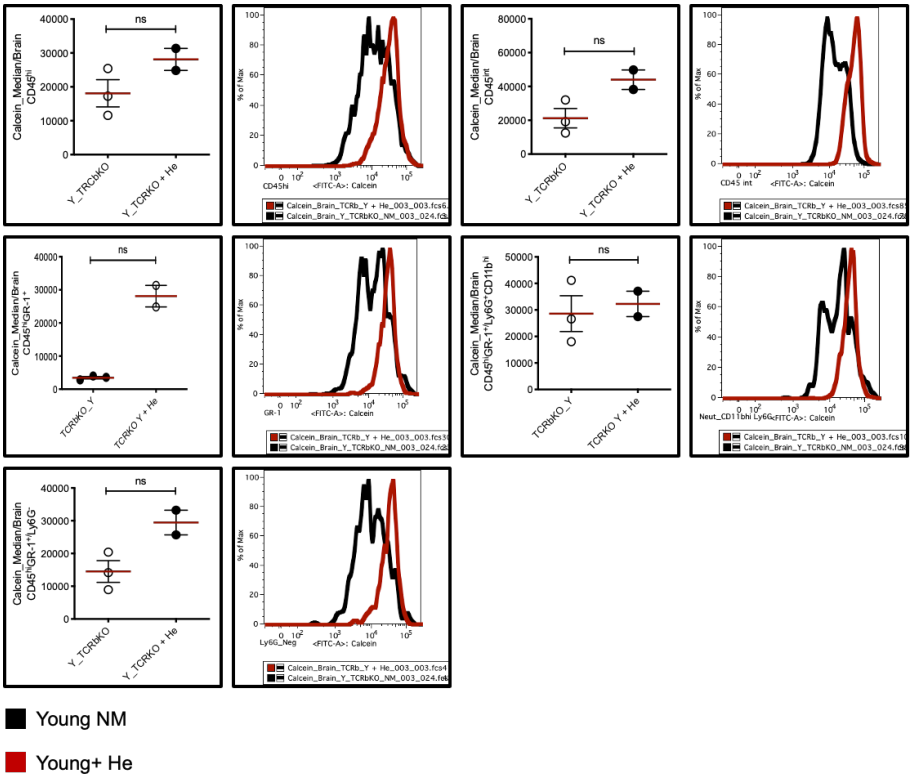

Fig. 109- Fe accumulation in infiltrated peripheral and resident immune cells in the brain of TCRKβ-KO. Young NM and peripheral Heme-treated TCRKβ-KO mice (8-12 weeks old) were used for the experiment. Graphs show: CD45hi-Leukocytes, GR-1- Monocytes and neutrophils, Ly6G neg-monocytes, Ly6G pos- neutrophils and resident cells: CD45int-Microglia. The results were expressed as mean ± standard deviation. Asterisks refer to a statistically significant difference. ns $p > 0.05$, defined by applying the non-parametric Mann-Whitney t test.

When we compared TCRKβ-KO mice, young and old, we found no differences between these groups (Fig.110), contrary to WT mice, where aged mice showed a significantly higher amount of Fe in immune cells.

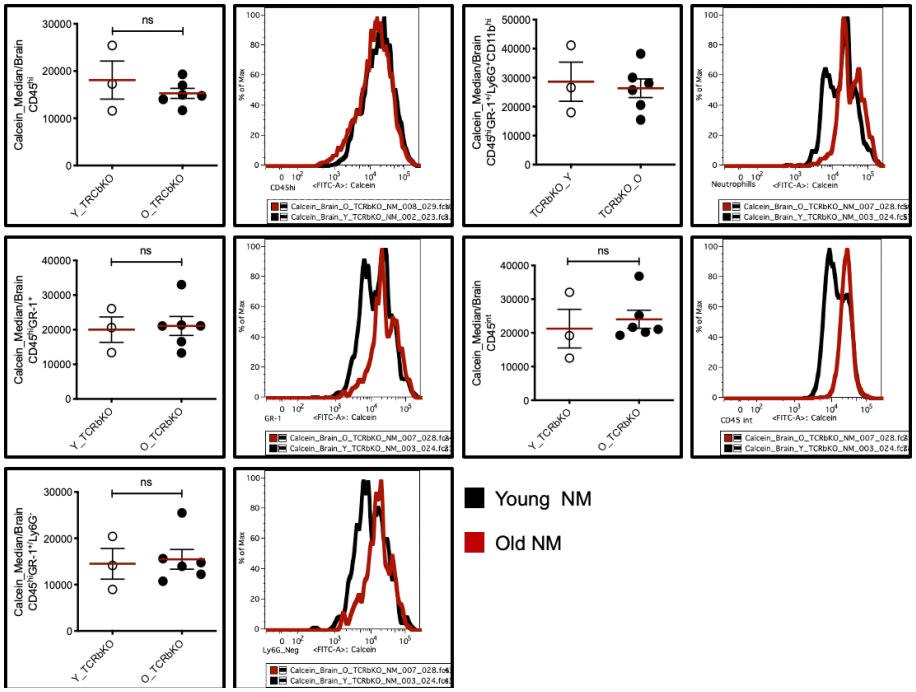

Fig. 110- Fe accumulation in infiltrated peripheral and resident immune cells in the brain of TCRKβ-KO. Young (8-12 weeks old) and old (52-60 weeks old) TCRKβ-KO mice were used for the experiment. The graphs show: CD45hi- Leukocytes, GR-1- Monocytes and neutrophils, Ly6G neg- monocytes, Ly6G pos- neutrophils and the resident cells: CD45int-Microglia. The results were expressed as mean ± standard deviation. Asterisks refer to a statistically significant difference. ns $p > 0.05$, defined by applying the non-parametric Mann-Whitney t test.

Peripheral Heme-treated old TCRKβ-KO mice presented a similar profile to peripheral Heme-treated young TCRKβ-KO animals. Heme injection significantly reduces the Fe accumulation in the myeloid population (Fig.111).

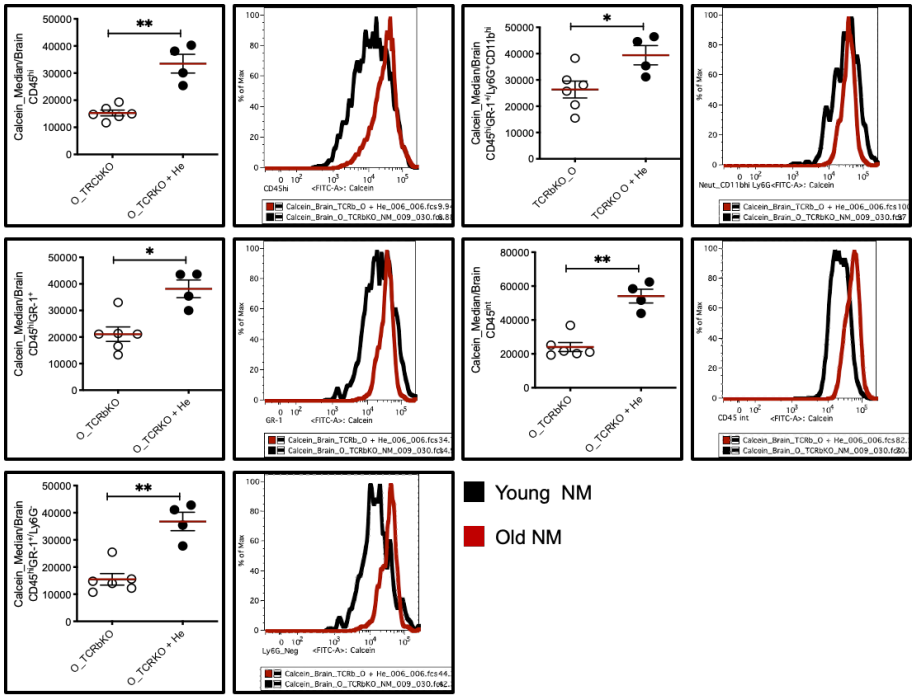

Fig. 111- Quantification of brain Fe accumulation in infiltrated peripheral and resident immune cells. Old NM and peripheral Heme-treated (52-60 weeks old) TCRKβ-KO mice were used for the experiment. Graphs show: CD45hi-Leukocytes, GR-1- Monocytes and neutrophils, Ly6G neg- monocytes, Ly6G pos- neutrophils and the resident cells: CD45int-Microglia. The results were expressed as mean ± standard deviation. Asterisks refer to a statistically significant difference. * $p < 0.05$, defined by applying the non-parametric Mann-Whitney t test.

We then analyzed the same conditions in RAG2-KO mice. As shown in the graph below, Fe accumulation in young peripheral Heme-treated RAG2-KO mice is lower than in the non-treated group, regardless of the population analyzed.

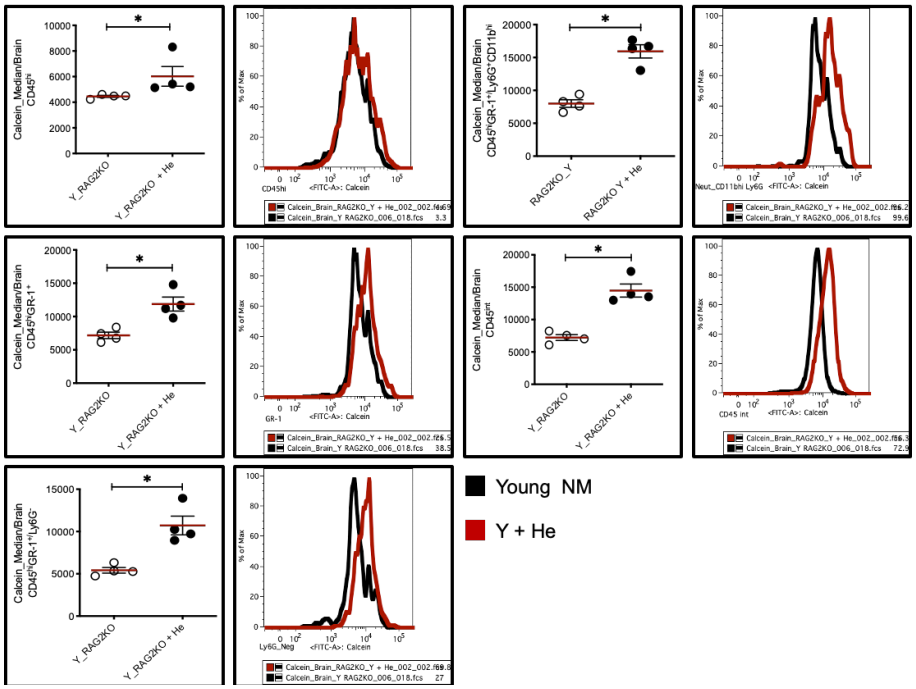

Fig. 112- Quantification of brain Fe accumulation in infiltrated peripheral and resident immune cells. Young NM and Heme-treated RAG2-KO mice (8-12 weeks old) were used for the experiment. Graphs show: CD45hi-Leukocytes, GR-1- Monocytes and neutrophils, Ly6G neg- monocytes, Ly6G pos- neutrophils and the resident cells: CD45int-Microglia. The results were expressed as mean ± standard deviation. Asterisks refer to a statistically significant difference. * $p < 0.05$, defined by applying the non-parametric Mann-Whitney t test.

We then compared RAG2-KO mice, young and old, and found no significant changes in Fe content (Fig.113), similar to TCRKβ-KO mice.

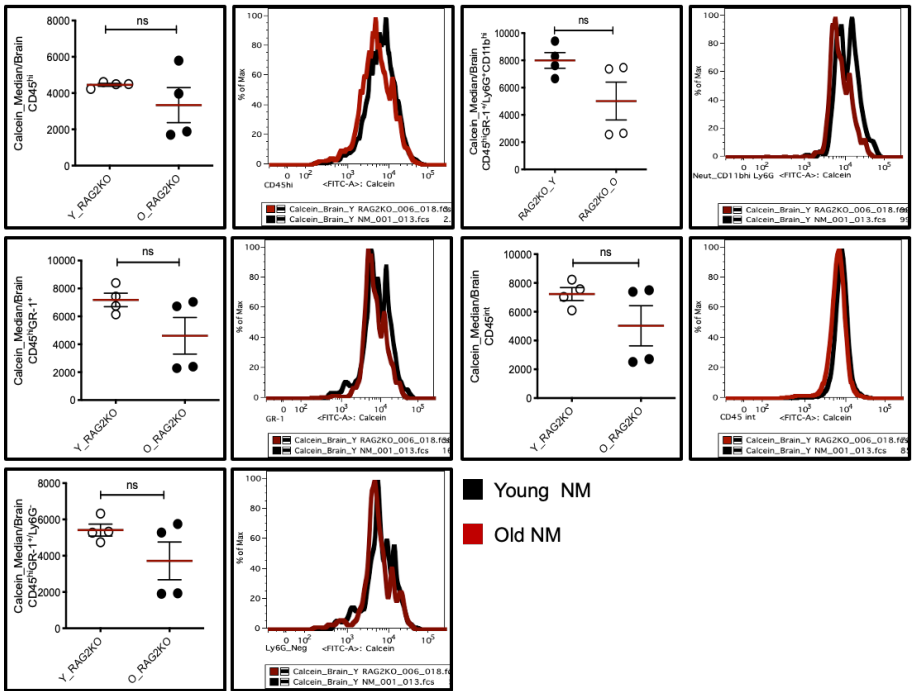

Fig. 113- Quantification of brain Fe accumulation in infiltrated peripheral and resident immune cells. Young (8-12 weeks old) and old (52-60 weeks old) RAG2-KO mice were used for the experiment. The graphs show: CD45hi- Leukocytes, GR-1- Monocytes and neutrophils, Ly6G neg- monocytes, Ly6G pos- neutrophils and the resident cells: CD45int-Microglia. The results were expressed as mean ± standard deviation. Asterisks refer to a statistically significant difference. ns $p > 0.05$, defined by applying the non-parametric Mann-Whitney t test.

Peripheral Heme-treated RAG2-KO old mice presented a significantly diminished Fe accumulation in immune cells, regardless of the population analyzed (Fig.114).

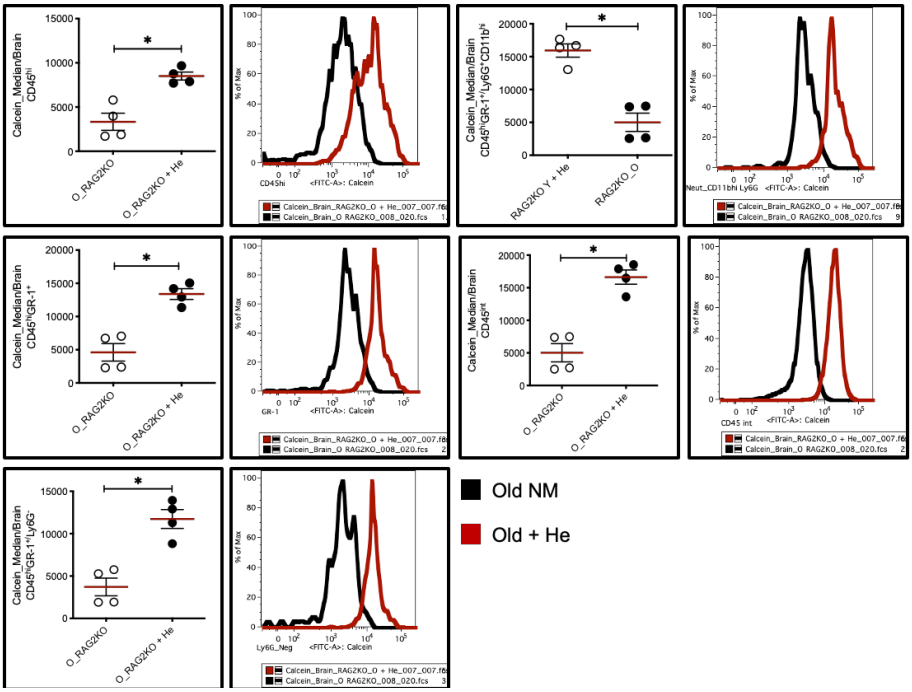

Fig. 114- Quantification of brain Fe accumulation in infiltrated peripheral and resident immune cells. Old NM and Heme-treated (52-60 weeks old) RAG2-KO mice were used for the experiment. The graphs show: CD45hi-Leukocytes, GR-1- Monocytes and neutrophils, Ly6G neg- monocytes, Ly6G pos- neutrophils and the resident cells: CD45int-Microglia. The results were expressed as mean ± standard deviation. Asterisks refer to a statistically significant difference. * $p < 0.05$, defined by applying the non-parametric Mann-Whitney t test.

4.5 Iron accumulation in the circulation of immunocompromised mice cells

Given the results obtained, we analyzed the effect of exacerbated peripheral Heme/Fe administration in the circulation of the immunocompromised mice.

The results shown in the graph below are in agreement with what observed in the brain of peripheral Heme-treated TCRKβ-KO young mice, in the sense that Heme reduces the Fe content in immune cells (Fig.115)

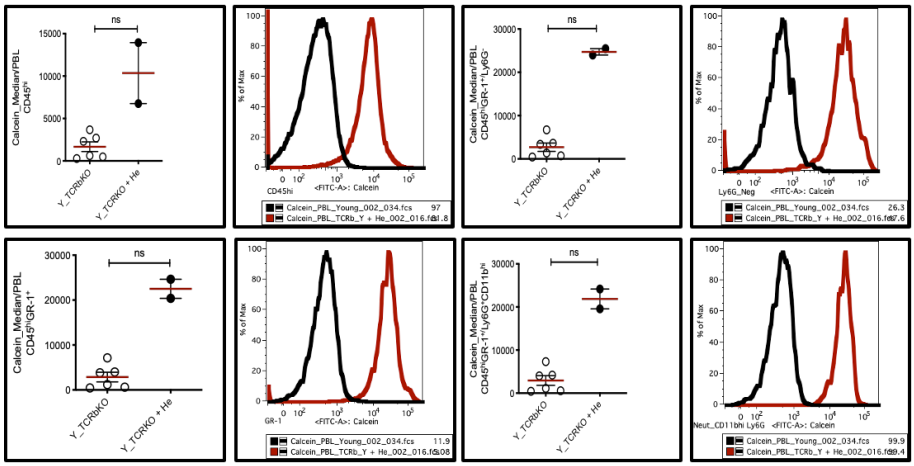

Young NM

Young + He

Fig. 115- Quantification of brain Fe accumulation in infiltrated peripheral and resident immune cells. Young NM and Heme-treated TCRKβ-KO mice (8-12 weeks old) were used for the experiment. The graphs show: CD45hi- Leukocytes, GR-1- Monocytes and neutrophils, Ly6G neg- monocytes, Ly6G pos- neutrophils. The results were expressed as mean ± standard deviation. Asterisks refer to a statistically significant difference. ns $p > 0.05$, defined by applying the non-parametric Mann-Whitney t test.

When comparing young to old NM TCRKβ-KO mice, we found no statistical differences (Fig.116). However, old mice appear to have higher Fe accumulation.

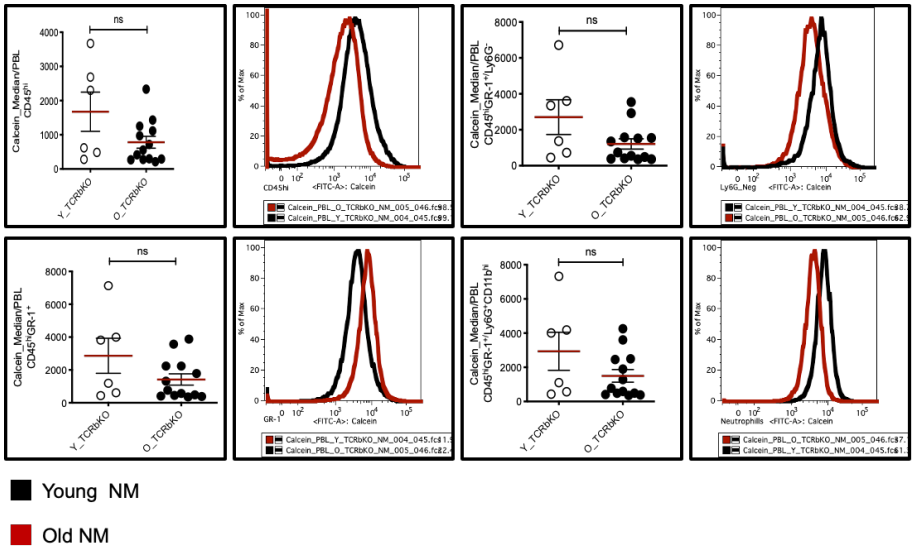

Fig. 116- Quantification of brain Fe accumulation in infiltrated peripheral and resident immune cells. Young (8-12 weeks old) and old (52-60 weeks old) TCRKβ-KO mice were used for the experiment. The graphs show: CD45hi- Leukocytes, GR-1- Monocytes and neutrophils, Ly6G neg- monocytes, Ly6G pos- neutrophils. The results were expressed as mean ± standard deviation. Asterisks refer to a statistically significant difference. ns $p > 0.05$, defined by applying the non-parametric Mann-Whitney t test.

Upon Heme injection, the Fe present in circulating immune cells of old TCRKβ-KO mice significantly reduces the inflammatory response (Fig.117), similar to what occurring into the brain.

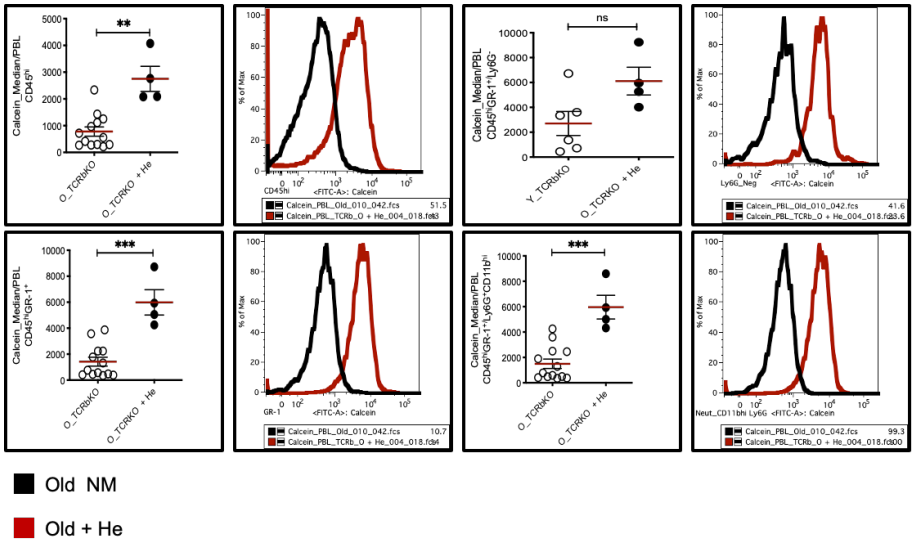

Fig. 117- Quantification of brain Fe accumulation in infiltrated peripheral and resident immune cells. Old NM and Heme-treated (52-60 weeks old) TCRKβ-KO mice were used for the experiment. The graphs show: CD45hi-Leukocytes, GR-1- Monocytes and neutrophils, Ly6G neg- monocytes, Ly6G pos- neutrophils. The results were expressed as mean ± standard deviation. Asterisks refer to a statistically significant difference. ns $p > 0.05$, ** $p < 0.01$, *** $p < 0.001$, defined by applying the non-parametric Mann-Whitney t test.

We further analyzed the presence of Fe loaded immune cells in RAG2-KO mice. Heme administration into young RAG2-KO had different effect in the circulation, although Fe levels are maintained (Fig.118).

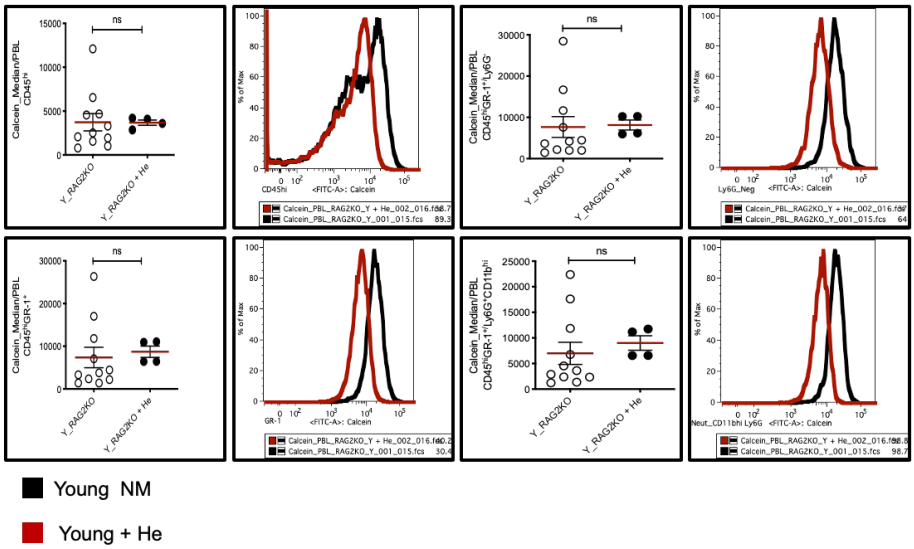

Fig. 118- Quantification of brain Fe accumulation in infiltrated peripheral and resident immune cells. Young NM and Heme-treated RAG2-KO mice (8-12 weeks old) were used for the experiment. The graphs show: CD45hi- Leukocytes, GR-1- Monocytes and neutrophils, Ly6G neg- monocytes, Ly6G pos- neutrophils. The results were expressed as mean ± standard deviation. Asterisks refer to a statistically significant difference. ns $p > 0.05$, defined by applying the non-parametric Mann-Whitney t test.

Fe content is lower in old NM RAG2-KO mice, despite the lack of significance. However, monocytes display a significant reduction in Fe when compared to young NM RAG2-KO mice (Fig.119).

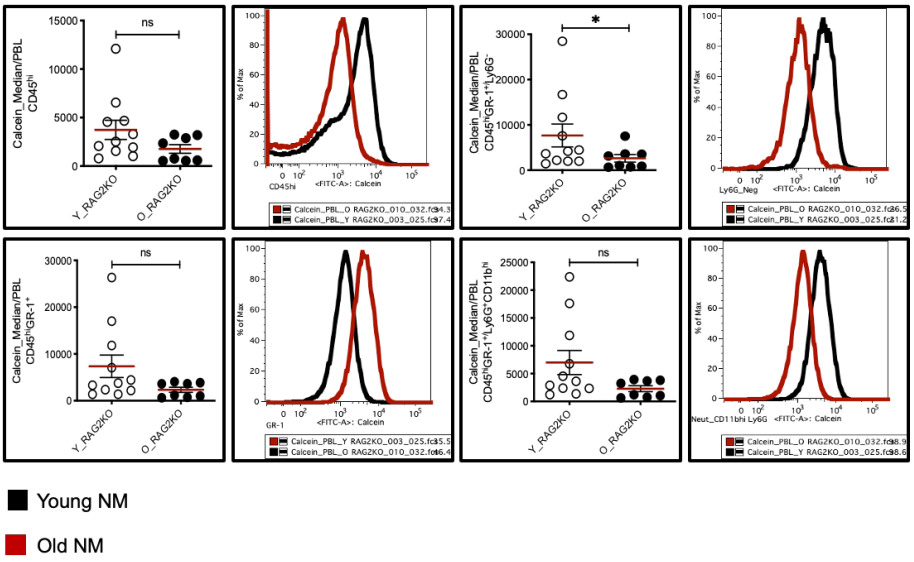

Fig. 119- Quantification of brain Fe accumulation in infiltrated peripheral and resident immune cells. Young (8-12 weeks old) and old (52-60 weeks old) RAG2-KO mice were used for the experiment. The graphs show: CD45hi- Leukocytes, GR-1- Monocytes and neutrophils, Ly6G neg- monocytes, Ly6G pos- neutrophils. The results were expressed as mean ± standard deviation. Asterisks refer to a statistically significant difference. ns $p > 0.05$, defined by applying the non-parametric Mann-Whitney t test.

Circulating immune cells in RAG2-KO old mice displays similar profile as the one observed in the brain, which presents a reduced Fe accumulation upon periphery Heme injection (Fig.120).

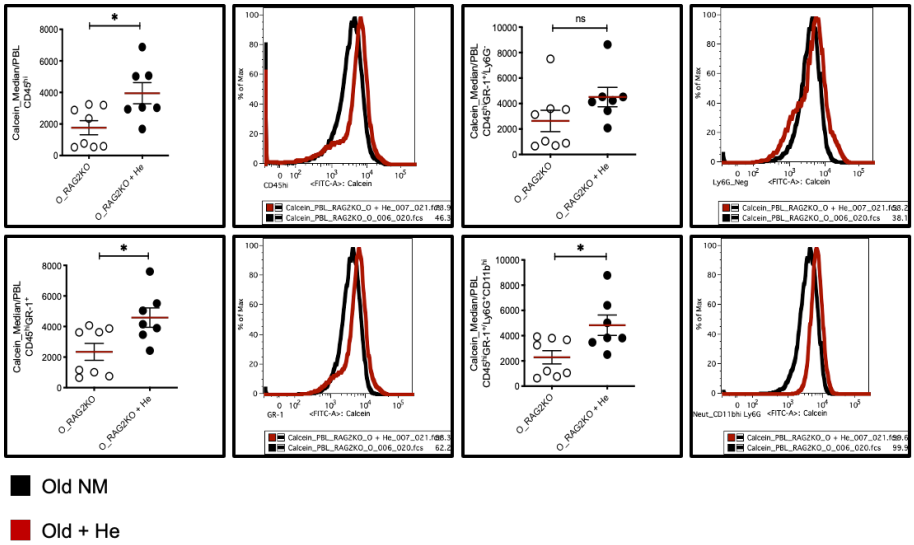

Fig. 120- Quantification of brain Fe accumulation in infiltrated peripheral and resident immune cells. Old (52-60 weeks old) RAG2-KO mice were used for the experiment. The graphs show: CD45hi-Leukocytes, GR-1- Monocytes and neutrophils, Ly6G neg- monocytes, Ly6G pos- neutrophils. The results were expressed as mean ± standard deviation. Asterisks refer to a statistically significant difference. ns $p > 0.05$, * $p < 0.05$, defined by applying the non-parametric Mann-Whitney t test.

4.6 Fe chelation therapy can reduce inflammation in aged mice

So far, our data demonstrated that exogenous and peripheral Heme administration increases Fe content in the brain and primes this organ towards the infiltration of pro-inflammatory immune cells. Since aged mice present an increased Fe accumulation in the brain, when compared to young animals, we wanted to assess whether the peripheral administration of Fe chelators might prevent the aged-related neuroinflammatory phenotype. It is known than deferiprone (DFP) is currently used for the treatment of neurodegenerative diseases, such as PD and AD [195][196].

Our aim was to demonstrate that DFP could act in a preventive manner, decreasing the contribution of the immune system on the development of brain inflammation and Fe accumulation, which then culminate in neuronal death.

Old mice were treated with DFP for a period of 15 or 30 days (given every other day at a dose of 15mg/kg, once a day, i.p.), and the inflammatory profile in the brain was evaluated in relation to non-treated animals of the same age.

The treatment of 15 days showed promising results. Although the results obtained were not significant, the number of invading cells decreases. Contrarily, 30 days of DFP treatment significantly increases the number of infiltrated immune cells.

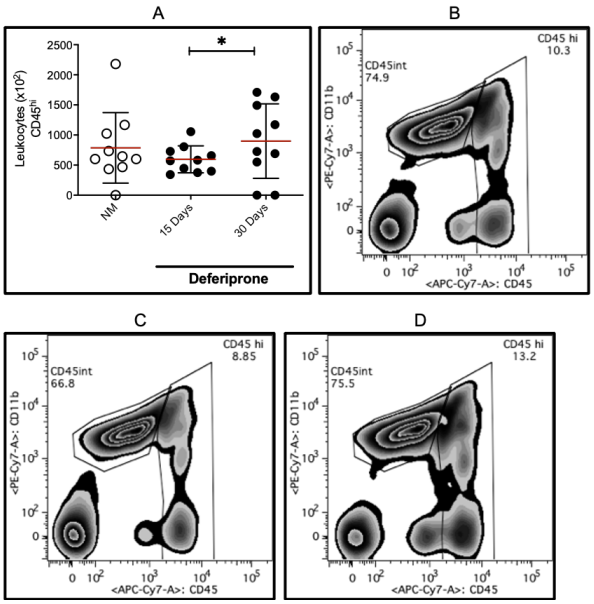

Fig. 121- Brain infiltration of immune cells in old mice after DFP treatment. Old mice were injected i.p. with DFP for a period of 15 or 30 days, every other day. Graph (A) shows the number of peripheral leukocytes (CD45hi). The differences were also observed in graphs obtained from freshly isolated brain leukocytes from (B) old NM, (C) old treated 15 days with DFP and (D) old treated 30 days with DFP. The results were referred to old NM mice; and

expressed as mean ± standard deviation (10 animals per group). Asterisks refer to a statistically significance. * p<0.05, defined by applying the one-way ANOVA test.

When evaluating the inflammatory profile of leukocytes, we obtained similar results. DFP administration was capable to reverse the inflammation associated with increasing age after 15 days of treatment, but not after 30 days (Fig.122).

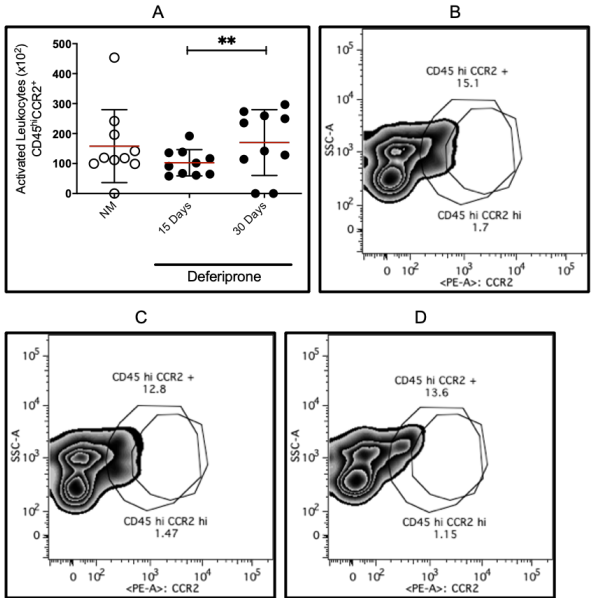

Fig. 122- Leukocytes' activation in the brain of old mice after DFP treatment. Old mice were injected i.p. with DFP for a period of 15 or 30 days, every other day. Graph (A) shows the number of activated leukocytes (CD45hiCCR2+). The differences were also observed in graphs obtained from freshly isolated brain leukocytes from (B) old NM, (C) old treated 15 days with DFP and (D) old treated 30 days with DFP. The results were referred to old NM mice; and expressed as mean ± standard deviation (10 animals per group). Asterisks refer to a statistically significance. **p<0.01, defined by applying the one-way ANOVA test.

Activated monocytes also decrease after 15 days of DFP treatment, but significantly increase after 30 days (Fig.123).

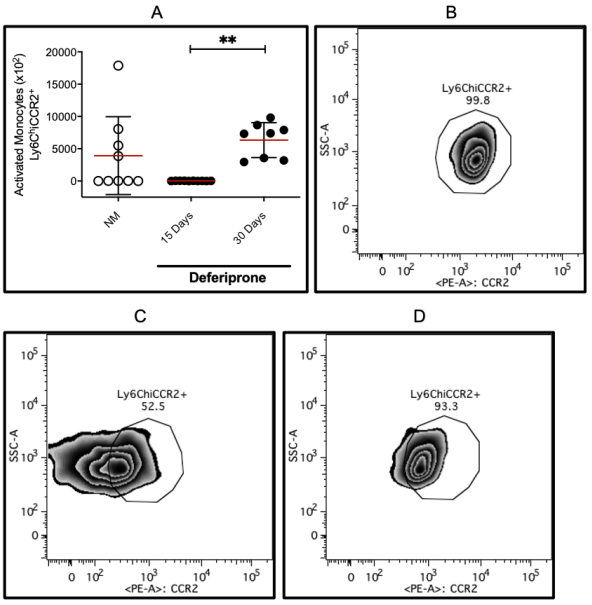

Fig. 123- Monocytes' activation in old mice after DFP treatment. Old mice were injected i.p. with DFP for a period of 15 and 30 days, every other day. Graph (A) shows the number of activated monocytes (Ly6ChiCCR2+). The differences were also observed in graphs obtained from freshly isolated brain leukocytes from (B) old NM, (C) old treated 15 days with DFP and (D) old treated 30 days with DFP. The results were referred to old NM mice; and expressed as mean ± standard deviation (10 animals per group). Asterisks refer to a statistically significance. **p<0.01, defined by applying the one-way ANOVA test.

We then assessed whether DFP could also revert the pro-inflammatory profile of microglia, which indeed was the case. Microglia activation decreases after 15 days treatment (Fig.124).

It is important to note that prolonged DFN administration, i.e., for 30 days, showed an opposite effect in the absence of pathological condition.

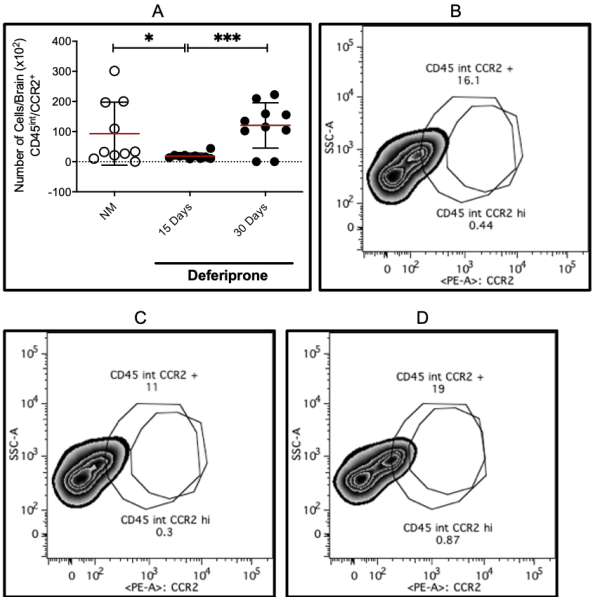

Fig. 124- Microglia activation in old mice after DFP treatment. Old mice were injected i.p. with DFP for a period of 15 or 30 days, every other day. Graph (A) shows the number of activated monocytes (CD45intCCR2+). The differences were also observed in graphs obtained from freshly isolated brain leukocytes from (B) old NM, (C) old treated 15 days with DFP and (D) old treated 30 days with DFP. The results were referred to old NM mice; expressed as mean ± standard deviation (10 animals per group). Asterisks refer to a statistically significance. **p<0.01, defined by applying the one-way ANOVA test.

We then accessed whether the lymphocytic compartment could also be affected by DFP treatment and found the same tendency. While T cells decrease after 15 days treatment (Fig.125), their count is enhanced by 30 days treatment, as observed in previous results.

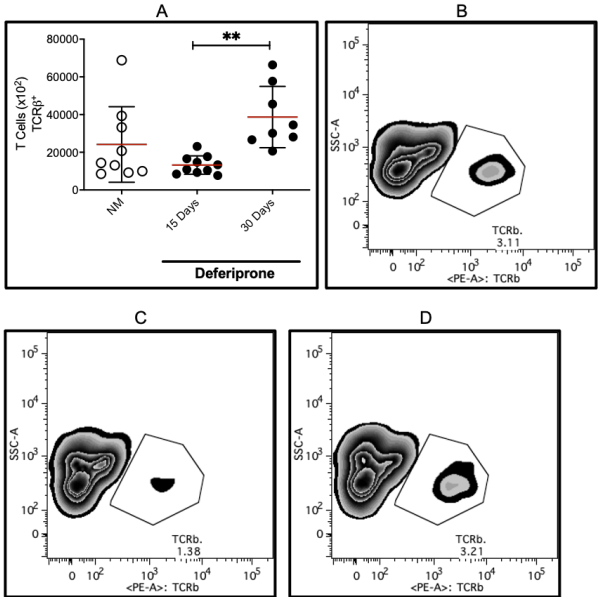

Fig. 125- T cells infiltration in the brain after DFP treatment. Old mice were injected i.p. with DFP for a period of 15 or 30 days, every other day. Graph (A) shows the number of infiltrated T cells (TCRβ+). The differences were also observed in graphs obtained from freshly isolated brain leukocytes from (B) old NM, (C) old treated 15 days with DFP and (D) old treated 30 days with DFP. The results were referred to old NM mice; expressed as mean ± standard deviation (10 animals per group). Asterisks refer to a statistically significance, defined by applying the one-way ANOVA test.

CD4 and CD8 also exhibited the same pattern (Fig.126 and 127), and similar results were also obtained for their activation state.

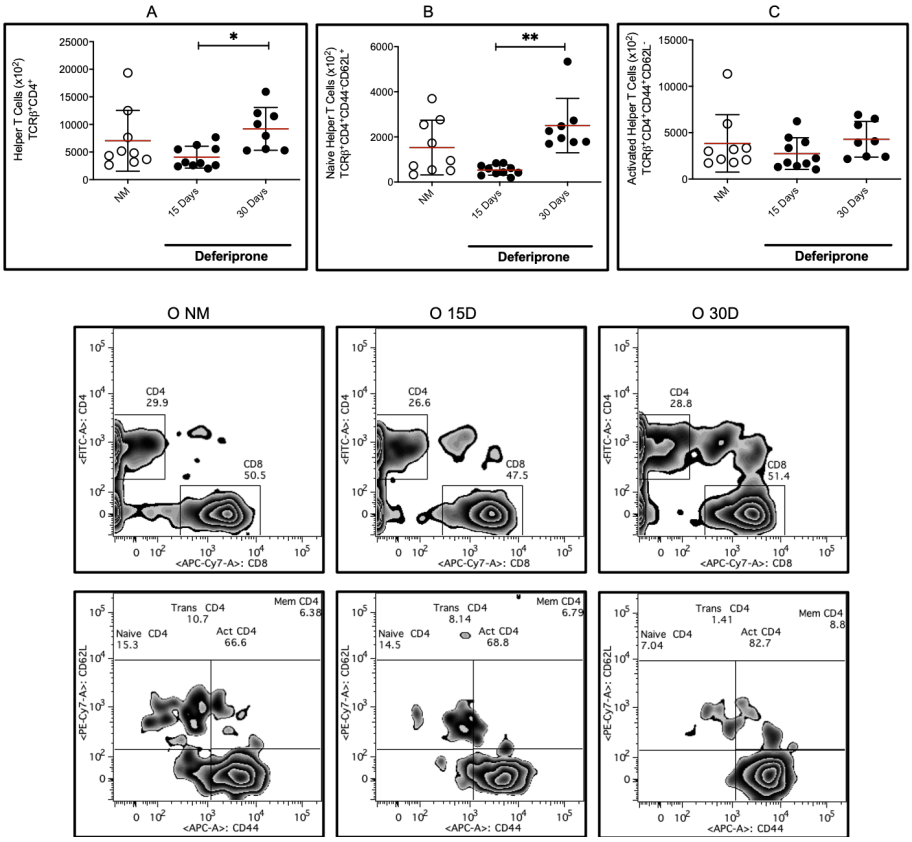

Fig. 126- Helper T cells activation after DFN treatment. Old mice were injected i.p. with DFN for a period of 15 or 30 days, every other day. Graph (A) shows the number of helper T cells (TCRβ+CD4+), (B) Naïve helper T cells (CD4+CD62L+CD44-) and (C) Activated helper T cells (CD4+CD62L-CD44+). The differences were also observed in graphs obtained from freshly isolated brain leukocytes from old NM, old treated 15 days with DFN, and old treated 30 days with DFN. The results were referred to old NM mice; expressed as mean ± standard deviation (10 animals per group). Asterisks refer to a statistically significance. *p<0.05, **p<0.01, defined by applying the one-way ANOVA test.

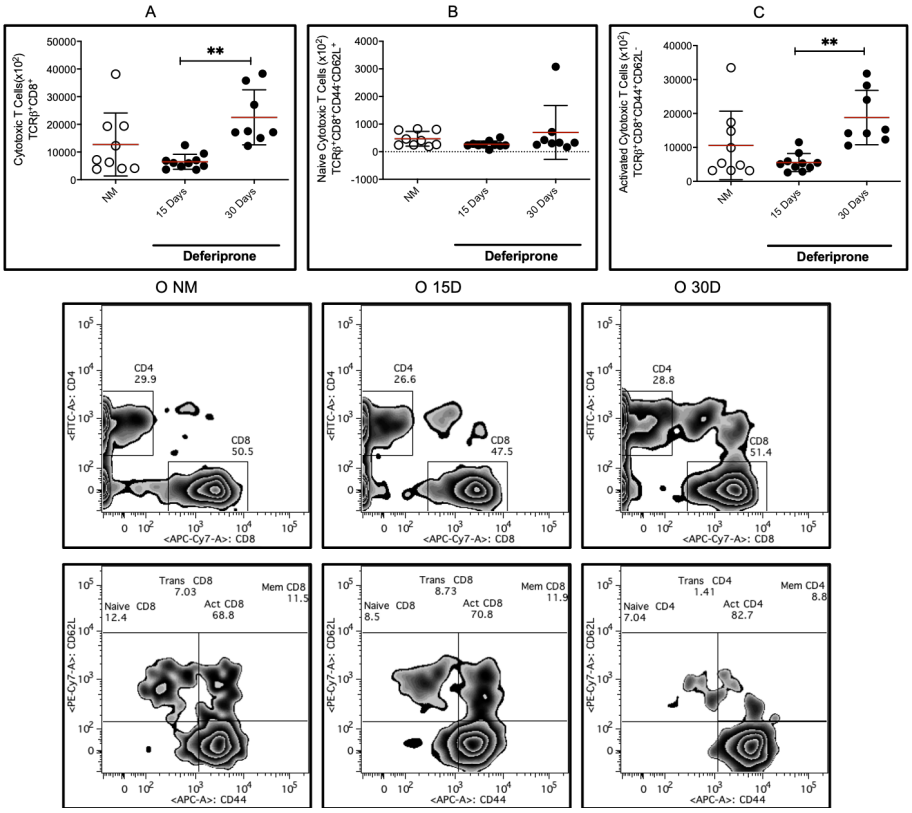

Fig. 127- Cytotoxic T cells activation after DFP treatment. Old mice were injected i.p. with DFN for a period of 15 or 30 days, every other day. Graph (A) shows the number of cytotoxic T cells (TCRβ+CD8+), (B) Naïve cytotoxic T cells (CD8+CD62L+CD44-) and (C) Activated cytotoxic T cells (CD8+CD62L-CD44+). The differences were also observed in graphs obtained from freshly isolated brain leukocytes from old NM, old treated 15 days with DFN, and old treated 30 days with DFN. The results were referred to old NM mice; expressed as mean ± standard deviation (10 animals per group). Asterisks refer to a statistically significance. *p<0.05, **p<0.01, defined by applying the one-way ANOVA test.

CHAPTER 5

5.1 Pharmacological PD mice model

To better understand the role Heme/Fe in sensitizing to the development of PD, we performed experiments in a pharmacological model of PD, induced by the neurotoxin precursor MPTP. The use of this compound is well accepted as MPTP-treated mice are known to display several features of PD, such as nigral cell loss, striatal dopamine loss, motor impairment and behavioral deficits.

When we analyzed the peripheral infiltration of immune cells into the brain, we observed that MPTP did not cause any effect in young mice, when administered at sub-acute dosages. Whereas, when old mice were treated with the same concentration present a significant increase in peripheral immune cells brain infiltrates (Fig.128).

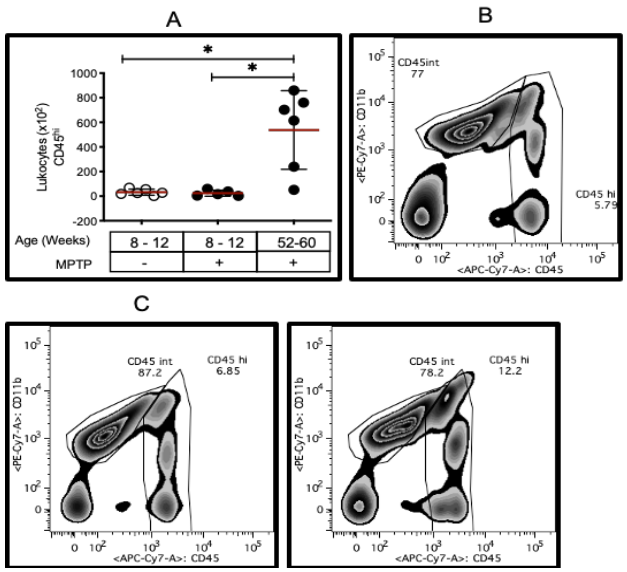

Fig. 128- Peripheral infiltration into the brain after MPTP treatment. Young (8-12 weeks old) and old (52-60 weeks old) MPTP-treated animals were used for the experiment. Graph (A) shows the number of infiltrated cells in the brain

(CD45hi), (B) Young mice, (C) MPTP-treated young mice and (D) MPTP-treated old mice. The results were referred to young non-manipulated mice; and expressed as mean ± standard deviation (5-6 animals per group). Asterisks refer to a statistically significance. *p<0.05, defined by applying the non-parametric Kruskal-Wallis test, as appropriate.

As observed in the graph below, the inflammatory profile follows the same tendency. In young mice, where the level of inflammation is lower and often undetectable, as shown in the previous results, sub-acute administration of MPTP causes no effect. However, when inflammation increases, as in old mice, MPTP is capable to boost immunity, as indicated by the increased number of CCR2 expressing cells (Fig.129).

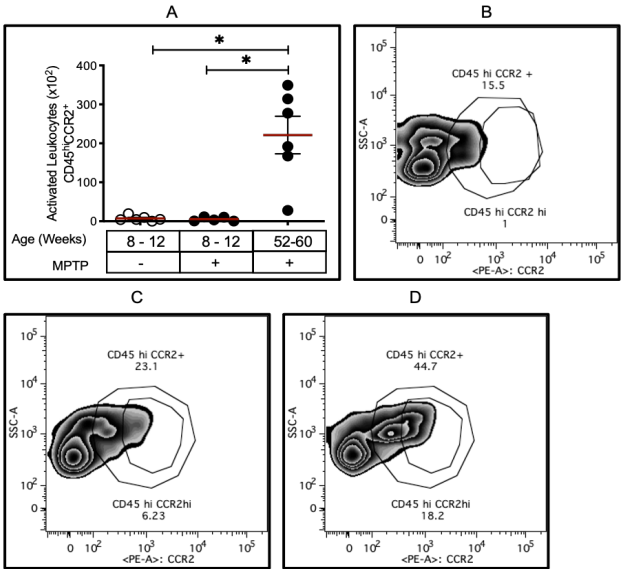

Fig. 129- Lymphocytes' activation in the brain after MPTP treatment. Young (8-12 weeks old) and old (52-60 weeks old) MPTP-treated animals were used for the experiment. Graph (A) shows the number of recruiting lymphocytes cells in the brain (CD45hiCCR2+), (B) Young mice, (C) MPTP-treated young mice and (D) MPTP-treated old mice. The results were referred to young non-manipulated mice; and expressed as mean ± standard deviation (5-6 animals per group). Asterisks refer to a statistically significance. *p<0.05, defined by applying the non-parametric Kruskal-Wallis test.

In accordance with previous graphs, old mice treated with MPTP showed an increased number of inflammatory monocytes when compared to young mice exposed to the same treatment (Fig.130).

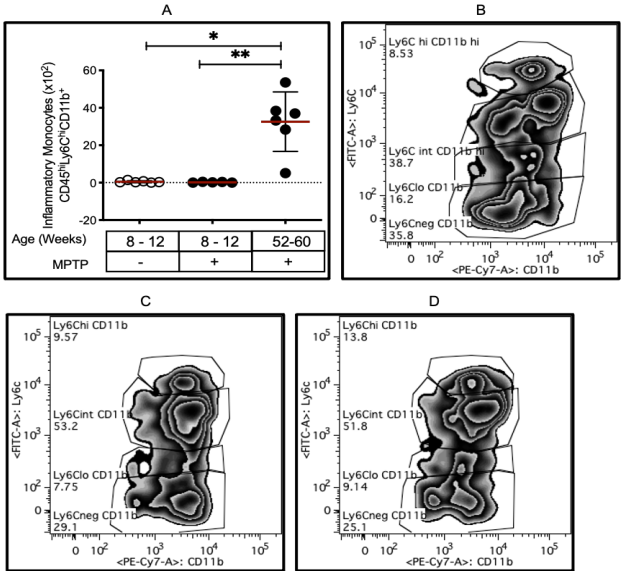

Fig. 130- Inflammatory monocytes increase in the brain after MPTP treatment. Young (8-12 weeks old) and old (52-60 weeks old) MPTP-treated animals were used for the experiment. Graph (A) shows the number of inflammatory monocytes in the brain (CD45hiLy6ChiCD11b+), (B) Young mice, (C) MPTP-treated young mice and (D) MPTP-treated old mice. The results were referred to young non-manipulated mice; expressed as mean ± standard deviation (5-6 animals per group). Asterisks refer to a statistically significance. *p<0.05, **p<0.01, defined by applying the non-parametric Kruskal-Wallis test.

When assessing T cell subsets, CD4 and CD8, and their activation state we found similar patterns than previous data. Old mice present an increased number of CD4 and CD8 T cells and enhanced activation upon MPTP administration (Fig.131 and 132).

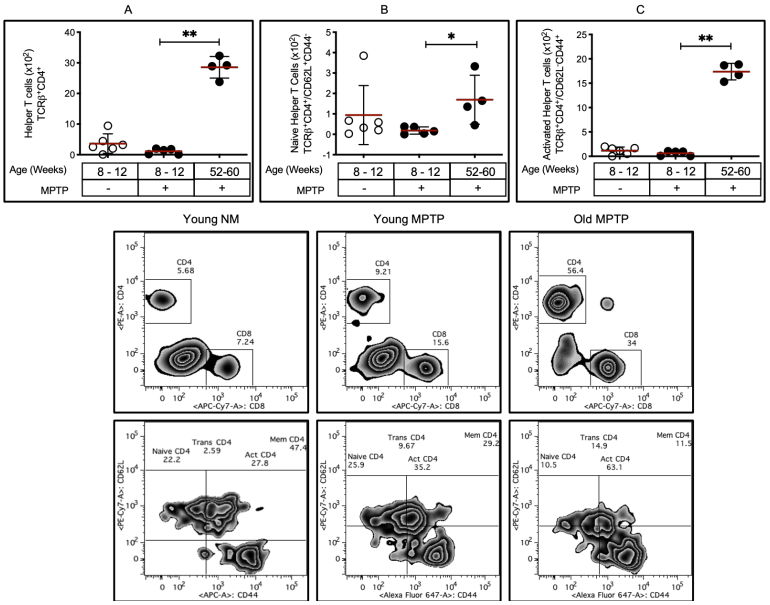

Fig. 131- Helper T cells' activation after MPTP treatment. Young (8-12 weeks old) and old (52-60 weeks old) MPTP-treated animals were used for the experiment. Graph (A) shows of helper T cells (TCRβ+CD4+), (B) Naïve helper T cells (TCRβ+CD4+CD62L+CD44-), (C) Activated helper T cells (TCRβ+CD4+CD62L-CD44+). The results were referred to young NM mice; expressed as mean ± standard deviation (5-6 animals per group). Asterisks refer to a statistically significance. *p<0.05, **p<0.01, defined by applying the non-parametric Kruskal-Wallis test.

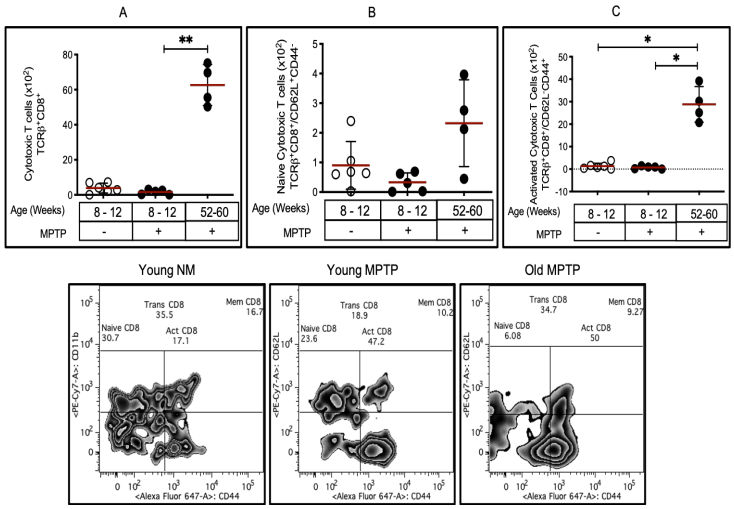

Fig. 132- Cytotoxic T cells activation after MPTP treatment. Young (8-12 weeks old) and old (52-60 weeks old) MPTP-treated animals were used for the experiment. Graph (A) shows of cytotoxic T cells (TCRβ+CD8+), (B) Naïve cytotoxic T cells (TCRβ+CD8+CD62L+CD44-), (C) Activated cytotoxic T cells (TCRβ+CD4+CD62L-CD44+). The results were referred to young NM mice; expressed as mean ± standard deviation (5-6 animals per group). Asterisks refer to a statistically significance. *p<0.05, **p<0.01, defined by applying the non-parametric Kruskal-Wallis test.

5.2 α-Synuclein Immunization

Accumulation of misfolded fibrillar α-Syn is one of the main hallmarks of PD [197]. Reports show that Heme/Fe accumulation driven-oxidative stress promotes α-syn aggregation, and by doing so it increases neuroinflammation and sensitize to the development of PD [104][105].

To better understand the Heme/Fe interaction with α-syn, as one of the inducing factor for PD, we performed experiments mimicking this condition in mice. To facilitate the entering of α-syn into the brain, prior immunizations with pertuxis toxin were carried out. Then, intranasal administration of α-syn, followed Heme peripherally administered.

As expected, Heme administration significantly increases the infiltration of peripheral immune cells into the brain (Fig.133). Conversely, α-syn alone showed no effect. However, when Heme administration was followed by α-syn, it slightly reduced the infiltration caused by Heme alone, suggesting the possibility of α-syn protecting against Heme cytotoxicity by scavenging this molecule.

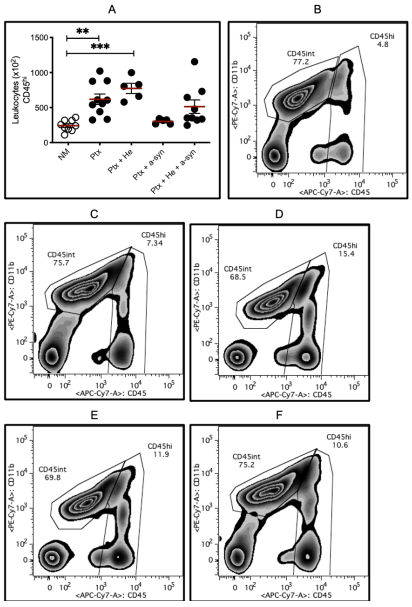

Fig. 133- Peripheral infiltration into the brain after α-syn and Heme treatment. Young (8-12 weeks old) Heme and/or α-syn-treated animals were used for the experiment. Graph (A) shows the number of infiltrated cells in the brain (CD45hi), (B) NM Young mice, (C) PTX-treated young mice, (D) PTX + Heme treated young mice, (E) PTX + α-syn treated young mice and (F) PTX + Heme + α-syn. The results were referred to young NM mice; expressed as mean ± standard deviaiton (4-9 animals per group). Asterisks refer to a statistically significance. *p<0.05, defined by applying the non-parametric Kruskal-Wallis test.

As leukocytes' infiltration increases, so it does inflammation, as shown in the graph below. Heme boosts neuroinflammation by enhancing the number of CCR2 positive leukocytes, as treatment with α-syn alone continues to have no effect on innate immune cells. Although no significant results were detected, treatment with Heme followed by α-syn stimulation slightly reduced the Heme-driven neuroinflammatory phenotype (Fig.134).

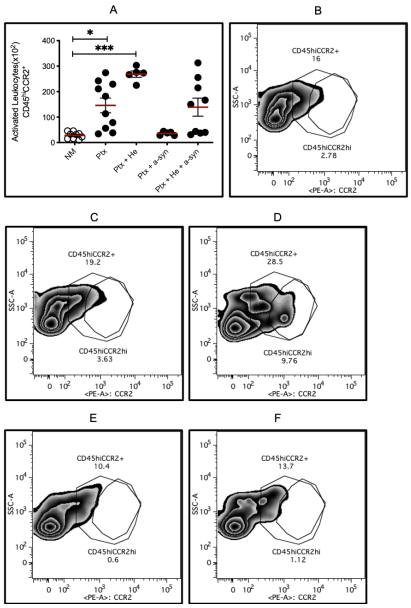

Fig. 134- Peripheral leukocytes activation in the brain after α-syn and Heme treatment. Young (8-12 weeks old) Heme and/or α-syn-treated animals were used for the experiment. Graph (A) shows the number of infiltrated cells in the brain (CD45hiCCR2+), (B) NM Young mice, (C) PTX-treated young mice, (D) PTX + Heme treated young mice, (E) PTX + α-syn treated young mice and (F) PTX + Heme + α-syn. The results were referred to young NM mice; expressed as mean ± standard deviation (4-9 animals per group). Asterisks refer to a statistically significance. *p<0.05, defined by applying the non-parametric Kruskal-Wallis test.

When analyzing specific populations, like inflammatory monocytes, we observed the same pattern as previously analyzed immune cells (Fig.135). The difference between Heme-treated mice and α-syn/Heme-treated mice is significant, confirming that α-syn is affording protection against Heme activation.

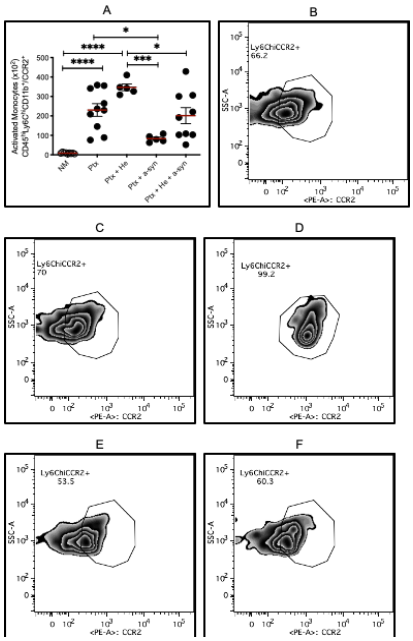

Fig. 135- Monocytes' and leukocytes activation in the brain after peripheral Heme and α-syn treatment. Young (8-12 weeks old) Heme and/or α-syn-treated animals were used for the experiment. Graph (A) shows the number of infiltrated cells in the brain (Ly6ChiCCR2+), (B) NM Young mice, (C) PTX-treated young mice, (D) PTX + Heme treated young mice, (E) PTX + α-syn treated young mice and (F) PTX + Heme + α-syn. The results were referred to young NM mice; expressed as mean ± standard deviation (4-9 animals per group). Asterisks refer to a statistically significance. *p<0.05, defined by applying non-parametric Kruskal-Wallis test.

CHAPTER 6

6. *In vitro* Assays

To better understand the molecular mechanisms by which increased doses of Heme/Fe mediate its cytotoxic effect, we conducted *in vitro* experiments, using BV-2 cells and isolated primary mouse microglia. To note that the protocol we used to obtain an enriched microglia culture was established in our laboratory.

6.1 Heme induces proliferation in BV-2 cell line

A Heme/Fe dose-response assay was carried out to assess the concentration of the compound that does not affect cell viability but elicit inflammation. Once that dose was found, we performed a time response assay with the same aim.

As shown below, Heme was not capable to induce cell death, even at higher concentrations. This lack of cytotoxicity was observed either in BV-2 or primary isolated microglia (Fig.136). After 4 or 8 hrs Heme stimulation, the proliferation of both BV-2 and primary microglia increases. After 16 and 24 hrs treatment, Heme showed no effect in BV2. Primary microglia treated with 50μM, for 16 hrs, proliferate more when compared to non-treated control cells. However, 24 hrs treatment showed no effect, as in BV-2 cells.

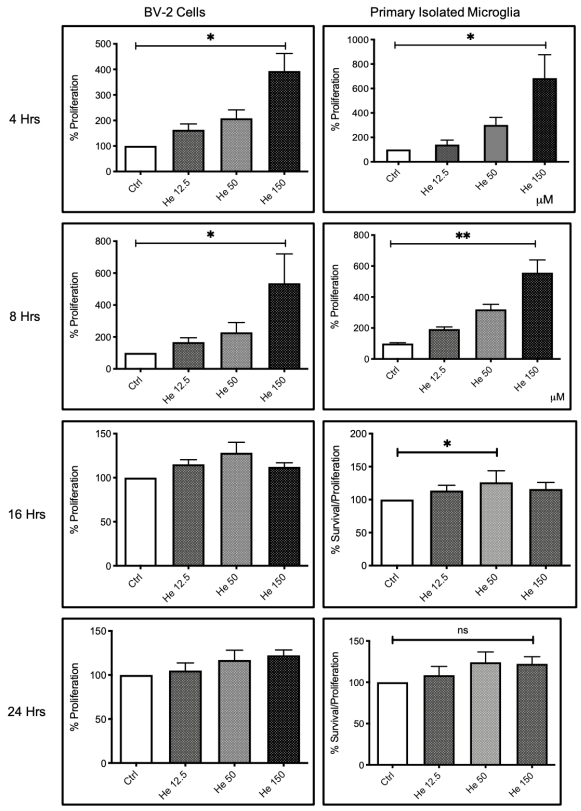

Fig. 136- BV2 response to Heme/Fe stimulation in a dose and time-dependent matter. BV2 cells and primary microglia were treated with Heme at the indicated concentrations, in serum-deprived medium, for 4 or 8 hrs; or for 16 or 24 hrs if maintained in complete medium. Cell viability and proliferation were evaluated by Crystal Violet. The result is representative of four different experiments, carried out in sextuplicate, showing the same trend. The results are expressed as mean ± standard deviation and referred to non-treated controls. Asterisks refer to a statistically significant difference. * $p < 0.05$, ** $p < 0.01$, defined by applying the student's t test.

6.2 Excess Heme concentration abrogates inflammation

The pro-inflammatory effect of Heme in these cells was assessed by quantifying pro-inflammatory cytokines, such as IL-6 and TNF, after 4 hours treatment. Although we observed that microglia remained viable even at higher Heme concentrations (150μM), their

ability to develop an inflammatory response decrease with the dose that was used. The production of IL-6 was completely inhibited when cells were stimulated with higher Heme concentrations. This effect also occurred when referring to TNF production, measured upon cell stimulation with 150μM Heme (Fig.137). The release of these pro-inflammatory cytokines, in response to higher doses of Heme was also measured in primary microglia. Our results demonstrated that the production of IL-6 and TNF was inhibited 4 hrs after Heme stimulation, at 50 and 150μM.

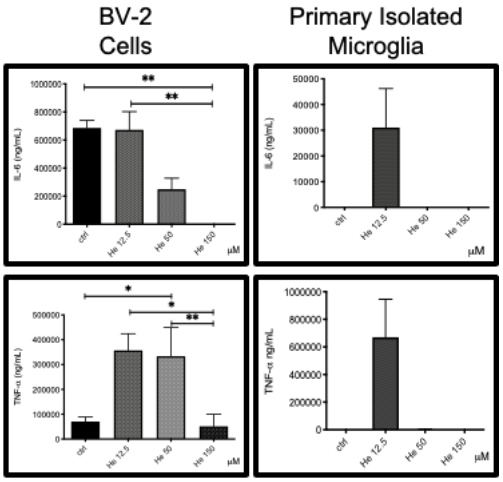

Fig. 137- Quantification of pro-inflammatory cytokines upon Heme/Fe stimulation. BV2 and primary microglia cells were treated with Heme at indicated concentrations, maintaining cells in serum-deprived medium, for 4 hrs. The production of IL-6 and TNF-α was measured by ELISA and expressed as mean ± standard deviation and referred to non-treated control cells. The result is representative of three independent experiments, carried out with sextuplicate. Asterisks refer to a statistically significant difference. * $p < 0.05$, defined by applying the Student's t test.

6.3 Increased Heme concentration inhibits ROS generation

To evaluate Heme pro-oxidant effect, we quantified total (DCF) and mitochondrial (MitoSox) ROS generation, using specific probes. We observed that in response to high concentration of Heme treatment, namely at 150 μM, primary microglia are not responsive, contrarily to BV-2 cells (Fig.138). These results are in agreement with the reduced inflammatory response of brain infiltrated immune cells observed in old mice, which present high levels of Heme/Fe accumulation, when exposed to higher Heme concentration. Our findings suggest that higher Heme concentration is capable to suppress microglia activation, as inhibiting ROS production.

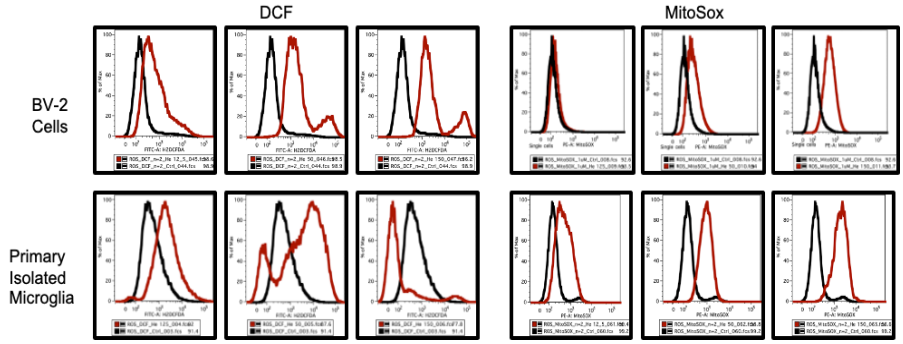

Fig. 138- ROS generation upon Heme/Fe administration. BV2 and primary microglia cells were treated with Heme at indicated concentrations, maintaining cells in serum-deprived medium, for 4 hours. The generation of ROS was assessed by flow cytometry using cell permeable probes, i.e., CM-H2DCFDA and MitoSox, respectively.

To further confirm that the inflammatory effect caused by Heme is due to the Fe atom inside that molecule, we performed experiments with the Fe chelator, DFP. Pre-treatment of BV-2 cells with DFP,

administered 1 hour before Heme and maintained thereafter for 4 Hrs, was observed capable to reduce the generation of ROS.

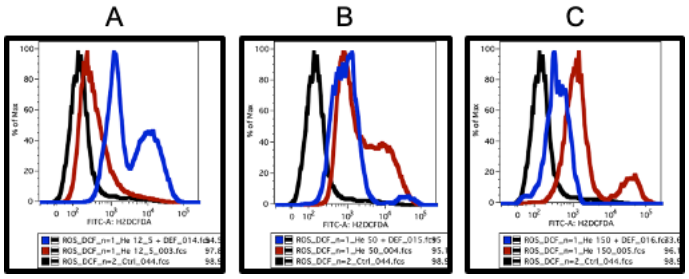

Fig. 139- ROS generation upon Heme/Fe administration. BV-2 cells were treated with DFN 1hr before Heme and maintained thereafter for 4hrs. Heme treatment lasted 4 hrs. The histograms (A) show DFN +/- 12.5 μM Heme, (B) DFN +/- 50 μM Heme and (C) DFN +/- 150 μM Heme. The generation of ROS was assessed by flow cytometry using a cell permeable probe, i.e. CM-H2DCFDA.

Since these effects are mediated by Fe, we also assessed whether the pharmacological inhibition of Fe-mediated cell death, known ferroptosis, with ferrostatin-1 (Fer-1) could prevent the Heme-driven pro-inflammatory phenotype observed in these cells. BV2 cells were treated with indicated doses of Heme and 25 μM of Fer-1 was adminstered for 4 hours. The results showed that the pro-oxidant effect of Heme in these cells was inhibited by Fer-1. This treatment suppressed ROS production, protecting mainly mitochondria from the development of oxidative stress.

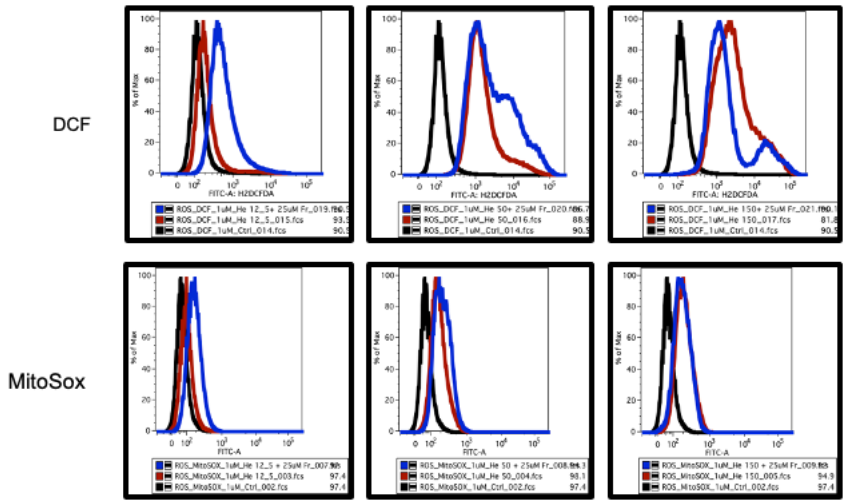

Fig. 140- Heme-driven ROS inhibition by Fer-1. BV-2 cells were treated with Heme at indicated concentrations, maintaining cells in serum-deprived medium, for 4 hrs. The generation of ROS was assessed by flow cytometry using cell permeable probes, i.e., CM-H2DCFDA and MitoSox, respectively.

DISCUSSION

CHAPTER 1

The importance of Heme relies on its ability to promote the occurrence of several biological functions, among which cell survival, differentiation, proliferation, etc. [34]–[36]. Nevertheless, due to the Fe atom contained within the protoporphyrin ring it can turn cytotoxic, as inducing the generation of ROS. The lipophilic nature of Heme favors the appearance of oxidative stress, when intercalating into membranes. Whether this might contribute to underlie the pathogenesis of neurodegenerative diseases is likely the case, as Heme/Fe overload is postulated to be one of the causes of neuronal loss and neuroinflammation [198][199].

In keeping with this notion, we aimed to characterize the pro-inflammatory role of Heme in the brain. To do so, we administrated Heme, i.p., to young mice (8-12 weeks) and assessed the inflammatory profile of these animals by flow cytometry.

Our results demonstrate that the peripheral injection of Heme significantly impairs the integrity of the BBB, possibly due to its pro-oxidant effect. This notion is supported by the fact that free Heme alone can cause ROS generation, given the ability of the Fe atom to participate in Fenton's reaction and promote the production of free radicals [2]. Our data are in agreement with our hypothesis, since Heme treatment causes in mice an increase in Fe the brain, leading to exacerbated oxidative stress, which further induces BBB dysfunction. At molecular levels, ROS are responsible for tight junction modifications, mitochondrial impairment and microglial activation [200],

an effect also confirmed in mice models [201], [202]. Similar to what we observed, Imai et al. showed that Heme administration causes a deleterious effect in the brain including: increased BBB permeability, Fe accumulation in endothelial cells and neuronal damage [203]. However, in this study Heme was injected directly into the striatum and not in the periphery contrary to our experimental model, which provides new insides towards risk factors for an increasing susceptibility to neuronal loss.

When assessing whether peripheral Heme/Fe treatment could cause neuroinflammation, our data demonstrated a significant increase in the peripheral leukocytes in the brain, suggesting that Heme-driven BBB disruption might contribute to this phenomenon. Inflammatory neutrophils (Ly6GhiCCR2+) represented the largest leukocyte population entering the brain, followed by inflammatory monocytes (Ly6ChiCCR2+). Our results are supported by the notion that Heme also acts as a chemoattractant molecule [204], altering brain microvascular endothelial cells and upregulating the expression of cellular adhesion molecules [205] to then facilitate the migration of leukocytes into inflamed tissue, boosting neuroinflammation [1].

We then assessed microglia's proinflammatory response. Their count (CD45int) and level of activation were significantly elevated in Heme-treated young mice, when compared control. A TLR4-dependent activation was already described [206].

Evaluating the infiltration of adaptive immune T cells (TCRβ+) into the brain, we found that, even in homeostatic conditions and besides the presence of T cells in the brain, microglia represent the larger CNS population. In agreement, also Mrdjen et al. showed the existence of a substantial amount of peripheral immune cells in the brain of 8-weeks-old C57BL/6 mice, both from the innate and adaptive immune system [207]–[209].

When Heme is administered, i.p., the number of T cells increased significantly as well as the activation of T helper (th) ($CD4^+$) and cytotoxic T cells (CTLs) (CD8). It is known that upon CNS injury or disease, peripheral immune cells are actively recruited to the brain [210], through a molecular mechanism not fully elucidated. Investigations report the existence of T cell infiltration and microglia activation in the brain of pharmacological PD models as well as in *post-mortem* brain of PD patients [194]. Subbarayan et al. even found a relation between T cells and microglia, where in a α-syn PD rat model, CD4 T and CD8 T cells as well as MHCII microglia activation were detected in the SN along with α-syn expression. Given that the peripheral injection of Heme is responsible for the activation of circulating immune cells by breaching the BBB and entering the brain, this molecule can play a role in the development of PD by promoting neuroinflammation and neuronal impairment [211].

We hypothesize that immune cells buffered Heme/Fe to prevent cytotoxicity, which was confirmed also by the quantification of calcein quenching in Macrophages, B cells, Natural killer cells, T cells and Helper T cells. However, this circulating compartment enters the brain and is finally responsible also for the appearance of Heme/Fe-loaded microglia.

This was confirmed by the results obtained when comparing Heme-treated mice vs. non-manipulated controls. By promoting Fe overload in the brain, it is this peripheral compartment that contributes to neuroinflammation. This notion was also supported by the data obtained when analyzing the inflammatory states of PBLs and spleen tissue. Total leukocytes and their activation in the peripheral compartment increased upon Heme administration. However, activated neutrophils and monocytes counts decreased, possibly indicating the migration of this population into tissues, like the brain.

Spleen leukocytes showed no major effects upon Heme administration, suggesting that leukocytes might have left the periphery, an effect justifying the increase of these cells in the brain, recruited also by an upregulated expression of CCR2 in microglia, in addition to inflammatory monocytes (Ly6Chi), known to promote monocytes and T cells mobilization to the site of inflammation [212][213].

Hence, our results show that peripheral Heme administration is capable to strongly impact the brain that, causing a neuroinflammation, aggravated by an impaired BBB permeability.

Linking all findings with PD, also Reale and colleagues observed that these patients present a higher expression of CCR2 in the cerebral spinal fluid (CSF) and plasma [214], which is in agreement with our data.

CHAPTER 2

Heme/Fe accumulation in the brain physiologically occurs during aging, as the appearance of sub-acute neuroinflammation. Whether this combination could favor the development of neurodegenerative disorders, like PD, was our starting hypothesis. Also, because in humans, brain Heme/Fe accumulation could be associated with silent microhemorrhages occurring with advancing age and that also cause oxidative stress. Thus, to demonstrate this possibility, we performed a series of experiments comparing young (8-12 weeks) vs. old non-manipulated mice (52-60 weeks). The presence of brain Fe accumulation in aged animals was confirmed, along with an increased BBB disruption favoring the infiltration of activated peripheral immune cells. These data were in agreement with the

literature, showing an enhanced level of pro-inflammatory mediators in the brain of elderly, a phenomenon boosted in patients suffering from age-related diseases, as PD [48]. We believe that microglia activation is a consequence of the peripheral inflammation, as increased microglia proliferation was reported under inflammatory conditions [215][216]. Besides the fact that our data indicated no difference between the conditions analyzed, old mice presented an increased inflammatory profile. The positive loop created by the sustained inflammation observed might contribute to cause neuronal death, thus believing it is an age-driven inflammation what underlies the development of neurodegeneration.

The results obtained, when comparing young and old animals, are similar to those observed when analyzing young mice exposed or not to Heme. These findings validate our hypothesis that the proinflammatory effect of this molecule sensitizes, when accumulating in the brain during aging, to the development of neurodegenerative diseases.

Complementary profiles were observed in peripheral compartments. However, since no major changes were found in spleen and blood, we believe that inflammatory cells were already migrated to the brain, at the time of the analysis.

CHAPTER 3

Considering that Heme/Fe enhances inflammation and aging *per se* is an inflammatory process, we hypothesized that increasing Heme concentration in old mice would exacerbate the pro-inflammatory condition, causing ultimately neuronal loss. To assess

whether that would have been the case, we investigated the effect of exogenous peripheral Heme administration into old mice (52-60 weeks).

To our surprise, we observed a significant decrease in inflammatory cells in the brain of peripherally Heme-treated old animals, accompanied by a reduced microglia count, activation and recruiting capacity, measured by using expression markers as MHCII and CCR2, respectively.

Among the populations of immune cells that less infiltrated the brain of peripherally Heme-treated mice, we found both neutrophils and monocytes. These cells also presented a reduced activation, when compared to previous results.

Regarding the adaptive immune system, in the brain of peripherally Heme-treated old mice, total leukocyte count was decreased, as their activation. Also, immune cell sub-populations, like CD4 and CD8 were decreased. Although naïve CD4 and CD8 presented no major changes when compared to old NM control mice, their activation drastically diminishes upon Heme administration.

When assessing the peripheral compartment, while the immune profile observed in circulation is similar to the brain, in the spleen, the leukocyte counts were significantly reduced.

Since Heme administration to old mice seemed to decrease inflammation to levels like those observed in young non-manipulated animals, we arose the question of whether cells might become unresponsive. This could explain the lower ability to recruit observed in the brain of these animals, which, as occurs for microglia [210], reflects the decreased neuroinflammation [217]. We also hypothesize that the response obtained could be due to cell exhaustion, described in the literature as the response to a continuous PAMPs exposure [218]–[220]. This mechanism is well characterized in T cell population,

retained in suboptimal functions, as not effective in promoting an active pathogen clearance [219]. However, our data demonstrated that despite in lower number, CD4 and CD8 are still present and activated upon peripheral administration of Heme/Fe, this being necessary for microglia to upregulate MHCII [221].

When quantifying Fe accumulation in peripheral immune cells found in the brain or simply in PBLs, by using the calcein probe, we found that cells isolated from Heme-treated old mice presented a lower Fe accumulation when compared to old non-treated mice. However, PBL cells from Heme-treated old showed a higher Fe accumulation. This strongly indicates that Heme/Fe loaded cells infiltrates the brain, where exacerbate inflammation by inducing a general immune system shutdown.

CHAPTER 4

The results obtained demonstrated that the circulating compartment plays a crucial role in priming the brain towards the development of neuroinflammation. Thus, we assessed whether its depletion might revert the inflammatory process. To test our hypothesis, we first assessed the effect of Heme administration into young (8-12 weeks) and old (52-60 weeks) TCRβ-KO (mature T cells depleted) and RAG2-KO (mature T and B cells depleted) mice. The ability of this mice to be less susceptible to Heme/Fe-driven inflammation was expected.

Contrary to young WT mice, young TCRβ-KO and RAG2-KO did not present an increased infiltration of peripheral immune cells upon Heme administration. When we assessed leukocytes activation by quantifying CCR2 expression, we also found no changes in immune

deficient mice. However, in RAG2-KO mice, leukocytes presented a lower level of MHC II, which increases upon Heme stimulation.

Furthermore, our data demonstrated that when mice lack mature lymphocytes displayed a remarkably reduced susceptibility to Heme-driven neuroinflammation, as measured by the number of activated neutrophils and monocytes. Similarly, microglia presented the same pattern. Although no significant difference was shown between microglia activation in non-manipulated and Heme-treated TCRβ-KO and RAG2-KO mice, the inflammatory profile of these cells tended to decrease.

Neuroinflammation, Fe accumulation in the SNpc and oxidative stress, among others [222]–[224], constitute PD features, promoting neuroinflammation and neuronal death [225]. Brochard et al. showed that the depletion of the lymphocytic compartment rendered mice less susceptible to MPTP, as presenting a reduced infiltration of peripheral immune cells and attenuated dopaminergic cell death [194].

When analyzing the peripheral compartment of these animals, no major effects were observed in both spleen and PBL. Nevertheless, immunocompromised mice presented lower numbers of total leukocytes, which were also less activated, when compared to WT mice. A lower inflammatory profile was also found in response to peripheral Heme administration. Like observing in the brain, the levels of inflammation in RAG2-KO mice are lower than those in TCRβ-KO mice.

In keeping with the results obtained from Heme-treated old mice, we assessed whether the observed phenotype was modulated by the depletion of mature lymphocytes. Immunocompromised mice presented lower infiltrate counts when compared to WT old non-manipulated mice. In agreement with previous data, old RAG2-KO

mice showed a lower susceptibility to both aging and Heme administration effects.

We also observed that peripheral Heme-treated old TCRβ-KO and RAG2-KO showed an increased number of CCR2 expressing cells in the brain. The same could not be found when assessing MHC II expression. However, while TCRβ-KO mice showed no difference between as for neutrophils, exogenous Heme administration in RAG2KO mice decreased their count.

Next, we assessed whether Heme might have influenced microglia from old TCRβ-KO mice. No differences were observed contrarily to RAG2KO mice, where Heme decreases the pro-inflammatory phenotype of these cells in aged mice.

Like the previous experiments, we quantified Fe accumulation in the immune cells of these mice, finding that peripheral Heme administration in young TCRKβ-KO mice does not induce a significant Fe accumulation. When compared to its old counterpart, we found no differences, contrarily to what we observed in WT animals. Heme-treated old TCRKβ-KO mice had significantly reduced Fe accumulation in the myeloid population, further proving the role of lymphocytes in promoting Fe-driven neuroinflammation.

When performing the same analyses in RAG2-KO mice, regardless of the population analyzed, we observed that Fe accumulation in young Heme-treated RAG2-KO mice is lower and there is no significant difference in young vs. old RAG2-KO mice, like in TCRKβ-KO mice.

The profile in peripheral compartments of TCRKβ-KO young mice is the same than in the brain. No changes were observed when comparing young to old non-manipulated TCRKβ-KO mice. Heme-treated old TCRKβ-KO mice also presented a lower Fe accumulation.

Conversely, in circulation, RAG2-KO lower Fe accumulation if compared to young or upon Heme administration, further suggesting that depletion of the lymphocytic compartment confers protection against Heme-mediated inflammation.

Considering that the accumulation of Heme/Fe, during aging, primes the brain toward an inflammatory state, we assessed whether the peripheral administration of DFP a Fe chelator used in PD treatment and capable to cross the BBB, could revert this aged-related phenotype. Our aim was to demonstrate it could act in a preventive manner, decreasing the contribution of the immune system to the development of brain inflammation and Fe accumulation, which then culminate in neuronal death.

To do so we injected old mice with DFP for a period of 15 or 30 days. Our data showed a decrease in leukocytes infiltration into the brain as well as their activation after 15 days of DFP treatment. Regarding cell activation, the number of CCR2 expressing monocytes decreased after 15 days; a phenotype that is completely reverted after 30 days of DFP treatment. Similar data were also observed for T cells and sub-populations of CD4 and CD8, as well as their activation, which is diminished at day 15 and reverted at day 30. The same for microglia, which activation is significantly reduced after 15 days of DFP treatment, contrarily to what occurring after 30 days of treatment.

Our results show that aged mice are have increased Fe accumulation and increased neuroinflammation, considered both features of PD [226]. The use of DFP showed promising results in decreasing neuroinflammation in aged mice, due to its ability to chelate excess Fe [226], [227]. The data obtained further confirm that Fe accumulation is one of the leading cause of neuroinflammation and neurodegeneration, a notion also supported by the beneficial effect of DFP in ameliorating the progression of neurodegenerative diseases,

like PD [172]. Nowadays, four clinical trials of Fe chelation have been successfully completed in PD, whether DFP was shown to decrease Fe content in the SN, dentate and caudate nucleus, improve motor disfunction and retard disease progression. Nevertheless, if the treatment is suspended, Fe accumulates again [175][174], suggesting that DFP should be used in combination with other therapies.

CHAPTER 5

To further understand aging as the main risk factor for PD, we investigated the effect of MPTP in mice young vs. old.

MPTP is a neurotoxin precursor, widely used to study PD. Once injected, MPTP easily crosses the BBB into the brain parenchyma. In the CNS, it is uptaken by glia cells and converted into the toxic metabolite 1-methyl-4-phenylpyridinum (MPP+), which presents a high affinity for dopaminergic neurons, where causing oxidative stress and neuronal damage [228].

When injecting MPTP in young (8-12 weeks) and old (52-60 weeks) mice, we observed that while a sub-acute dose did not cause any effect in young mice, aged animals present a significant increase in neuroinflammation. This indicates that PD is a multifactorial disease, requiring an inflammatory state to occur and brain Fe accumulation, the importance of which was also evaluated by performing experiments with purified α-syn exposure. Heme/Fe driven-oxidative stress promotes α-syn aggregation, which presenting a ferrireductase activity, boosts ROS by reducing Fe^{3+} into Fe^{2+} [104]. When treating young mice (8-12 weeks) with Heme and α-syn, we observed that this latter acted in a preventing manner, diminishing Heme-mediated neuroinflammation. No effects were observed by α-syn alone.

CHAPTER 6

To better understand the molecular mechanism by which increased doses of Heme/Fe might turn microglia unresponsive, *in vitro* experiments were performed in BV-2 cells and isolated mouse primary microglia.

A dose-response of Heme was carried out, showing that, despite the increased proliferation, when experiments are carried out in serum-deprived medium, microglia become unresponsive. Pro-inflammatory cytokines, IL-6 was fully inhibited upon Heme stimulation at the highest concentration (150μM), as TNF. Similar results were also obtained in primary isolated microglia. This effect was observed only when treated cells at higher Heme concentrations, maintaining a pro-inflammatory profile at lower doses. Possibly, these latter mimic microhemorrhage conditions, where microglia are known to migrate to the site of injury and increase proliferation [229].

We then quantified the pro-oxidant effect of Heme by measuring total (DCF) and mitochondrial (MitoSox) ROS generation, finding that also oxidative stress is inhibited at higher concentration of Heme (150 μM). Contrarily, BV-2 cells were still responsive, and their phenotype was reverted by DFN.

Given the predominant role of Fe in mediating these effects, we assessed whether the pharmacological inhibition of ferroptosis with ferrostatin-1 (Fer-1) could also prevent the Heme-driven pro-inflammatory phenotype of these cells. The results obtained met our expectations, in the sense that the pro-oxidant effect of Heme in BV2 cells was inhibited by Fer-1 treatment. ROS production in mitochondria was significantly reduced by Fer-1.

Overall, our study demonstrated that inflammation and

Heme/Fe accumulation are risk factors for the development of PD and as such could be used as prognostic markers for neurodegeneration.

CONCLUSION

Heme is vital for a variety of biological processes. However, it can also be cytotoxic. In this work we reported the interplay between aging and Heme accumulation as one of the causes for neuroinflammation and increased susceptibility to neurodegeneration, as priming the brain for neuronal damage.

Our data showed the existence of a communication between the periphery and the brain, already at basal level. In this study, we demonstrated that the infiltration of Fe loaded peripheral immune cells into the brain occurs under inflammatory conditions. Since aging is a sub-chronic pathology, we demonstrate that advancing age promotes Heme/Fe accumulation in the brain and primes this organ to the development of neurodegenerative diseases, such as PD.

By activating immune cells and causing neuronal death, microglia were shown to be a consequence of a chain of events started in the periphery. Treatment with DFN abrogates these effects, as scavenging Fe prevents aging-driven neuroinflammation.

BIBLIOGRAPHY

[1] F. F. Dutra and M. T. Bozza, “Heme on innate immunity and inflammation,” *Front. Pharmacol.*, vol. 5 MAY, no. May, pp. 1–20, 2014.

[2] R. Larsen, Z. Gouveia, P. Miguel, and R. Gozzelino, “Heme cytotoxicity and the pathogenesis of immune-mediated inflammatory diseases,” vol. 3, no. May, pp. 1–17, 2012.

[3] R. Gozzelino, “The Pathophysiology of Heme in the Brain.,” *Curr. Alzheimer Res.*, vol. 13, no. 2, pp. 174–84, 2016.

[4] T. Korolnek and I. Hamza, “Like iron in the blood of the people: The requirement for heme trafficking in iron metabolism,” *Frontiers in Pharmacology*, vol. 5 JUN, no. June. pp. 1–13, 2014.

[5] S. Kumar and U. Bandyopadhyay, “Free heme toxicity and its detoxification systems in human,” vol. 157, pp. 175–188, 2005.

[6] D. Chiabrando, F. Vinchi, V. Fiorito, S. Mercurio, and E. Tolosano, “Heme in pathophysiology: A matter of scavenging, metabolism and trafficking across cell membranes,” *Front. Pharmacol.*, vol. 5, no. April, pp. 1–24, 2014.

[7] X. Yuan *et al.*, “Regulation of intracellular heme trafficking revealed by subcellular reporters,” *Proc. Natl. Acad. Sci. U. S. A.*, vol. 113, no. 35, pp. E5144–E5152, 2016.

[8] V. Vijayan, F. A. D. T. G. Wagener, and S. Immenschuh, “The macrophage heme-heme oxygenase-1 system and its role in inflammation,” *Biochem. Pharmacol.*, vol. 153, no. February, pp. 159–167, 2018.

[9] R. G. Kranz, C. Richard-Fogal, J.-S. Taylor, and E. R. Frawley, “Cytochrome c Biogenesis: Mechanisms for Covalent Modifications and Trafficking of Heme and for Heme-Iron Redox Control,” *Microbiol. Mol. Biol. Rev.*, vol. 73, no. 3, pp. 510–528, 2009.

[10] S. Niwa, K. Takeda, M. Kosugi, E. Tsutsumi, T. Mogi, and K. Miki, “Crystal structure of heme A synthase from Bacillus subtilis,” *Proc. Natl. Acad. Sci. U. S. A.*, vol. 115, no. 47, pp. 11953–11957, 2018.

[11] Sarah E. J. Bowman and Kara L. Bren, “The Chemistry and Biochemistry of Heme c: Functional Bases for Covalent Attachment,” *Nat Prod Rep.*, vol. 23, no. 1, pp. 1–7, 2008.

[12] R. Gozzelino and P. Arosio, “Iron homeostasis in health and

disease," *Int. J. Mol. Sci.*, vol. 17, no. 1, pp. 2–14, 2016.
[13] R. S. Ajioka, J. D. Phillips, and J. P. Kushner, "Biosynthesis of heme in mammals," *Biochim. Biophys. Acta - Mol. Cell Res.*, vol. 1763, no. 7, pp. 723–736, 2006.
[14] D. Chiabrando, S. Mercurio, and E. Tolosano, "Heme and erythropoieis: More than a structural role," *Haematologica*, vol. 99, no. 6, pp. 973–983, 2014.
[15] I. Hamza and H. A. Dailey, "One ring to rule them all: Trafficking of heme and heme synthesis intermediates in the metazoans," *Biochim. Biophys. Acta - Mol. Cell Res.*, vol. 1823, no. 9, pp. 1617–1632, 2012.
[16] J. Hooda, A. Shah, and L. Zhang, "Heme, an essential nutrient from dietary proteins, critically impacts diverse physiological and pathological processes," *Nutrients*, vol. 6, no. 3, pp. 1080–1102, 2014.
[17] I. U. Heinemann, M. Jahn, and D. Jahn, "The biochemistry of heme biosynthesis," vol. 474, pp. 238–251, 2008.
[18] R. Gozzelino, "The Pathophysiology of Heme in the Brain," pp. 174–184, 2016.
[19] B. Wu, Y. Wu, and W. Tang, "Heme Catabolic Pathway in Inflammation and Immune Disorders," *Front. Pharmacol.*, vol. 10, no. July, pp. 1–15, 2019.
[20] V. Hvidberg, M. B. Maniecki, C. Jacobsen, P. Højrup, H. J. Møller, and S. K. Moestrup, "Identification of the receptor scavenging hemopexin-heme complexes," *Blood*, vol. 106, no. 7, pp. 2572–2579, 2005.
[21] L. E. Fredenburgh, M. A. Perrella, and S. A. Mitsialis, "The role of heme oxygenase-1 in pulmonary disease," *Am. J. Respir. Cell Mol. Biol.*, vol. 36, no. 2, pp. 158–165, 2007.
[22] B. Ma, J. P. Day, H. Phillips, B. Slootsky, E. Tolosano, and S. Doré, "Deletion of the hemopexin or heme oxygenase-2 gene aggravates brain injury following stroma-free hemoglobin-induced intracerebral hemorrhage," *J. Neuroinflammation*, vol. 13, no. 1, pp. 1–12, 2016.
[23] S. Immenschuh, V. Vijayan, S. Janciauskiene, and F. Gueler, "Heme as a target for therapeutic interventions," *Front. Pharmacol.*, vol. 8, no. APR, pp. 1–15, 2017.
[24] F. P. Guengerich, "Destruction of Heme and Hemoproteins Mediated by Liver Microsomal Reduced Nicotinamide Adenine Dinucleotide Phosphate-Cytochrome P-450 Reductase," *Biochemistry*, vol. 17, no. 17, pp. 3633–3639, 1978.
[25] S. B. Brown, H. Hatzikonstantinou, and D. G. Herries, "The role of peroxide in haem degradation. A study of the oxidation of ferrihaems by hydrogen peroxide," *Biochem. J.*, vol. 174, no. 3,

pp. 901–907, 1978.
[26] K. V. Lyles and Z. Eichenbaum, “From host heme to iron: The expanding spectrum of heme degrading enzymes used by pathogenic bacteria,” *Front. Cell. Infect. Microbiol.*, vol. 8, no. JUN, pp. 1–13, 2018.
[27] E. Nagababu and J. M. Rifkind, “Heme degradation by reactive oxygen species,” *Antioxidants Redox Signal.*, vol. 6, no. 6, pp. 967–978, 2004.
[28] A. A. Khan and J. G. Quigley, “Heme and FLVCR-related transporter families SLC48 and SLC49,” *Mol. Aspects Med.*, vol. 34, no. 2–3, pp. 669–682, 2013.
[29] and B. H. P. Jacky Chung, Caiyong Chen, “NIH Public Access,” vol. 19, no. 3, pp. 156–162, 2012.
[30] I. Yanatori, M. Tabuchi, Y. Kawai, Y. Yasui, R. Akagi, and F. Kishi, “Heme and non-heme iron transporters in non-polarized and polarized cells,” *BMC Cell Biol.*, vol. 11, 2010.
[31] M. D. K. and B. H. Paw, “Intracellular iron and heme trafficking and metabolism in developing erythroblasts,” *Physiol. Behav.*, vol. 176, no. 1, pp. 139–148, 2017.
[32] D. Chiabrando, V. Fiorito, S. Petrillo, and E. Tolosano, “Unraveling the Role of Heme in Neurodegeneration,” vol. 12, no. October, pp. 1–14, 2018.
[33] X. Yuan, O. Protchenko, C. C. Philpott, and I. Hamza, “Topologically conserved residues direct heme transport in HRG-1-related proteins,” *J. Biol. Chem.*, vol. 287, no. 7, pp. 4914–4924, 2012.
[34] H. Ohta, I. Kimura, M. Konishi, and N. Itoh, “Neudesin as a unique secreted protein with multi-functional roles in neural functions, energy metabolism, and tumorigenesis,” *Front. Mol. Biosci.*, vol. 2, no. MAY, pp. 1–5, 2015.
[35] T. Burmester and T. Hankeln, “Neuroglobin: A respiratory protein of the nervous system,” *News Physiol. Sci.*, vol. 19, no. 3, pp. 110–113, 2004.
[36] I. Kimura *et al.*, “Neuferricin, a novel extracellular heme-binding protein, promotes neurogenesis,” *J. Neurochem.*, vol. 112, no. 5, pp. 1156–1167, 2010.
[37] S. M. Bailey, U. S. Udoh, and M. E. Young, “Circadian regulation of metabolism,” *J. Endocrinol.*, vol. 222, no. 2, 2014.
[38] and B. R. C. Michael V. Airola‡, Jing Du§, John H. Dawson§, “Heme Binding to the Mammalian Circadian Clock Protein Period 2 is Non-Specific,” *Bone*, vol. 23, no. 1, pp. 1–7, 2010.
[39] S. L. Freeman *et al.*, “Heme binding to human CLOCK affects interactions with the E-box,” *Proc. Natl. Acad. Sci. U. S. A.*, vol. 116, no. 40, pp. 19911–19916, 2019.

[40] V. Fiorito and D. Chiabrando, “Mitochondrial Targeting in Neurodegeneration : A Heme Perspective,” no. Figure 1, pp. 12–14, 2018.
[41] H. Atamna, “Heme , iron , and the mitochondrial decay of ageing,” vol. 3, pp. 303–318, 2004.
[42] A. Morita *et al.*, “Temporal evolution of heme oxygenase-1 expression in reactive astrocytes and microglia in response to traumatic brain injury,” *Brain Hemorrhages*, vol. 1, no. 1, pp. 65–74, 2020.
[43] N. Schallner *et al.*, “Microglia regulate blood clearance in subarachnoid hemorrhage by heme oxygenase-1,” *J. Clin. Invest.*, vol. 125, no. 7, pp. 2609–2625, 2015.
[44] P. A. Yates, R. Sirisriro, V. L. Villemagne, S. Farquharson, C. L. Masters, and C. C. Rowe, “Cerebral microhemorrhage and brain β-amyloid in aging and Alzheimer disease,” *Neurology*, vol. 77, no. 1, pp. 48–54, 2011.
[45] J. Fiehler, “Cerebral microbleeds: Old leaks and new haemorrhages,” *Int. J. Stroke*, vol. 1, no. 3, pp. 122–130, 2006.
[46] D. J. Pinero and J. R. Connor, “Iron in the brain: An important contributor in normal and diseased states,” *Neuroscientist*, vol. 6, no. 6, pp. 435–453, 2000.
[47] A. Irimia, J. D. Van Horn, and P. M. Vespa, “Cerebral microhemorrhages due to traumatic brain injury and their effects on the aging human brain,” *Neurobiol. Aging*, vol. 66, pp. 158–164, 2018.
[48] G. Gelders, V. Baekelandt, and A. Van der Perren, “Linking neuroinflammation and neurodegeneration in parkinson’s disease,” *J. Immunol. Res.*, vol. 2018, 2018.
[49] M. G. Erkkinen, M. Kim, and M. D. Geschwind, “Major Neurodegenerative Diseases,” 2018.
[50] J. Hagemeier, J. J. G. Geurts, and R. Zivadinov, “Brain iron accumulation in aging and neurodegenerative disorders,” *Expert Rev. Neurother.*, vol. 12, no. 12, pp. 1467–1480, 2012.
[51] N. G. Bazan, A. Halabi, M. Ertel, and N. A. Petasis, “Neuroinflammation,” *Basic Neurochem.*, pp. 610–620, 2012.
[52] S. Voet, S. Srinivasan, M. Lamkanfi, and G. Loo, “Inflammasomes in neuroinflammatory and neurodegenerative diseases,” *EMBO Mol. Med.*, vol. 11, no. 6, pp. 1–16, 2019.
[53] D. Kempuraj *et al.*, “Brain and peripheral atypical inflammatory mediators potentiate neuroinflammation and neurodegeneration,” *Front. Cell. Neurosci.*, vol. 11, no. July, pp. 1–16, 2017.
[54] and J. P. G. Damon DiSabato1, Ning Quan2, “Neuroinflammation: The Devil is in the Details Damon,” *J*

Neurochem., vol. 156, no. 2, pp. 136–153, 2016.
[55] V. Castelli *et al.*, “Neuronal cells rearrangement during aging and neurodegenerative disease: Metabolism, oxidative stress and organelles dynamic,” *Front. Mol. Neurosci.*, vol. 12, no. May, pp. 1–13, 2019.
[56] N. A. Flaris, T. L. Densmore, M. C. Molleston, and W. F. Hickey, “Characterization of microglia and macrophages in the central nervous system of rats: Definition of the differential expression of molecules using standard and novel monoclonal antibodies in normal CNS and in four models of parenchymal reaction,” *Glia*, vol. 7, no. 1, pp. 34–40, 1993.
[57] I. Yang, S. J. Han, G. Kaur, C. Crane, and A. T. Parsa, “The role of microglia in central nervous system immunity and glioma immunology,” *J. Clin. Neurosci.*, vol. 17, no. 1, pp. 6–10, 2010.
[58] U. B. Eyo and L. J. Wu, “Bidirectional microglia-neuron communication in the healthy brain,” *Neural Plast.*, vol. 2013, 2013.
[59] J. Y. Bertrand, A. Jalil, M. Klaine, S. Jung, A. Cumano, and I. Godin, “Three pathways to mature macrophages in the early mouse yolk sac,” *Blood*, vol. 106, no. 9, pp. 3004–3011, 2005.
[60] T. Chitnis and H. L. Weiner, “Series Editors : Marco Colonna and David Holtzmann CNS inflammation and neurodegeneration,” *J. Clin. Invest.*, vol. 127, no. 14, pp. 1–11, 2017.
[61] C. Sousa, K. Biber, and A. Michelucci, “Cellular and molecular characterization of microglia: A unique immune cell population,” *Front. Immunol.*, vol. 8, no. MAR, 2017.
[62] K. M. Lenz and L. H. Nelson, “Microglia and beyond: Innate immune cells as regulators of brain development and behavioral function,” *Front. Immunol.*, vol. 9, no. APR, 2018.
[63] M. L. Dubbelaar, L. Kracht, B. J. L. Eggen, and E. W. G. M. Boddeke, “The Kaleidoscope of Microglial Phenotypes,” *Front. Immunol.*, vol. 9, no. July, p. 1753, 2018.
[64] B. Ajami, J. L. Bennett, C. Krieger, W. Tetzlaff, and F. M. V. Rossi, “Local self-renewal can sustain CNS microglia maintenance and function throughout adult life,” *Nat. Neurosci.*, vol. 10, no. 12, pp. 1538–1543, 2007.
[65] S. Hosmane *et al.*, “TRIF mediates microglial phagocytosis of degenerating axons.,” *J. Neurosci.*, vol. 32, no. 22, pp. 7745–7757, 2012.
[66] B. Chamak, V. Morandi, and M. Mallat, “Brain macrophages stimulate neurite growth and regeneration by secreting thrombospondin,” *J. Neurosci. Res.*, vol. 38, no. 2, pp. 221–

233, 1994.
[67] M. W. Salter and B. Stevens, “Microglia emerge as central players in brain disease,” *Nat. Med.*, vol. 23, no. 9, pp. 1018–1027, 2017.
[68] C. A. Colton, “Heterogeneity of microglial activation in the innate immune response in the brain,” *J. Neuroimmune Pharmacol.*, vol. 4, no. 4, pp. 399–418, 2009.
[69] K. A. Kigerl *et al.*, “Pattern recognition receptors and the central nervous system repair,” pp. 5–16, 2016.
[70] K. Helmut, U. K. Hanisch, M. Noda, and A. Verkhratsky, “Physiology of microglia,” *Physiol. Rev.*, vol. 91, no. 2, pp. 461–553, 2011.
[71] N. Esen and T. Kielian, “Central Role for MyD88 in the Responses of Microglia to Pathogen-Associated Molecular Patterns,” *J. Immunol.*, vol. 176, no. 11, pp. 6802–6811, 2006.
[72] B. L. Fiebich, C. R. A. Batista, S. W. Saliba, N. M. Yousif, and A. C. P. de Oliveira, “Role of microglia TLRs in neurodegeneration,” *Front. Cell. Neurosci.*, vol. 12, no. October, pp. 1–10, 2018.
[73] J. A. Rodríguez-Gómez *et al.*, “Microglia: Agents of the CNS Pro-Inflammatory Response,” *Cells*, vol. 9, no. 7, pp. 1–46, 2020.
[74] C. E. Shiau, K. R. Monk, W. Joo, and W. S. Talbot, “An anti-inflammatory nod-like receptor is required for microglia development,” *Cell Rep.*, vol. 5, no. 5, pp. 1342–1352, 2013.
[75] J. D. Cherry, J. A. Olschowka, and M. K. O’Banion, “Neuroinflammation and M2 microglia: The good, the bad, and the inflamed,” *J. Neuroinflammation*, vol. 11, no. 1, pp. 1–15, 2014.
[76] P. J. Murray, J. E. Allen, E. A. Fisher, and T. Lawrence, “Experimental Guidelines,” *Immunity.*, vol. 41, no. 1, pp. 14–20, 2015.
[77] M. A. Cuadros and J. Navascués, “The origin and differentiation of microglial cells during development,” *Prog. Neurobiol.*, vol. 56, no. 2, pp. 173–189, 1998.
[78] G. J. Harry, “Microglia during development and aging,” *Pharmacol. Ther.*, vol. 139, no. 3, pp. 313–326, 2013.
[79] W. Zhang *et al.*, “Role and mechanism of microglial activation in iron-induced selective and progressive dopaminergic neurodegeneration,” *Mol. Neurobiol.*, vol. 49, no. 3, pp. 1153–1165, 2014.
[80] Z. Szepesi, O. Manouchehrian, S. Bachiller, and T. Deierborg, “Bidirectional Microglia–Neuron Communication in Health and Disease,” *Front. Cell. Neurosci.*, vol. 12, no. September, pp. 1–

26, 2018.
[81] C. Y. Liu, X. Wang, C. Liu, and H. L. Zhang, “Pharmacological Targeting of Microglial Activation: New Therapeutic Approach,” *Front. Cell. Neurosci.*, vol. 13, no. November, pp. 1–19, 2019.
[82] R. H. Hoek *et al.*, “Down-regulation of the macrophage lineage through interaction with OX2 (CD200),” *Science (80-.).*, vol. 290, no. 5497, pp. 1768–1771, 2000.
[83] A. C. Martins, J. I. Almeida, I. S. Lima, A. S. Kapitão, and R. Gozzelino, “Iron Metabolism and the Inflammatory Response,” *IUBMB Life*, vol. 69, no. 6, 2017.
[84] C. A. Colton and D. M. Wilcock, “Assessing Activation States in Microglia,” *CNS Neurol. Disord. - Drug Targets*, vol. 9, no. 2, pp. 174–191, 2012.
[85] Z. Zhang, Z. Zhang, H. Lu, Q. Yang, H. Wu, and J. Wang, “Microglial Polarization and Inflammatory Mediators After Intracerebral Hemorrhage,” *Mol. Neurobiol.*, vol. 54, no. 3, pp. 1874–1886, 2017.
[86] Z. V. Zheng and K. C. G. Wong, “Microglial activation and polarization after subarachnoid hemorrhage,” *Neuroimmunol. Neuroinflammation*, vol. 2019, pp. 1–12, 2019.
[87] S. Lin *et al.*, “Heme activates TLR4-mediated inflammatory injury via MyD88/TRIF signaling pathway in intracerebral hemorrhage,” *J. Neuroinflammation*, vol. 9, no. 1, p. 46, 2012.
[88] Y. Cai *et al.*, “Activated Microglia Are Less Vulnerable to Hemin Toxicity due to Nitric Oxide-Dependent Inhibition of JNK and p38 MAPK Activation,” *J. Immunol.*, vol. 187, no. 3, pp. 1314–1321, 2011.
[89] R. Gozzelino, V. Jeney, and M. P. Soares, “Mechanisms of Cell Protection by Heme Oxygenase-1,” *Annu. Rev. Pharmacol. Toxicol.*, vol. 50, no. 1, pp. 323–354, 2010.
[90] Y. F. Zhou *et al.*, “Hepcidin protects neuron from hemin-mediated injury by reducing iron,” *Front. Physiol.*, vol. 8, no. MAY, pp. 1–9, 2017.
[91] A. Ndayisaba, C. Kaindlstorfer, and G. K. Wenning, “Iron in neurodegeneration - Cause or consequence?,” *Front. Neurosci.*, vol. 13, no. March, pp. 1–15, 2019.
[92] J. Sian-Hülsmann, S. Mandel, M. B. H. Youdim, and P. Riederer, “The relevance of iron in the pathogenesis of Parkinson’s disease,” *J. Neurochem.*, vol. 118, no. 6, pp. 939–957, 2011.
[93] S. Bharath, M. Hsu, D. Kaur, S. Rajagopalan, and J. K. Andersen, “Glutathione, iron and Parkinson’s disease,” *Biochem. Pharmacol.*, vol. 64, no. 5–6, pp. 1037–1048, 2002.
[94] D. L. Abeyawardhane and H. R. Lucas, “Iron Redox Chemistry

and Implications in the Parkinson's Disease Brain," *Oxid. Med. Cell. Longev.*, vol. 2019, 2019.
[95] S. Elmore, "Apoptosis: A Review of Programmed Cell Death," *Toxicol. Pathol.*, vol. 35, no. 4, pp. 495–516, 2007.
[96] K. Venderova and D. S. Park, "Programmed cell death in Parkinson's disease," *Cold Spring Harb. Perspect. Med.*, vol. 2, no. 8, pp. 1–23, 2012.
[97] M. M. Tompkins, E. J. Basgall, E. Zamrini, and W. D. Hill, "Apoptotic-like changes in Lewy-body-associated disorders and normal aging in substantia nigral neurons," *Am. J. Pathol.*, vol. 150, no. 1, pp. 119–131, 1997.
[98] T. Chernova, J. R. Steinert, C. J. Guerin, P. Nicotera, I. D. Forsythe, and A. G. Smith, "Neurite degeneration induced by heme deficiency mediated via inhibition of NMDA receptor-dependent extracellular signal-regulated kinase 1/2 activation," *J. Neurosci.*, vol. 27, no. 32, pp. 8475–8485, 2007.
[99] R. Yilmaz *et al.*, "Serum Inflammatory Profile for the Discrimination of Clinical Subtypes in Parkinson's Disease," *Front. Neurol.*, vol. 9, no. December, pp. 1–9, 2018.
[100] W. Poewe *et al.*, "Parkinson disease," *Nat. Rev. Dis. Prim.*, vol. 3, pp. 1–21, 2017.
[101] M. T. Hayes, "Parkinson's Disease and Parkinsonism," *Am. J. Med.*, vol. 132, no. 7, pp. 802–807, 2019.
[102] Y. Chao, S. C. Wong, and E. K. Tan, "Evidence of inflammatory system involvement in Parkinson's disease," *Biomed Res. Int.*, vol. 2014, 2014.
[103] K. P. MacPherson, M. E. de Sousa Rodrigues, A. F. Cintron, and M. G. Tansey, *Neuroinflammation in Age-Related Neurodegenerative Diseases.* 2018.
[104] B. Chen, X. Wen, H. Jiang, J. Wang, N. Song, and J. Xie, "Interactions between iron and α-synuclein pathology in Parkinson's disease," *Free Radic. Biol. Med.*, vol. 141, no. April, pp. 253–260, 2019.
[105] J. Sian-Hulsmann and P. Riederer, "The role of alpha-synuclein as ferrireductase in neurodegeneration associated with Parkinson's disease," *J. Neural Transm.*, vol. 127, no. 5, pp. 749–754, 2020.
[106] L. Stefanis, "α-Synuclein in Parkinson's disease," *Cold Spring Harb. Perspect. Med.*, vol. 2, no. 2, pp. 1–23, 2012.
[107] P. R. Angelova *et al.*, "Alpha synuclein aggregation drives ferroptosis: an interplay of iron, calcium and lipid peroxidation," *Cell Death Differ.*, 2020.
[108] S. Ayton and P. Lei, "Nigral iron elevation is an invariable feature of Parkinson's disease and is a sufficient cause of

neurodegeneration," *Biomed Res. Int.*, vol. 2014, 2014.
[109] B. A. Hijaz and L. A. Volpicelli-Daley, "Initiation and propagation of α-synuclein aggregation in the nervous system," *Mol. Neurodegener.*, vol. 15, no. 1, pp. 1–12, 2020.
[110] L. Qu, H. Xu, W. Jia, H. Jiang, and J. Xie, "Rosmarinic acid protects against MPTP-induced toxicity and inhibits iron-induced α-synuclein aggregation," *Neuropharmacology*, vol. 144, no. May 2018, pp. 291–300, 2019.
[111] W. Li, H. Jiang, N. Song, and J. Xie, "Oxidative stress partially contributes to iron-induced alpha-synuclein aggregation in SK-N-SH cells," *Neurotox. Res.*, vol. 19, no. 3, pp. 435–442, 2011.
[112] U. Ganguly *et al.*, "Interaction of α-synuclein and Parkin in iron toxicity on SH-SY5Y cells: Implications in the pathogenesis of Parkinson's disease," *Biochem. J.*, vol. 477, no. 6, pp. 1109–1122, 2020.
[113] D. Brück, G. K. Wenning, N. Stefanova, and L. Fellner, "Glia and alpha-synuclein in neurodegeneration: A complex interaction," *Neurobiol. Dis.*, vol. 85, pp. 262–274, 2016.
[114] S. A. Ferreira and M. Romero-Ramos, "Microglia response during Parkinson's disease: Alpha-synuclein intervention," *Front. Cell. Neurosci.*, vol. 12, no. August, pp. 1–17, 2018.
[115] S. Kaczanowski, "Apoptosis: Its origin, history, maintenance and the medical implications for cancer and aging," *Phys. Biol.*, vol. 13, no. 3, 2016.
[116] J. E. Ricci *et al.*, "Disruption of mitochondrial function during apoptosis is mediated by caspase cleavage of the p75 subunit of complex I of the electron transport chain," *Cell*, vol. 117, no. 6, pp. 773–786, 2004.
[117] R. Singh, A. Letai, and K. Sarosiek, "Regulation of apoptosis in health and disease: the balancing act of BCL-2 family proteins," *Nat. Rev. Mol. Cell Biol.*, vol. 20, no. 3, pp. 175–193, 2019.
[118] K. Wimmer, M. Sachet, and R. Oehler, "Circulating biomarkers of cell death," *Clin. Chim. Acta*, vol. 500, no. April 2019, pp. 87–97, 2020.
[119] S. Nagata, "Apoptosis and Clearance of Apoptotic Cells," *Annu. Rev. Immunol.*, vol. 36, no. 1, pp. 489–517, 2018.
[120] T. Yasuda, Y. Nakata, and H. Mochizuki, "α-Synuclein and neuronal cell death.," *Mol. Neurobiol.*, vol. 47, no. 2, pp. 466–483, 2013.
[121] P. Li *et al.*, "Cytochrome c and dATP-dependent formation of Apaf-1/caspase-9 complex initiates an apoptotic protease cascade," *Cell*, vol. 91, no. 4, pp. 479–489, 1997.
[122] H. Li, H. Zhu, C. J. Xu, and J. Yuan, "Cleavage of BID by

caspase 8 mediates the mitochondrial damage in the Fas pathway of apoptosis," *Cell*, vol. 94, no. 4, pp. 491–501, 1998.
[123] Y. Akao, W. Maruyama, H. Yi, M. Shamoto-Nagai, M. B. H. Youdim, and M. Naoi, "An anti-Parkinson's disease drug, N-propargyl-1(R)-aminoindan (rasagiline), enhances expression of anti-apoptotic Bcl-2 in human dopaminergic SH-SY5Y cells," *Neurosci. Lett.*, vol. 326, no. 2, pp. 105–108, 2002.
[124] M. Oñate *et al.*, "The necroptosis machinery mediates axonal degeneration in a model of Parkinson disease," *Cell Death Differ.*, 2019.
[125] T. Zhou *et al.*, "Microglia polarization with M1/M2 phenotype changes in rd1 mouse model of retinal degeneration," *Front. Neuroanat.*, vol. 11, no. September, pp. 1–11, 2017.
[126] J. Nirmala and M. Lopus, "An overview of cell death mechanisms in eukaryotes," *Cell Mol. Toxicol.*, 2019.
[127] S. Zhang, M. B. Tang, H. Y. Luo, C. H. Shi, and Y. M. Xu, "Necroptosis in neurodegenerative diseases: a potential therapeutic target," *Cell Death Dis.*, vol. 8, no. 6, p. e2905, 2017.
[128] J. Yuan, P. Amin, and D. Ofengeim, "Necroptosis and RIPK1-mediated neuroinflammation in CNS diseases," *Nat. Rev. Neurosci.*
[129] N. Callizot, M. Combes, A. Henriques, and P. Poindron, "Necrosis, apoptosis, necroptosis, three modes of action of dopaminergic neuron neurotoxins," *PLoS One*, vol. 14, no. 4, pp. 1–19, 2019.
[130] M. Conrad *et al.*, "Regulation of lipid peroxidation and ferroptosis in diverse species," *Genes Dev.*, vol. 32, no. 9–10, pp. 602–619, 2018.
[131] S. J. Dixon and B. R. Stockwell, "The Hallmarks of Ferroptosis," *Annu. Rev. Cancer Biol.*, vol. 3, no. 1, pp. 35–54, 2019.
[132] T. Hirschhorn and B. R. Stockwell, "The development of the concept of ferroptosis," *Free Radic. Biol. Med.*, vol. 133, pp. 130–143, 2019.
[133] J. Li *et al.*, "Ferroptosis: past, present and future," *Cell Death Dis.*, vol. 11, no. 2, 2020.
[134] M. Conrad and D. A. Pratt, "The chemical basis of ferroptosis," *Nat. Chem. Biol.*, vol. 15, no. 12, pp. 1137–1147, 2019.
[135] "Stockwell, 2017.pdf." .
[136] F. P. Bellinger *et al.*, "Glutathione peroxidase 4 is associated with neuromelanin in substantia nigra and dystrophic axons in putamen of Parkinson's brain," *Mol. Neurodegener.*, vol. 6, no. 1, 2011.

[137] B. Do Van *et al.*, “Ferroptosis, a newly characterized form of cell death in Parkinson’s disease that is regulated by PKC,” *Neurobiol. Dis.*, vol. 94, pp. 169–178, 2016.
[138] S. J. Guiney, P. A. Adlard, A. I. Bush, D. I. Finkelstein, and S. Ayton, “Ferroptosis and cell death mechanisms in Parkinson’s disease,” *Neurochem. Int.*, vol. 104, pp. 34–48, 2017.
[139] D. Charvin, R. Medori, R. A. Hauser, and O. Rascol, “Therapeutic strategies for Parkinson,” *Nat. Publ. Gr.*, 2018.
[140] H. Gao, B. Liu, W. Zhang, and J. Hong, “Novel anti-inflammatory therapy for Parkinson ’ s disease,” vol. 24, no. 8, pp. 395–401, 2003.
[141] J. M. Ellis and M. J. Fell, “Current approaches to the treatment of Parkinson’s Disease,” *Bioorganic Med. Chem. Lett.*, vol. 27, no. 18, pp. 4247–4255, 2017.
[142] J. A. Borovac, “Side effects of a dopamine agonist therapy for Parkinson’s disease: A mini-review of clinical pharmacology,” *Yale J. Biol. Med.*, vol. 89, no. 1, pp. 37–47, 2016.
[143] G. Emilien, J. M. Maloteaux, M. Geurts, K. Hoogenberg, and S. Cragg, “Dopamine receptors - Physiological understanding to therapeutic intervention potential,” *Pharmacol. Ther.*, vol. 84, no. 2, pp. 133–156, 1999.
[144] N. Gerhards, L. Neubauer, P. Tudzynski, and S. M. Li, “Biosynthetic pathways of ergot alkaloids,” *Toxins (Basel).*, vol. 6, no. 12, pp. 3281–3295, 2014.
[145] B. Konta and W. Frank, “The treatment of Parkinson’s disease with dopamine agonists.,” *GMS Health Technol. Assess.*, vol. 4, p. Doc05, 2008.
[146] S. Hisahara and S. Shimohama, “Dopamine Receptors and Parkinson’s Disease,” *Int. J. Med. Chem.*, vol. 2011, pp. 1–16, 2011.
[147] A. W. K. Yeung, M. G. Georgieva, A. G. Atanasov, and N. T. Tzvetkov, “Monoamine oxidases (MAOs) as privileged molecular targets in neuroscience: Research literature analysis,” *Front. Mol. Neurosci.*, vol. 12, no. May, pp. 1–12, 2019.
[148] P. Riederer and G. Laux, “MAO-inhibitors in Parkinson’s Disease,” *Exp. Neurobiol.*, vol. 20, no. 1, pp. 1–17, 2011.
[149] K. C. Teo and S. Ho, “Monoamine oxidase-B (MAO-B) inhibitors : implications for disease-modification in Parkinson ’ s disease,” pp. 1–10, 2013.
[150] A. O. Pires, F. G. Teixeira, B. Mendes-pinheiro, C. Serra, and N. Sousa, “Old and New Challenges in Parkinson ’ s Disease Therapeutics Progress in Neurobiology Old and new challenges in Parkinson ’ s disease therapeutics,” no. January

2018, 2017.
[151] I. B. Nadel, “The Unified Parkinson’s Disease Rating Scale (UPDRS): Status and Recommendations,” *Ezra Pound Context*, vol. 18, no. 7, pp. 159–168, 2012.
[152] L. M. Collins, A. Toulouse, T. J. Connor, and Y. M. Nolan, “Neuropharmacology Contributions of central and systemic in fl ammation to the pathophysiology of Parkinson ’ s disease,” *Neuropharmacology*, vol. 62, no. 7, pp. 2154–2168, 2012.
[153] I. Kurkowska-Jastrzębska *et al.*, “Dexamethasone protects against dopaminergic neurons damage in a mouse model of Parkinson’s disease,” *Int. Immunopharmacol.*, vol. 4, no. 10–11, pp. 1307–1318, 2004.
[154] M. Long-smith, A. M. Sullivan, and Y. M. Nolan, “The influence of microglia on the pathogenesis of Parkinson ’ s disease Progress in Neurobiology The influence of microglia on the pathogenesis of Parkinson ’ s disease,” no. January 2019, 2009.
[155] E. C. Hirsch and S. Hunot, “Neuroinfl ammation in Parkinson ’ s disease : a target for neuroprotection ?,” vol. 8, no. April, 2009.
[156] E. Esposito, V. Di Matteo, A. Benigno, M. Pierucci, G. Crescimanno, and G. Di Giovanni, “Non-steroidal anti-inflammatory drugs in Parkinson’s disease,” *Exp. Neurol.*, vol. 205, no. 2, pp. 295–312, 2007.
[157] N. P. Rocha, A. S. De Miranda, and A. L. Teixeira, “Insights into neuroinflammation in Parkinson’s disease: From biomarkers to anti-inflammatory based therapies,” *Biomed Res. Int.*, vol. 2015, 2015.
[158] S. Cankaya, B. Cankaya, U. Kilic, E. Kilic, and B. Yulug, “The therapeutic role of minocycline in Parkinson’s disease,” *Drugs Context*, vol. 8, pp. 1–14, 2019.
[159] W. N. N.-P. I. Quispe-Tintaya, “A Pilot Clinical Trial of Creatine and Minocycline in Early Parkinson Disease: 18-Month Results,” *Physiol. Behav.*, vol. 176, no. 3, pp. 139–148, 2008.
[160] R. Filograna, M. Beltramini, L. Bubacco, and M. Bisaglia, “Anti-Oxidants in Parkinson ’ s Disease Therapy : A Critical Point of View,” pp. 260–271, 2016.
[161] 2 Claire Henchcliffe Meredith Spindler1 M Flint Beal1, “Coenzyme Q10 effects in neurodegenerative disease,” pp. 597–610, 2009.
[162] T. C. Rodick1, D. R. S. J. R. B. K. W. Huggins1, G. Ren3, and S. T. Mathews, “Potential role of coenzyme Q 10 in health and disease conditions,” 2018.
[163] M. F. Beal, R. T. Matthews, A. Tieleman, and C. W. Shults, “Ž

MPTP . induced loss of striatal dopamine and dopaminergic axons in aged mice," pp. 109–114, 1998.
[164] and A. G. K. Huajun Jin1, Arthi Kanthasamy1, Anamitra Ghosh1, Vellareddy Anantharam1, Balaraman Kalyanaraman2, "OF PARKINSON ' S DISEASE : PRECLINICAL AND CLINICAL," vol. 1842, no. 8, pp. 1282–1294, 2015.
[165] C. W. Shults, "Therapeutic role of coenzyme Q10 in Parkinson's disease," *Pharmacol. Ther.*, vol. 107, no. 1, pp. 120–130, 2005.
[166] A. J. Braakhuis, R. Nagulan, and V. Somerville, "Review Article The Effect of MitoQ on Aging-Related Biomarkers : A Systematic Review and Meta-Analysis," vol. 2018, 2018.
[167] A. Kumar, "A review on mitochondrial restorative mechanism of antioxidants in Alzheimer ' s disease and other," vol. 6, no. September, pp. 1–13, 2015.
[168] X. Zhao, M. Zhang, C. Li, X. Jiang, Y. Su, and Y. Zhang, "Review Article Benefits of Vitamins in the Treatment of Parkinson ' s Disease," vol. 2019, 2019.
[169] A. S. Mahyar Etminan, Sudeep S Gill, "Intake of vitamin E , vitamin C , and carotenoids and the risk of Parkinson ' s disease : a meta-analysis," 2005.
[170] T. Schirinzi *et al.*, "Dietary Vitamin E as a Protective Factor for Parkinson ' s Disease : Clinical and Experimental Evidence," vol. 10, no. February, pp. 1–7, 2019.
[171] C. A. Weber and M. E. Ernst, "Antioxidants , Supplements , and Parkinson ' s Disease Antioxidants , Supplements , and Parkinson ' s Disease," no. January, 2015.
[172] R. Galanello, "Deferiprone in the treatment of transfusion-dependent thalassemia: A review and perspective," *Ther. Clin. Risk Manag.*, vol. 3, no. 5, pp. 795–805, 2007.
[173] R. C. Hider and A. V. Hoffbrand, "The role of deferiprone in iron chelation," *N. Engl. J. Med.*, vol. 379, no. 22, pp. 2140–2150, 2018.
[174] A. Martin-Bastida *et al.*, "Brain iron chelation by deferiprone in a phase 2 randomised double-blinded placebo controlled clinical trial in Parkinson's disease," *Sci. Rep.*, vol. 7, no. 1, pp. 1–9, 2017.
[175] G. Abbruzzese *et al.*, "A pilot trial of deferiprone for neurodegeneration with brain iron accumulation," *Haematologica*, vol. 96, no. 11, pp. 1708–1711, 2011.
[176] S. R. Oliveira, J. D. Amaral, and C. M. P. Rodrigues, "Mechanism and disease implications of necroptosis and neuronal inflammation," *Cell Death Dis.*, vol. 9, no. 9, pp. 10–

12, 2018.
[177] A. Iannielli *et al.*, “Pharmacological Inhibition of Necroptosis Protects from Dopaminergic Neuronal Cell Death in Parkinson ’ s Disease Models Article Pharmacological Inhibition of Necroptosis Protects from Dopaminergic Neuronal Cell Death in Parkinson ’ s Disease Models,” pp. 2066–2079, 2018.
[178] P. A. Dionísio *et al.*, “Ablation of RIP3 protects from dopaminergic neurodegeneration in experimental Parkinson’s disease,” *Cell Death Dis.*, vol. 10, no. 11, 2019.
[179] J. R. Wu *et al.*, “Necrostatin-1 protection of dopaminergic neurons,” *Neural Regen. Res.*, vol. 10, no. 7, pp. 1120–1124, 2015.
[180] Q. S. Lin *et al.*, “RIP1/RIP3/MLKL mediates dopaminergic neuron necroptosis in a mouse model of Parkinson disease,” *Lab. Investig.*, 2019.
[181] M. Arakawa and Y. Ito, “N-acetylcysteine and neurodegenerative diseases: Basic and clinical pharmacology,” *Cerebellum*, vol. 6, no. 4, pp. 308–314, 2007.
[182] A. Agil *et al.*, “Plasma lipid peroxidation in sporadic Parkinson’s disease. Role of the L-dopa,” *J. Neurol. Sci.*, vol. 240, no. 1–2, pp. 31–36, 2006.
[183] D. T. Dexter *et al.*, “Increased Nigral Iron Content and Alterations in Other Metal Ions Occurring in Brain in Parkinson’s Disease,” *J. Neurochem.*, vol. 52, no. 6, pp. 1830–1836, 1989.
[184] D. Devos *et al.*, “Targeting chelatable iron as a therapeutic modality in Parkinson’s disease,” *Antioxidants Redox Signal.*, vol. 21, no. 2, pp. 195–210, 2014.
[185] K. Ito, Y. Eguchi, Y. Imagawa, S. Akai, H. Mochizuki, and Y. Tsujimoto, “MPP+ induces necrostatin-1-and ferrostatin-1-sensitive necrotic death of neuronal SH-SY5Y cells,” *Cell Death Discov.*, vol. 3, no. December 2016, pp. 1–10, 2017.
[186] F. Gouel *et al.*, “The protective effect of human platelet lysate in models of neurodegenerative disease: involvement of the Akt and MEK pathways,” *J. Tissue Eng. Regen. Med.*, vol. 11, no. 11, pp. 3236–3240, 2017.
[187] R. R. Crichton, R. J. Ward, and R. C. Hider, “The efficacy of iron chelators for removing iron from specific brain regions and the pituitary—Ironing out the brain,” *Pharmaceuticals*, vol. 12, no. 3, 2019.
[188] M. Greter, I. Lelios, and A. L. Croxford, “Microglia versus myeloid cell nomenclature during brain inflammation,” *Front. Immunol.*, vol. 6, no. MAY, pp. 1–7, 2015.
[189] S. Menezes *et al.*, “The Heterogeneity of Ly6Chi Monocytes

Controls Their Differentiation into iNOS+ Macrophages or Monocyte-Derived Dendritic Cells," *Immunity*, vol. 45, no. 6, pp. 1205–1218, 2016.
[190] Y. Ma, V. Abbate, and R. C. Hider, "Iron-sensitive fluorescent probes: Monitoring intracellular iron pools," *Metallomics*, vol. 7, no. 2, pp. 212–222, 2015.
[191] Y. Ma, Z. Liu, R. C. Hider, and F. Petrat, "Determination of the Labile Iron Pool of Human Lymphocytes using the Fluorescent Probe, CP655," *Anal. Chem. Insights*, vol. 2, no. 44, p. 117739010700200, 2007.
[192] J. Xu, M. D. Knutson, C. S. Carter, and C. Leeuwenburgh, "Iron Accumulation with Age , Oxidative Stress and Functional Decline," vol. 3, no. 8, 2008.
[193] R. Gozzelino and P. Arosio, *THE IMPORTANCE OF IRON IN CONDITIONS*. .
[194] V. Brochard *et al.*, "Infiltration of CD4+ lymphocytes into the brain contributes to neurodegeneration in a mouse model of Parkinson disease," vol. 119, no. 1, 2009.
[195] A. E. Lang and A. J. Espay, "Disease Modification in Parkinson's Disease: Current Approaches, Challenges, and Future Considerations," *Mov. Disord.*, vol. 33, no. 5, pp. 660–677, 2018.
[196] A. F. Carvalho, B. K. Puri, M. Berk, A. J. Walker, G. Morris, and M. Maes, "Why should neuroscientists worry about iron? The emerging role of ferroptosis in the pathophysiology of neuroprogressive diseases," *Behav. Brain Res.*, vol. 341, pp. 154–175, 2017.
[197] G. Zhang *et al.*, "New Perspectives on Roles of Alpha-Synuclein in Parkinson's Disease," *Front. Aging Neurosci.*, vol. 10, no. November, pp. 1–20, 2018.
[198] Z. I. Cabantchik, A. Munnich, M. B. Youdim, and D. Devos, "Regional siderosis: a new challenge for iron chelation therapy," *Front. Pharmacol.*, vol. 4, no. December, pp. 1–7, 2013.
[199] R. R. Crichton, D. T. Dexter, and R. J. Ward, "Brain iron metabolism and its perturbation in neurological diseases.," *J. Neural Transm.*, vol. 118, no. 3, pp. 301–314, 2011.
[200] K. Song *et al.*, "Oxidative Stress-Mediated Blood-Brain Barrier (BBB) Disruption in Neurological Diseases," *Oxid. Med. Cell. Longev.*, vol. 2020, 2020.
[201] O. I. Butt, P. W. Buehler, and F. D'Agnillo, "Blood-brain barrier disruption and oxidative stress in guinea pig after systemic exposure to modified cell-free hemoglobin," *Am. J. Pathol.*, vol. 178, no. 3, pp. 1316–1328, 2011.

[202] M. Katsu, K. Niizuma, H. Yoshioka, N. Okami, H. Sakata, and P. H. Chan, “Hemoglobin-induced oxidative stress contributes to matrix metalloproteinase activation and blood-brain barrier dysfunction in vivo,” *J. Cereb. Blood Flow Metab.*, vol. 30, no. 12, pp. 1939–1950, 2010.
[203] T. Imai *et al.*, “Intracellular Fe 2+ accumulation in endothelial cells and pericytes induces blood-brain barrier dysfunction in secondary brain injury after brain hemorrhage,” *Sci. Rep.*, vol. 9, no. 1, pp. 1–16, 2019.
[204] B. N. Porto *et al.*, “Heme induces neutrophil migration and reactive oxygen species generation through signaling pathways characteristic of chemotactic receptors,” *J. Biol. Chem.*, vol. 282, no. 33, pp. 24430–24436, 2007.
[205] N. S. Merle *et al.*, “P-selectin drives complement attack on endothelium during intravascular hemolysis in TLR-4/hemedependent manner,” *Proc. Natl. Acad. Sci. U. S. A.*, vol. 116, no. 13, pp. 6280–6285, 2019.
[206] M. T. Bozza and V. Jeney, “Pro-inflammatory Actions of Heme and Other Hemoglobin-Derived DAMPs,” *Front. Immunol.*, vol. 11, no. June, pp. 1–13, 2020.
[207] D. Mrdjen *et al.*, “High-Dimensional Single-Cell Mapping of Central Nervous System Immune Cells Reveals Distinct Myeloid Subsets in Health, Aging, and Disease,” *Immunity*, vol. 48, no. 2, pp. 380-395.e6, 2018.
[208] C. Ní Chasaide and M. A. Lynch, “The role of the immune system in driving neuroinflammation,” *Brain Neurosci. Adv.*, vol. 4, p. 239821281990108, 2020.
[209] H. González, D. Elgueta, A. Montoya, and R. Pacheco, “Neuroimmune regulation of microglial activity involved in neuroinflammation and neurodegenerative diseases,” *J. Neuroimmunol.*, vol. 274, no. 1–2, pp. 1–13, 2014.
[210] A. D. Greenhalgh, S. David, and F. C. Bennett, “Immune cell regulation of glia during CNS injury and disease,” *Nat. Rev. Neurosci.*, vol. 21, no. 3, pp. 139–152, 2020.
[211] S. T. T. Schetters, D. Gomez-Nicola, J. J. Garcia-Vallejo, and Y. Van Kooyk, “Neuroinflammation: Microglia and T cells get ready to tango,” *Front. Immunol.*, vol. 8, no. JAN, 2018.
[212] H. X. Chu, T. V. Arumugam, M. Gelderblom, T. Magnus, G. R. Drummond, and C. G. Sobey, “Role of CCR2 in inflammatory conditions of the central nervous system,” *J. Cereb. Blood Flow Metab.*, vol. 34, no. 9, pp. 1425–1429, 2014.
[213] A. Santaella *et al.*, “Cerebrospinal fluid monocyte chemoattractant protein 1 correlates with progression of Parkinson’s disease,” *npj Park. Dis.*, vol. 6, no. 1, pp. 1–5,

2020.
[214] M. Reale *et al.*, “Peripheral cytokines profile in Parkinson’s disease,” *Brain. Behav. Immun.*, vol. 23, no. 1, pp. 55–63, 2009.
[215] 3 Mahalakshmi Shankaran, 1* Michael E. Marino, 1 Robert Busch, 1 Carole Keim, 1 Chelsea King, 1 Jean Lee, 1 Salena Killion, 1 Mohamad Awada, 1 and Marc K. Hellerstein2, “Measurement of Brain Microglial Proliferation Rates In Vivo in Response to Neuroinflammatory Stimuli: Application to Drug Discovery,” *J. Neurosci. Res. 852374–2384*, vol. 3253, no. April, pp. 3244–3253, 2007.
[216] S. Fukushima, E. Furube, M. Itoh, T. Nakashima, and S. Miyata, “Robust increase of microglia proliferation in the fornix of hippocampal axonal pathway after a single LPS stimulation,” *J. Neuroimmunol.*, vol. 285, pp. 31–40, 2015.
[217] A. N. Mohebiany *et al.*, “Microglial A20 Protects the Brain from CD8 T-Cell-Mediated Immunopathology,” *Cell Rep.*, vol. 30, no. 5, pp. 1585-1597.e6, 2020.
[218] A. Schietinger and P. D. Greenberg, “Tolerance and exhaustion: Defining mechanisms of T cell dysfunction,” *Trends Immunol.*, vol. 35, no. 2, pp. 51–60, 2014.
[219] E. J. Wherry and M. Kurachi, “Molecular and cellular insights into T cell exhaustion,” *Nat. Rev. Immunol.*, vol. 15, no. 8, pp. 486–499, 2015.
[220] M. I. Tores, M. A. López-Casado, C. P. de León, P. Lorite, and T. Palomeque, “Physiology and Pathology of Immune Dysregulation: Regulatory T Cells and Anergy,” *Physiol. Pathol. Immunol.*, 2017.
[221] M. S. Subbarayan, C. Hudson, L. D. Moss, K. R. Nash, and P. C. Bickford, “T cell infiltration and upregulation of MHCII in microglia leads to accelerated neuronal loss in an α-synuclein rat model of Parkinson’s disease,” *J. Neuroinflammation*, vol. 17, no. 1, pp. 1–16, 2020.
[222] W. M. K. JEAN LHERMITTE, PARIS, “ON THE OCCURRENCE OF ABNORMAL DEPOSITS OF IRON IN THE BRAIN IN PARKINSONISM WITH SPECI,” *J. Neurol. Psychopathol.*, vol. V, no. 19, 1924.
[223] P. L. McGeer, S. Itagaki, B. E. Boyes, and E. G. McGeer, “Reactive microglia are positive for HLA-DR in the: Substantia nigra of Parkinson’s and Alzheimer’s disease brains,” *Neurology*, vol. 38, no. 8, pp. 1285–1291, 1988.
[224] I. S. Lima, A. C. Pêgo, J. T. Barros, A. R. Prada, and R. Gozzelino, “Cell death-osis of dopaminergic neurons and the role of iron in Parkinson’s disease,” *Antioxid. Redox Signal.*,

vol. 2050, no. 180, pp. 1–21, 2020.
[225] M. Pajares, A. I Rojo, G. Manda, L. Boscá, and A. Cuadrado, “Inflammation in Parkinson’s Disease: Mechanisms and Therapeutic Implications,” *Cells*, vol. 9, no. 7, pp. 1–32, 2020.
[226] R. J. Ward, D. T. Dexter, A. Martin-bastida, and R. R. Crichton, “Is chelation therapy a potential treatment for parkinson’s disease?,” *Int. J. Mol. Sci.*, vol. 22, no. 7, 2021.
[227] D. M. O’Hara, S. K. Kalia, and L. V. Kalia, “Emerging disease-modifying strategies targeting α-synuclein for the treatment of Parkinson’s disease,” *Br. J. Pharmacol.*, vol. 175, no. 15, pp. 3080–3089, 2018.
[228] C. N. Mat Taib and M. Mustapha, “MPTP-induced mouse model of Parkinson’s disease: A promising direction of therapeutic strategies,” *Bosn. J. Basic Med. Sci.*, no. x, pp. 1–12, 2020.
[229] S. J. Ahn, J. Anrather, N. Nishimura, and C. B. Schaffer, “Diverse Inflammatory Response after Cerebral Microbleeds Includes Coordinated Microglial Migration and Proliferation,” *Stroke*, vol. 49, no. 7, pp. 1719–1726, 2018.

ANNEXES

PUBLICATIONS

- Martins AC, Almeida JI, **Lima IS**, Kapitão AS and Gozzelino R. Iron metabolism and the inflammatory response. IUBMB Life. 2017.

Research Communication

Iron Metabolism and the Inflammatory Response

Ana C. Martins
Joana I. Almeida
Illyane S. Lima
Antonino S. Kapitão
Raffaella Gozzelino *

Chronic Diseases Research Center (CEDOC)/NOVA Medical School, NOVA University of Lisbon, Portugal

Abstract

Iron (Fe) is essential to almost all organisms, as required by cells to satisfy metabolic needs and accomplish specialized functions. Its ability to exchange electrons between different substrates, however, renders it potentially toxic. Fine tune-mechanisms are necessary to maintain Fe homeostasis and, as such, to prevent its participation into the Fenton reaction and generation of oxidative stress. These are particularly important in the context of inflammation/infection, where restricting Fe availability to invading pathogens is one, if not, the main host defense strategy against microbial growth. The ability of Fe to modulate several aspects of the immune response is associated with a number of "costs" and "benefits", some of which have been described in this review.

Keywords: *iron; inflammation; infection; immunity; iron metabolism*

Introduction

Iron (Fe) is a very abundant atom, representing almost 5% of the earth's crust. Most forms of Fe are insoluble, i.e. not biologically useful. Thus, essential is the role played by proteins, e.g. ferroxidases and ferrireductases, which are capable to convert Fe into a more soluble form and increase its accessibility. The poor solubility of Fe, which in neutral solutions corresponds to 10^{-18} M for the most abundant forms Fe^{3+} and to 10^{-2} M for most ferrous salts Fe^{2+}, could be seen as part of an entire strategy to avoid Fe toxicity (1). In fact, if from one side this metal is essential to almost all organisms, on the other, it becomes toxic when accumulating above certain thresholds. The ability of Fe to stably interconvert between the most common oxidative forms Fe^{2+} and Fe^{3+} favors its participation into the Fenton reaction and the generation of highly reactive hydroxyl radicals (2). These subsequently damage DNA, lipids and proteins, causing cells to undergo Fe-mediated oxidative stress and programmed cell death. Thus, maintaining Fe homeostasis is a necessary step for the correct cell functioning and to prevent Fe-mediated tissue damage (3).

Abbreviations: *CO, Carbon Monoxide; DcytB, Duodenal Membrane Associated Cytochrome b Ferroreductase; DMT1, Divalent Metal Transporter 1; Fe, Iron; Fe-S, Iron Sulfur; FtH, Ferritin H Chain; FtL, Ferritin L Chain; FPN, Ferroportin; HFE, Hemochromatosis Gene; HH, Hereditary Hemochromatosis; HO, Heme Oxygenase; IL, Interleukin; IRE, Iron Responsive Element; IRP, Iron Responsive Protein; NCOA4, Nuclear Receptor Coactivator 4; Nramp, Natural Resistance-Associated Macrophage Protein; NTBI, Non-transferrin bound iron; ROS, Reactive Oxygen Species; Tf, Transferrin; TfR, Transferrin Receptor; TNF, Tumor Necrosis Factor; Zip14, Plasma Membrane Metal-Ion Transporter SLC39A14*

Volume 69, Number 6, June 2017, Pages 442–450

**Address correspondence to: Raffaella Gozzelino, Chronic Diseases Research Center (CEDOC)/NOVA Medical School, NOVA University of Lisbon, Inflammation and Neurodegeneration Laboratory, Rua Câmara Pestana no. 6, Edificio II, Lisbon, Portugal.*
E-mail: raffaella.gozzelino@nms.unl.pt and raffaellagozzelino@gmail.com

Received 28 February 2017; Accepted 6 April 2017
DOI 10.1002/iub.1635
Published online 5 May 2017 in Wiley Online Library (wileyonlinelibrary.com)

Iron Absorption

In humans, dietary Fe absorption is strictly regulated and influenced by the type of food ingested. While compounds, e.g. phytates, act as inhibitors of Fe uptake, others like vitamin C increase Fe entry and facilitate its reduction to Fe^{2+} (4).

Dietary Fe absorption varies between 1 and 2 mg. This represents only a small fraction of its daily requirement, which accounts for approximately 30 mg. Both inorganic and organic Fe can be absorbed. Different forms of this latter are found in Fe-binding compounds e.g. lactoferrin and plant phytoferritin. These are particularly important in individuals fed with poor Fe diets or during the neonatal period (5–7). The lower the levels of Fe in the body, the higher its intestinal uptake. The expression of the divalent metal transporter 1 (DMT1) (8) and of the duodenal membrane associated cytochrome b ferroreductase (DcytB) on enterocytes enables the reduction and

- **Lima IS** & Pêgo AC, Barros T, Prada AR, Gozzelino R. Cell death-osis of dopaminergic neurons and the role of iron in Parkinson's disease. Antioxidants and Redox Signaling, 2021.

ANTIOXIDANTS & REDOX SIGNALING
Volume 00, Number 00, 2021

DOI: 10.1089/ars.2020.8229

Cell Death-Osis of Dopaminergic Neurons and the Role of Iron in Parkinson's Disease

Illyane Sofia Lima,[1,*] Ana Catarina Pêgo,[1,*] João Tomas Barros,[1] Ana Rita Prada,[1] and Raffaella Gozzelino[1,2]

Abstract

Significance: There is still no cure for neurodegenerative diseases, such as Parkinson's disease (PD). Current treatments are based on the attempt to reduce dopaminergic neuronal loss, and multidisciplinary approaches have been used to provide only a temporary symptoms' relief. In addition to the difficulties of drugs developed against PD to access the brain, the specificity of those inhibitory compounds could be a concern. This because neurons might degenerate by activating distinct signaling pathways, which are often initiated by the same stimulus.

Recent Advances: Apoptosis, necroptosis, and ferroptosis were shown to significantly contribute to PD progression and, so far, are the main death programs described as capable to alter brain homeostasis. Their activation is characterized by different biochemical and morphological features, some of which might even share the same molecular players.

Critical Issues: If there is a pathological need to engage, in PD, multiple death programs, sequentially or simultaneously, is not clear yet. Possibly the activation of apoptosis, necroptosis, and/or ferroptosis correlates to different PD stages and symptom severities. This would imply that the efficacy of therapeutic approaches against neuronal death might depend on the death program they target and the relevance of this death pathway on a specific PD phase.

Future Directions: In this review, we describe the molecular mechanisms underlying the activation of apoptosis, necroptosis, and ferroptosis in PD. Understanding the interrelationship between different death pathways' activation in PD is of utmost importance for the development of therapeutic approaches against disease progression. *Antioxid. Redox Signal*. 00, 000–000.

Keywords: Parkinson's disease, cell death, iron, apoptosis, necroptosis, ferroptosis

Introduction

Life expectancy increased globally in the last few decades, with estimates indicating that, in 2050, the elderly will represent 16% of the entire world population (181). While this is a clear advantage for human life, it could also become a health concern. This because aging is a risk factor for the development of many pathologies (82), and the incidence of noncommunicable diseases significantly increased in the last decades.

Among these, neurodegenerative diseases stand out. Their chronic and long-lasting nature also constitutes an economic burden to society, given the costs for medical care, treatment, and patients' follow-up. This strengthens the need to identify, on one hand, biological markers aiding in providing an early diagnosis, and on the other hand, therapeutic approaches capable to ameliorate and possibly retard clinical manifestations. In 2015, neurodegenerative diseases were detected in more than 47 million people worldwide, a number expected to increase up to 131.5 million by 2050 (180).

[1]Inflammation and Neurodegeneration Laboratory, Centro de Estudos de Doenças Crónicas (CEDOC)/NOVA Medical School, Universidade NOVA de Lisboa, Lisbon, Portugal.
[2]Universidade Técnica do Atlântico (UTA), São Vicente, Cabo Verde.
*These authors contributed equally to this work.